Palaeooceanographic modeling in global and regional scale:

An example from the Burdigalian Seaway Upper Marine Molasse (Early Miocene)

Dissertation
Zur Erlangung des Grades eines Doktors der Naturwissenschaften

der Geowissenschaftlichen Fakultät
der Eberhard-Karls-Universität Tübingen

vorgelegt von

Ulrich Bieg

aus Aalen

2005

Tag der mündlichen Prüfung: *16.12.2005*
Dekan: *Prof. K.-G. Nickel, Ph.D.*
1. Berichterstatter : *PD Dr. M.-P. Süss*
2. Berichterstatter : *PD Dr. J. Kuhlemann*

SUMMARY

This thesis consits of 5 major parts. Most of the chapters are separate publications (mainly published, under review or in preparation).

Chapter 1: A general introduction is given to the reader on the control of foreland basins. After the numerical background of the global and regional M_2 simulations, a workflow is outlined, to process geocoded ArcView data towards a 3D gOcad model, generating input files for Quoddy. Quoddy is a Fortran77 finite element program that simulates tides and velocity fields in shallow waters.

Chapter 2: An introduction to the palaeogeography of the early Miocene in global scale is given in chapter 2. The study presents the results of a global tidal M_2 simulation. Aim of the study is to evaluate proper tidal amplitudes at the open gateways of the Burdigalian Seaway, which linked the western Mediterranean (Marseille, France) with the Paratethys (Linz, Austria). The derived tidal amplitudes are used to drive the shallow water model in chapter 3.

> **Bieg, U., Thomas, M., Cordero, F., Süss, M.P., Kuhlemann J.** (2003): Global M $_2$ Simulation for the Early Miocene delivering border conditions for a forthcoming tidal simulation of the Circum-Mediterranean realm; *Zbl. Geol. Paläont. Teil I*, **Heft 3/4**, 259-276.

Chapter 3: A stratigraphic and palaeogegraphic framework is established for the maximum flooding of the peri-Alpine foreland basin during the OMM. Shallow water simulations are introduced, providing information on the tidal response and meso-scale currents of the seaway, using different boundary conditions. The simulations are driven by M_2 waves and provide information on tidal amplitudes and bottom velocities. Calculated residual currents yield insights into net-sediment transport directions.

> **Bieg, U., Süss, M.P., Kuhlemann J.** (accepted): Simulation of Tidal Flow and Circulation Patterns in the Burdigalian Seaway (Upper Marine Molasse, Early Miocene); *IAS Special Publication.*

Chapter 4: A field study in SW Germany is carried out to develop a sequence stratigraphic model, which allows to correlate marginal sequences with the basin. The nearshore cross-bedded Randengrobkalk was evaluated for tidal-/wave- or current influences. The successions are separated in different facies types according to the ratio of siliciclastics (quarz grains) to carbonate (fossiliferous debris), sedimentary structures and microfacies.

Summary

Chapter 5: This chapter respans the question which boundary conditions may have driven the regional currents in the Burdigalian Seayway. A twofold approach has been carried out. (1) Enhanced palaeogeographic reconstructions for the circum-Mediterranean realm have been used for further global M_2 simulations. This yields a tidal range, which might have co-oscillated with the open gateways of the Burdigalian Seaway, giving us a conservative but also an optimistic idea about the expected tidal amplitudes. (2) To accomodate the shift of tidal loci, during the transgression, palaeogeographic sketch maps have been derived for the OMM key stages. To generate an overall idea about net-sediment transport directions, the regional model of the Burdigalian Seawy was also forced by wind and fresh water influx from the surrounding rivers and fan deltas. This yields information on the sensitivity of residual velocities in terms of the different driving forces.

ZUSAMMENFASSUNG

Die Doktorarbeit gliedert sich in 5 Kapitel. Bei den Kapiteln handelt es sich um einzelne Studien, die bereits publiziert wurden, sich im Begutachtungsprozeß befinden oder als Manuskript vorliegen.

Kapitel 1: Das erste Kapitel vermittelt einen Überblick über die Steuerungsmechanismen von Vorlandbecken. Darüber hinaus werden die numerischen Methoden und ein "Workflow" vorgestellt, wie man von einer ArcView Anwendung mit Liniendaten über ein 3D Gittermodell in gOcad zu den Geometrie- und Parameter-Dateien kommt, die als Eingabe für QUOODY (einem Fortran77 Finite-Elemente Programm zur Modellierung von Gezeiten und Strömungen) benutzen werden.

Kapitel 2: Im zweiten Kapitel findet der Leser eine Einführung in die globale paläogeographische Entwicklung des frühen Miozäns. Basierend auf einer Rekonstruktion der Kontinent/Meer Verteilung wird eine globale Simulation der halbtägigen, durch den Mond gesteuerten Gezeitenwelle (M_2) vorgestellt. Ziel der Studie ist es für den paläogeograpisch stark veränderten Mittelmeerraum Gezeitenamplituden abzuleiten und diese für das in Kapitel 3 vorgestellte Flachwassermodell als Randbedingung zu verwenden.

> **Bieg, U., Thomas, M., Cordero, F., Süss, M.P., Kuhlemann J.** (2003): Global M $_2$ Simulation for the Early Miocene delivering border conditions for a forthcoming tidal simulation of the Circum-Mediterranean realm; *Zbl. Geol. Paläont. Teil I*, **Heft 3/4**, 259-276.

Kapitel 3: Das Flachwassermodell umfaßt den Burdigalischen Seeweg, der sich von Marseille (Frankreich) bis Linz (Österreich) erstreckt. Er verbindet die aktiven Gezeitenmeere des Mittelmeerraums mit der Paratehys. Kapitel 3 führt in die Ausbreitung von Gezeitenwellen ein und erklärt wie es durch die spezielle Beckengeometrie zu einer Verstärkung der Gezeitenwirkung kommen kann. Dabei werden verschiedene Randparameter benutzt und die Simulationsergebnisse erklärt. Neben den berechneten Gezeitenamplituden werden besonders die Geschwindigkeitsfelder untersucht. Ziel ist es die Netto-Sedimenttransportrichtung für unterschiedliche Randbedingungen zu erörtern.

> **Bieg, U., Süss, M.P., Kuhlemann J.** (accepted): Simulation of Tidal Flow and Circulation Patterns in the Burdigalian Seaway (Upper Marine Molasse, Early Miocene); *IAS Special Publication.*

Kapitel 4: In Kapitel 4 wird eine Feldstudie vorgestellt. Ziel der Studie ist es, ein sequenzstratigraphisches Modell für die küstennahen OMM Ablagerungen während der maximalen Transgression zu entwerfen. Auf dieser Grundlage ist es möglich, rand- und beckenwärtige OMM Ab-

folgen stratigraphisch zu korrelieren. Der an der nördlichen Küste abgelagerten Randengrobkalk (Raum Tengen) wurde dazu anhand seiner Mikrofazies, den Sedimentstrukturen und der Lithofazies in verschiedene Fazies Bereiche untergliedert. Dabei wurde neben Sequenzgrenzen auch die maximale Überflutungsfläche definiert.

Kapitel 5: Abgeschlossen wird die Arbeit mit einer Studie bei der neben erweiterten globalen Gezeitensimulationen auch Flachwassersimulationen vorgestellt werden, die sowohl durch Gezeiten, als auch durch Wind und Süßwasszuflüsse angetrieben werden. Grundlage der Flachwassersimulationen ist eine detailierte paläogeographische Rekonstruktion des Nordalpinen Vorlandbeckens für unterschiedliche Ausdehnungszustände des OMM Meeres. Diese erlauben es die Veränderung des Gezeitensystems hinsichtlich der Lage der amphidromischen Systeme und der Gezeitenamplituden zu erklären. Dadurch daß das Flachwassermodell neben den Gezeiten auch durch Wind und Süsswasserzuflüsse angetrieben wird, erlaubt dies eine allumfassende Beurteilung des Netto-Sedimenttransports.

Contents

Chapter 1

Introduction & Methods

1.1 Aim & Concept

Sedimentological research carried out in the eighties showed that sediments of the Burdigalian seaway have mainly been deposited under a strong meso- to macrotidal regime (e.g. Homewood et al. 1985). Tidally related deposits like sand waves, bidirectional cross-stratification, neap-spring tidal bundle sequences have been recognized within the whole seaway from France (e.g. Tessier & Gigot 1989; Assemat 1991; Crumeyrolle et al. 1991; Allen & Bass 1993),

Switzerland (e.g. Homewood & Allen 1981; Allen 1984; Diem 1985; Allen et al. 1985; Homewood et al. 1985; Homewood et al. 1986) to South Germany, Austria (e.g. Hülsemann 1955; Faupl & Roetzel 1987,1990; Krenmayr 1991; Salvermoser 1999) and Hungary (e.g. Sztanó 1994, 1995; Sztanó & deBoer 1995).

The proposed tidal ranges in the order of 2 to 4m are high if we consider, that the active open oceans (Paratehtys and Western Mediterranean) are far away and the open gateways of the Burdigalian Sea "only" co-oscillate with them. So far there have been just local ("outcrop scale") ideas about tidal currents (strength and direction) and tidal ranges, which could not be compiled in a sufficient way to generate maps of meso-scale current systems and contoured maps of tidal ranges.

This might be the reason that there are disputed concepts about net-sediment transport, which might have been directed towards the East (Lemcke 1973, Freudenberger & Schwerd 1996), West (Kuhlemann 2000) or opposed to each other, with a mixing zone in the mid of the central German Molasse Basin (Füchtbauer 1967, Sissingh 1997), or alternatively according to Allen et al. (1985) tides operated within distinct cells, which act as essentially closed systems for sediment transport. According to heavy mineral analysis it was proposed by Büchi & Hofmann (1960), Schreiner (1966), Hofman (1976), Allen et al. (1985) that tidal currents transported sediment alongshore from the extra Alpine source, the Bohemian Massif, towards the Swiss realm in the West.

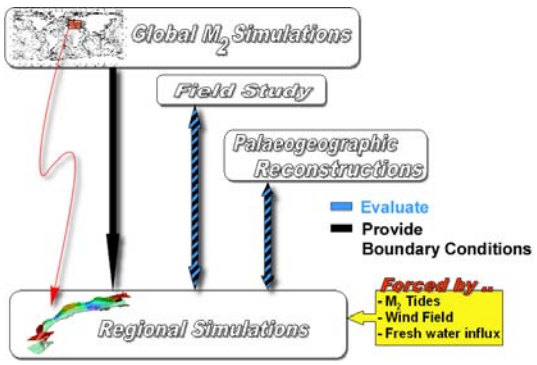

Figure 1.1: *Workflow chart of the study: Numerical simulations accounting the regional, Burdigalian Seaway, rank a central position within the study. The flanking topics should deliver proper constraints for the regional model.*

Regional Simulations: This study intends to find proper boundary conditions for the Burdigalian Seaway to explain the high tidal ranges but also the controversial net-sediment transport directions. To achieve this, the state-of-the-art prognostic time-domain shallow-water model, Quoddy, was used. The numerical model was initiated as a unlayered (barotropic) or layered (barocline) model. The simulation period spans some few weeks and hence is termed "short term

model". The "long term" (some 10ky) behaviour of the depositional system and coastline evolution have not been accounted. To evaluate the sensitivity of the model according to net-sediment transport directions, it was driven by:

- M_2 waves. The semi-diurnal lunar tide was chosen, as tidal deposits of the OMM show mostly a 14-day neap-spring cycle (e.g. Allen et al. 1985),
- river influx from the surrounding domains, e.g. fan deltas,
- uniform wind field (storm event).

Global M_2 Simulations: Based on an approach of Seiler (1989) and Seiler (1991) global M_2 simulations provided boundary conditions for the open gateways of the regional model (Burdigalian Seaway). Different reconstruction possibilities of the cicum-mediterranean realm have been tested in terms of:

- widened and deepened seaways towards the active oceans (Atlantic and Indian ocean).
- different land/sea distributions as proposed by Dercourt et al. (1993) or Rögl (1998).

Palaeogeographic Reconstructions: Basin shape of the Burdigalian Seaway was reconstructed for different key stages, displaying the changes of basin width and depth during the transgression of the Upper Marine sea. This is of crucial importance as the tidal regimes shifted their loci with the ongoing transgression. The reconstructions were used to generate different three-dimensional grids which have been utilized for the numerical studies .

Field Study: For the time of the maximum transgression, marginal deposits of the Upper Marine Molasse sea have been studied in the vicinity of Tengen and Zollhaus (South-Germany). Crossbedding types of the Randengrobkalk were evaluated for tidal-, wave- and current influences but also separated into a transgressional and regressional series.

1.2 The North Alpine Foreland Basin (NAFB)

1.2.1 General introduction

The OMM (Upper Marine Molasse) has been deposited in the North Alpine Foreland Basin. Peripheral foreland basins, in general, develop in response to the load of the thickened crust that resulted from continent continent collision (Allen et al. 1986, Beaumont 1981, Dickinson 1974). The sedimentary infill of foreland basins record the interaction between the growth of the thrust wedge, the isostatic adjustments of the cratonic lithosphere to thrust loading and additional bending moments, eustasy and the surface processes that redistribute material from the mountain belt into the surrounding basins (Sinclair 1997). In the following the basin fill history and its depencency on the interplay of tectonics and eustatic sea-level rise is discussed.

The peripheral North Alpine foreland basin (NAFB) developed in response to continental collision between the African and Eurasian plates during early Tertiary times (Dewey et al. 1973). The underthrusting of the southward-facing Tethyan passive margin below the overriding African plate generated a submarine trench, that is considered to mark the time of initiation of the Alpine foreland basin (Allen et al. 1991). As a mechanical response to the tectonic load of the evolving alps (Homewood et al. 1986, Sinclair et al. 1991, Schlunegger et al. 1997) the european lithosphere downflexed and generated the asymmetric accommodation space of the NAFB.

Several attempts to correlate foreland basin stratigraphy to orogenic evolution of the adjacent hinterland were done by Beaumont (1981), Piffner (1986), Homewood et al. (1986), Sinclair (1991), Sinclair et al. (1991), Sinclair & Allen (1992)and Schlunegger et al. (1997) modelled the shape of the NAFB. These authors concluded, that the formation of the NAFB must be considered as a flexural response of a weak (T_e about 10km) elastic plate (see also contrasting ideas by Jin et al. (1995) and discussion by Zweigel & Zweigel (1998)) to the Alpine loads. However, the Alpine stack of upper crustal material alone (topographic load) appears not to be adequately to describe the shape of the flexed plate. Instead, a subsurface, deep crustal load exerted by the Adriatic mantle and associated

lower crustal wedge in combination with the topographic load is likely to explain the overall shape of the flexed plate to a first order approximation.

1.2.2 Basin fill history

Sedimentologically, the basin fill can be divided into two stages; a Paleocene to mid-Oligocene deep marine (*flysch*) stage, followed by a mid-Oligocene to late Miocene shallow marine and continental (*molasse*) stage (see discussion in (Sinclair et al. 1991; Sinclair & Allen 1992). Comparisons between rates of exhumation in the Alps and preserved volume of sediment in the basin suggest that the Molasse represents the late filled/overfilled stage of the evolution of the NAFB (Sinclair 1997; Sinclair & Allen 1992).

The wedge of Molasse deposits that accumulated between the Early Oligocene and the Middle Miocene comprises two coarsening and thickening upward megasequences (see Fig. 1.2). They are traditionally subdivided into four units (Matter et al. 1980) for which the conventional German abbreviations are used:

- Lower Marine Molasse (UMM),
- Lower Freshwater Molasse (USM),
- Upper Marine Molasse (OMM),
- Upper Freshwater Molasse (OSM).

Lower Marine Molasse (UMM):
The first megasequence starts with the development of the 35- to 30-Ma-old Lower Marine Molasse Group (UMM). This unit forms the transition from the underfilled to the filled stage of basin evolution, presumably as the increase of sediment supply rates was larger than the creation of accommodation space (cf. Kuhlemann 2000). The stratigraphy of underfilled peripheral foreland basins can be synthesized into three units, named by Sinclair (1997) the "underfilled trinity", which are commonly superimposed during basin migration.

Lower Freshwater Molasse (USM):
The UMM is overlain by fluvial clastics of the 30- to 20-Ma-old Lower Freshwater Molasse Group (USM). This units consits of several kilometers of alluvial fan conglomerates at the thrust front (cf. Kempf & Matter 1999). Towards the more distal parts of the basin, the conglomerates interfinger with meander belt sandstones, floodplain mudstones and lacustrine depositional systems.

Upper Marine Molasse (OMM):
The second megasequence started with a marine transgression at ca. 20 Ma, resulting in the establishment of the shallow marine depositional systems of the Upper Marine Molasse Group (OMM) between 20 and 16.5 Ma for the Swiss area (Kempf 1998) and 18 - 17.6 Ma for the German area. At the Alpine thrust front the marine deposits interfinger with fan delta conglomerates, which were sourced in the Central Alps (e.g. Schaad et al. 1992, Keller 1989).

Upper Freshwater Molasse (OSM):
The OMM is overlain by the Continental Upper Freshwater Molasse Group (OSM). Deposition of the OSM started at ca. 16.5 Ma. The youngest deposits of this unit display ages between 13 Ma (proximal position , Kempf et al. 1999) and 10.5 Ma (distal position, Berger 1992). At present the Molasse basin is uplifted and eroded, and no deposits younger than Tortonian are preserved.

At approx. 17 Ma a retreat of the marine to barackish environment (Doppler 1989; Reichenbacher et al. 1998; Reichenbacher et al. 1998) established a large west-directed river system (Glimmersande), termed Palaeo-Rhône by Kuhlemann et al. (2001). The regression of the OMM sea is mainly due to an increase of sediment supply towards the NAFB due to an important uplift in the Eastern Alps. This uplift is caused by the termination of thrusting along the eastern part of the Alpine front (Decker & Peresson 1996).

Mass balance calculations

Temporal variations in sediment discharge to the NAFB were derived by various authors (Hay et al. 1992, Kuhlemann 2000, Kuhlemann et al. 2001; Schlunegger et al. 2001) using the volume of preserved rocks in the basin.

The similarities in trends between the progradational sequences of the Molasse deposits and the sediment discharge curve suggest that temporal variations in erosional processes in the Alpine hinterland predominantly controlled the stratigraphic development of the Molasse sequences. Specifically the change from the underfilled to the overfilled stage of basin foreland evolution (transition from the UMM to USM)

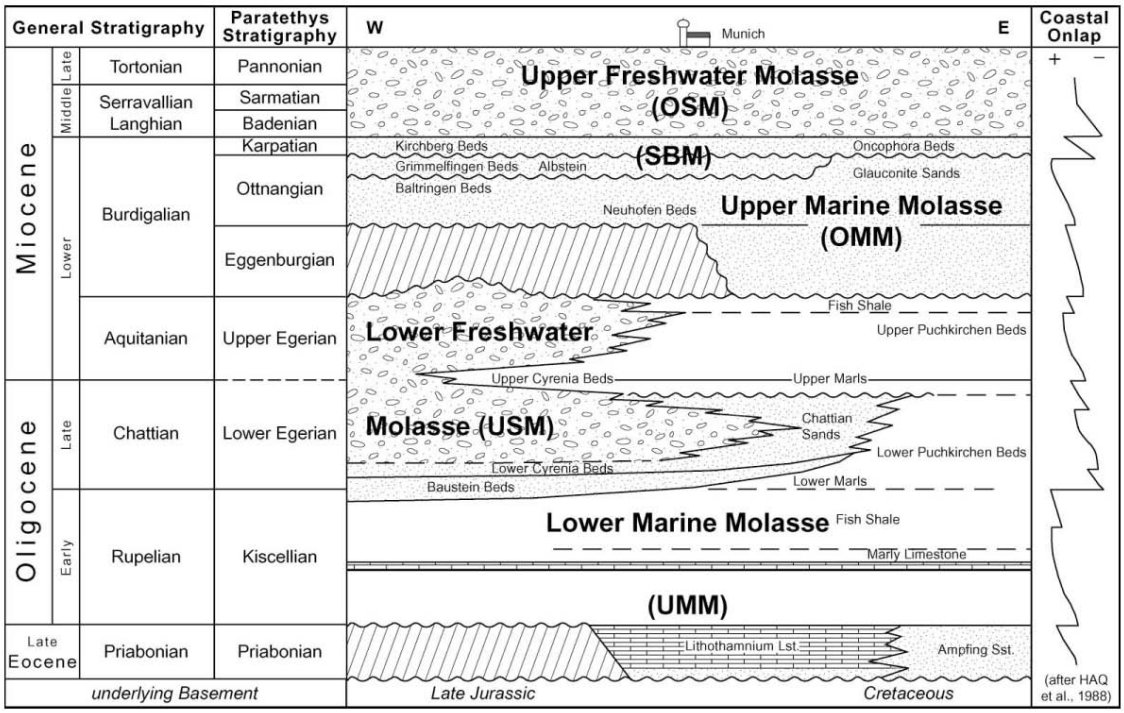

Figure 1.2: *Schematic west-east chart with a generalized stratigraphic and facies evolution of the central NAFB and the coastal onlap curve of Haq et al. (1988) - taken from Kuhlemann & Kempf (2002).*

coincides with a continuous increase in sediment discharge (Sinclair 1997). Similarly, the changes from terrestrial (USM) to shallow marine (OMM) and subsequently to terrestrial conditions (OSM) correlate with corresponding temporal trends of sediment discharge (Schlunegger et al. 2001).

Despite differences in the boundary conditions for mass balance calculations of Hay et al. (1992), Schlunegger (1999) and Kuhlemann (2000), they all reveal similar trends (see Fig. 1.3), that are characterized by a significant increase (150-300%) of denudation rates between 30 and 20 Ma. At ca. 20 Ma surface erosion decreases to 25-40% of the previous time interval. The results imply that sediment export can be ignored (Schlunegger 1999) and that the basin was not significantly overfilled during the late Oligocene and Early Miocene (see Kuhlemann et al. 2001 for contrasting interpretations).

After 16 Ma, average erosion rates started to increase again. Kuhlemann (2000) suggests a significant increase, whereas the data of Hay et al. (1992) and Schlunegger (1999) imply a small increase. As we have to consider that SW-directed transport started to occur somewhat after 18Ma, the calculations of Schlunegger (1999) might represent underestimates.

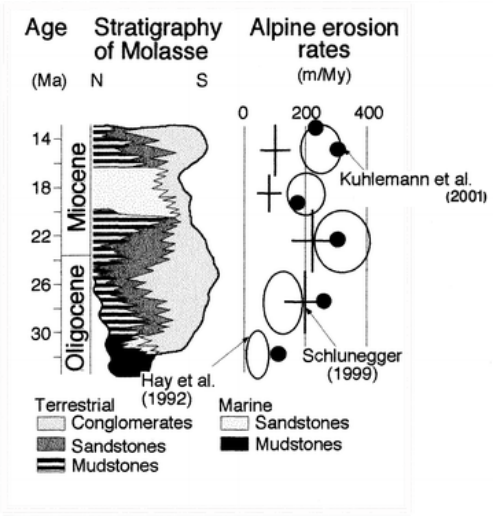

Figure 1.3: *Average Alpine erosion rates which are based on the preserved volume of sediment in the Molasse Basin of central and western Switzerland (Schlunegger 1999) and in the German and Swiss part of the Molasse Basin as well as in sedimentary basins in the north and the south (Hay et al. 1992; Kuhlemann et al. 2000) - the figure is taken from Schlunegger et al. (2001).*

1.2.3 Interplay between Alpine tectonics and foreland basin evolution

The 'Two-phase' foreland basin concept

Foreland basins are controlled by the interplay between episodic thrusting and erosional unloading. This concept is called "two phase" foreland basin system (Heller et al. 1988; Jordan and Flemings 1991). In this concept periods of tectonic activity (Fig. 1.4, phase 1) lead to thrust wedge loading and enhanced flexural subsidence at the rear of the basin, whereas the frontal forebulge experiences uplift and migrates towards the thrust front. The associated fluvial pattern in the foreland is that of a longitudinal river interlocked between the basin margin alluvial fans and the forebulge high. During a phase of tectonic quiescence (Fig. 1.4, phase 2) the thrust wedge is eroded and the amplitude of the forebulge diminishes while migrating outward. As a result of the erosion of the thrust wedge, the lithosphere is unloaded and the sediment accommodation space in the foreland basin is reduced. This is partly a self-sustaining process, as new material is continuously added from below and removed in efficient high-relief drainage basins. The reduction of the basin accommodation space, combined with a high rate of sediment supply leads to a widespread progradation of alluvial fans, which now establish a dominant transversal drainage system (Burbank 1992). Renewed tectonic activity results in a retreat of the alluvial fans by the increase of flexural accommodation space created close to the tectonic front. In addition, the flexural response again results in forebulge uplift, temporal erosion of distal foreland basin sediments and the creation of unconformities. Accordingly a respective tectonic/quiescence pattern is reflected as multiple cycles of gravel progradation in the foreland basin alternating with well-sorted axial sediments and forebulge unconformities.

A relatively instantaneous, elastic response of the lithosphere upon thrust loading and erosional uploading is assumed in the "two-phase" foreland basin concept. Yet, another style of lithospheric behaviour, the visco-elastic response, is frequently advocated in literature and applied in model studies of foreland basins (Quinland and Beaumont 1984; Tankard 1986). Visco-elastic models take into account time-dependent lithospheric processes such as thermo-mechanical weakening. These models are used to explain changes in basin geometry without changes in surface load. Inherently visco-elastic models involve a relaxation time between loading of the orogenic wedge.

Orogenic evolution of the Western and Eastern Alps during Miocene times and its implication on basin fill

There are fundamental topographic differences between the Central (mainly Swiss) Alps and the Eastern (mainly Austrian) Alps. The Central Alps have generally a higher relief than the Eastern. This is due to differences in Miocene to recent tectonics, which is characterized by ongoing crustal thickening in the Central Alps (Schmid et al. 1996) and lateral extrusion tectonics in the Eastern Alps. Late Tertiary lateral extrusion in the Eastern Alps (Ratschbacher et al. 1991) is a combination of gravity-driven orogenic collapse and crustal escape driven by tangential forces. Lateral extrusion mainly occurred in Early and Middle Miocene time (ca. 23-13 Ma). Both metamorphic core complexes of the Eastern (Tauern window) and Central Alps (Lepontine dome) were exposed contemporaneously at $\sim$ 14-13 Ma (Spiegel et al. 2000) at the surface as a consequence of tectonic unroofing during Miocene lateral extrusion (Frisch et al. 2000; Steck & Hunziker 1994). In contrast to the Eastern Alps, Penninic basement units had already been exposed between 25 and 20 Ma in the Ccentral Alps. But these units belong to the Upper to Middle Penninic hanging wall of the Lepontine dome. At 21. Ma the sediment discharge of the Alps dropped dramatically. This event occurred coeval with the reduction of thrust advance rates in the Swiss Molasse zone to at least one third (Homewood et al. 1986). In the easternmost part pf the orogen, thrusting continued until $\sim$17 Ma (Decker and Peresson 1996).

Eastern Alps

In Early Miocene times, the area of the western Eastern Alps were already mountainous, whereas the eastern part of the orogen formed lowlands or hilly areas (Frisch et al. 1998). Enhanced block movement in the course of the extrusion process around the Early/Middle Miocene boundary led to the formation of intramontane sedimentary basins and fault-induced reorientation of the drainage pattern, which

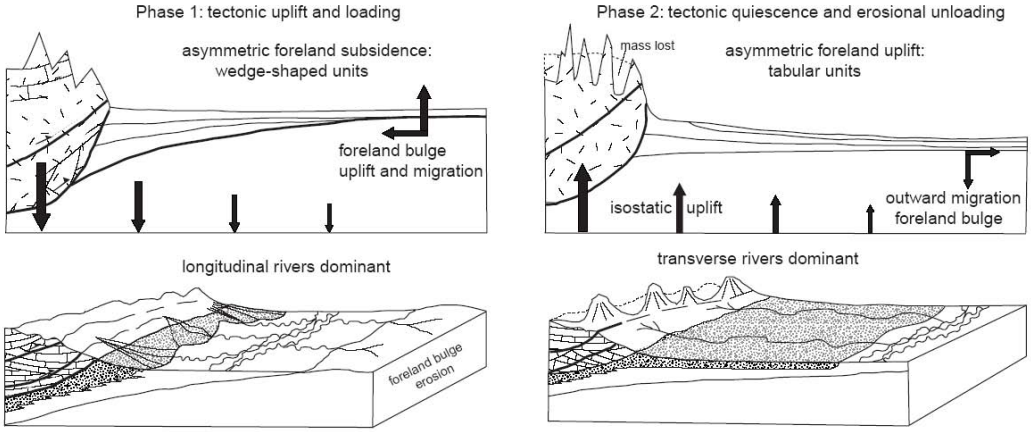

Figure 1.4: *Two-phase foreland basin concept. The Thrust wedge loading (phase 1) leads to flexural subsidence, whereas the frontal forebulge experiences uplift and migrates towards the thrust front. The fluvial pattern in the foreland is that of a longitudinal river interlocked between the basin margin alluvial fans and the forebulge high. during a period of tectonic quiescence (phase 2), the thrust wedge is eroded and the drainage is dominated by transverse alluvial fans (taken from Clevis (2003), modified after Burbank (1992)).*

formed the basis of the modern river system in the area east of the Tauern window. The main extrusion period occurred at about Ottnangian or Karpathian until the early Badenian (ca. 18-15 Ma). A number of intramontane basins formed as pull-apart or transtensional structures along major strike-slip fault zones (Ennstal, Mur-Mütztal, Lavanttal). Enahnced block movement during tectonic extrusion around the Early/Middle Miocene boundary led to the rearrangement of north-directed drainage system east of the (later) Tauern window (Miocene "tectonic revolution"). Augenstein sediments - (Frisch et al. 2000) attributed an Early Miocene age to palaeosurface and palaeosoil formation, which was interrupted by the ca. 18 Ma tectonic event, during which fault-bounded valleys dissected the palaeosurface.

Between 18 and 17 Ma, a short termed, drastic increase of sediment discharge rates is observed. At this time the final thrusting phase in Lower Austria resulted in a collision of the Alpine nappe stack with the Bohemian spur (Decker and Peresson 1996), which formed a rigid indenter of the European continental margin in Lower Austria. In this region, the Molasse zone is nowadays very narrow. The most uplifted and eroded area, the Amstetten swell (Kapountek et al. 1965), formed a drainage divded and forced the NW-trending East Alpine rivers towards westerly directions (Kuhlemann 2000). The collision initiated the closure of the marine gateway between the central Paratethys and the Western Mediterranean (Lemcke 1988) and the retreat of the OMM sea. The Bohemian spur formed an obstacle, triggering an anticlockwise rotation of East Alpine tectonic units (Márton et al. 2000) and simulataneous pull-apart opening of the Vienna basin E of the Bohemian spur (Decker and Peresson 1996).

Central/Western Alps

The Swiss alps are a doubly vergent orogen (cf. Beaumont et al. 1996, Kühni & Pfiffner 2001). The internal structure of the orogen is made up of a complex series thick-skinned and thin-skinned thrust sheets. They are the result of Cretaceous and Tertiary orogenic events.

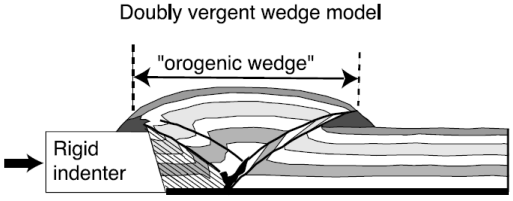

Figure 1.5: *Schematic sketch of a doubly vergent orogen due to continent-continent collision.*

The decrease of Early Miocene erosion rates, is in general considered to be the result of

changes in rate and pattern of crustal uplift, exposed source rock lithologies and palaeoclimate (Schlunegger 2001, Whipple & Tucker 1999, Kühni & Pfiffner 2001).

At $\sim$ 20 Ma average erosion rates in the Alps decreased of 25-40 %, as the orogenic crystalline core of the Alps became exposed. This also resulted in an reorganisation of drainage pattern from orogen-normal to an orogen-parallel orientation. It appears that erosion rates decreased more rapidly than crustal uplift rates (Schlunegger et al. 2001). Schlunegger & Pfiffner (2001) propose that the climate change resulted in an instantaneous decrease of sediment discharge and vertical topographic growth until the re-establishment of steady-state. This is in contrast to Kuhlemann (2000) who found no detectable influence on Alpine erosion rates due to the Miocene climate "change", pointing out that changes in erosion rates are mainly caused by lateral extrusion. Underfilling of the NAFB at ca. 20Ma coincides with a significant modification in the structural evolution of the Alps from a period of crustal thickening in the central part of the orogen to a phase of frontal accretion in the foreland. Schlunegger (1997) hypothesized that the marine ingression at that time was triggered by a decrease in average erosion rates. Further constraints how erosion influenced the structural evolution of the Swiss Alps can be found in Schlunegger (1999) and Schlunegger & Willett (1999). However, despite the formation of enhanced relief, the volume of sediment preserved in the NAFB, suggests that there was a significant decrease in the discharge of sediment from the central Alps at 20 Ma, compared with the preceeding 10 My (Kuhlemann 2000, Schlunegger & Willett 1999).

Dispersal systems, basin drainage directions

At the Oligocene/Miocene boundary palaeoclimate changed from humid and hot conditions towards a climate with high temperature and low humidity (Schlunegger 1999). The aridization is associated with a change in depositional pattern from alluvial fans to lakes and floodplains, suggesting also decreasing sediment discharge.

As a result of surface uplift the drainage pattern of the Alpine hinterland changed from an across-strike to present day along-strike orientation (Schlunegger et al. 1998; Schlunegger & Willett 1999). During this stage of the drainage basin evolution ($\sim$ 20-15 Ma), the North Alpine palaeorivers were deflected around the hinge of the growing Aar massif and changed to the present-day orogen-parallel dispersion (Rhine and Rhone rivers). At some 15Ma present-day Alpine drainage network was already established, cutting further down the Alps (Schlunegger et al. 1998). The total size of Alpine drainage basin remained nearly constant from 30 Ma to the present (Schlunegger & Willett 1999). Reconstruction of the evolution of drainage pattern of the Swiss Alps presented by Schlunegger et al. (1998) was subsequently modified by Eynatten et al. (1999).

Within the central Swiss molasse basin there are three major dispersal systems (Rigi, Höronen, Napf), distinguished by characteristic heavy mineral suites, conglomerate clast population and the presence of key clasts. These systems record the three major phases of denudation of the Alpine edifice (Schlunegger et al. 1997). The Rigi system eroded the Austroalpine and Penninc nappes of eastern Switzerland from 30 to 25,5 Ma as a result of backthrusting and uplift of these units along the insubric line. Subsequent uplift of the Aar massif some 40 km to the north appears to have controlled the duration of the Höronen and Napf dispersal systems, spanning 24-22 Ma and 21,5 to 15 Ma, respectively. They record downcutting into the crystalline cores of the Penninic and Austroalpine nappes of eastern (Höronen) and western (Napf) Switzerland. Due to lateral extension, newly created or reactivated fault systems cut off the headwaters of the old drainage pattern (Kuhlemann et al. 2001) and established new catchments such as the Lake Constance-Pfänder fan system (Berger 1996).

1.3 Numerical Methods and Workflow to generate a shelf-scale shallow water model

1.3.1 Generation of a 3D Palaeogeographic Model

In the following a workflow is outlined how to process from two-dimensional data towards a three dimensional grid. The 3D grid with its extent and bathymetry is used as input geometry file for Quoddy. A general overview about Quoddy is also presented in the section.

ArcView - 2D approach - Fig. 1.6

ArcView was used to digitize the reconstructed extent of the Burdigalian seaway (see Fig. 1.6). As a base map, the HYDRO1K of the USGS (`http://edcdaac.usgs.gov/gtopo30/hydro/`) was used. The map was geocoded to the equal-area Lambert projection. Informations concerning palaeo-coastlines and palaeo-bathymetry were digitized according to local (e.g. Allen & Bass 1993; Berger 1996; Krenmayr & Roetzel 1996) and regionl (e.g. Demarcq & Perriaux 1984; Sissingh 1997; Sissingh 1998; Sissingh 2001; Kuhlemann & Kempf 2002; Berger et al. in press a,b) datasets. The shape files have been exported and used within gOcad for further processing.

gOcad - 3D approach - Fig. 1.7

Within gOcad the shapefiles have been imported and used to generate a delauney triangulated unstructured mesh. Because of the velocity distribution, calculated by Quoddy, the size of the triangles in the unstructured finite element grid has to be proportional to both bathymetry and the bathymetric gradient. Generally triangles are smaller in regions with shallow water depth and larger where the bathymetric gradient is less steep. The variable mesh is especially useful in coastal regions where the depth of water varies greatly.

Order of generation	Border labels
1:	land
2:	island
3:	nonzero normal velocity
4:	geostrophic outflow
5:	surface elevation

Table 1.1: *The table shows in which order the "borders" have to be created.*

Order of generation	Properties
1:	Amplitude
2:	Phase
3:	Residual

Table 1.2: *The table shows in which order the properties have to be created.*

After a mesh was created, borders have to be created and labeled according to Tab. 1.1. Numbers in Tab. 1.1 indicate what has to be created at first (1) and at least (5). Border nodes have to be assigned with boundary values for the Quoddy simulation (see Tab. 1.2). The order in which the user has to create borders and properties is of crucial importance for the C++ program (see Appendix) which extracts geometry and border informations from the gOcad surface file to generate proper input-files for Quoddy.

1.3.2 The prognostic time domain model - QUODDY

Numerical Methods

Quoddy, a state-of-the-art finite element compehensive circulation model from the Dartmouth College, is employed. The Fortran 77 source code is free available under `http://www-nml.dartmouth.edu/Software/quoddy/` (currently in version 5.2).

> "A comprehensive model is one which provides shelf-scale geographic coverage; adequate local resolution of topography, coast and flow features; and internal physics to capture all important shelf processes at tidal time" — Lynch et al. (1996)

It is described in detail by Lynch et al. (1996) and Lynch & Werner (1987). The governing equations are the canonical set: continuity and transport equations for horizontal momentum, heat, salt and turbulence. The model is three-dimensional with a free-surface, partially mixed vertically, hydrostatic, and fully nonlinear. All terms are resolved in tidal time. A level 2.5 turbulence closure scheme (Mellor & Yamada 1982; Galperin et al. 1988; Blumberg et al. 1992) determines the vertical mixing. The horizontal mixing is represented by a mesh- and shear-dependent eddy viscosity similar to Smagorinsky (1963).

Variable horizontal resolution is achieved with an unstructured mesh of conventional linear triangles. In the vertical, a general terrain following coordinate system is used, that incorporates flexible, non-uniform vertical discretization. Therefore continuous tracking of the free surface, including proper resolution of surface and bottom boundary layers is accomplished.

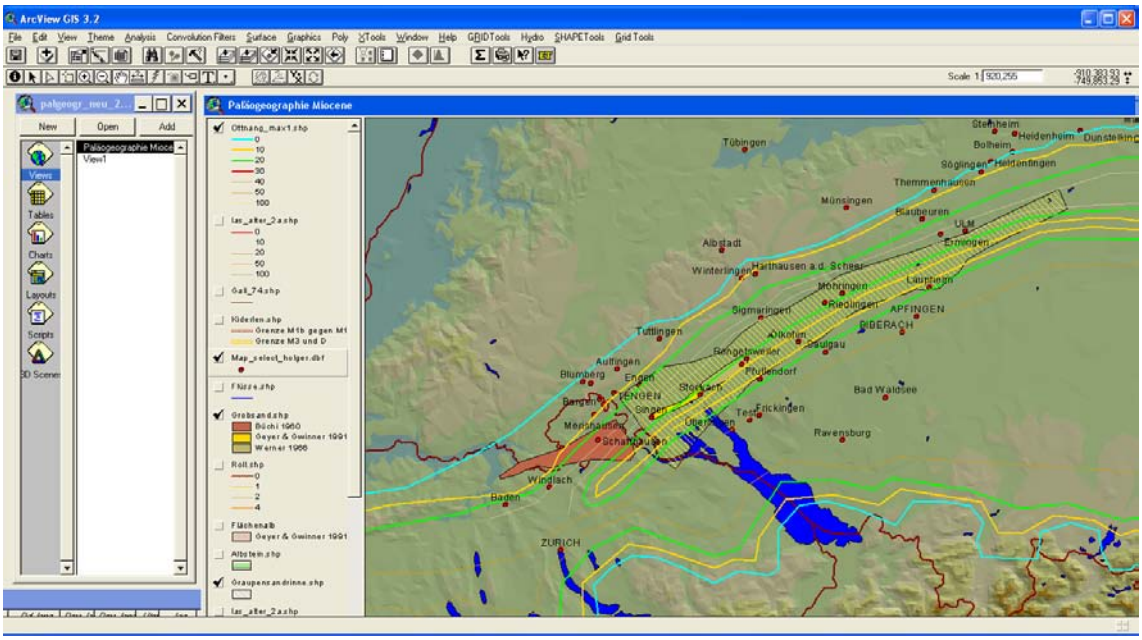

Figure 1.6: *Generation of a palaeogeographic map within ArcView. Palaeocoastlines and bathymetry were digitized on the geocoded HYDRO1K map.*

In general it has to be mentioned that Quoddy cannot be used to simulate drying and wetting of e.g. a tidal flat. If there are requisites like this, BELLAMY another simulation tool from the Dartmouth College has to be used.

Governing equations

The 3D-hydrodynamic equations are solved with the conventional Boussinesq and hydrostatic assumptions. Temperature and salinity are transported, and density is determined via an equation of state. The subgrid-scale dissipation is represented in eddy viscosity (diffusivity) form. This is parameterized in terms of stratification plus turbulent kinetic energy and missing length, both of which evolve at the macroscale.

There are six canonical three-dimensional state variables (see also Tab. 1.3) for which the conventional transport equations are witten.

Continuity Equation:

$$\nabla \cdot = \frac{\sigma}{\rho} \tag{1.1}$$

$$\frac{\delta \eta}{\delta t} + \nabla_{xy} \cdot \int_{-h}^{\eta} v dz = \int_{-h}^{\eta} \frac{\sigma}{\rho} dz + (P - E) \tag{1.2}$$

We have the two horizontal components of the momentum equations:

$$\frac{dv}{dt} + f \times v + g \nabla_{xc} \zeta - \frac{\delta}{\delta z}(N_m \frac{\delta v}{\delta z}) = - \frac{g}{\rho_0} \int_z^{\zeta} \nabla_{xy} \rho dz + F_m + \frac{\sigma}{\rho}(\nu_\sigma - \nu) \tag{1.3}$$

Heat and Salt conservations:

$$\frac{dT}{dt} - \frac{\partial}{\partial z}(N_h \frac{\partial T}{\partial z}) = \Gamma_\tau + \frac{\sigma}{\rho}(T_\sigma - T) \tag{1.4}$$

$$\frac{dS}{dt} - \frac{\partial}{\partial z}(N_h \frac{\partial T}{\partial z}) = \Gamma_s + \frac{\sigma}{\rho}(S_\sigma - S) \tag{1.5}$$

A constitutive relationship relates the density to the temperature and salinity (Gill 1982):

$$\rho = \rho(T, S) \tag{1.6}$$

For further mathematical expressions concerning boundary conditions (atmoshperic shear stress, quadratic slip condition for the bottom etc.), wave coninuity equation and vertical meshing see e.g. Lynch et al. (1996). The solution method for the free surface ζ and the horizontal velocity is described in Lynch & Werner (1991). It is based on the Galerkin weak-form, with nodal quadrature for evaluation of the inner products. A semi-implicit time-stepping procedure is used to solve the implicit wave equation (Lynch et al. 1996).

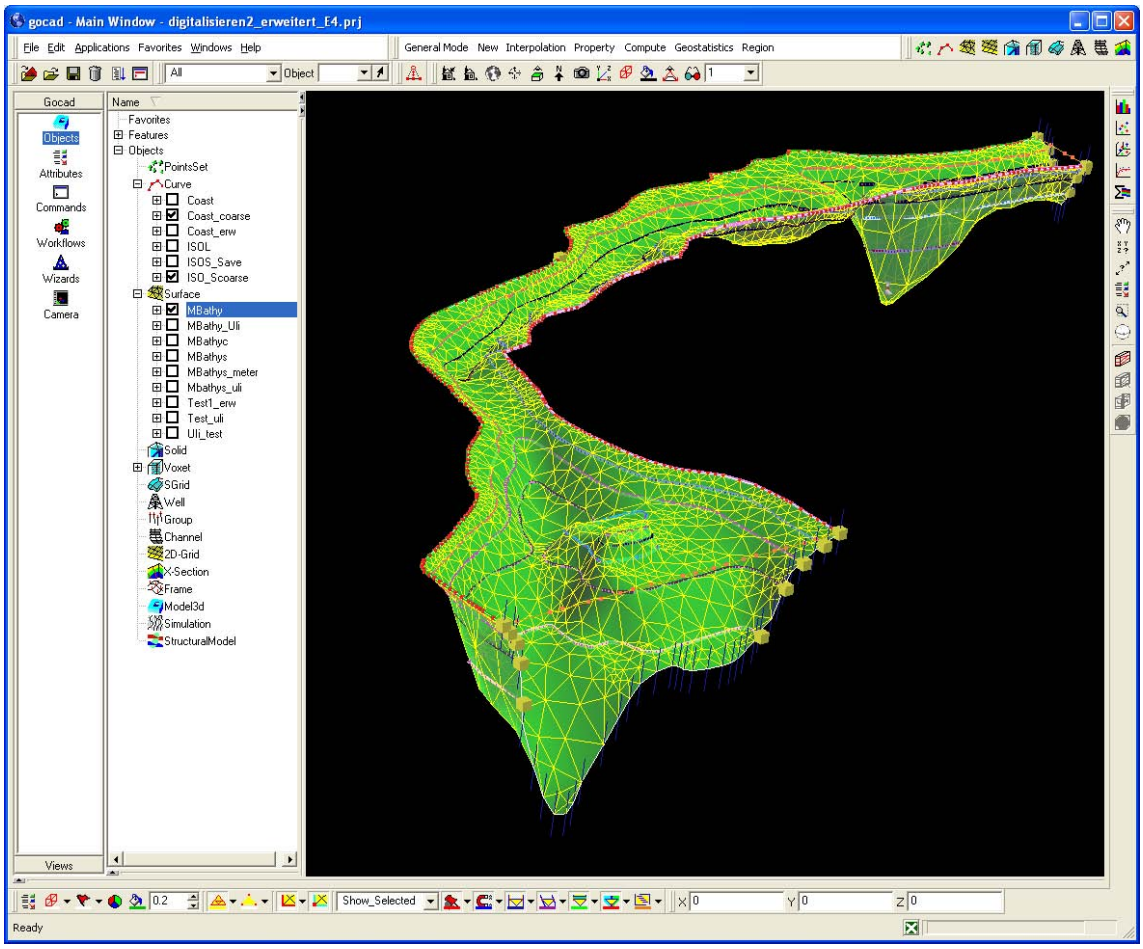

Figure 1.7: *Import of coastlines as DXF- or Shape-File in gOcad. Generation of a unstructured delauney triangulated mesh.*

Forcing processes of the Quoddy model

To drive Quoddy with other forcing mechanisms than tidal waves, the TIDE_Q5_1.1.USER.f file has to be enhanced.

Wind-induced model
A uniform wind field is so far used and applied to the model after the dynamic equilibrium with the tide has been achieved. This was done by adding the ATMOSQ5 (Listing 6.3 in the Appendix section) and WINDSTRESS (Listing 6.4 in the Appendix section) subroutine to the TIDE_Q5_1.1_USER.f file.

Introducing point sources
Quoddy can also be driven by point sources. As boundary conditions, the fresh water influx from e.g. fan deltas in Switzerland and rivers in Germany have been evaulated for their influence on the residual velocieties. This was done by adding the subroutine POINTSOURCE (Listing 6.5 in the Appendix section) to the TIDE_Q5_1.1_USER.f file.

Passive Particle Tracking
Tracking passive lagrangian tracers on a finite element domain was realized with DOG3DDT (`http://www.opnml.unc.edu/Particle_Tracking/part_track.html`), that operates as a subroutine to Quoddy. Drogues were placed along different isobaths to infer transport pathways and accumulations of sediment particles.

Pre- and Post-Processing

Preprocessing of the geometry and input files
When using the geometry files from gOcad, it is highly recommended to re-order the numbers

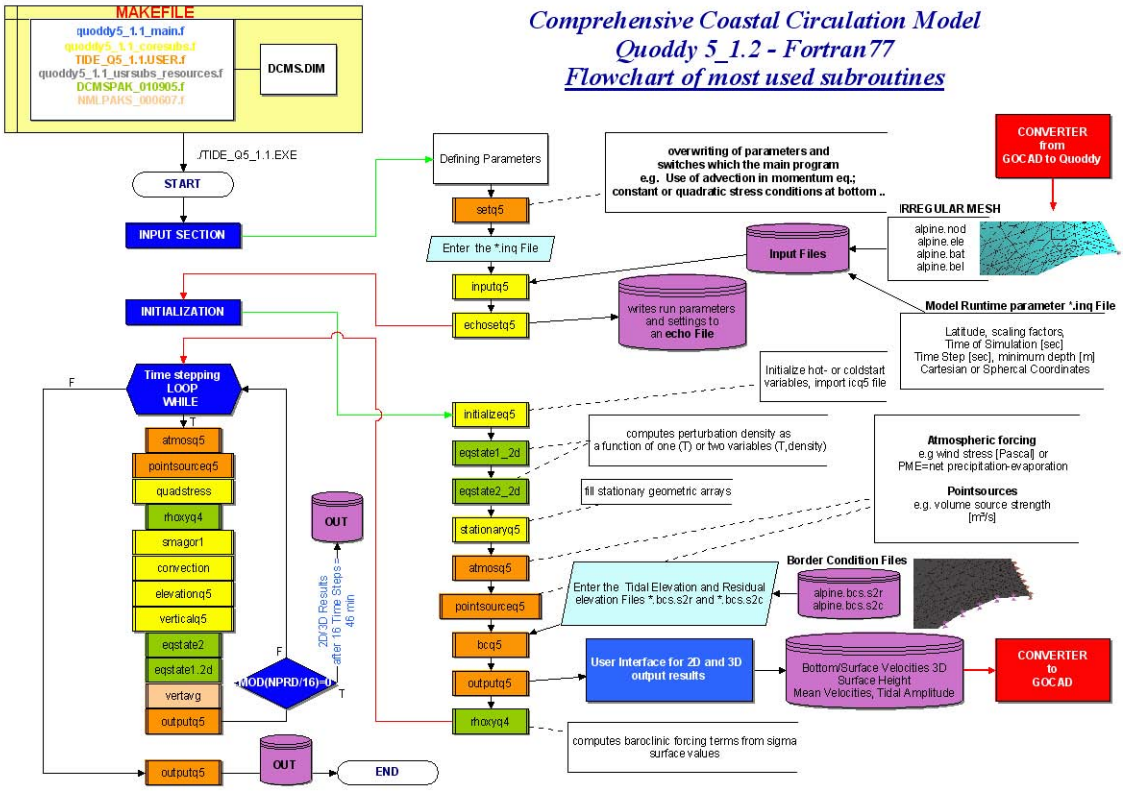

Figure 1.8: *Flowchart of the Quoddy Fortran 77 source code structure.*

of the FEM grid. This makes Quoddy work more efficient and "memory-conservative". Quoddy solves the matrix $Ax = b$ by direct factorization. For efficiency, the bandwidth of the matrix needs to be clustered as good as possible about the diagonal (see Fig. 1.9). The grid rearrangement was done in Matlab using the "Symmetric Reverse Cuthill-McKee" routine or the "Collins method".

```
o=loadgrid('ottnang')
%[he,hx,hz]=redbw_collins(o.e,o.x,o.y,o.z) % Collins
[re,rx,ry,rz,rbnd,perm]=reduce(o.e,o.x,o.y,o.z) % Cuthill-McKee
write_bat(rx,'test.bat')
write_ele(re,'test.ele')
write_nod(rx,ry,'test.nod')
```

Listing 1.1: *Reducing the bandwith of the matrix by using the "Cuthill-McKee" method*

Before a model run the time stepping increment has also to be adjusted within the .inq file. This time step has to fit the Courant stability criterion. The Courant-Friedrich-Lévy (CFL) condition discretes the time step to be kept small enough in time to propagate through the space discretization.

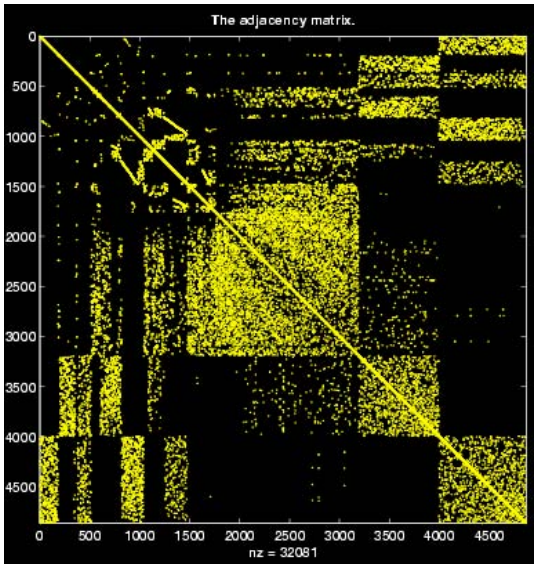

Figure 1.9: *"Footprint" of the exportet gOcad FEM matrix, indicating the spread-out and 'blocked' connectivity and thus the necessity of rearranging the matrix.*

Within the model domain the depth is set to 10m in the .inq file. The phase speed of a shallow wave in 10 meters is approximately $\sqrt{9.81 \cdot 10} = 9.9 m/sec$. The smallest element area is 3144 m^2,

Notation	Description
$v(x,y,z,t)$	fluid velocity, with Cartesian components (u,v,w)
$\overline{v}(x,y,t)$	is the vertical average of v
$\zeta(x,y,t)$	is the free surface elevation
$h(x,y)$	is the bathymetric depth
H(x,y,t)	is the total fluid depth , $H = h + \zeta$
$\rho(x,y,z,t)$	is the fluid density, $\rho_0$is a reference value
$T(x,y,z,t)$	is the fluid temperature
$S(x,y,z,t)$	is the fluid salinity
$q^2(x,y,z,t)/2$	is the turbulent kinetic energy
$l(x,y,z,t)$	is the turbulent mixing length
$N_m(x,y,z,t)$	is the vertical eddy viscosity
$N_h(x,y,z,t)$	is the vertical eddy diffusivity for heat and salt
$N_q(x,y,z,t)$	is the vertical eddy diffusivity for $q^2$and $q^2 l$
F_m,F_τ, F_S	are non-advective horizontal exchanges of momentum, heat and salt
g	is gravity
f	is the Coriolis vector, directed vertically with magnitude f
∇	is the gradient operator;$\nabla_{x,y}$ is its horizontal part
$\frac{d}{dt}$	is the material derivative, $\frac{\delta}{\delta t} + v \cdot \nabla$
(x,y)	are the cartesian coordinates
z	is the vertical coordinate, positive upward; $-h \leq z \leq \zeta$
t	time

Table 1.3: *Notations of the most used variables.*

which means that the smallest element edge is about 80m.

$$C = \frac{\sqrt{g \cdot H} dt}{dx} \tag{1.7}$$

For reliable computations, the Courant number C is tried to approach the order of 0.1. This means that the time step dt has to be adjusted and put into the .inq File.

Useful Matlab routines

The "Ocean Processes Numerical Modeling Laboratory" (http://www.opnml.unc.edu/) provides useful matlabroutines for handling output files from QUODDY. Other useful Matlab routines and programs can be downloaded at:

TRIANGLE: `http://www-2.cs.cmu.edu/~quake/triangle.html`

BATTRI: `www-nml.dartmouth.edu/Software/battri/`

VIZICQ4: `http://eta.marine.unc.edu/`

FDCONT1.2: `http://www.opnml.unc.edu/OPNML_Matlab/fdcont/FDCONT.html`

```
% ---- Landmask erstellen %%%%%
%peri=loadgrid('test');
%lndmake(peri,'test.bel');
%plotbnd(peri);
% ------
rrs = get(0,'screensize');
rrf = get(0,'defaultfigurepos');
m = min((rrs(3)-200)/rrf(3), (rrs(4)-200)/rrf(4));
defpos = [100,100,1400,1000];
set(0,'defaultfigurepos',defpos);
set(0,'ShowHiddenHandles','On')
nx=50;ny=nx;
peri=loadgrid('test');
bfd=genbfd(peri,[nx ny],0);

% --- Amplitudenwerte
data=read_s2c('tidal_zeta4.s2c');
% --- Residual velocities
data1=read_v2r('resid_vbar4.v2r');
[c,h]=fdcontour(bfd,data(:,2),0,1,0.05,0);
colorbar ('horiz');
plotbnd(peri);
axis off;
axis equal;

lndfill(peri,[1 1 1]*.75)
hbbrian_=plotbnd(peri);

ufe=data1(:,2);
vfe=data1(:,3);
hvec=fdvector(bfd,ufe,vfe,0.05,1,'cm/s');
```

Listing 1.2: *This is a simple example of how to visualize some of the Quoddy output files.*

1.4 References

Allen, P.A. & Bass, J.P. (1993): Sedimentology of the Upper Marine Molasse of the Rhône-Alp region, Eastern France: Implications for basin evolution. *Eclogae geologicae Helvetiae*, **86**: 121-171.

Allen, P.A., Crampton, S.L. & Sinclair, H.D. (1991): The inception and early evolution of the North Alpine Foreland Basin, Switzerland. *Basin Res.*, **3**: 143-163.

Allen, P.A., Homewood, P. & Wiliams, G.D. (1986): Foreland basins: an introduction. In: *Foreland Basins* (Eds P.A. Allen and P. Homewood), *IAS, Special Publications*, **8**, pp. 3-12. Blackwell Scientific Publications, Oxford.

Allen, P.A., Mange-Rajetzky, M., Matter, A. & Homewood, P. (1985): Dynamic palaeogeography of the open Burdigalian seaway, Swiss Molasse basin. *Eclogae geologicae Helvetiae*, **78**: 351-381.

Assemat, S. (1991): Récherche et analyse des tidalites dans la molasse marine marine miocène du domaine subalpin, dans la région de Frangy-Rumilly-Aix-les-Bains. *Mém. D.E.A. Univ. de Savoie, Chambéry.*

Beaumont, C. (1981): Foreland Basins. *Geophys. J. R. astr. Soc.*, **65**: 291-329.

Beaumont, C., Ellis, S., Hamilton, J. & Fullsack, P. (1996): Mechanical model for subduction-collision tectonics of Alpine-type compressional orogens. *Geology*, **24**: 675-678.

Berger, J.-P. (1992): Correlative chart of the European Oligocene and Miocene: Application to the Swiss Molasse Basin. *Eclogae geol. Helv.*, **85**: 573-609.

Berger, J.-P. (1996): Cartes paléogéographiques-palinspastiques du bassin molassique suisse (Oligocène inférieur - Miocène moyen). *Neues Jahrbuch für Geologie und Paläontologie, Abhandlungen*, **202**: 1-44.

Berger, J.-P., Reichenbacher, B., Becker, D., Grimm, M., Grimm, K., Picot, L., Storni,

A., Pirkenseer, C., Derer, C. & Schäfer, A. (in press, a): Palaeogeography of the Upper Rhine Graben (URG) and the Swiss Molasse Basin (SMB) from Eocene to Pliocene. *Int. J. Earth Sciences (Geol. Rundsch.)*.

Berger, J.-P., Reichenbacher, B., Becker, D., Grimm, M., Grimm, K., Picot, L., Storni, A., Pirkenseer, C. & Schäfer, A. (in press, b): Eocene-Pliocene time scale and stratigraphy of the Upper Rhine Graben (URG) and the Swiss Molasse Basin (SMB). *Int. J. Earth Sciences (Geol. Rundsch.)*.

Blumberg, A.F., Galperin, B. & O'Connor, D.J. (1992): Modeling vertical structure of open-channel flows. *ASCE, J. Hydraulic Engg.*, **118**: 1119-1134.

Büchi, U.P. & Hofmann, F. (1960): Die Sedimentationsverhältnisse zur Zeit der Muschelsandsteine und Grobkalke im Gebiet des Beckennordrandes der Oberen Meeresmolasse zwischen Aarau und Schaffhausen. *Bulletin der Vereinigung Schweizerischer Petroleum-Geologen und -Ingenieure*, **27**: 11-22.

Burbank, D.W. (1992): Causes of recent Himalayan uplift, deduced from the depositional patterns in the Ganges basin. *Nature*, **357**: 680-682.

Crumeyrolle, P., Rubinio, J.-L. & Clauzon, G. (1991): Miocene depositional sequences within a tectonically -controlled transgressive-regressive cycle. In: *Spec. Publ. internat. Assoc. Sedimentol.* (Eds D.I.M. McDonald), **12**, pp. 373-390.

Decker, K. & Peresson, H. (1996): Tertiary kinematics in the Alpine-Carpathian-Panonian System; links between thrusting, transform faulting and crustal extension. In: *Oil and gas in Alpidic thrust belts and basins of Central an Eastern Europe. EAPG Spec. Publ.* (Eds G. Wessely and W. Liebl), **9**, pp. 69-77.

Demarcq, G. & Perriaux, J. (1984): Neogene. In: *Synthèse géologique du Sud-Est de la France: Stratigraphie et paléogeographie* (Eds D.-P.e. al.), **Bureau de Récherches Géologiques et Minières, Mémoire 125**, pp. 469-519.

Dercourt, J., Ricou, L.E. & Vrielynck, B. (1993): *Atlas Tethys Palaeoenvironmental Maps.* Gauthier-Villars, Paris, 307 pp.

Dewey, J.F., Pitman, W.C.I., Ryan, W.B.F. & Bonnin, J. (1973): Plate tectonics and the evolution of the Alpine System. *Geol. Soc. Amer. Bull.*, **84**: 3137-80.

Dickinson, W.R. (1974): Plate tectonics and sedimentation. In: *Tectonics and Sedimentation* (Eds W.R. Dickinson), **22**, pp. 1-27. Society of Economic Palaeontologists and Mineralogists Special Publication.

Diem, B. (1985): Analytical method for estimating palaeowave climate and water depth from wave ripple marks. *Sedimentology*, **32**: 705-720.

Doppler, G. (1989): Zur Stratigraphie der nördlichen Vorlandmolasse in Bayrisch-Schwaben. *Geologica Bavarica*, **94**: 83-133.

Faupl, P. & Roetzel, R. (1987): Gezeitenbeeinflußte Ablagerungen der Innviertler Gruppe (Ottnangien) in der oberösterreichischen Molassezone. *Jahrbuch der Geologischen Bundesanstalt Wien*, **130**: 415-447.

Faupl, P. & Roetzel, R. (1990): Die Phosphoritsande und Fossilreichen Grobsande; Gezeitenbeeinflusste Ablagerungen der Innviertler Gruppe (Ottnangien) in der oberoesterreichischen Molassezone. *Jahrbuch der Geologischen Bundesanstalt Wien*, **132**: 157-180.

Freudenberger, W. & Schwerd, K. (1996): *Erläuterungen zur Geologischen Karte von Bayern 1:500000.* Bayerisches Geologisches Landesamt, München.

Frisch, W., Dunkl, I. & Kuhlemann, J. (2000): Post-collisional orogen-parallel large-scale extension in the Eastern Alps. *Tectonophysics*, **327**: 239-265.

Frisch, W., Kuhlemann, J., Dunkl, I. & Brügel, A. (1998): Palinspastic reconstruction and topographic evolution of the Eastern Alps during Late Tertiary tectonic extrusion. *Tectonophysics*, **297**: 1-15.

Galperin, B., Kantha, L.H., Hassid, S. & Rosati, A. (1988): A quasi-equilibrium turbulent energy model for geophysical flows. *Journal of Atmospheric Science*, **45**: 55-62.

Gill, A.E. (1982): *Atmosphere-Ocean Dynamics.* Academic Press, 599-603 pp.

Haq, B.U., Hardenbol, J. & Vail, P.R. (1988): Mesozoic and Cenozoic chronostratigraphy and cycles of sea-level change. In: *Sea-level changes: An integrated approach* (Eds C.K. Wilgus et al.), *SEPM, Special Publications*, **42**, pp. 71-108. SEPM (Society of Economic Paleontologists and Mineralogists), Tulsa.

Hay, W.W., Wold, C.N. & Herzog, J.M. (1992): Preliminary mass-balanced 3-D reconstructions of the Alps and surrounding areas during the Miocene. In: *Computer graphics in geology, three-dimensional computer graphics in modeling geologic structures and simulating geologic processes* (Eds R. Pflug and J.W. Harbaugh), **42**, pp. 99-100. Lecture Notes in Earth Sciences.

Heller, P.L., Angevine, C.I. & Wilson, N.S. (1988): Two phase stratigraphic model of foreland basin sequences. *Geology*, **16**: 501-504.

Hofmann, F. (1976): Überblick über die geologische Entwicklungsgeschichte der Region Schaffhausen seit dem Ende der Jurazeit. *Bull. Ver. Schweizer Petrol.-Geol. u. -Ing.*, **42**: 1-16.

Homewood, P. (1981): Faciès et environnements de dépôt de la Molasse de Fribourg. *Eclogae geologicae Helvetiae*, **74**: 29-36.

Homewood, P. & Allen, P. (1981): Wave-, tide-, and current-controlled sandbodies of Miocene molasse, Western Switzerland. *American Association of Petroleum Geologists, Bulletin*, **65**: 2534-2545.

Homewood, P., Allen, P.A. & Williams, G.D. (1986): Dynamics of the Molasse Basin of western Switzerland. In: *Foreland Basins* (Eds P.A. Allen and P. Homewood), *IAS, Special Publications*, **8**, pp. 199-217. Blackwell Scientific Publications, Oxford.

Homewood, P., Allen, P.A. & Yang, C.S. (1985): Palaeotidal range estimates from the Miocene Molasse. In: *Abstr. 6th int. Ass. Sediment. Reg. Mtg.*, pp. 200-201, Lleida.

Hülsemann, J. (1955): Großrippeln und Schrägschichtungs-Gefüge im Nordsee Watt und in der Molasse. *Senck. leth.*, **36**: 359-388.

Jin, J., Aigner, T., Luterbacher, H.P., Bachmann, G.H. & Müller, M. (1995): Sequence stratigraphy and depositional history in the south-eastern German Molasse Basin. *Marine and Petroleum Geology*, **12**: 929 - 940.

Jordan, T.E. & Flemings, P.B. (1991): Large-Scale Stratigraphic Architecture, Eustatic Variation, and Unsteady Tectonism: A Theoretical Evaluation. *Journal of Geophysical Research*, **96**: 6681-6699.

Kapountek, J., Kröll, A., Papp, A. & Turnovsky, K. (1965): Die Verbreitung von Oligozän und Unter- und Mittelmiozän in Niederösterreich. *Erdöl-Erdgas-Zeitschrift*, **81**: 109-115.

Keller, B. (1989): *Fazies und Stratigraphie der Oberen Meeresmolasse (Unteres Miozän) zwischen Napf und Bodensee*. Unpubl. PhD Thesis, Universität Bern, Bern, 402 p pp.

Kempf, O. (1998): *Magnetostratigraphy and facies evolution of the Lower Freshwater Molasse (USM) of eastern Switzerland*, Berne, 138 pp.

Kempf, O. & Matter, A. (1999): Magnetostratigraphy and depositional history of the Upper Freshwater Molasse (OSM) of eastern Switzerland. *Eclogae geol. Helv.*, **92**: 97-103.

Kempf, O., Matter, A., Burbank, D.W. & Mange, M. (1999): Depositional and structural evolution of a foreland basin margin in a magnetostratigraphic framework: the eastern Swiss Molasse basin. *International Journal of Earth Sciences*, **88**: 253-275.

Krenmayr, H.G. & Roetzel, R. (Eds) (1996): *Oligozäne und miozäne Becken- und Gezeitensedimente in der Molassezone Oberösterreichs, Exkursionsführer Sediment '96, Exkursion B2*, **33**. Geologische Bundesanstalt, Wien, 17 Abb., 43 pp.

Kuhlemann, J. (2000): Post-collisional sediment budget of circum-Alpine basins (Central Europe). *Memoire di Scienze Geologiche Padova*, **52**: 1-91.

Kuhlemann, J., Frisch, W., Dunkl, I. & Székely, B. (2001): Quantifying tectonic versus erosive denudation by the sediment budget: the Miocene core complex of the Alps. *Tectonophysics*, **330**: 1-23.

Kuhlemann, J., Frisch, W., Dunkl, I., Székely, B. & Spiegel, C. (2001): Miocene shifts of drainage divide in the Alps and their foreland basin. *Z. Geomorph. N. F.*, **45**: 239-265.

Kuhlemann, J. & Kempf, O. (2002): Post-Eocene evolution of the North Alpine Foreland Basin and its response Alpine tectonics. *Sedimentary Geology*, **152**: 45-78.

Kühni, A. & Pfiffner, O.A. (2001): Drainage patterns and tectonic forcing: a model study for the Swiss Alps. *Basin Research*, **13**: 169-197.

Lemcke, K. (1973): Zur nachpermischen Geschichte des nördlichen Alpenvorlandes. *Geologica Bavarica*, **69**: 5-48.

Lemcke, K. (1988): *Geologie von Bayern. - I. Teil: Das bayerische Alpenvorland vor der Eiszeit*, **I**. E. Schweizerbart'sche Verlagsbuchhandlung, Stuttgart, 175 p pp.

Lynch, D.R., Ip, J.T.C., Naimie, C.E. & Werner, F.E. (1996): Comprehensive Coastal Circulation Model with Application to the Gulf of Maine. *Continental Shelf Research*, **12**: 37-64.

Lynch, D.R. & Werner, F.E. (1987): Three-Dimensional Hydrodynamics on Finite Elements. Part I: Linearized Harmonic Model. *International Journal for Numerical Methods in Fluids*, **7**: 871-909.

Lynch, D.R. & Werner, F.E. (1991): Three-Dimensional Hydrodynamics on Finite Elements. Part II: Non-linear Time-stepping Model. *International Journal for Numerical Methods in Fluids*, **12**: 507-533.

Márton, E., Kuhlemann, J., Frisch, W. & Dunkl, I. (2000): Miocene rotations in the Eastern Alps - paleomagnetic results from intramontane basin sediments. *Tectonophysics*, **323**: 163-182.

Matter, A., Homewood, P., Caron, C., Rigassi, D., Stuijvenberg, J.v., Weidmann, M. & Winkler, W. (1980): Flysch and Molasse of western and central Switzerland (Excursion No. 5). In: *Geology of Switzerland, a guide-book* (Eds R. Trümpy), *Schweizerische Geologische Kommission*, **Part B**, pp. 261-293. Wepf, Basel.

Mellor, G.L. & Yamada, T. (1982): Development of a turbulence closure model for geophysical fluid problems. *Reviews of Geophysics Space Physics*, **20**: 851-875.

Pfiffner, O.A. (1986): Evolution of the north Alpine foreland basin in the Central Alps. In: *Foreland Basins* (Eds P.A. Allen and P. Homewood), *IAS, Special Publications*, **8**, pp. 219-228. Blackwell Scientific Publications, Oxford.

Quinland, G.M. & Beaumont, C. (1984): Appalachian thrusting, lithospheric flexure and Paleozoic stratigraphy of the eastern Interior of North America. *Canadian Journal of Earth Science*, **21**: 973-996.

Ratschbacher, L., Frisch, W., Linzer, H.G. & Merle, O. (1991): Lateral extrusion in the Eastern Alps. Part 2: Structural analysis. *Tectonics*, **10**: 257-271.

Reichenbacher, B., Böttcher, R., Bracher, H., Doppler, G., Engelhardt, W.v., Gregor, H.-J., Heissig, K., Heizmann, E.P.J., Hofmann, F., Kälin, D., Lemcke, K., Luterbacher, H., Martini, E., Pfeil, F.H., Reiff, W., Schreiner, A. & Steininger, F.F. (1998): Graupensandrinne - Ries - Impakt: zur Stratigraphie der Grimmelfinger Schichten,Kirchberger Schichten und Oberen Süßwassermolasse: Kommentar zur 'Revision der Stratigraphie der süddeutschen Brackwassermolasse'. *Z. dt. geol. Ges.*, **149**: 127-161.

Reichenbacher, B., Doppler, G., Schreiner, A., Böttcher, R., Heissig, K. & Heizmann, E.P.J. (1998): Lagerungsverhältnisse von Grimmelfinger Schichten und Kirchberger Schichten: Kommentar zur 'Revision der Stratigraphie der süddeutschen Brackwassermolasse'. *Zeitschrift der deutschen geologischen Gesellschaft*, **149**: 321-326.

Rögl, F. (1998): Palaeogeographic Considerations for Mediterranean and Paratethys Seaways (Oligocene to Miocene). *Ann. Naturhist. Mus. Wien*, **99A**: 279-310.

Salvermoser, S. (1999): Zur Sedimentologie gezeitenbeeinflusster Sande in der Oberen Meeresmolasse und Süssbrackwassermolasse (Ottnangium) von Niederbayern und Oberösterreich. *Münchner Geologische Hefte (A)*, **26**: 1-179.

Schaad, W., Keller, B. & Matter, A. (1992): Die Obere Meeresmolasse (OMM) am Pfänder: Beispiel eines Gilbert-Deltakomplexes. *Eclogae geologicae Helvetiae*, **85**: 145-168.

Schlunegger, F. (1997): Controls of erosional denudation on the stratigraphy of foreland basins and on strain partitioning in the orogen: the Alps and the Molasse basin. *GAEA Heidelbergensis*, **3**: 305-306.

Schlunegger, F. (1999): Controls of surface erosion on the evolution of the Alps: constraints from the strati-

graphies of the adjacent foreland basins. *International Journal of Earth Sciences*, **88**: 285-304.

Schlunegger, F., Leu, W. & Matter, A. (1997): Sedimentary sequences, Seismic Facies, Subsidence Analysis, and Evolution of the Burdigalian Upper Marine Molasse Group (OMM), Central Switzerland. *American Association of Petroleum Geologists, Bulletin*, **81**: 1185-1207.

Schlunegger, F., Matter, A., Burbank, D.W. & Klaper, E.M. (1997): Magnetostratigraphic constraints on relationships between evolution of the central Swiss Molasse basin and Alpine orogenic events. *Geological Society of America, Bulletin*, **109**: 225-241.

Schlunegger, F., Melzer, J. & Tucker, G. (2001): Climate, exposed source rock lithologies, crustal uplift and surface erosion: a theoretical analysis calibrated with data from the Alps/North Alpine Foreland Basin system. *International Journal of Earth Sciences*, **90**: 484-499.

Schlunegger, F. & Pfiffner, O.A. (2001): The sedimentary response of the North Alpine Foreland Basin to changes in erosional processes in the Alps (Excursion P9). In: *IAS 2001, 21st Meeting* (Eds H. Funk and U.G. Wortmann), *Excursion Guides*, pp. 85-99. IAS (International Association of Sedimentologists), Davos.

Schlunegger, F. & Willett, S.D. (1999): Spatial and temporal variations in exhumation of the central Swiss Alps and implications for exhumation mechanisms. In: *Exhumation Processes: Normal faulting, ductile Flow and Erosion* (Eds M.T. Brandon and S.D. Willett), **154**, pp. 157-179. Geol. Soc. London Spec. Publ.

Schmid, S.M., Pfiffner, O.A., Froitzheim, N., Schönborn, G. & Kissling, E. (1996): Geophysical-geological transect and tectonic evolution of the Swiss-Italian Alps. *Tectonics*, **15**: 1036-1064.

Schreiner, A. (1966): Zur Stratigraphie der Oberen Meeresmolasse zwischen der Oberen Donau und dem Überlinger See (Baden-Württemberg). *Jber. u. Mitt. oberrh. geol. Ver.*, **48**: 91-104.

Seiler, U. (1989): *An investigation to the Tides of the World Ocean and their Instantaneous Angular Momentum Budgets.* PhD, Univ. of Hamburg, Germany, 101 pp.

Seiler, U. (1991): Periodic changes of the angular momentum budget due to the tides of the world ocean. *Journal of Geophysical Research*, **96**: 10,287-10,300.

Sinclair, H.D. (1997): Tectonostratigraphic model for underfilled peripheral foreland basins: An Alpine perspective. *GSA Bull.*, **109**: 324-346.

Sinclair, H.D. & Allen, P.A. (1992): Vertical versus horizontal motions in the Alpine orogenic wedge: stratigraphic response in the foreland basin. *Basin Res.*, **4**: 215-233.

Sinclair, H.D., Coakley, B.J., Allen, P.A. & Watts, A.B. (1991): Simulation of foreland basin stratigraphy using a diffusion model of mountain belt uplift and erosion: an example from the central Alps, Switzerland. *Tectonics*, **10**: 599-620.

Sissingh, W. (1997): Tectonostratigraphy of the North Alpine Foreland Basin: correlation of Tertiary depositional cycles and orogenic phases. *Tectonophysics*, **282**: 223-256.

Sissingh, W. (1998): Comparative Tertiary stratigraphy of the Rhine Graben, Bresse Graben and Molasse Basin: correlation of Alpine foreland events. *Tectonophysics*, **300**: 249-284.

Sissingh, W. (2001): Tectonostratigraphy of the West Alpine Foreland: correlation of Tertiary sedimentary sequences, changes in eustatic sea-level and stress regimes. *Tectonophysics*, **333**: 361-400.

Smagorinsky, J. (1963): General circulation experiments with the primitive equations I. The basic experiment. *Monthly Weather Review*, **91**.

Spiegel, C., Kuhlemann, J., Dunkl, I., Frisch, W., Eynatten, H.v. & Balogh, K. (2000): The erosion history of the Central Alps: Evidence from zircon fission track data of the foreland basin sediments. *Terra Nova*, **12**: 163-170.

Steck, A. & Hunziker, J. (1994): The Teriary structural and thermal evolution of the central Alps - compressional and extensional strucutres in an orogenic belt. *Tectonophysics*, **238**: 229-254.

Sztanó, O. (1994): *The tide-influences Pétervására sandstone, early Miocene, Northern Hungary: Sedimentology, Palaeogeography and basin development.* Phd., Universiteit Utrecht, Utrecht, 155 pp.

Sztanó, O. (1995): Palaeogeographic significance of tidal deposits; an example from an early Miocene Paratethys embayment, northern Hungary. *Palaeogeography, Palaeoclimatology, Palaeoecology*, **113**: 173-187.

Sztanó, O. & de Boer, P.L. (1995): Basin dimensions and morphology as controls on amplification of tidal motions (the early Miocene North Hungarian Bay). *Sedimentology*, **42**: 665-682.

Tankard, A.J. (1986): On the depositional response to thrusting and lithospheric flexure: examples from the Appalachian and Rocky Mountain Basins. In: *Foreland Basins* (Eds P.A. Allen and P. Homewood), *IAS, Special Publications*, **8**, pp. 369-394. Blackwell Scientific Publications, Oxford.

Tessier, B. & Gigot, P. (1989): A vertical record of different tidal cyclicities: an example from the Miocene Molasse of Digne (Haute Provence, France). *Sedimentology*, **36**: 767-776.

von Eynatten, H., Schlunegger, F., Graup, R. & Wijbrans, J.R. (1999): Exhumation of the Central Alps: evidence from 40Ar/39Ar laserprobe dating of detrital white micas from the Swiss Molasse Basin. *Terra Nova*, **11**: 284-289.

Zweigel, J., Aigner, T. & Luterbacher, H. (1998): Eustatic versus tectonic controls on Alpine foreland basin fill: sequence stratigraphy and subsidence analysis in the SE German Molasse. In: *Cenozoic Foreland Basins of Western Europe* (Eds A. Mascle, C. Puigdefàbregas, H.P. Luterbacher and M. Fernàndez), *Geological Society Special Publication*, **134**, pp. 299-323, London.

Zweigel, J. & Zweigel, P. (1998): DISCUSSION: Plan-view curvatures of foreland basins and its implications for the palaeostrength of the lithosphere underlying the Western Alps. *Basin Research*, **10**: 271-278.

Chapter 2

Global M_2 Simulation for the Early Miocene delivering border conditions for a forthcoming tidal simulation of the Circum-Mediterranean realm

2.1 Abstract

Abstract: Tidal waves show a high sensitivity to the geometry and depth of ocean basins. Hence ancient marginal seas are expected to have experienced rapid changes of their tidal environment in earth history. The aim of this study is to compute a global M_2 tidal model, which is based on a global reconstruction of paleogeography and paleobathymetry for the Early Miocene. The model is used to identify areas with divergent amplitudes relative to todays M_2 oscillation system. The Early Miocene global M_2 simulation reflects changes in tidal amplitudes in the major ocean basins as well as in open seaways to the Western and Eastern Mediterranean Sea and Panama. As the semidiurnal M_2 tide shows a near resonant behaviour in the Southern Atlantic, small changes in ocean basin configuration changed the amplitudes in a significant amount over a large area. Highly divergent amplitudes have been observed in the wide and deep seaway from the Atlantic to the Western Tethys as well as in the area of the shallow connection of the Eastern Tethys to the Indian Ocean. Also highly divergent amplitudes are generated at the open Isthmus of Panama. In the Pacific Ocean only minor changes can be deduced from the simulation.

Zusammenfassung: Die Ausbreitung von Gezeitenwellen zeigt eine hohe Empfindlichkeit bezüglich der Geometrie und Tiefenverteilung der ozeanischen Becken. Es ist daher zu erwarten, dass im Laufe der Erdgeschichte die randlichen Schelf und Flachwasserbereiche einer starken Veränderung des Gezeitenregimes unterlagen. Das Ziel dieser Studie ist es, ein globales M_2 Gezeitenmodell zu berechnen, das auf einer globalen Rekonstruktion der Paläogeographie und Paläobathymetrie des frühen Miozäns beruht. Mit Hilfe dieses Modells werden Gebiete, in denen sich die Amplituden von denen des heutigen M_2-Oszillationsmodells unterscheiden, identifiziert. Die Simulation der frühmiozänen M_2-Gezeiten offenbart änderungen in den großen Ozeanbecken sowie in den geöffneten Seewegen im Bereich des Westlichen und östlichen Mittelmeers und im Seeweg von Panama. Da sich die halbtägige M_2-Gezeit im Südatlantik nahezu im Resonanzzustand befindet, haben kleine änderungen in der Konfiguration des Ozeanbeckens bereits erhebliche Auswirkungen auf die Amplituden über einen größeren Bereich. Sehr unterschiedliche Amplituden wurden in den Seewegen zwischen Atlantik und der westlichen Tethys, sowie im Bereich der flachen Verbindung zwischen der östlichen Tethys und dem Indischen Ozean beobachtet. Gleichermaßen wurden sehr unterschiedliche Amplituden im Bereich des geöffneten Isthmus von Panama simuliert.

Im Pazifik können nur geringere Veränderungen im Rahmen der Simulationsergebnisse abgeleitet werden.

2.2 Introduction

The purpose of this study is to evaluate the response of the global M_2 oscillation system to the global palaeogeography and palaeobathymetry at 18 Ma. In more detail we want to examine the palaeotides at the entrance of the Indian Seaway and the transition from the Atlantic to the Western Mediterranean. This should provide for a better understanding of the tidal dynamics in the Mediterranean relam due to reconstructed connections to the open marine Atlantic and Pacific Ocean. This study should shed light on the well-known tidal deposits (e.g. Allen 1981, Allen 1984, Homewood & Allen 1981, Homewood *et al.* 1986, Allen *et al.* 1985, Keller 1989, Salvermoser 1999, Faupl & Roetzel 1987, Faupl & Roetzel 1990, Sztanó 1994, Sztanó & de Boer 1995) of the Burdigalian seaway linking the Mediterranean realm with the Paratethys indicating meso- to macrotidal conditions, which remained largely unexplained.
The generated information should be used for a forthcoming tidal simulation of the circum-Mediterranean realm.

2.3 Methods

2.3.1 Palaeogeography

In order to establish proper boundary conditions for the phase and amplitude of the global M_2 tidal model, palaeogeographic and bathymetric conditions at 18 Ma had to be restored.

As a base for the reconstruction of ocean basins and continental positions mainly the Cenozoic basemap of Scotese *et al.* (1988) has been used. This map is mainly based on palaeomagnetic and palaeontologic evidence and reflects widely the existing palaeogeographic knowledge of continent distribution. For correct tidal modeling the width and depth of seaways is of crucial importance, as they are gateways for currents and sediments. However their reconstruction is difficult, as the width of ancient seaways was mostly less than 1 degree, which is less than the numerical resolution of the underlying grid. As an approximation for the paleobathymetry we use the the ETOPO5 data set of the National Geophysical Data Center in Boulder Colorado (NGDC 1988). Areas without palaeobathymetric information, which appeared due to continental realignments, were filled with approximated data based on surrounding depth information. According to HAQ *et al.* (1988) the eustatic sea-level was approximately 100 m higher than today. While the resulting changes in palaeogeography seldom exceed the resolution of 1° in the model, this had to be considered where necessary.

2.3.2 The numerical tidal model

The numerical simulation was performed with the unconstrained barotropic tidal model described by Seiler (1989), which is based on the vertically integrated hydrodynamical equations of motions, the equation of continuity, and includes secondary effects arising from terrestrial tides as well as from loading and self-attraction of the water column. The numerical model is forced exclusively with the potential of partial tides, thus, apart from coast lines and depth distributions, no empirical data had to be incorporated. The spatial resolution is a constant of 1° in longitude and latitude, the time step used here is 1.5 minutes. The tidal model has been successfully applied in numerous studies, e.g., determiniation of the present-day oceanic angular momentum budget (Seiler 1991) and changes in the tidal oscillation system since the last glacial maximum (Thomas & Sündermann 1999).

2.4 Global Palaeogeography of the early Miocene 18 Ma

The palaeogeographic reconstruction of coast lines and ocean basins is based on two different types of data: geophysical measurements and geological/palaeontological indicators. The evolution of the deep ocean basins themselves can be traced using the age structure of the underlying oceanic crust with its sea-floor spreading isochrones (Sclater *et al.* 1981, Larson *et al.* 1985, Scotese *et al.* 1988). The original shape of the epicontinental seas on the other hand, can be deduced from the extent of marine sediments on the adjacent ocean margins and continents. Such reconstructions from Scotese *et al.* (1979) and Ziegler *et al.* (1982) are the base for the maps presented by Scotese *et al.* (1988).

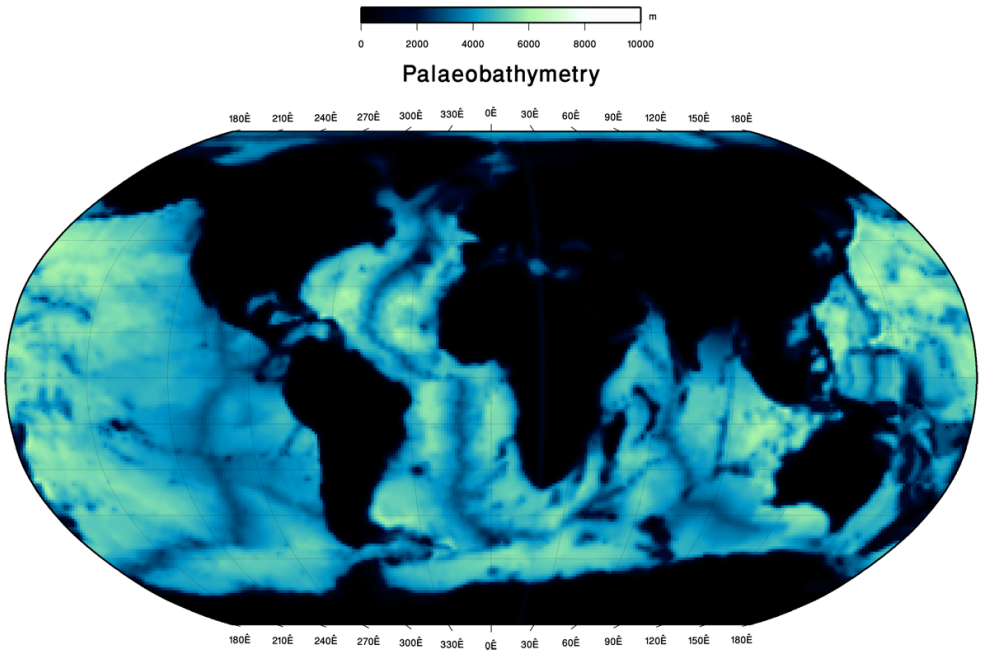

Figure 2.1: *Map of the global bathymetry during the Early Miocene. Bathymetry data are modified from ETOPO5. Due to continental realignments, areas without palaeobathymetric information were filled with approximated data from surrounding depth information.*

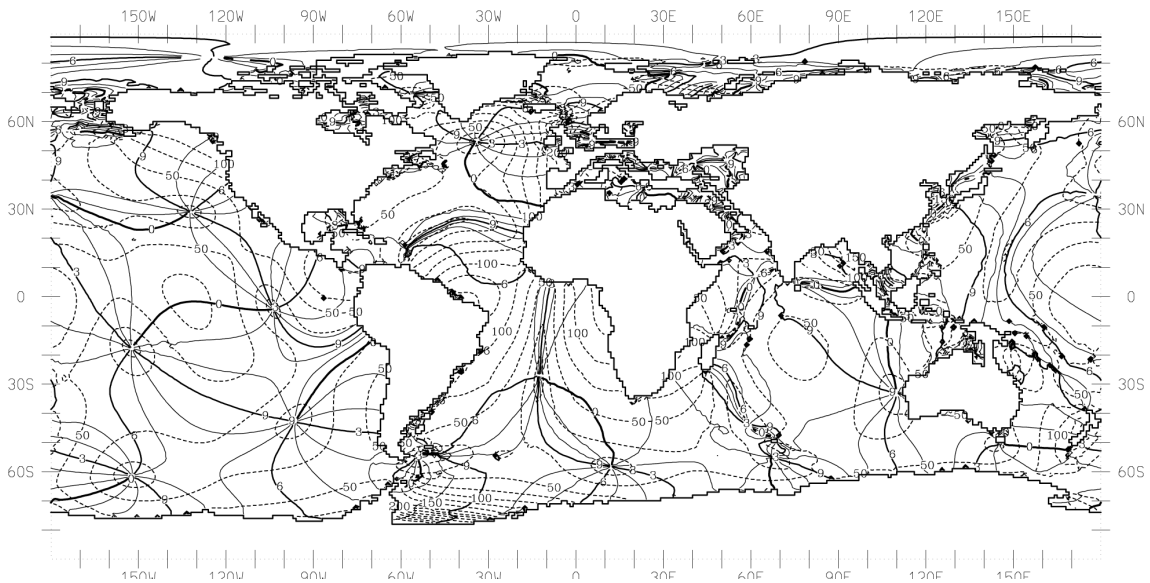

Figure 2.2: *Simulated global oscillation system of the dominant semi-diurnal M_2 -tide of the Early Miocene (18 Ma) with a computation grid of 1° latitude and longitude. Co-tidal lines are shown as full lines with respect to Greenwich Mean Time, co-range lines as broken lines (cm).*

To reflect more accurately the palaeogeography of the Tethys, this area was reconstructed using the palaeoenvironmental atlas of the Tethys Ocean by Dercourt *et al.* (1993) and maps of Rögl (1999). Faunal relations provide additional important information on the gateways between marine basins.

Compared to the overall changes during earth history, the land-sea distribution during the last 18 million years was not significantly different from todays. However there were some small, but important variations in the distribution of oceanic gateways such as the Panama Strait between the Pacific and Atlantic Ocean and the gateway between the Pacific and Indian Ocean (Collins *et al.* 1996, Tsuchi 1997). The impact of the opening or closure of these gateways has been demonstrated by regional compilations on the climatic record of marine sequences. It has been shown that these palaeogeographic changes profoundly influenced the mechanics of the oceanic conveyor belts and induced significant climatic changes during the Neogene (Mikolajewicz *et al.* 1993).

Many studies (see Bice *et al.* 2000) have attempted to quantify the potential influences of changes in plate configuration on climate trends (air mass changes with mountain uplift, poleward heat transport, global ocean thermohaline circulation). The timing of closure of the two major Pacific ocean gateways, the Indonesian and Central American Seaways, have been discussed with reference to climatically warm periods which apparently occurred as response to these closures (Tsuchi 1997).

In general the following gateways were already opened or about to close 18 Ma ago:

- The Indonesian seaway closed, e.g. Gaspari & Kennett (1993), Kennett *et al.* (1985), Tsuchi (1997).
- The Tasman Sea was open for deep water since 40 Ma, e.g. Kennett *et al.* (1985).
- The Drake Passage was open for deep water since 22 Ma, e.g. Kennett *et al.* (1985).
- The Panama/Central American Seaways was open for deep water until 4.5 Ma, e.g. Haug & Tiedemann (1998).
- The Denmark Strait was open for shallow water, but not yet for deep water, e.g. Kennett *et al.* (1985).
- The Gibraltar Strait was wider and deeper, e.g. Blanc (2002).
- The Indic seaway was linking the Indian Ocean and the eastern Paratethys realm, e.g. Rögl & Steininger (1984)

Below we will discuss in more detail the aspects of the evolution of these important links between the marine basins during the Miocene.

2.4.1 North/South Atlantic and North European seaway

The shape of the Atlantic Ocean by 18 Ma is based on plate reconstructions of Sclater *et al.* (1977, 1981), whereas palaeobathymetry is derived from Owen *et al.* (1979). During Cenozoic times the Norwegian-Greenland Sea opened and provided a shallow gateway to the Polar. By 18 Ma, there was no deep-water exchange between the North Atlantic and the Norwegian-Greenland Sea, since the Denmark Strait NW of Iceland was still at shallow depth (Kennett *et al.* 1985).

2.4.2 Isthmus of Gibraltar

The Strait of Gibraltar is a Pliocene structure (Comas *et al.* 1999), formed after the Messinian Salinity Crisis (5.5 Ma; Krijgsman *et al.* 1999). In the Early Miocene, the Mediterranean was connected to the Atlantic Ocean by the shallow Iberian and the Rifian corridor in the North of Morocco (Esteban *et al.* 1996, Martín *et al.* 2001). By 18 Ma, the gateway between Morocco and Iberia was fairly wide (Dercourt 1993).

2.4.3 Major changes in the Mediterranean Tethys, Eastern Tethys and Paratethys area (see Fig. 2.3)

During the Tertiary a change in relative African-European plate motions occurred during which the earlier counter-clockwise rotation and transcurrent motion became a mainly convergent motion (Dewey *et al.* 1973, Hsü 1971, Mckenzie 1970, Neev 1975). By Early Miocene times, this collision broke up the Tethys oceanic realm which had existed since the early Mesozoic and

resulted in the T 9-Tethys phase of Dewey *et al.* (1973) and Stanley (1986). This phase is characterized by the formation of several relatively small basins and troughs in the circum-Tethys realm during the Neogene. These basins and troughs are the Mediterranean and Paratethys seas, the Mesopotamian Basin, and the oceanic trough, which stretched towards the Indo-Pacific Ocean.

In the western part of the Mediterranean Tethys, counter-clockwise rotation of the Corsica and Sardinia blocks and clockwise rotation of the Balearic Islands were largely terminated at 18 Ma, shaping the Algero-Provençal basin (Gelabert *et al.* 2002). The Gibraltar arc migrated westward towards the Atlantic Ocean and the Alboran basin started to form.

In Early Burdigalian times, the marine connnection in the Alpine Foredeep established a Mediterranean-Paratethys seaway, known as the Burdigalian Seaway. This marine seaway connected the Eastern Paratethys region with the Western Mediterranean Sea across Hungaria, Austria, Bavaria, Switzerland, and the Rhône Valley. The Slovenian corridor between the Mediterranean and the Central Paratethys was closed by 18 Ma. The extent of the marine realm in the area of the later Pannonian Basin rapidly decreased (Rögl 1999). The Mediterranean Tethys and the Eastern Tethys were still connected by fairly narrow gateways open for shallow subtropical marine circulation.

The Great Caucasus started to emerge to the North of the Black Sea Basin and Caspian Basin, which were still connected. The Black Sea and Caspian basin as part of the Paratethys marine domain were connected to the Eastern Mediterranean Sea by a corridor toward the Sivas Basin (Dercourt *et al.* 1993).

By 18 Ma tropical to subtropical climate conditions reestablished in the Circum-Mediterranean realm, faciliated by the equatorial Indo-Pacific-Atlantic current system (Hochuli 1978).

2.4.4 Indian-Ocean seaway

In the late Oligocene a marine connection established between the Indo-Pacific and the Paratethys (Rögl 1999). A wide marine realm between the Afro-Arabian and Eurasian-Turkish plate systems with carbonate platforms on either side provided access from the Indo-Pacific ocean to the Eastern Mediterranean and the Eastern and Central Paratethys (Steininger & Rögl 1984). This paleogeography is consistent with the configuration resulting from plate tectonic reconstructions in this area (Dewey *et al.* 1973, p. 3169, fig. 18; Hsü 1971).

In the Early Miocene, the Paratethys area is characterized by a uniform, widespread faunal renewal (Steininger *et al.* 1975). Tropical-subtropical faunal elements (upper NN2 Zone) continued to migrate to the Mediterranean and Paratethys (Rögl 1999). Faunal assamblages indicate a connection between the Paratethys and the Indo-Pacific Ocean, concurrent with a worldwide transgressive phase. The seaway can be traced from the Persian Gulf and western Iran, including the Quom Basin, across Iraq and the Mesopotamian trough to eastern Turkey and across southern Russia (Crimea area) into the Paratethys. Moreover, it can be traced by fossiliferous sediments across the Mesopotamian Basin and northwest Syria into the Levantine Sea (Eastern Mediterranean), on the basis of a transgressive phase into Red Sea rift zone (Dercourt *et al.* 1993).
The Zagros region emerged (Reyre & Mohafez 1970), possibly shortly after 18 Ma. The Arabian platform, covered by shallow water carbonates, was progressively overthrusted by the Zagros fold belt.

2.4.5 Indian Ocean and Indonesian Seaway

The present Indian Ocean evolved since the Early Cretaceous when Gondwana dispersed into the continental fragments of Africa, India, Antarctica and Australia (Ogg *et al.* 1992). Since the Indian Ocean Plate was subducted northward underneath the Eurasian Plate, the Sunda Arc extended eastward as far as Flores in the Early Miocene (Hamilton 1979). The Middle to Late Miocene circulation patterns within the Pacific Ocean and between the tropical Pacific and Indian Oceans were strongly changed by the shallowing and closure of the Indonesian

Seaway (Kennett *et al.* 1985, Gasperi & Kennett 1993). Tectonic reconstructions and biogeographic data indicate that the Neogene Indonesian Seaway was effectively restricted during the early Middle Miocene (17-15 Ma) and completely severed by about 6 Ma, suppressing further interchange between surface water of the tropical Pacific and Indian Oceans (Nishimura & Supaka 1997).

2.4.6 Red Sea rifting started in the early Miocene (ca. 25 -20 Ma

The late Burdigalian-early Langhian marine cycle represents the largest Neogene Mediterranean transgression. It is coeval with a very intensive phase of rifting and the most uniform marine faunal association in the Red Sea. Restriction and temporal isolation of the Red Sea marks the beginning of a new cycle of sedimentation, that varies between complete marine invasion and complete desiccation of the Red Sea basin (Rogers 1993).

2.4.7 The Tasman Sea and Australia

The Tasman Sea was opened between 90 Ma and 53 Ma separating the Lord Howe Rise and Western New Zealand from Australia (Weissel & Hayes 1972). The Tasmanian Seaway and the Drake Passage opened to deep water during the Cenozoic, eventually leading to the establishment of circum-Antarctic currents, which prevented tropical heat from reaching Antarctica and led to the development of Antarctic ice sheets (Kennett & Shackleton 1976, Lawver *et al.* 1992 and Latimer 2002).

The history of separation of Australia from Antarctica is well known (Weissel & Hayes 1972) and started around 55 Ma. 20 Ma ago, the Australian continent was still situated more than 1250 km farther to the south and a wide opening between the Indian and Pacific oceans existed (Linthout *et al.* 1997). The Australian margin and its northern extensions in New-Guinea, Irian Jaya and East Sulawesi constituted a very extensive carbonate shelf (Dercourt *et al.* 1993).

2.4.8 Panama Strait

By 18 Ma the Central American Seaway is still open for deep-water circulation, possibly in more than one sill. Shoaling of the Central American Seaway is thought to have been gradual , starting by 13 Ma and ending by about 1.9 Ma (Haug & Thiedemann 1998) .

2.4.9 Bering Strait

It has been proposed that the Bering Strait was closed 18 Ma ago and opened during the Late Miocene or earliest Pliocene epochs. MAarincovich & Gladenkov (1999) suggested an age of 4.8 - 5.5 Ma for the first opening since the middle Cretaceous, when the Bering Strait connected the Arctic and Pacific boreal marine realms, and separated Asia from North America.

2.4.10 Drake Passage

The Drake Passage opened in the latest Oligocene to early Miocene (25-20 Ma) (Keller & Baron 1983). Barker & Burrell (1977) showed that the Shackleton Fracture Zone provided a deep gap suitable for development of the Antarctic Circumpolar Current by 23.5 +/- 2.5 Ma. Thus we reduced the width of the Drake Passage in our reconstruction.

2.5 Palaeotides - Changes in the Oscillation System

As the amphidromic systems have not undergone significant changes since the last 18Ma years, Fig. 2.3 only depicts the difference of amplitudes between the M_2 simulation of the Lower Miocene and the present day simulation presented by Thomas & Sündermann (1999).

The various ocean basins have their individual natural modes of oscillation, which influence their responses to the tide generating forces. In general, the amplitudes of the semidiurnal tides are significantly higher than that of diurnal tides, because the oceans have a near resonant response to forcing at semidiurnal frequencies, especially at the M_2 frequency.

Obviously, most significant changes of amplitudes are restricted to coastal and shelf regions, while the deep oceans are in general only slightly affected by topographic changes since the Lower Miocene.
In the northern part of the Pacific Ocean amplitudes are simulated to have been reduced with respect to the recent situation in the Gulf of Alaska and near the Bering Sea. This change

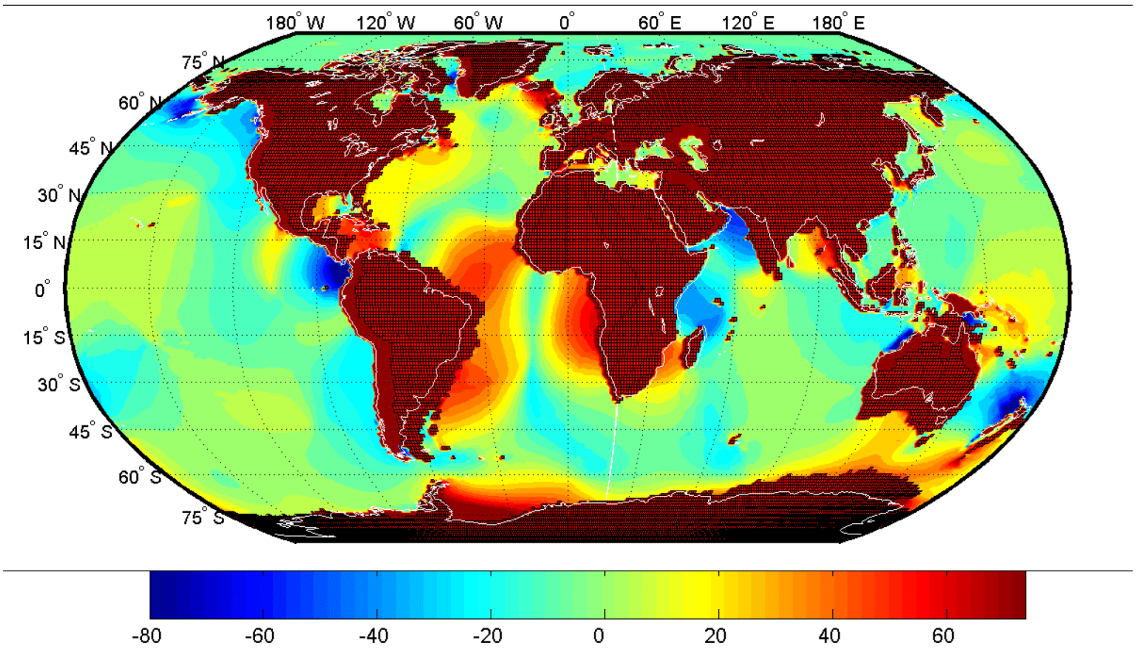

Figure 2.3: *The map shows differences between simulated Early Miocene M 2 amplitudes and present-day amplitudes simulated by Thomas & Sündermann (1999). Shaded areas present positions of continents for the Early Miocene, white lines show recent coastlines. Color contours represent differences in tidal amplitudes (cm) with respect to the present day values.*

results from the built-up of an amphidromic point near the mouth of the Bering Strait. Noticeable modifications are found in the Western part of the Southern Pacific Ocean. While today amplitudes are increased at the northern coasts of New Zealand, tidal amplitudes were modelled significantly to be higher North-East of Australia and especially South of New Zealand and in the Tasman Sea in the Miocene. The latter amplification was supported by a at the time narrower Tasman Strait between Australia and Antarctica. The present-day M_2 tide develops only small amplitudes in the Gulf of Mexico and the Caribbean Sea. However because of the Isthmus of Panama was opened in the Lower Miocene tidal waves were able to penetrate from the Pacific Ocean into the Gulf of Mexico and the Caribbean Sea. Thus, amplitudes were smaller then today at the western side of the Isthmus of Panama, as there was no reflection; on the other hand tidal amplification appeared in the Gulf of Mexico and the Caribbean Sea.

In the Northern Indian Ocean most remarkable differences appear in the Arabian Sea and the Bay of Bengal. Lower amplitudes in the Arabian Sea with respect to the present-day state are caused by a northward shift of an amphidrome Southwest of India; the amplitude amplification in the Bay of Bengal is related to slight palaeobathymetric changes in this region.

Marginal changes of the land-sea-distribution in the western Indian Ocean, especially a slight shift of Madagascar, were accompanied by significant lower tidal amplitudes North of Madagascar and amplifications at the Southeast African coasts.

Although the Indonesian Seaway was constricted 18 Ma ago, only slight changes in the amplitudes are appearent. Major changes in order of 30 cm were modelled nearby the Philippines. Palaeogeographic changes within the Sunda Islands and Kalimantan caused no significant change in tidal amplitudes.

In the Southern Ocean, there is a circumpolar zone around 60° S. It was suggested that this would allow a resonant response to the tidal forces (Pugh 1987). As expected the computed tides of the Southern Ocean show for the present and the Lower Miocene a general Westward propagation. The narrowness of the Drake

Passage between South America and Graham Land had no strong influence on the pattern of wave propagation. Also the westward shift of South America from the Early Miocene to the present has no remarkable influence on the M_2-wave in the Southern Pacific, but leads to a significant change of resonance conditions in the southern Atlantic.

In the Atlantic Ocean the pattern of the amphidromic system of the principal lunar semidiurnal M_2 tide has been modelled to be equal to today. In general phase differences do not exceed 2 to 3 hours. However, in contrast to the present day setting, the narrowed Atlantic Ocean had a significant impact on resonance conditions resulting in compared higher M_2-amplitudes along the coast of North America, in the central Atlantic, and along the coasts of South America and Southwest Africa. Due to the movement of Greenland and the subsequent constriction of the North-European Sea, tidal waves amplified to a maximum of 60 cm in magnitude between Greenland, Iceland and North-Western United Kingdom.

Near the western coast of France and Spain palaeotidal amplitudes in general were modelled to have been about 10 cm higher (Fig. 2.3). The dimension of the Mediterranean and Paratethys basins were too restricted for direct tidal forcing to have much effect on it. As the "Strait of Gibraltar" was wide and deep, penetration of the tidal waves from the Atlantic Ocean into the Mediterranean Tethys resulted in tidal amplitudes in the order of 60 cm at the former position of Sardinia and Corsica (Fig. 2.4). Similary at the eastern end of the Mediterranean Sea in the area of the entrance to the Indian Seaway tidal amplitudes were nearly in the order of 50 cm. Thus, ancient tidal amplitudes in general exceed the amplitudes of today in the order of 10 to 60 cm (Fig. 2.3, 2.4). Co-tidal lines in the Paratethys realm (Fig. 2.4) show a high sensibility to palaeobathymetric changes. Calculated co-range lines show that because of the narrow access to the Paratethys only small tidal amplitudes of less than 20 cm were able to develop.

2.6 Discussion and Conclusions

The numerical simulations of the global M_2 oscillation systems for the present-day and Early Miocene suggest, that tidal amplitudes in deep ocean basins as well as the large scale pattern of the amphidromic systems are only slightly affected by topographic changes during the last 18 Ma. However, on the shelves the tidal wave propagation is significantly influenced by closure/opening or shortening/widening of seaways.

In the Eastern part of the North Atlantic the propagation of the tidal wave as well as amplitudes is quite similar to present-day conditions (Fig. 2.3). In contrast to today's situation, 18 Ma ago the Indian Ocean was linked via a shallow seaway with the Eastern Tethys, which allowed propagation of the tidal wave through the shallow and wide gateway. Thus, tidal amplitudes in the Gulf of Oman at 18 Ma were reduced with respect to present conditions (Fig. 2.3).
The presented simulation suggests that Mediterranean tides are mainly influenced by tidal amplitudes from the eastern Atlantic and in particular by topographic conditions at the Strait of Gibraltar. As described before, the Gibraltar Strait was taken into account with a single cell during the simulation. Although this might be close to the ancient situation, the numerical model was not able to allow a significant flow rate from Northern and Southern cells and amplitudes are comparable to today. Consequently the resulting amplitudes represent a lower estimate. According to Martel *et al.* (1994) and new results presented by Bieg *et al.* (2003) a semidiurnal M_2 tide with an initialisation amplitude of 0.5 m in the Mediterranean Tethys near Marseille and in the Paratethys near Linz (Austria) cannot have generated a meso- or even macrotidal setting in the Swiss area. Therefor it has been suggested that, 18 Ma ago, the tidal wave from the Atlantic my have exceeded nowadays tides in the Mediterranean with amplitudes increased for about 40 cm near the former position of Sardinia and Corsica.
It is therefore necessary to study the variability of the presented palaeo-oscillation system in subsequent simulations with alternative gateway configurations. In addition to open ocean excitation, tides in the Mediterranean Sea depend on the width and depth of the strait of Gibraltar and the seaway between the Indian Ocean and the Eastern Tethys. As a consequence a new simulation with a broader gateway in the Gibraltar region and an extended Indian Seaway is in preparation which is expected to give a maximum estimate of tidal amplitudes in the circum-

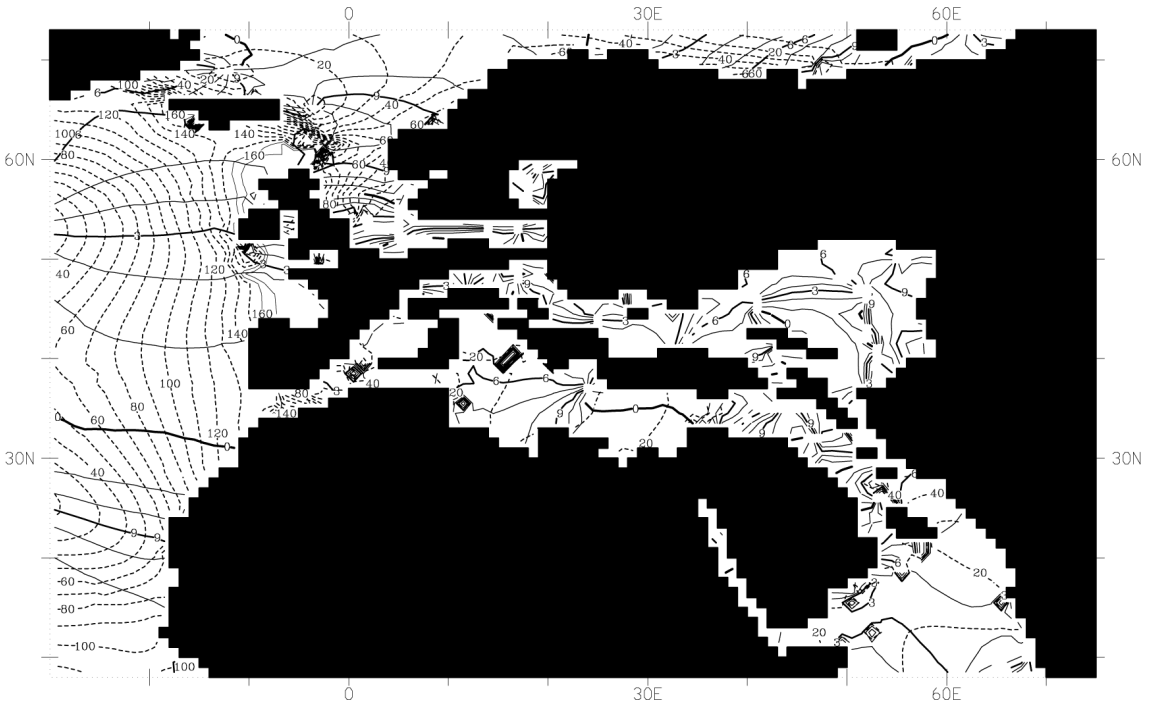

Figure 2.4: *Closeup view of the circum-Mediterranean, showing the paleogeographic situation ∼ 18 Ma ago. Co-tidal lines are shown as full lines with respect to Greenwich Mean Time, co-range lines as broken lines (cm).*

Tethys area. Further, shallow water effects due to nonlinear friction and reflection of the tidal wave may have to be considered to get a more reliable estimate of tidal amplitudes in shelve regions in the Early Miocene.

2.7 Acknowledgements

The study is funded by the DFG (SU 242/3-1). We also want to thank the DKRZ (Deutsches Klimarechenzentrum) for allowing us to use its infrastructure.

2.8 References

Allen, J.R.L. (1981): Palaeotidal speeds and ranges estimated from cross-bedding sets with mud drapes. *Nature*, **293**: 394-396.

Allen, P.A. (1984): Reconstruction of ancient sea conditions with an example from the Swiss Molasse. *Marine Geology*, **60**: 455-473.

Allen, P.A., Mange-Rajetzky, M., Matter, A. and Homewood, P. (1985): Dynamic palaeogeography of the open Burdigalian seaway, Swiss Molasse basin. *Eclogae geologicae Helvetiae*, **78**: 351-381.

Barker, P.F. and Burrell, J. (1977): The opening of the Drake Passage. *Marine Geology*, **25**: 15-34.

Bice, K.L., Scotese, C.R., Seidov, D., Barron, E.J. (2000): Quantifying the role of geographic change in Cenozoic ocean heat transport using uncoupled atmosphere atmosphere and ocean models. *Palaeogeography, Palaeoclimatology, Palaeoecology*, **161**: 295-310.

Bieg, U., Süss, M.P., Thomas, M. and Kuhlemann, J. (2003): Quantitative 3D Modelling of Sedimentary Transport Mechanisms in the Burdigalian Seaway, Molasse Basin (Lower Miocene). In: *SEDIMENT 2003 - 18th Meeting of Sedimentologists and 1st Regional meeting of SEPM Central European Section - Wilhelmshaven, Germany, 10-14 June 2003* (Eds A. Wehrmann), *TERRA NOSTRA*, **03/3**, pp. 200. Alfred-Wegener-Stiftung, Wilhelmshaven.

Blanc, P.-L. (2002): The opening of the Plio-Quaternary Gibraltar Strait: assessing the size of a cataclysm. *Geodinamica Acta*, **15**: 303-317.

Collins, L.S., Coates, A.G., Berggren, W.A., Aubry, M.-P. and Zhang, J. (1996): The late Miocene Panama isthmian strait. *Geology (Boulder)*, **24**: 687-690.

Comas, M.C., Platt, J.P., Soto, J.I. and Watts, A.B. (1999): The origin and tectonic history of the Alboran basin: insights from leg 161 results. *Proc. Ocean drill. Prog., Sci. Res.*, **161**: 555-580.

Dercourt, J., Ricou, L.E. and Vrielynck, B. (1993): *Atlas Tethys Palaeoenvironmental Maps.* Gauthier-Villars, Paris, 307 pp.

Dewey, J.F., Pitman, W.C.I., Ryan, W.B.F. and Bonnin, J. (1973): Plate tectonics and the evolution of the Alpine System. *Geol. Soc. Amer. Bull.*, **84**: 3137-80.

Esteban, M., Braga, J.C., Martin, J. and de Santisteban, C. (1996): Models for carbonate stratigraphy from Miocene reef complexes of Mediterranean

regions. In: *Concepts in Sedimentology and Paleontology* (Eds E.K.E. Franseen, Mateu; Ward, William C; Rouchy, Jean-Marie), **5**, pp. 277-294.

Faupl, P. and Roetzel, R. (1987): Gezeitenbeeinflußte Ablagerungen der Innviertler Gruppe (Ottnangien) in der oberösterreichischen Molassezone. *Jahrbuch der Geologischen Bundesanstalt Wien*, **130**: 415-447.

Faupl, P. and Roetzel, R. (1990): Die Phosphoritsande und Fossilreichen Grobsande; Gezeitenbeeinflusste Ablagerungen der Innviertler Gruppe (Ottnangien) in der oberoesterreichischen Molassezone. *Jahrbuch der Geologischen Bundesanstalt Wien*, **132**: 157-180.

Gasperi, J.T. and Kennett, J.P. (1993): Vertical thermal structure evolution of Miocene surface waters: western equatorial Pacific DSDP Site 289. *Marine Micropaleontology*, **22**: 253-254.

Gelabert, B., Sàbat, F. and Rodríguez-Perea, A. (2002): A new proposal for the late Cenozoic geodynamic evolution of the western Mediterranean. *Terra Nova*, **14**: 93-100.

Hamilton, W. (1979): Tectonics of the Indonesian Region. *Geol. Survey Prof. Pap.*, **1078**: 1-345.

Haug, G.H. and Tiedemann, R. (1998): Effect of the formation of the Isthmus of Panama on Atlantic Ocean thermohaline circulation. *Nature*, **393**: 673-676.

Homewood, P. and Allen, P. (1981): Wave-, tide-, and current-controlled sandbodies of Miocene molasse, Western Switzerland. *American Association of Petroleum Geologists, Bulletin*, **65**: 2534-2545.

Homewood, P., Allen, P.A. and Williams, G.D. (1986): Dynamics of the Molasse Basin of western Switzerland. In: *Foreland Basins* (Eds P.A. Allen and P. Homewood), *IAS, Special Publications*, **8**, pp. 199-217. Blackwell Scientific Publications, Oxford.

Hsü, K. (1971): Origin of the Alps and western Mediterranean. *Nature*, **233**: 44-48.

Keller, G. and Barron, J. (1983): Paleoceanographic implications of Miocene deep-sea hiatuses. *Geological Society of America Bulletin*, **94**: 590-613.

Kennett, J.P., Keller, G. and Srinivasan, M.S. (1985): Miocene planktonic foraminiferal biogeography and paleoceanographic development of the Indo-Pacific region. *Geological Society of America Memoir*, **163**: 197-236.

Larson, R.L., Pitman II, W.C., Golovchenko, X., Cande, S.C., Dewey, J.F., Haxby, W.F. and Labrecque, J.L. (1985): *The Bedrock Geology of the World*. Freeman, New York.

Linthout, K., Helmers, H. and Sopaheluwakan, J. (1997): Late Miocene obduction and microplate migration around the southern Banda Sea and the closure of the Indonesian Seaway. *Tectonophysics*, **281**: 17-30.

Marincovich, L.J. and Gladenkov, A.Y. (1999): Evidence for an early opening of the Bering Strait. *Nature*, **397**.

Martel, A.T., Allen, P.A. and Slingerland, R. (1994): Use of tidal-circulation modeling in paleogeographical studies: An example from the Tertiary of the Alpine perimeter. *Geology*, **22**: 925-928.

Martín, J.M., Braga, J.C. and Betzler, C. (2001): The Messinian Guadalhorce corridor: the last northern, Atlantic-Mediterranean gateway. *Terra Nova*, **13**: 418-424.

McKenzie, D.P. (1970): Plate tectonics of the Mediterranean region. *Nature*, **226**: 239-243.

Mikolajewicz, U., Maier-Reimer, E., Crowley, T.J. and Kim, K.-Y. (1993): Effect of Drake and Panamanian gateways on the circulation of an ocean model. *Paleoceanography 8*409-426.

Neev, D. (1975): Tectonic evolution of the Middle East and the Levantine Basin (easternmost Mediterranean). *Geology (Boulder)*, **3**: 683-686.

Ogg, J.G., Kodama, K. and Wallick, B.P. (1992): Lower Cretaceous magnetostratigraphy and paleolatitudes off Northwest Australia, ODP Site 765 and DSDP Site 261, Argo abyssal plain, and ODP site 766, Gascoyne abyssal plain. *Proceedings of the Ocean Drilling Program, Scientific Results*, **123**: 523-548.

Owen, H.G., Sclater, J.G., Hellinger, S. and Tapscott, C. (1979): The paleobathymetry of the Atlantic Ocean from the Jurassic to present; discussion and reply. *Journal of Geology*, **87**: 116-118.

Reyre, D.M., S (1970): Une premiere contribution des accords NIOC-ERAP a la connaissance geologique de l'Iran, premiere partie. Preliminary contribution by NIOC-ERAP to the geology of Iran, part 1. *Revue de l'Institut Francais du Petrole et Annales des Combustibles Liquides*, **25**: 687-713.

Rogers, J.J.W. (1993): *A History of the Earth*. Cambridge University Press, New York, 312 pp.

Rögl, F. (1999): Mediterranean and Paratethys. Facts and Hypotheses of an Oligocene to Miocene Paleogeography (short overview). *Geologica Carpathica*, **50**: 339-349.

Rögl, F. and Steininger, F.F. (1984): *Neogene Patatethys, Mediterranean and Indo-pacific Seaways*. Fossils and Climate. John Wiley & Sons.

Salvenmoser, S. (1999): Zur Sedimentologie gezeitenbeeinflusster Sande in der Oberen Meeresmolasse und Süssbrackwassermolasse (Ottnangium) von Niederbayern und Oberösterreich. *Münchner Geologische Hefte (A)*, **26**: 1-179.

Sclater, J.G., Parsons, B. and Jaupart, C. (1981): Oceans and continents; similarities and differences in the mechanisms of heat loss. *Journal of Geophysical Research. B*, **86**: 11,535-11,552.

Sclater, J.G.H., S; Tapscott, C (1977): The paleobathymetry of the Atlantic Ocean from the Jurassic to the present. *Journal of Geology*, **85**: 509-522.

Scotese, C.R., Bambach, R.K., Barton, C., Voo, R.v.d. and Ziegler, A.M. (1979): Paleozoic base maps. *Journal of Geology*, **87**: 217-277.

Scotese, C.R., Gahagan, L.M. and Larson, R.L. (1988): Plate tectonic reconstructions of the Cretaceous and Cenozoic ocean basins. *Tectonophysics*, **155**: 27-48.

Seiler, U. (1989): *An investigation to the Tides of the World Ocean and their Instantaneous Angular Momentum Budgets*. PhD, Univ. of Hamburg, Germany, 101 pp.

Seiler, U. (1991): Periodic changes of the angular momentum budget due to the tides of the world ocean. *Journal of Geophysical Research*, **96**: 10,287-10,300.

Stanley, S.M. (1986): *Earth and life through time*. W. H. Freeman and Co., New York, NY, United States (USA), Johns Hopkins Univ., Baltimore, MD, United States (USA), 690 pp.

Steininger, F., Rögl, F. and Martini, E. (1975): Current Oligocene/Miocene biostratigraphic concept of the Central Paratethys (Middle Europe). *Newsl. Stratigr.*, **4**: 174-202.

Steininger, F.F. and Roegl, F. (1984): Paleogeography and palinspastic reconstruction of the Neogene of the Mediterranean and Paratethys. *Geological Society Special Publications*, **17**: 659-668.

Sztanó, O. (1994): *The tide-influences Pétervására sandstone, early Miocene, Northern Hungary: Sedimentology, Palaeogeography and basin development.* Phd., Universiteit Utrecht, Utrecht, 155 pp.

Sztanó, O. and de Boer, P.L. (1995): Basin dimensions and morphology as controls on amplification of tidal motions (the early Miocene North Hungarian Bay). *Sedimentology*, **42**: 665-682.

Thomas, M. and Sündermann, J. (1999): Tides and tidal torques of the world ocean since the last glacial maximum. *Journal of Geophysical Research*, **104**: 3159-3183.

Tsuchi, R. (1997): Marine climatic responses to the Neogene tectonics of the Pacific Ocean seaways. *Tectonophysics*, **281**: 113-124.

Weissel, J.K. and Hayes, D.E. (1972): *Oceanography of the South Pacific. Analysis of Magnetic Data from South of Australia.* N.Z. Comm. Unesco, Wellington, 345 pp.

Ziegler, A.M., Scotese, C.R. and Barnett, S.F. (1982): Mesozoic and Cenozoic paleogeographic maps. In: *Tidal Friction and Earth's Rotation, vol. II* (Eds P. Brosche, Sündermann, J.). Springer Verlag, New York.

Chapter 3

Simulation of Tidal Flow and Circulation Patterns in the Burdigalian Seaway (Upper Marine Molasse, Early Miocene)

3.1 Abstract

During Ottnangian times the Burdigalian Seaway has linked the Mediterranean realm in the South with the Paratethys realm in the Northeast. The seaway reached its maximum extend in the German part of the Molasse basin during the Ottnangian. A stratigraphic framework has been established that allows to reconstruct the palaeobathymetry of the Burdigalian Seaway during its maximum extend during the Ottnangian. To reconstruct tidal currents and amplitudes, a fully non-linear 3D hydrodynamic model has been applied. Residual currents are interpreted to represent net-transport directions of sediments within the Burdigalian Seaway. The model is forced at its open boundaries with the semi-diurnal M2 waves. The sensitivity of the tidal model has been tested, using different tidal amplitudes and phases at the open model boundaries. Based on this, the model indicates high mesotidal ranges as deduced from outcrops in Switzerland, Germany and Austria. A complex system of convergent and divergent currents mainly along circular flow paths in the seaway have been generated.

3.2 Introduction

A basinwide transgression during the early Miocene ($\sim$ 20 Ma), flooded the Alpine foredeep generating shallow marine conditions between southeastern France and Eastern Austria via Switzerland and Southern Germany. The Burdigalian Seaway (Fig. 3.1 and Fig. 3.4) has a length of about 1200 km, linking the deep marine Western Mediterranean realm with the Paratethys in the Northeast. The investigated tidal deposits of the Upper Marine Molasse are part of the North Alpine Foreland Basin (NAFB) that was formed during the Oligocene and Miocene, as a mechanical response to the tectonic load of the evolving Alpine thrust wedge (e.g. Homewood et al. 1986; Sinclair et al. 1991; Schlunegger et al. 1997b).

The development of the Burdigalian Seaway occurred coeval with a reduction of thrust advance rates of the Alpine orogenic wedge and with strongly reduced sediment discharge in the western and central part of the North Alpine Foreland Basin (Kuhlemann 2000; Schlunegger & Hinderer 2001). It can be also correlated to a global eustatic sea level rise (e.g. Crumeyrolle et al. 1991; Haq et al. 1988; Zweigel et al. 1998). The investigated stratigraphic unit, the Upper Marine Molasse (OMM), has a total preserved thickness of approximately 1000 m adjacent to the Alpine thrust front and thins to 70-100 m near the northern edge of the Swiss part of the Molasse basin (Berger 1983; Allen et al. 1985; Keller 1989). The cumulative sedimentary thickness of the Molasse basin in Germany reaches almost 5000 m (Bachmann & Müller 1992; Lemcke 1988).

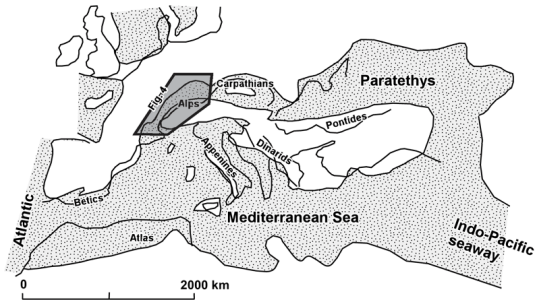

Figure 3.1: *Palaeogeography of the circum-Mediterranean region during the early Miocene (Burdigalian, ca. 20 Ma.) with a reconstructed Indo-Pacific connection and a wider connection of the western Tethys area with the Atlantic Ocean. The shallow marine Burdigalian Seaway (marked area, Fig. 3.4) came into existence and linked the western Tethys with the Paratethys realm in the northeast (modified from Allen et al. 1985 and Rögl 1999).*

During the Burdigalian (ca. 20-17 Ma) shallow marine conditions prevailed for ∼3 million years. Sediments consist of wave- and tide-dominated shallow marine sandstones, siltstones and mudstones and conglomerates of marginal fan-deltas (e.g. Keller 1989). It has been sugested that tidal waves from the open marine Atlantic Ocean were able to enter the Mediterranean realm and co-oscillate with the Burdigalian Seaway at the open boundary in the South (Martel et al. 1994). A proposed shallow water connection to the Indian Ocean (Fig. 3.1) in the East (e.g. Rögl & Steininger 1984; Rögl 1999) probably allowed tidal currents to enter the Paratethys. Sedimentological research carried out in the eighties showed that sediments of the Burdigalian Seaway (Fig.1) have mainly been deposited under a strong meso- to macrotidal regime (e.g. Homewood et al. 1985). Tidally related deposits like sand waves, bidirectional cross-stratification, neap-spring tidal bundle sequences have been recognized within the whole seaway from France (Tessier & Gigot 1989; Assemat 1991; Crumeyrolle et al. 1991; Allen & Bass 1993; Rögl 1999), Switzerland (Allen 1981; Allen 1984; Homewood & Allen 1981; Diem 1985; Allen et al. 1985; Homewood et al. 1986) to South Germany and Upper/Lower Austria (Salvenmoser 1999, Faupl & Roetzel 1987; Faupl & Roetzel 1990; Hülsemann 1955; Krenmayr 1991).

Until Martel et al. (1994) demonstrated in a numerical model, that two propagating tidal waves can generate meso- to macro tidal ranges in the Swiss region the observation of mesotidal ranges in the Swiss part of the Burdigalian Seaway stayed unexplained. As Martel's model was of a limited spatial extent (Marseille to Geneva) and provides only information on tidal amplitudes, we increased Martel's model domain, linking the shallow water Burdigalian Seaway with the deeper marine parts of the Mediterranean Sea in the South and the Paratethys realm in the North. Using a state-of-the-art finite element circulation model, described in detail by Lynch et al. (1997) and Lynch et al. (1996), we calculated tidal amplitudes and current velocities within the seaway applying different border conditions for the open model boundaries. We calculated vertically averaged residual velocities to describe net transport direction. These might provide useful information about sediment transport paths.

Many studies (e.g. Faupl & Roetzel 1987; Faupl & Roetzel 1990; Salvermoser 1999) provided detailed quantitative local information on the current direction of ebb- and flood. However, these studies do not allow the reconstruction of mesoscale currents within the as calculated by the numerical simulation. Also owing to the complexity of the Burdigalian palaeogeography, our geometric reconstruction of the shoreline is a best estimate without considering small-scale details, such as tidal flats behind a coastal barrier in the model. (e.g. Allen & Bass 1993: Fig. 26). Consequently, it is not the aim of the study to fit single local palaeocurrent directions to the simulations. Instead, we only compare the palaeocurrents of the offshore subtidal deposits qualitatively.

3.3 Stratigraphy of the Upper Marine Molasse (OMM)

The clastic sediments of the central Molasse basin are traditionally subdivided into four lithostratigraphic groups Matter et al. (1980): Lower Marine Molasse (UMM), Lower Freshwater Molasse (USM), Upper Marine Molasse (OMM), and Upper Freshwater Molasse (OSM). We use the conventional German abbreviations for convenience. These lithostratigraphic units form two shallowing-upward megasequences (e.g. Schlunegger et al. 1996): The first megasequence comprises the Rupelian Lower Marine Molasse and the Chattian and Aquitanian fluvial clas-

tics of the Lower Freshwater Molasse, the second megasequence, starting with the Burdigalian transgression, consists of shallow-marine sand-, silt- and mudstones (Upper Marine Molasse), which interfinger with conglomeratic fan-delta deposits adjacent to the thrust front (e.g. Keller 1989; Schlunegger et al. 1993; Demarcq & Perriaux 1984; Lemcke 1988; Allen & Bass 1993). The top of this megasequence form Mid-Late Miocene fluvial clastics of the Upper Freshwater Molasse. We are interested in the maximum extend of the marine water body during the OMM (Fig.2) as an upper limit bathymetric boundary condition of the tidal simulations. To define depositional sequences we used the lithostratigraphic framework of Schreiner (1976), Lemcke (1988), Keller (1989), Doppler (1989), Bachmann & Müller (1991), Crumeyrolle et al. (1991), Roetzel & Rupp (1991), Luterbacher et al. (1992) and Schreiner & Luterbacher (1999). For further details see also the discussion in Kuhlemann & Kempf (2002). The biostratigraphic correlation for the western and eastern part is based on Berggren et al. (1995), Rögl (1996) and Steininger et al. (1996). According to these studies, it must be concluded that the Burdigalian megasequence is made up by two depositional sequences, the Eggenburgian (21-18 Ma) and Ottnangian (18-17 Ma). The maximum flooding of the Burdigalian Seaway and hence the maximum distribution of marine sediments in the OMM occurred during a basin-wide transgression at the base of the Ottnangian around 18 Ma (Fig. 3.2).

3.3.1 The Ottnangian Maximum flooding surface (MFS, Fig. 3.2)

During the Burdigalian, a slow gradual rise in eustatic sea level is assumed by the global eustatic sea level curve of Haq et al. (1987), Haq et al. (1988) (2nd-order supercycle TB 2 see Fig. 3.2). This rise led to a basin-wide marine transgression in the Molasse basin. The transgression must be taken as an indication for less than 100 m elevation above sea-level during the previous USM stage (cf. Berger 1996).

During the initial Eggenburgian (ca. 21-18 Ma) transgression (TB 2.1, Fig. 3.2), a wave dominated transgressive systems tract accumulated thick deposits on the more subsiding margin of the basin in eastern France (Crumeyrolle et al. 1991). This "first" Burdigalian transgression encroached from the West and East into the Northern Alpine Foreland Basin (NAFB) (Büchi & Schlanke 1977). In the French and Swiss parts of the Burdigalian Seaway a shallow, micro-tidal and mostly wave-dominated marine estuary was established (e.g. Keller 1989), which narrowed west of Lake Constance to a small channel, connecting the shallow Swiss seaway with the remnant deep sea in the East (Bavaria/Austria) (Kuhlemann & Kempf 2002: Plate: 4). This transgression ended with the deposition of Montaugier Lithosome, the Grobsandzug, the Neuhofener Beds and equivalent sediments that are interpreted to represent a first regional high stand systems tract (Crumeyrolle 1991; Allen & Bass 1993; Bachmann & Müller 1991). In Switzerland it was suggested that the regression at the end of the St. Gallen formation and the development of the sequence boundary, separating the Luzern and St. Gallen formations, were additionally controlled by an uplift in the distal parts of the basin (Schlunegger et al. 1997a; Kuhlemann & Kempf 2002).

The following second rapid transgression at the base of the Ottnagian (TB 2.2, Fig. 3.2) is attributed to combined effects of load-induced flexural subsidence and eustatic sea-level rise. The Ottnagian transgression (TB 2.2, Fig.2; ca. 18 Ma) established an overall seaway from the Rhône valley to Austria (Rögl & Steininger 1983). In the French part of the basin the Ottnagian transgression is recognized by a pronounced marine onlap onto the margin of the Massif Central (Allen & Bass 1993). At this time the Burdigalian Seaway reached its maximum extend and depth. The transgression encroached far onto the German foreland and cut a cliff into the Franconian platform (e.g. Bachmann & Müller 1991). However, as described below, we must assume that the Maximum Flooding Surface of the second transgression occurred above the deposition of the Randengrobkalk.

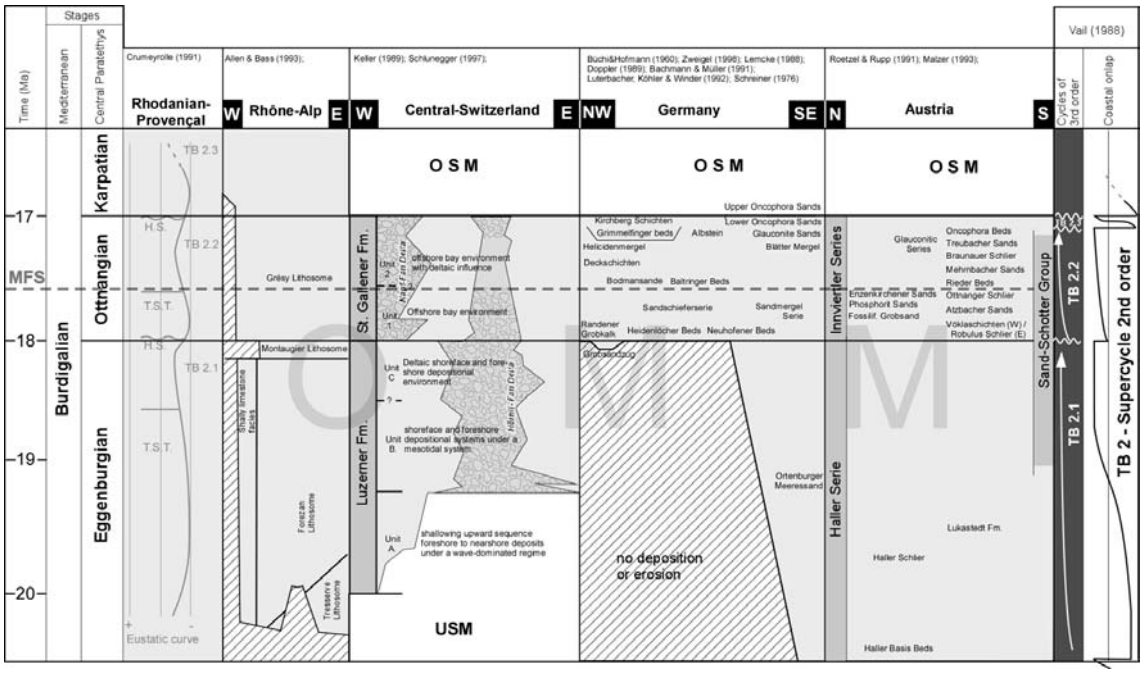

Figure 3.2: *Simplified stratigraphic overview of the Early Miocene between France (West) and Austria (East). The Figure shows the two depositional sequences of the Eggenburg and Ottnangian. The study concentrates on the maximum extent of the Burdigalian Seaway at the base of the Ottnangian (shortly after 18 Ma =MFS). Stratigraphic time scale after Berggren et al. 1995; Rögl 1996; Steininger et al. 1996.*

3.4 Basin Shape and Palaeobathymetric reconstruction of the Burdigalian Seaway

Until now, no detailed reconstruction of the palaeobathymetry and palaeogeography for the Burdigalian Seaway during the OMM exists. Many available studies in Switzerland, France, Germany and Austria concentrate on local features (e.g Büchi et al. 1961; Büchi & Hofmann 1960). Other more comprehensive studies focus on the entire evolution of the peripheral Molasse basin (e.g. Bachmann & Müller 1992) and do not cover the Burdigalian stage in sufficient detail. Thus, it was necessary to reconstruct the Budigalian Seaway by collecting mesoscale information about its extent and subsequently earning information on palaeobathymetry.

3.4.1 Basin shape and basin evolution

The palaeobathymetry and extent of the Burdigalian Seaway is substantially influenced by its coexisting structural framework. In addition, after the deposition of the OMM the Burdigalian Seaway was partly structurally deformed and eroded. Hence, it is necessary to first define the style of structural evolution of the seaway and subsequently to reconstruct the original extend of the seaway using balancing restoration techniques (e.g. Ford et al. 1999, Laubscher 1992).

The depositional area of the Upper Marine Molasse in France is presumably fault-controlled. It is suggested that in the course of seafloor spreading in the Mediterranean Sea (Séranne et al. 1995, Ford et al.1999) an extensional regime was initiated (Fig. 3.3, 3.4). This led to enhanced basin subsidence and facilitated the Burdigalian marine transgression towards the North. It has been shown (Demarcq & Perriaux 1984; Ford et al. 1999), that the first Burdigalian (TB2.1) marine transgression migrated from the Gulf of Lion into the Rhodanian-Provençal basin and flooded both the footwall and the hanging wall of the Durance fault (Fig. 3.3). The sea occupied an elongated seaway (Demarcq 1970), with a gulf-like morphology (Crumeyrolle et al. 1991; Tessier & Gigot 1989), which was bordered by the Alpine front in the East (Fig.

3.3). The Digne-Valensole basin formed a large embayment connected with the Rhodanian-Provençal gulf. The Rhodano-Provençal gulf was dissected by emergent areas (Demarcq & Perriaux 1984) and extended northward through the Basse-Dauphiné graben to the North Alpine Foreland Basin (NAFB). We postulate that at the beginning of the Ottnangian, during the TB2.2 transgression these emergent areas have been completely flooded to allow tidal penetration into the northern areas more easily.

However, due to uplift and erosion caused by subsequent Alpine deformation, reconstruction of the original geometry of the Burdigalian Seaway in the Digne-Valensole area is difficult to achieve. While Demarcq & Perriaux (1984: Fig. 9.34) favoured a narrow, eastward directed embayment; Martel et al. (1994) preferred a broad opening towards the Mediterranean Sea. In our reconstruction (Fig. 3.4) we used the more conservative model of Demarcq & Perriaux (1984), extending their reconstruction of the seaway according to the data of Lickorish & Ford (1998). Isolated remnants of the OMM series occur across the southern Subalpine Chains (SSC, Fig. 3.3) and are best preserved in the southern parts of the Digne thrust sheet. Using sequential balancing techniques, Lickorish & Ford (1998) restored a section through the southern part of the SSC, constrained by the Tertiary stratigraphy, deriving a SW-directed shortening of 21.5 km, similar to that obtained by Ritz (1991: 24 -25 km).

The seaway extended northward through the peri-Alpine foreland basins (Rhône-Alp, Savoy, Base-Dauphiné) to the North Alpine Foreland Basin (NAFB) (Debrand-Passard et al. 1984; Martel et al. 1994). The Savoy basin appears as a strait between the wider and deeper Swiss part of the OMM and the southern French alps area (Tessier & Gigot 1989, Allen & Bass 1993). In the Early Miocene the seaway in the Savoy region was about 35-40 km wider than the distribution of present-day outcrops initially suggest (Allen & Bass 1993). Based on these data we used an average basin width of approximately 30-40 km in the Savoy region (Fig. 3.4) for our simulations.

In Switzerland the seaway was wider and deeper then in the adjacent Savoy region. The time span from 20 to 12 Ma is only poorly constrained in the western Swiss Molasse basin, since most of the corresponding sediments have been removed by uplift related erosion after 12 Ma in the course of Jura Mountain deformation. Hence the kinematics of the Jura is an important constrain for the reconstruction of the Swiss Molasse Basin. Palaeogeographic and palinspastic reconstructions for the western Swiss Molasse Basin are given by Berger (1996) and Kuhlemann & Kempf (2002).The Swiss Jura system is, as a whole, the result of the Middle to Late Miocene oblique convergence between Adria and Europe (Laubscher 1992). Folding and subsequent uplift of the Jura Mountains started in the Late Serravallian, when the entire western Molasse basin became incorporated into the Alpine orogenic wedge and was shortened by up to 30 km and displaced to the northwest (Guellec et al. 1990; Laubscher 1965; Laubscher 1992; Mugnier & Menard 1986). The present day western Swiss Molasse basin forms a piggyback basin above a décollement horizon in Mid-Triassic evaporites (Deville et al. 1994).
Pre-Middle Miocene erosion in the relict Molasse strata points towards the existence of a Late Oligocene-Early Miocene forebulge located in the present-day Jura Mountains (Guellec et al. 1990; Laubscher 1992; Naef et al. 1985). The palinspastic reconstruction of the Burdigalian seaway thus results in a width of approximately 70 km and fits well with results from Allen & Homewood (1984) who reconstructed marine conditions near Fribourg. In western Switzerland the Alpine thrust front between 22-12 Ma seemed to be in a fixed position southeast of Lausanne and the 'pinch-out' migration of Molasse strata to the NW seems to have markedly slowed down (Burkhard & Sommaruga 1998). Towards the East the basin remains at a constant width of about 100 km.

In Germany the Molasse basin widens to a maximum of approximately 150 km. The basal OMM transgression (see Fig. 3.3) entered only the southern parts of South-Germany, forming a narrow channel in front of the Alps (see e.g. Bachmann & Müller 1991: Fig. 20:13; Keller 1989: Fig.6-2; Kuhlemann & Kempf 2002: Plate 4). A more widespread transgression occurred at the base of the Ottnangian and flooded also more external parts of the basin. Along the northern margin a "cliff" was cut into the Upper

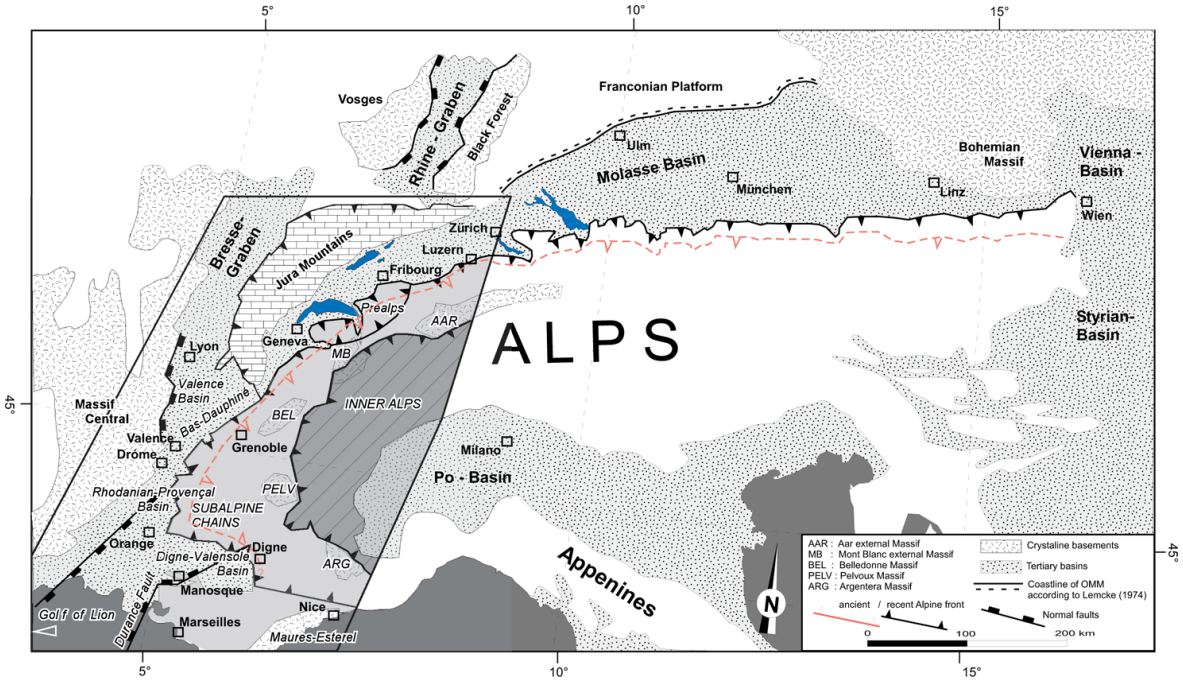

Figure 3.3: *Overview of the tertiary basins adjacent to the Alpine orogen. The rectangle highlights a schematic structural map of southeastern France (modified from Phillipe et al. 1998, Keller 1989, Beck et al. 1998, Ford et al. 1999). The Burdigalian North Alpine thrust front (red dashed line) was modified from Kuhlemann et al. (2002), Kuhlemann & Kempf (2002) and Wagner (1996b: Fig. 13). The ancient and recent Alpine thrust fronts represent the northern limit of the Helvetic/Penninic Units.*

Jurassic Limestones of the European foreland (e.g. Lemcke 1973; Lemcke 1988). According to Gall (1974) and Gall (1975) OMM sediments are also found above the cliff. However, a basin wide tracing of these deposits is not possible. Hence, we stay with the established, more conservative interpretation as presented for example by Bachmann & Müller (1991) and used the cliff as approximation of the coastline.
In Austria the recent foreland is only a narrow remnant of the original basin width. Wagner 1996: p. 224, Fig. 3.10a shows a facies reconstruction for Ottnagian times. Coastlines have been taken from Kuhlemann & Kempf (2002:plate 5), indicating a width of 50 km for the Ottnagian. East of the Bohemian Massif the Austrian Molasse basin widens again towards the Carpathian foreland.

During Eggenburgian times, the basin in Austria was approximately 500 m deep (Wagner et al. 1986). Bottom currents deeply eroded older sediments in front of the northward propagating Alpine orogen (Wagner 1996). Erosion was succeeded by rapid sedimentation through submarine slides and turbidites in the deeper part of the basin. In the Lower Miocene the imbricated Molasse thrust sheets reached approximately its present-day position (Wagner 1996, Fig. 3.10b). At 18 Ma the thrust front stopped to migrate northward (Malzer et al. 1993). The Ottnangian transgression widely flooded the entire NAFB and generated marine conditions from the Alpine-Carpathian foredeep to the Rhône valley and the Indian Ocean. Concurrently deep marine conditions in the Austrian section transformed into shallow marine conditions ("Innviertler Gruppe") of predominantly tidal deposits.

3.4.2 Sedimentary facies of the Burdigalian Seaway

According to Homewood & Allen (1981), Homewood et al. (1986) and Allen & Bass (1993) the OMM (in the Rhône area and Switzerland) was deposited in a wide variety of marine environments. Four major facies belts are distinguished (Homewood et al. 1986). These are: conglomerates and sandstones of the proximal fan-delta that were deposited in tide-influenced distributary channels, tidal

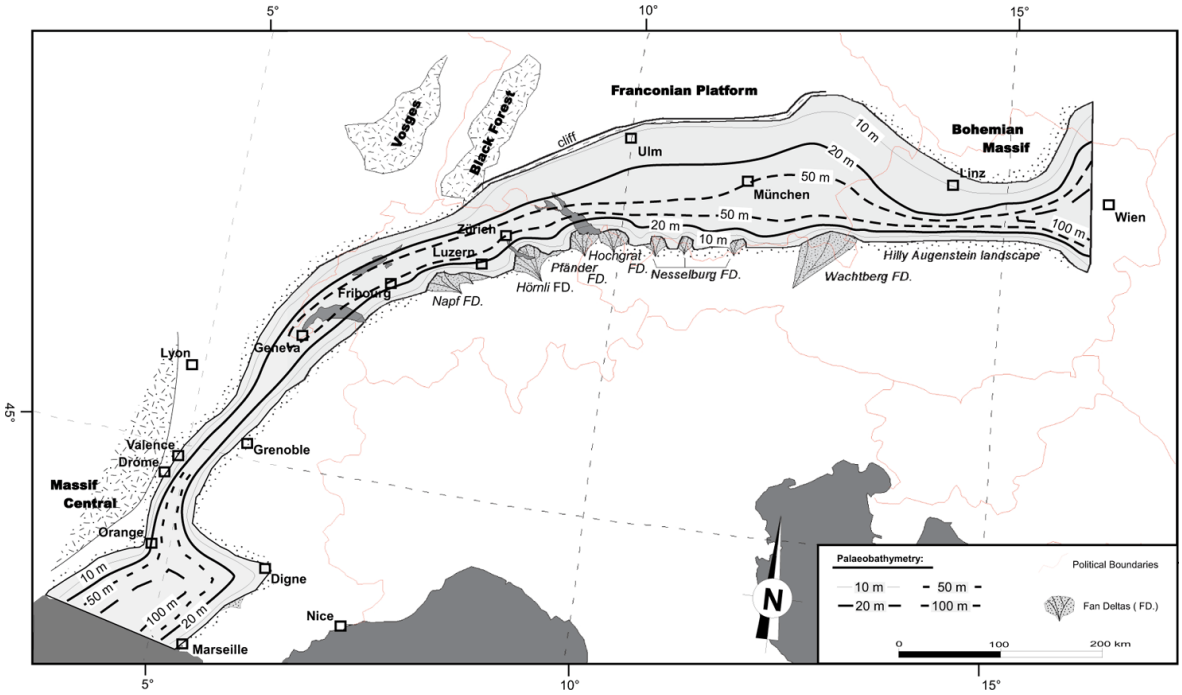

Figure 3.4: *Palaeogeographic and bathymetric reconstruction of the Upper Marine Molasse in Early Ottnangian times shortly after 18 Ma. At this time, a second, more enhanced transgression flooded the entire North Alpine Foreland Basin and generated an extended seaway between the Mediterranean and the Paratethys (from the Rhône area in the southwest to Upper Austria in the northeast). Contour lines indicate the estimated bathymetry. The map is projected in equal area Lambert projection.*

sand waves exhibiting bipolar palaeocurrent directions and intertidal sand flats are the most conspicuous features of the coastal facies belt. The nearshore facies is composed of thick, sandy subtidal shoals built of current-generated megaripples, intershoal swales containing horizontally stratified sandstones and mudstones, and swash bars or flood ramps with low angle accretionary bedding. Finally, the offshore facies belt contains sizeable coquina banks with very large-scale tabular cross-stratification (up to 20 m; Allen et al. 1985). In the Digne embayment, wave-dominated, deltaic systems were deposited during the Burdigalian transgression (Crumeyrolle et al. 1991). Sand shed from the rising relief was reworked into shoal and tidal inlet systems. The transgressive succession is capped by a series of thinner strata that consist of fine to medium glauconitic burrowed sand. This sand is considered to represent a condensed section, which occurs at the maximum stage of transgression, when shelf starvation enhances mineral authigenesis (Loutit et al. 1988).

In central and eastern Switzerland the Upper Marine Molasse consist of the Luzern (20-18 Ma) and St. Gallen (18-17 Ma) formations (magnetostratigraphic correlation was done by Schlunegger et al. 1996; Kempf et al. 1997; Kempf et al. 1999). Both formations exhibit an initial deepening and a subsequent shallowing upward sequence, that are comparable to the TB2.1 and TB2.2 sequences. The Luzern formation consists of predominantly sand- and mudstones that are locally interbedded with conglomerates. According to Keller (1989) three informal units are preserved in the Luzern Formation. Unit A comprises thick wave-dominated glauconitic sandstones alternating with mudstones; unit B is composed of an succession of fine- to medium-grained sandstones with mudstone interlayers, deposited by mesotidal currents, unit C, consist of alternating sand and mudstones that record deposition of both microtidal currents and strong wave-dominated conditions (Keller 1989). The top of unit C is interpreted as a sequence boundary (Schaad et al. 1992). At the base of the following St. Gallen formation, sand- and mudstones

were deposited in an approximately 20-m deep offshore bay environment. These deposits are overlain by a succession of deltaic sandstones and conglomerates (Keller 1989), also showing indicators of tidal dominance.

In Germany during the Ottnangian marine highstand (Fig. 3.2, TB 2.2), shelly beach rocks (e.g. "Randengrobkalk") were formed in near the northwestern basin margin, grading southward into intertidal and subtidal sand- and siltstones (Haus 1951; Kiderlen 1931; Luterbacher 1997; Luterbacher et al. 1992; Rutte 1952; Schreiner & Luterbacher 1999). Zweigel (1998) described well-preserved neap-spring tidal bundles with sigmoidal foreset laminae, similar to those found in the Swiss Molasse. In Upper Bavaria glauconitic sands were deposited, forming large sand-waves (Salvermoser 1999). With the transition of the marine sands to the Oncophora beds (Upper Ottnangium-Karpat) bidirectional tidal currents changed into non-tidal uni-directional currents (Salvermoser 1999).

In Austria the basin was considerably deeper during the deposition of the Eggenburgian. An Eggenburgian microfauna was determined in the upper few hundred meters of the Puchkirchen Formation (USM). After the most prominent submarine erosion across the Molasse basin, a new fauna immigrated in the Hall Group from the Indian Ocean (Rögl & Steininger 1983; Steininger & Rögl 1979). At the time of the deposition of the Hall Formation, the whole Molasse basin was filled with light grey to green-grey micaceous, sandy pelites, the so-called "Hall-Schlier", which are the distal parts of turbidites and contourites. The centre of the Hall basin accumulates the turbiditic and contouric sandstones and slides in erosional lows. The boundary between the Eggenburgian and Ottnangian cannot be determined precisely by biostratigraphic data. The correlation marker on logs and seismic lines is a regional submarine unconformity with sand layers on top (Wagner 1998). According to this information we used an estimated palaeodepth of 150 m to the former position of the Puchkirchen trough. Ottnangian sandstones recently were interpreted as subtidal sand waves, deposited under strong tidal current activity (Faupl & Roetzel 1987; Faupl & Roetzel 1990; Krenmayr 1991).

3.4.3 Reconstructed palaeobathymetry of the Burdigalian

Model Parameter	Value
Gravity	9,806 m/s^2
Latitude	47°
Coriolis	0.1067e^{-4}
τ_0	2.0e^{-4}
implicit time weighting factor for vertical diffusion of momentum	0.5
vertical diffusion of heat and salt	1.0
vertical diffusion of turbulence	1.0
θ	0.75
Quadratic bottom stress coefficient C_d	5e^{-3}
minimum bottom stress coefficient	1.0e^{-5}
Smagorinsky coefficient	0.28
Reference temperature	10.0 °C
Reference salinity	32 psu
Reference q^2	1.e^{-3}
Reference q^{2}l	1.e^{-3}
Minimum vertical viscosity	2.0 e^{-3}
Minimum value for q^2,q^{2}l,l	1.e^{-6}

Table 3.2: *Listing of a typical parameter set for the Burdigalian Seaway.*

To reconstruct the basin-wide palaeobathymetry, we used the estimates resulting from the previously reported sedimentary facies. Additional assumptions have been made to complete the model as suggested by Martel et al. (1994). An opposite trend in the evolution of palaeobathymetry during the deposition of the OMM is evident between the western part (France, Switzerland, Germany) and the eastern part (Austria) of the Molasse Basin. While bathymetry increased in most parts of the western basin during Early Ottnangian times, the seaway became shallower in the East (Tab. 1). For the Austrian part of the Molasse basin we assume a relatively shallow marine environment of about 20 to 50 m, as discussed in Krenmayr & Roetzel (1996). The association of the Skolithos (and Cruziana) ichnofacies supports the interpretation of a high-energy environment. According to Kuhlemann & Kempf (2002) and Wagner et al. (1986), a furrow of about 150 m depth close to the Alpine thrust front was reconstructed. The Molasse basin shows an asymmetric, wedge-shaped depth distribution with its deepest part near the Alpine thrust front and continuously shallowing towards its

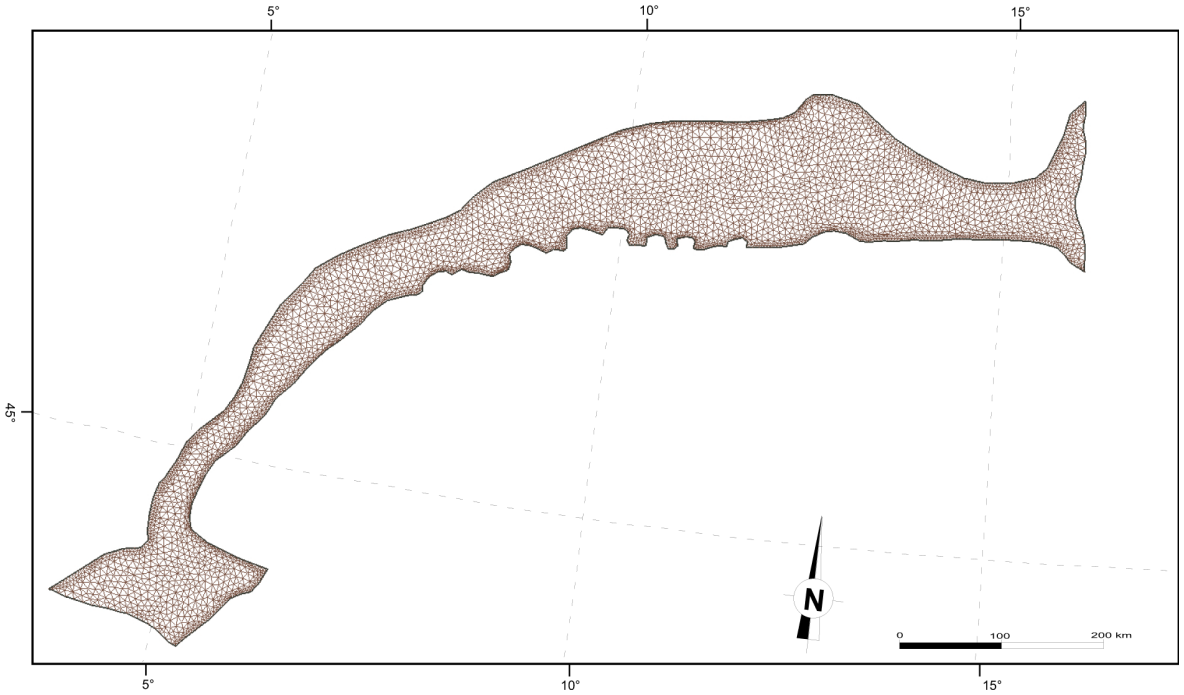

Figure 3.5: *Horizontal finite element mesh discretizing the Burdigalian seaway using linear triangles. Triangulation of the unstructured mesh was done depth dependent. Coastal features are resolved with a higher resolution than deeper areas.*

northern coastline.

3.5 The prognostic time-domain model

3.5.1 General model setup and shallow water physics

We employ a state-of-the-art finite-element circulation model, described in detail by Lynch et al. (1997) and Lynch et al. (1996). The nonlinear time-domain model follows the algorithmic approach of Lynch & Werner (1991) with improvements and extensions. Using a time-stepping finite element method algorithm, the model solves the nonlinear, three dimensional, shallow water equations with the conventional boussinesq and hydrostatic assumptions. The model is three-dimensional, hydrostatic, with a free surface, partially mixed vertically and fully nonlinear. It transports heat, salt and two momentum variables. Both barotropic and baroclinic motions are resolved in tidal time. In this study we used a simple barotropic approach. Vertical mixing is represented by a level 2.5 turbulence closure scheme (Blumberg et al. 1992; Galperin et al. 1988; Mellor & Yamada 1982). Horizontal mixing is represented by a mesh- and shear-dependent eddy viscosity similar to Smagorinsky (1963). The turbulent Reynolds stress and flux terms in the conservation equations for momentum and energy are parameterized in terms of eddy mixing coefficients. Dirichlet boundary conditions at the free surface for the turbulent quantities are included. Variable horizontal resolution is facilitated by the use of unstructured meshes of triangles. The comprehensive model provides shelf-scale geographic coverage to resolve local coastal features like tidal channels, estuaries, headlands, tidal inlets. Because of the representation of involved flow features and shallow water physics it is able to capture all important shelf processes in tidal time. Forcing terms include tides, surface wind stress and the barotropic pressure gradients computed from a prognostic evolving density field. Within this study the model is only driven by the M_2 constituents of tides, specified as a Dirichlet elevation boundary condition across the open ocean boundary at the both ends of the seaway. The describing elevation time series is a linear sinusoidal function.

	France	Switzerland	Germany	Austria
Eggenburgian	Allen & Bass 1993	Homewood & Allen 1981	Erosion	Wagner 1996a
(21-18 Ma)	30-50m	10m		500 m
Ottnangian	Keller 1989	Wenger 1987		Krenmayr 1991
(18-17 Ma)	Schaad 1992	30-50 m		Rögl et al. 1973
	Allen et al. 1985			50-150 m
	10-35 m			Faupl & Rötzl 1987
	Allen & Homewood 1984			<50 m
	25 - 60 m			

Table 3.1: *Palaeobathymetric estimates for the Eggenburgian and Ottnangian deposits of the Molasse basin. The determination of bathymetry is controversial when comparing sedimentary structures and benthic microfossils or ichnofossils (e.g. Krenmayr & Roetzel 1996). Depth information for the German part is poorly constrained. For discussion see text.*

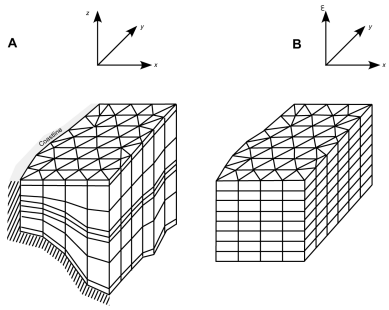

Figure 3.6: *Main features of the 3-D layered mesh: (A) element sides perfectly vertical, variable vertical mesh spacing allows resolution of boundary and internal layers, (B) mesh spacing is uniform in mapped (x,y,e) coordinate system (adopted from Lynch & Naimie 1993).*

The finite element solution is based on the Galerkin weighted residual method, which is discretized by simple linear elements (Fig. 3.6). The horizontal domain is discretized by triangular elements with linear basis functions in a Cartesian coordinate system. The vertical domain is resolved by a terrain following coordinate system that consists of a string of nodes connected by 1-D linear elements. The nodes are allowed to move vertically to track the time-dependent free surface elevation (Lynch 1982). The resulting FE-element is a 6-node prism that can squeeze and stretch vertically in time. The numerical implementation is described in detail discussed by Lynch & Werner (1991).

3.5.2 Computational Setup

Because of the velocities resulting from simple hydrodynamics, the size of the triangles in the unstructured finite element grid is proportional to both bathymetry and the bathymetric gradient. Generally triangles are smaller in regions with shallow water depth and where the gradients are large. The variable mesh is especially useful in coastal regions where the depth of water varies greatly. The minimum size of the elements is roughly 84000 m^2 and the maximum size is roughly 23E6 m^2. The model has 10 to 40 horizontal layers. The vertical spacing of the layers is not uniform. Layers are closer together near the top and bottom (Fig. 3.6). Minimum spacing is roughly one meter in the bottom boundary layer.

3.5.3 Model setup - Boundary Conditions

The presented model is only forced with tidal amplitudes at the open model boundaries (barotropic model). Transport of heat and density (baroclinic), both as forcing due to wind and point sources (rivers and fan deltas), is so far excluded and a topic for further research. The simulation is initiated with a time step of 15 sec., 4 non-linear iterations per time step and terminated after 12 M2 cycles, well after dynamical equilibrium is established. Bottom stress was employed using a nonlinear quadratic form with a drag coefficient value Cc.The drag coefficient value Cc has been discussed to range between .0025 or .0050 (see sections in Sündermann & Lenz 1983). Most authors have chosen a Cc value of 0.0025. Recently, Werner et al. (2003) published drag coefficient values of 3.0+/-0.1 x10-3 measured at the Georges Bank. Taking a Cd of 0.005, we used a rather high value to account for greater bed roughness due to tidal bedforms (see also Martel et al. 1994). Crumeyrolle et

al. (1991) proposed a macro-tidal regime for the Digne area in SE France. Initial simulation results showed that this can be fulfilled if a tidal-amplitude of 2 m is used at the southern open boundary of the model. On the eastern bounudary of the model mesotidal ranges (2 - 4 m) are assumed based on Faupl & Roetzel (1987) and Krenmayr & Roetzel (1996). In the frame of our simulations we tested tidal amplitudes of 2 and 1 m (Fig. 3.10, 3.13). The calculated residual velocities are giving the net vector of currents within one tidal cycle and can provide information on the time averaged and thus effective palaeotransport directions. Using systematically different phases lags between the two M2 constituents, we studied how the basinwide magnitude and direction of the residual velocities are established and in how far unique transport pattern may have existed.

3.6 Some semi-quantitative considerations about tidal waves

To explain the tidal amplitudes (respectively tidal ranges) and the complicate pattern of residual current velocities in the studied Burdigalian seaway (compare Fig. 3.10 to 3.14), we start with some principal considerations about tidal waves in a simple setup. First we will consider a 1D-case of two propagating two-dimensional, semi-diurnal, lunar M2 waves, travelling towards each other (Fig. 3.7). In the presented case both incident waves are initiated in-phase (for an out-of-phase example see Fig. 3.14). The length of the basin l is a multiple of the quarter wavelength of the M2 tidal wave (basin length is equivalent to 5/4 of the M2 wavelength), as must be assumed for the area of interest. Considering this, the two propagating waves superimpose each other, generating a standing wave (Fig. 3.7-A) with two nodes and 3 anti-nodes. We get a constructive interference between both propagating waves with a maximum of amplitudes in the middle of the travel line. Compared to the case of the Burdigalian seaway this point would be located near Lake Constance. In this simplified case friction is neglected. Considering friction the tidal amplitudes are damped with ongoing travel time. In the 2D-case (Fig. 3.7-A) this leads to a significant modification of the tidal systems, since the incoming wave has a significant higher amplitude than the outgoing wave.

In wide gulfs or seaways, the effect of earth rotation must be taken into consideration. If we include rotation to the system, both incoming waves are deflected to the right due to the coriolis force (northern hemisphere). The resulting pattern is known as a Kelvin wave. The effect of the coriolis force is to convert a standing wave into a rotary wave (Fig. 3.7-B). As the high tide crest of a wave moves up the channel, the flow of water is deflected to the right, causing a higher tide on the right bank and a lower tide on the left (Fig. 3.7-C). During low tide or at the high tide maximum of the counter-propagating wave, the flow of water reverses but is again reflected to the right of its path, so that there is now a weaker ebb-phase on the left bank and a stronger ebb-phase on the right. The net result is a greater range of tidal amplitudes on the right side of the seaway, than on the left.

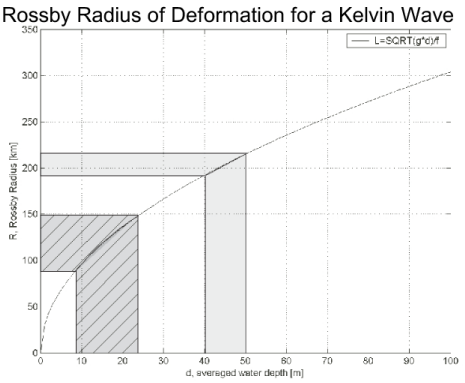

Figure 3.8: *Rossby radius of deformation, showing the requirement of a certain basin width and depth to accommodate an amphidromic system.*

To accommodate a rotary wave and thus to form an amphidromic system, a basin should have a certain width. The so called internal Rossby radius of deformation (Fig. 3.8) describes the exponential decay of a propagating wave (Fig. 3.8). For an averaged basin depth of 50 m, which was used for our study, the seaway should have a width of approximately 200 km to accommodate a complete rotary system. Due to strong frictional effects the amphidromic points are shifted from the center of the seaway to the border. We are now able to apply these theoretical ideas of progressive, standing-/Kelvin-waves and amphidromic sys-

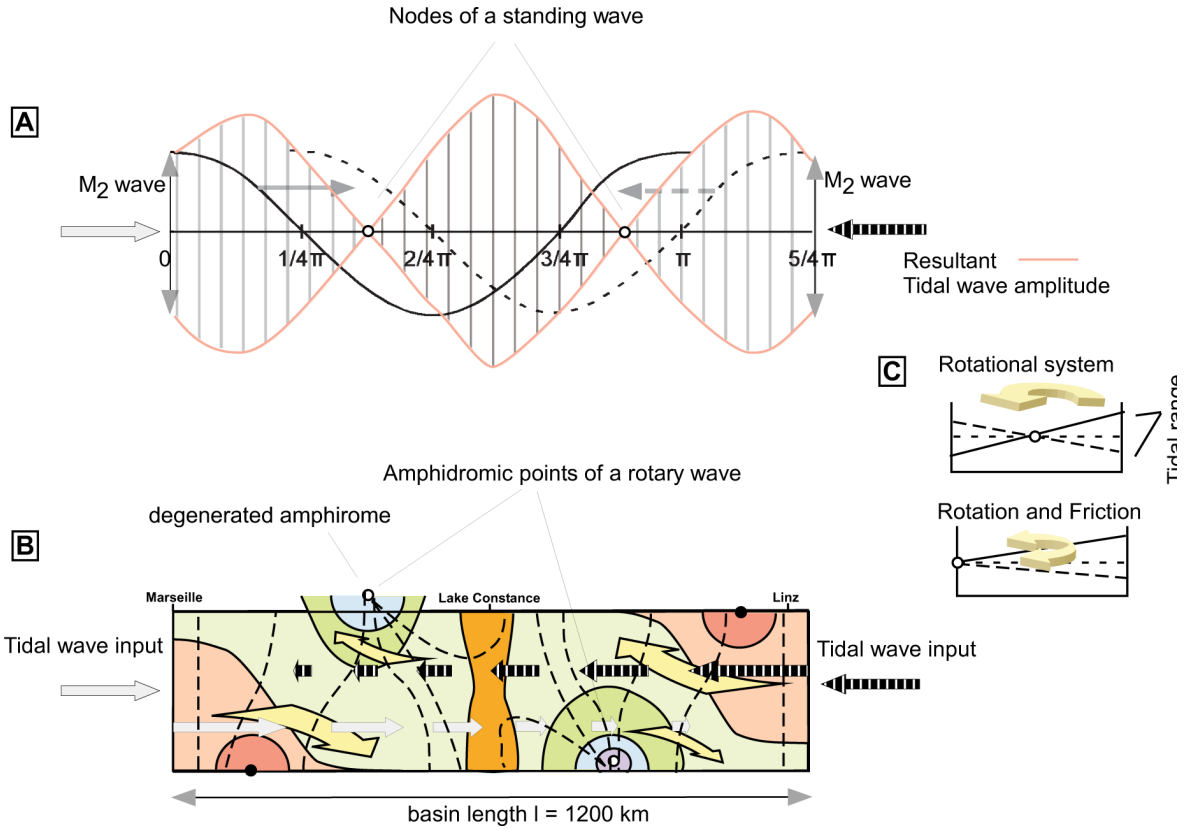

Figure 3.7: *Principal models of the Burdigalian Seaway, assuming two propagating M2 waves from opposite directions. The simplest one-dimensional case (A) shows a standing wave (red line) of two superimposing waves with two nodal points. Within a rotary system (B), the propagating Kelvin waves (yellow arrows) rotate around two amphidromic points anti-clockwise. Friction leads to shift the amphidromic point (C). Part (B) shows the combined effects of a standing wave, within a rotary system and included friction. Contours indicate co-range , dashed-lines indicate co-tidal lines of constant phase.*

tems to describe the dynamics of the simulated tides in the Burdigalian seaway.

3.7 Numerical simulation results

3.7.1 Reference Model - 2 incident M_2 waves of 2m amplitude, being in-phase

In accordance to the above described geological constrains we used, two sinusoidal M_2 waves (T=12,42 h) with an amplitude of 2 m being initiated in-phase as a reference.

Tidal Amplitudes

As in the previous section explained the most significant feature of the tidal system under the given geometric boundary conditions is the build up of two rotary waves, rotating around two static amphidromic points. According to the simulation the two modelled amphidromic points, with no tidal range, are located near Lake Neuenburg in Switzerland and in front of the Nesselburg fan deltas near Bad Tölz in South-Germany. In the Swiss part of the seaway the amphidromic point is located outside the left-hand boundary of the basin and hence the cotidal lines are focusing on an inland point; this situation is called a degenerated amphidrome. Highest amplitudes have been simulated in the area of Linz and in the South of Grenoble indicating amplitudes of up to 3 m. As previously described the highest tidal amplitudes in these areas can result from the deflection of both propagating M_2 waves to the right due to coriolis force. Additionally a funneling effect enhances amplification of tidal amplitudes in these regions. A rotary amphidromic system, which was postulated by Salvermoser (1999)

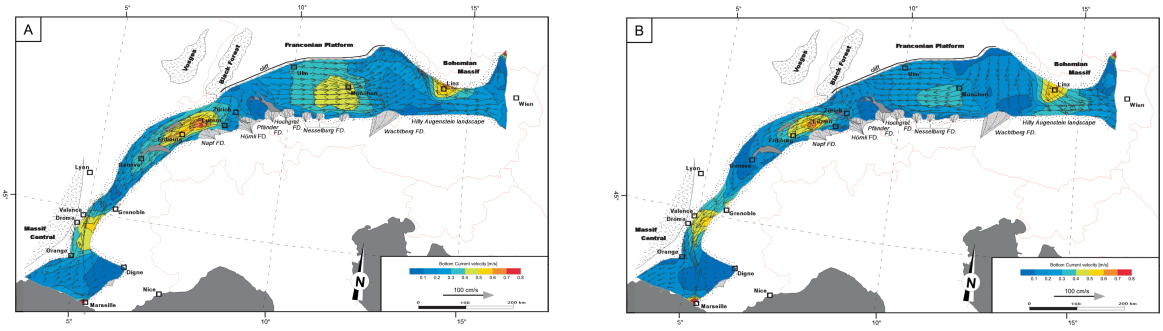

Figure 3.9: *Simulated bottom velocities during incoming flood [A] , respectively incoming ebb [B] in the reference model.*

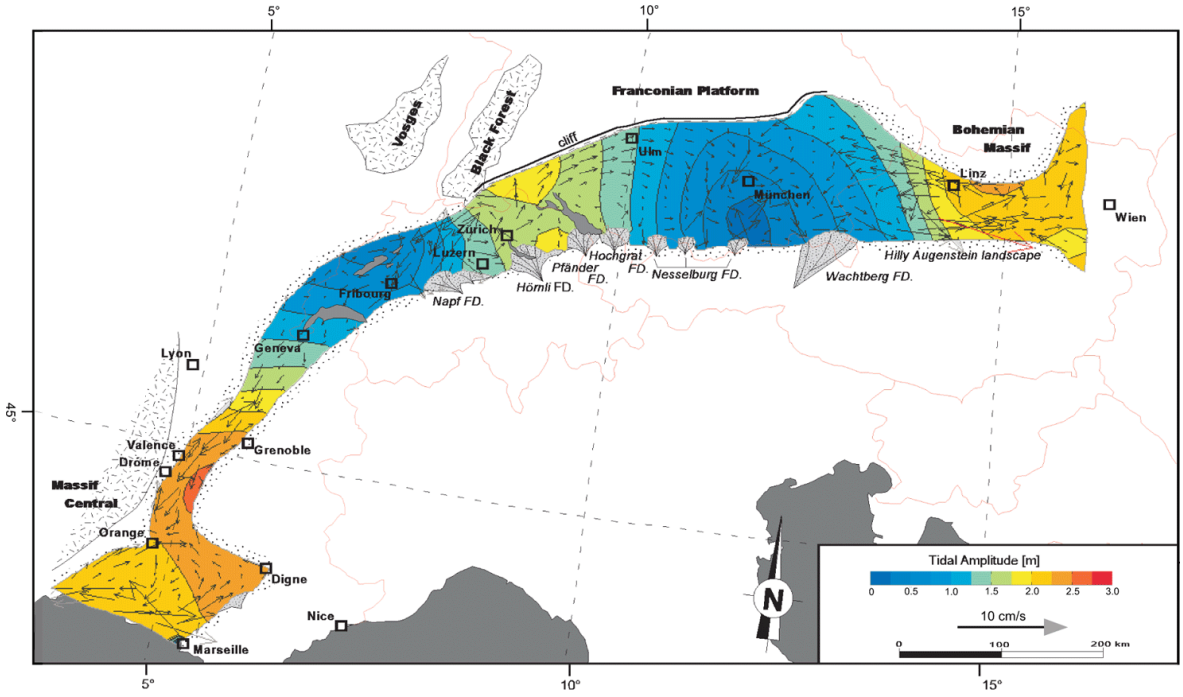

Figure 3.10: *Celerity of the vertically averaged residual currents [cm/s], indicating net transport directions of one ebb/flood cycle after dynamic equilibrium has been reached. Contour lines indicate tidal amplitudes [m]. The model has been forced with two propagating M_2 waves of 2 m amplitude. Coloured areas indicate tidal amplitudes [m].*

in Upper Bavaria/Lower Austria could not be modelled by this simulation. However, considering residual current directions within this region we can explained his observations. In the model it can be observed that residual currents are aligned in a nearly circular way in Upper Bavaria, resulting from a transition from in- to outflow currents.

High to meso-tidal amplitudes, reaching 1.5 to 2 m, are simulated in the mid of the model domain, near Lake Constance, where the two counter-propagating M_2 waves interfere constructive. Maximum tidal amplitudes within this zone can be observed between the Napf and Hörnli fan deltas, showing the tidal dominance within this area and in the vicinity of Tengen (North of Lake Constance).

To the West, in the Rhône-Alp region the banks of the seaway are too close together for the rotary tide to develop (see above for discussion), hence tidal amplitudes are aligned in a right angle to the coastline.

Residual Velocities
After the simulation has reached its dynamic equilibrium, vertically averaged residual current velocities of one ebb/flood cycle can be calculated. In the given model these residual current velocities (Fig. 3.10, 3.11) are interpreted to represent net-transport directions of suspended sediment, or in case that the residual tidal currents are strong enough, also for bedload transport. Residual current velocities of our simulations are within a range of 1-10 cm/s. Compared to peak tidal/ebb velocities (Fig. 3.9), residual velocities are in general less than 10% of the tidal (peak) currents. As an example the threshold velocity for the movement of sediment with median grain size of D50=0,3 mm is 1.4 cm/sec (Allen & Homewood 1984). Under these conditions small ripples can be formed. The transition to larger-scale bedforms (dunes) occurs at approximately 4.5 cm sec/s. Hence residual velocities in the order of 1-8 cm/s of our simulations would only be able to form small scale ripples. However the peak transport velocities were much higher and consequently averaged residual velocities are not very representative for the actual current velocities during the deposition of the sediments.

In the tubular Rhône-Alp region strong residual currents in the order of 5-7 cm/s are modelled, having a subordinate flow direction to the South (Fig. 3.10,3.11). In this area Allen & Bass (1993) interpreted palaeocurrents with a complex pattern and without a dominant direction. In the simulation the Rhône area acts like a bottle neck. Ebb and flood tidal currents have to pass this area and no dominating residual current directions can be established. During ebb and flood this area is under direct influence of the flood and ebb with strong north- or south- directed currents (Fig. 3.9) causing strong turbulences and local eddies.

In the vicinity of Geneva, residual velocities are very weak, being in the order of 1-2 cm/s. Residual currents are mainly directed towards the South. Towards Northeast the region up to Fribourg is characterized by two counter-propagating eddies and residual currents that are directed to the East. Within the seaway highest residual velocities are found in the vicinity of the Napf fan delta and at the opposite coastline of approximately 5-7 cm/s. The bays between the Napf, Hörnli and the Pfänder fan delta are characterized by two clockwise rotating eddies, that form two distinct circulation cells. North of the Napf fan delta convergent residual currents have been modelled, forming a zone of bedload convergence. North-west of Lake Constance (see 3.10 and 3.11), within the area of constructive interference of the two counter-propagating M_2 waves (compare Fig. 3.7), a zone of divergent, strong residual currents can be found, forming a zone of bedload parting (BLP). Summing up, no unique transport direction is modelled for the Swiss part of the seaway.

In front of the Hochgrat and Nesselburg fan deltas, east of the Lake Constance, off- and on-shore directed residual currents can be observed. The northern part of the German seaway is characterized by northeast directed residual currents forming a wide semi-circle with a small-scale enclosed vorticity in the middle part of the basin (Fig. 3.11). Tidal residual currents are alongshore in front of the cliffline. In Bavaria residual vectors are directed southwestward, forming a strong elongated counterclockwise rotating eddy. Residual currents in Austria are characterized by West to Northwest directed residual celerities ($\sim$ 3cm/s) at the Northern coastline and East to Northeast directed currents at the Southern coastline. Over all we observe net-flow towards the Paratethys, whereas the transport to the South-West from the Swiss area can be neglected.

Peak currents
Comparing peak currents of flood and ebb (Fig. 3.9-A,B) we can observe, that regions of two maximal co-oscillating counter-propagating M_2 waves (Fig. 3.7) that act like a divide for ebb and flood flow directions. Outside this "ebb/flood-divide" current branches continue on both sides in opposite directions. It is obvious that regions having the highest residual velocities have the strongest asymmetry between ebb and flood current velocities. For example in the vicinity of Fribourg strong ebb currents, which are in the order of 50-60 cm/s are in contrast to flood currents which are in the order of 40-50 cm/s, show a high asymmetry of tides. On the other hand, while highest residual velocities occur next to the southern and northern coastline west of Lake Constance, highest ebb/flood bottom velocities are aligned in the centre of the seaway

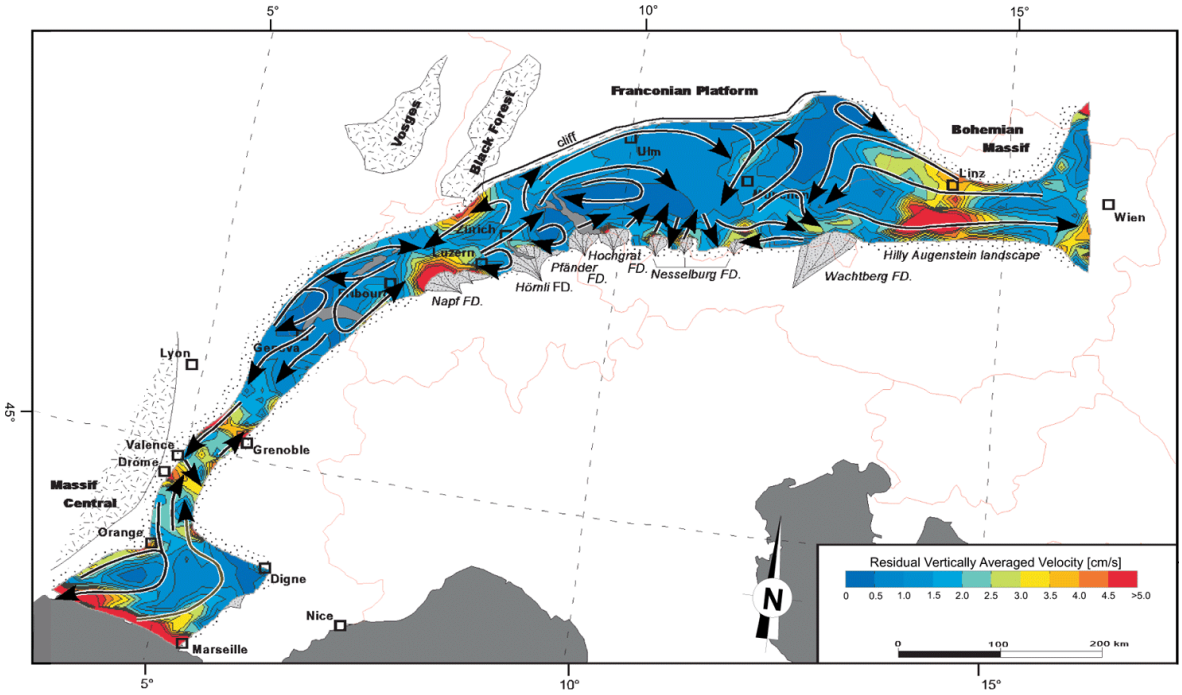

Figure 3.11: *Generalized meso-scale currents within the Burdigalian seaway, deduced from Fig. 9. Contour lines indicate the absolute value of vertically averaged residual velocities [cm/s]; residual values > 5 cm/s can be assumed from Fig. 3.10.*

parallel to the seaway-axis. Two exceptions can be found. One is in the vicinity of Linz and another on is found in the Rhône-Alp region. Here both highest residual velocities and high ebb/flood bottom currents are nearly at the same place. In the vicinity of Linz flood currents are stronger than ebb currents, showing an asymmetry towards the flood tide. Proposed flood peak current velocities in Upper Bavaria of 0,5 m/s (Salvermoser 1999) and 0,75 m/s in Lower Austria (Faupl & Roetzel 1987) can be confirmed with the simulation.

3.7.2 Alternative Models

In the previous chapter we discussed tidal amplitudes and velocity distributions for in-phase excitation with 2 co-oscillating M_2 waves having amplitudes of 2m. Next we will study alternative out-phase excitation and varying M_2 tidal amplitudes for the two M_2 waves. This should give us some ideas about the robustness of the model in terms of amplitudes, current strength and flow directions. We will also review if it is possible to initiate a south-west directed net-transport ("tidal pumping", Kuhlemann 2000) by modifying the reference model.

Alternative 1: One incident M_2 wave, initiated at the southwestern boundary

It was suggested by Sztanó (1995), that the seaway was blocked in Austria during the maximum flooding and acted like a semi-enclosed basin. A tidal wave comming from SE France should be reflected at the closed head of the basin (vicinity of Amstetten). Due to resonance between the incident and the reflected wave, a standing wave should be generated. Fig. 3.12 shows that this is not possible. The tidal wave is damped (tidal friction) on its long way from France to Austria. However the authors identified the standing wave as the main reason why high tidal amplitudes can be observed in the mid of the Burdigalian Seaway.

Alternative 2: Changing the M_2 Amplitude

Changing the M_2 amplitude for the northern open boundary to 1m, nearly the same distribution of tidal amplitudes within the seaway can be observed (Fig. 3.13). A remarkable difference is a general decrease of tidal amplitudes of about

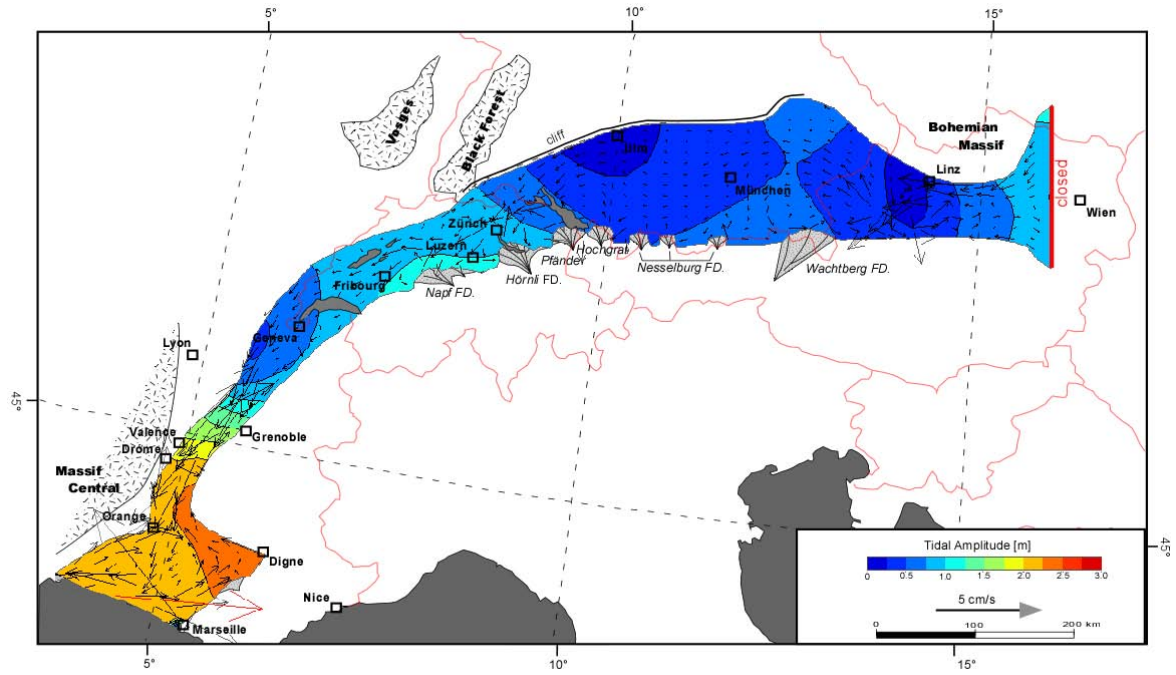

Figure 3.12: *Residual, vertically averaged velocities and tidal amplitudes of an alternative tidal model forced by one incident M_2 wave (2m amplitude) from the southwest (France). The open boundary in Austria was*

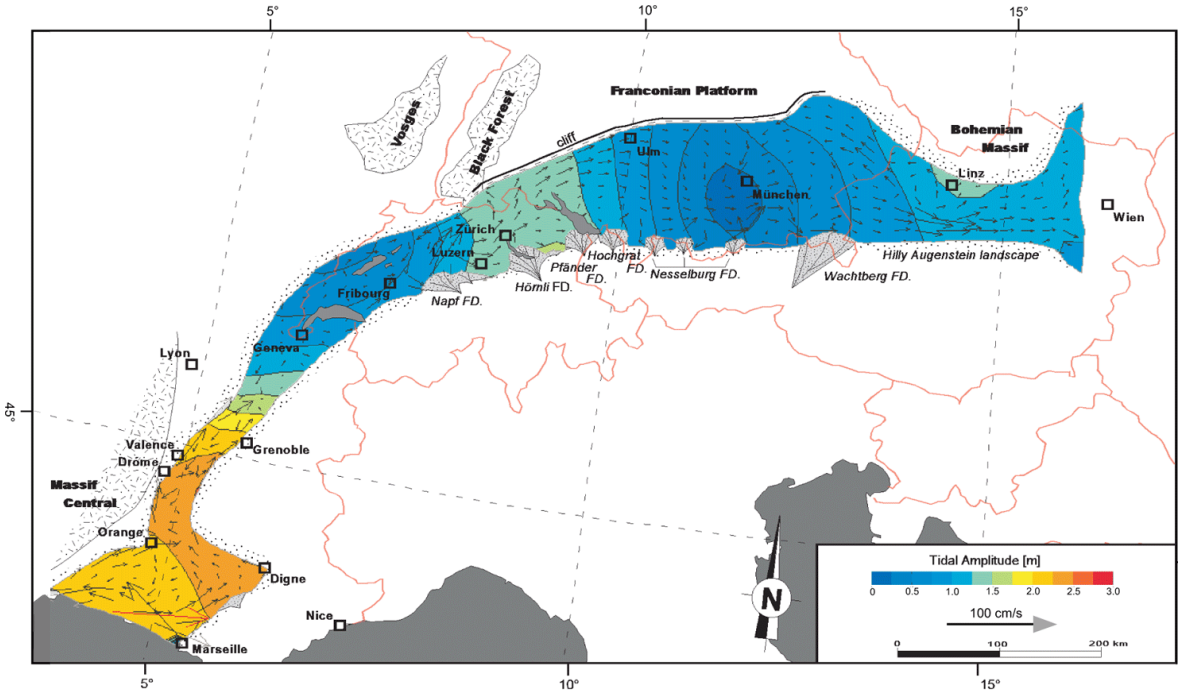

Figure 3.13: *Residual, vertically averaged velocities and tidal amplitudes of an alternative tidal model being forced by two incident M_2 waves. The M_2 constituent from the South was initiated in phase with an amplitude of 2 m, whereas the northern M_2 wave was initiated with 1m.*

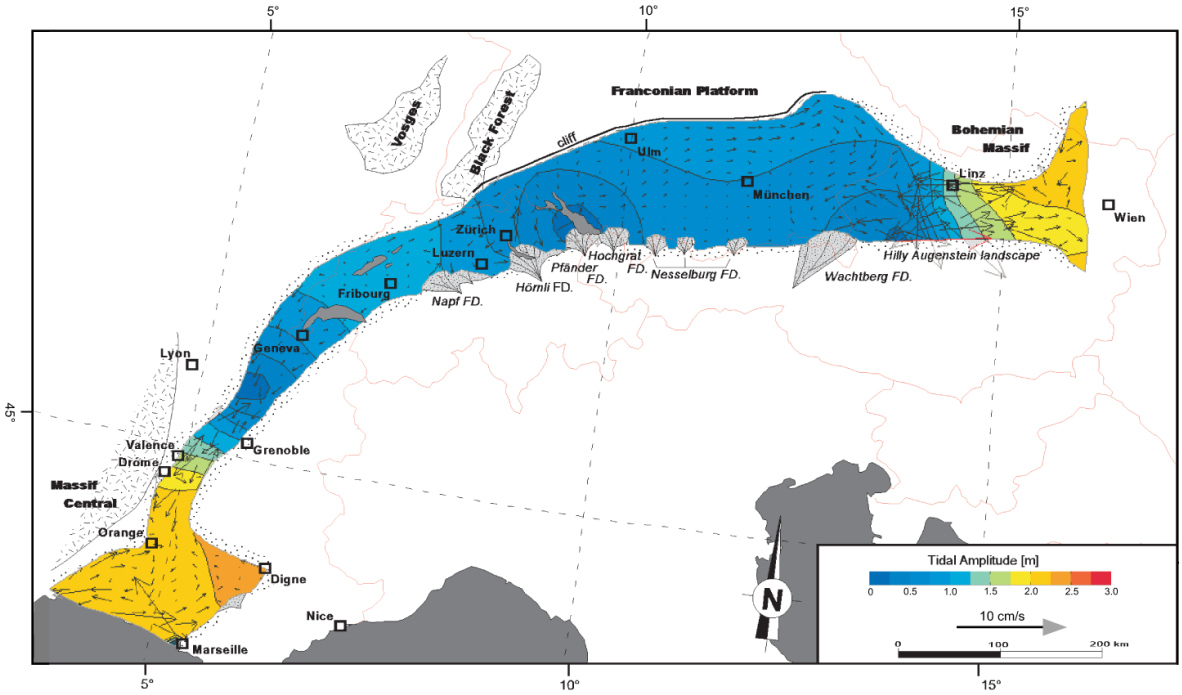

Figure 3.14: *Plot of residual, vertically averaged velocities and tidal amplitudes of an alternative tidal model being in equilibrium state. Both incident M_2 tidal waves have been initiated with an amplitude of 2m, but out-phase with a phaselag of 180°.*

half a meter within the whole seaway. Residual velocities show nearly the same directions. Noticeable differences to Fig. 3.10 are diverting residual currents in the Rhône area suggesting a bedload partition zone in this region and a strong eastward directed residual current at the southern coastline of the Austrian Molasse basin.

Alternative 3: Phaselag of 180° between the two M_2 waves

In a second test we excite the tidal model with two waves of the same amplitude (2 m), but with a phase difference of 180°. The model reacts as the simple considerations in Fig.7 suggest. The two counter-propagating waves interfere destructive in the region of the former maximum amplification, generating a amphidromic point with nearly stationary conditions (Fig. 3.7 A,B). Now, wave crest and trough superimpose destructive. The resulting basin wide tidal ranges, are within 1 - 1.25 m, indicating micro- to low meso-tidal conditions. Such a situation is in contradiction to the sedimentary observations for the Burdigalian seaway (e.g. Homewood et al. 1985). In addition unrealistic "no-flow" conditions in the vicinity of Fribourg are modelled that do not fit the field data.

3.8 Conclusion

We presented a tidal model for the Burdigalian seaway ranging from southern France to Austria. The model is based on and referenced to a palaeogeographic and palaeobathymetric restoration of the seaway during a time of maximum flooding in the Ottnangian. The simulations have shown that tides in the Burdigalian seaway depend upon the nature of the adjacent seas with which they co-oscillate. Additionally the tidal amplitudes and currents are a combination of progressive, standing and rotary waves, including modifying effects of friction and reflection. The best fit to the sedimentological observations is achieved by two 2 m in-phase M_2 tides, acting at the open model boundaries. The resulting two propagating tidal waves cause two rotary amphidromic systems in the seaway. Simulated tidal amplitudes indicate high meso-tidal ranges for the Swiss area (3-4 m), comparable to outcrop descriptions and previous simulations by Martel et al. (1994). Comparing vertically averaged residual velocities of a

ebb-flood cycle with ebb/flood peak velocities, it can be shown that residual velocities are about ten times smaller that ebb/flood peak velocities. Hence residual velocities are interpreted to represent net-transport directions, whereas peak velocities characterize sediment transport in e.g. ripples, dunes or large sandwaves. Based on the recording of velocities it can be shown, that there are symmetric and asymmetric tides depending on the duration and intensity of ebb and flood currents. Net-transport directions follow a complicate pattern of vortices, convergent or divergent currents. The tube-like transfer zone of tidal waves in the Rhône-Alp area is characterized by a diffusive pattern of netflow directions and strengthens with a subordinate flow direction to the South. The simulations so far do not show a clear southwest transport of sediments as proposed by Kuhlemann (2000). Further simulations are necessary to test additional factors like prevailing wind directions. Peak current velocities have been simulated up to 0,8 m/s. These values compare well with modern tide-influenced seas, where active migration of sand waves is possible (e.g. Dalrymple et al. 1990). Although residual velocities seem to be very small (1-8 cm/s), recent examples (e.g. Harris 1991) have shown, that this might have significant influence on the net sediment transport.

3.9 References

Allen, J.R.L. (1981): Palaeotidal speeds and ranges estimated from cross-bedding sets with mud drapes. *Nature*, **293**: 394-396.

Allen, P.A. (1984): Reconstruction of ancient sea conditions with an example from the Swiss Molasse. *Marine Geology*, **60**: 455-473.

Allen, P.A. and Bass, J.P. (1993): Sedimentology of the Upper Marine Molasse of the Rhône-Alp region, Eastern France: Implications for basin evolution. *Eclogae geologicae Helvetiae*, **86**: 121-171.

Allen, P.A. and Homewood, P. (1984): Evolution and mechanics of a Miocene tidal sandwave. *Sedimentology*, **31**: 63-81.

Allen, P.A., Mange-Rajetzky, M., Matter, A. and Homewood, P. (1985): Dynamic palaeogeography of the open Burdigalian seaway, Swiss Molasse basin. *Eclogae geologicae Helvetiae*, **78**: 351-381.

Assemat, S. (1991): Récherche et analyse des tidalites dans la molasse marine marine miocène du domaine subalpin, dans la région de Frangy-Rumilly-Aix-les-Bains. *Mém. D.E.A. Univ. de Savoie, Chambéry.*

Bachmann, G.H. and Müller, M. (1991): The Molasse Basin, Germany: evolution of a classic petroliferous foreland basin. In: *Generation, accumulation, and production of Europe's hydrocarbons* (Eds A.M. Spencer), *Special Publication of the European Association of Petroleum Geoscientists*, **1**, pp. 263-276. EAPG (European Association of Petroleum Geoscientists).

Bachmann, G.H. and Müller, M. (1992): Sedimentary and structural evolution of the German Molasse Basin. *Eclogae geologicae Helvetiae*, **85**: 519-530.

Berger, J.-P. (1983): Biostratigraphie de la transgression de la molasse marine superieure (OMM) en Suisse occidentale. *Eclogae Geologicae Helvetiae*, **76**: 729-732.

Berger, J.-P. (1996): Cartes paléogéographiques-palinspastiques du bassin molassique suisse (Oligocène inférieur - Miocène moyen). *Neues Jahrbuch für Geologie und Paläontologie, Abhandlungen*, **202**: 1-44.

Berggren, W.A., Kent, D.V., Swisher, C.C. and Aubry, M.-P. (1995): A revised Cenozoic geochronology and chronostratigraphy. In: *Geochronology, time scales and global stratigraphic correlations* (Eds W.A. Berggren, D.V. Kent, M.-P. Aubry and J. Hardenbol), *SEPM, Special Publications*, **54**, pp. 17-28, Tulsa.

Blumberg, A.F., Galperin, B. and O'Connor, D.J. (1992): Modeling vertical structure of open-channel flows. *ASCE, J. Hydraulic Engg.*, **118**: 1119-1134.

Büchi, U.P., Colombi, C., Fehr, W.R., Lemcke, K., Koewing, K., Hofmann, F., Füchtbauer, H. and Trümpy, R. (1961): Geologische Ergebnisse der Bohrung Küsnacht 1. *Bulletin der Vereinigung Schweizerischer Petroleum-Geologen und -Ingenieure*, **28**: 7-16.

Büchi, U.P. and Hofmann, F. (1960): Die Sedimentationsverhältnisse zur Zeit der Muschelsandsteine und Grobkalke im Gebiet des Beckennordrandes der Oberen Meeresmolasse zwischen Aarau und Schaffhausen. *Bulletin der Vereinigung Schweizerischer Petroleum-Geologen und -Ingenieure*, **27**: 11-22.

Büchi, U.P. and Schlanke, S. (1977): Zur Paläogeographie der schweizerischen Molasse. *Erdöl-Erdgas-Zeitung*, **93**: 57-69.

Burkhard, M. and Sommaruga, A. (1998): Evolution of the western Swiss Molasse basin: structural relations with the Alps and the Jura belt. In: *Cenozoic Foreland Basins of Western Europe* (Eds A. Mascle, C. Puigdefàbregas, H.P. Luterbacher and M. Fernàndez), *Geological Society Special Publication*, **134**, pp. 279-298.

Crumeyrolle, P., Rubinio, J.-L. and Clauzon, G. (1991): Miocene depositional sequences within a tectonically -controlled transgressive-regressive cycle. In: *Spec. Publ. internat. Assoc. Sedimentol.* (Eds D.I.M. McDonald), **12**, pp. 373-390.

Dalrymple, R.W., Knight, R.J., Zaitlin, B.A. and Middleton, R.V. (1990): Dynamics and facies model of a macro-tidal sand-bar complex, Cobequid Bay-Salmon River Estuary (Bay of Fundy). *Sedimentology*, **37**.

Debrand-Passard, S., Courbouleix, S. and Lienhardt, M.J. (1984): Synthese geologique du sud-est de la France. Geologic synthesis of southeastern France. *Memoires du B.R.G.M.*, **125-126**: 615.

Demarcq, G. (1970): *Etude stratigraphique du Miocène rhodanien.* Mem. BRGM, **61**, 257 pp.

Demarcq, G. and Perriaux, J. (1984): Neogene. In: *Synthèse géologique du Sud-Est de la France: Stratigraphie et paléogeographie* (Eds D.-P.e. al.), **Bu-**

reau de Récherches Géologiques et Minières, Mémoire 125, pp. 469-519.

Deville, E., Blanc, E., Tardy, M., Beck, C., Cousin, M. and Ménard, G. (1994): Thrust propagation and syntectonic sedimentation in the Savoy Tertiary Molasse basin (Alpine foreland). In: *Hydrocarbon and Petroleum Geology of France. Special Publications of of the European Association of Petroleum Geoscientists* (Eds A. Mascle), **4**, pp. 269-280. Springer-Verlag.

Diem, B. (1985): Analytical method for estimating palaeowave climate and water depth from wave ripple marks. *Sedimentology*, **32**: 705-720.

Doppler, G. (1989): Zur Stratigraphie der nördlichen Vorlandmolasse in Bayrisch-Schwaben. *Geologica Bavarica*, **94**: 83-133.

Faupl, P. and Roetzel, R. (1987): Gezeitenbeeinflußte Ablagerungen der Innviertler Gruppe (Ottnangien) in der oberösterreichischen Molassezone. *Jahrbuch der Geologischen Bundesanstalt Wien*, **130**: 415-447.

Faupl, P. and Roetzel, R. (1990): Die Phosphoritsande und Fossilreichen Grobsande; Gezeitenbeeinflusste Ablagerungen der Innviertler Gruppe (Ottnangien) in der oberoesterreichischen Molassezone. *Jahrbuch der Geologischen Bundesanstalt Wien*, **132**: 157-180.

Ford, M., Lickorish, W.H. and Kusznir, N.J. (1999): Tertiary foreland sedimentation in the Southern Subalpine Chains, SE France: a geodynamical appraisal. *Basin Research*, **11**: 315-336.

Gall, H. (1974): Neue Daten zum Verlauf der Klifflinie der oberen Meeresmolasse (Helvet) im südlichen Vorries. *Mitt. Bayer. Stattssamml. Paläont. hist. Geol.*, **14**: 81-101.

Gall, H. (1975): Der III. Zyklus der oberen Meeresmolasse (Helvet) am Südrand der Schwäbisch-Fränkischen Alb. *Mitt. Bayer. Stattssamml. Paläont. hist. Geol.*, **15**: 179-205.

Galperin, B., Kantha, L.H., Hassid, S. and Rosati, A. (1988): A quasi-equilibrium turbulent energy model for geophysical flows. *Journal of Atmospheric Science*, **45**: 55-62.

Guellec, S., Mugnier, J.L., Tardy, M. and Roure, F. (1990): Neogene evolution of the western alpine foreland in the light of ECORS data and balanced cross-section. In: *Deep structure of the Alps* (Eds F. Roure, P. Heitzmann and R. Polino), *Mémoire du Société Géologique de France*, **156**, pp. 165-184.

Haq, B.U., Hardenbol, J. and Vail, P.R. (1987): Chronology of fluctuating sea levels since the Triassic. *Science*, **235**: 1156-1167.

Haq, B.U., Hardenbol, J. and Vail, P.R. (1988): Mesozoic and Cenozoic chronostratigraphy and cycles of sea-level change. In: *Sea-level changes: An integrated approach* (Eds C.K. Wilgus et al.), *SEPM, Special Publications*, **42**, pp. 71-108. SEPM (Society of Economic Paleontologists and Mineralogists), Tulsa.

Harris, R.T. (1991): Reversal of subtidal dune asymmetries caused by seasonally reversing wind driven current in Torres Strait, Australia. *Continental Shelf Research*, **11(7)**: 979-1003.

Haus, H.A. (1951): Zur paläogeographischen Entwicklung des Molassetroges im Bodenseegebiet während des mittleren Miozäns. *Mitteilungsblatt der badischen geologischen Landesanstalt*, **1950**: 48-66.

Homewood, P. and Allen, P. (1981): Wave-, tide-, and current-controlled sandbodies of Miocene molasse, Western Switzerland. *American Association of Petroleum Geologists, Bulletin*, **65**: 2534-2545.

Homewood, P., Allen, P.A. and Williams, G.D. (1986): Dynamics of the Molasse Basin of western Switzerland. In: *Foreland Basins* (Eds P.A. Allen and P. Homewood), *IAS, Special Publications*, **8**, pp. 199-217. Blackwell Scientific Publications, Oxford.

Homewood, P., Allen, P.A. and Yang, C.S. (1985): Palaeotidal range estimates from the Miocene Molasse. In: *Abstr. 6th int. Ass. Sediment. Reg. Mtg.*, pp. 200-201, Lleida.

Hülsemann, J. (1955): Großrippeln und Schrägschichtungs-Gefüge im Nordsee Watt und in der Molasse. *Senck. leth.*, **36**: 359-388.

Keller, B. (1989): *Fazies und Stratigraphie der Oberen Meeresmolasse (Unteres Miozän) zwischen Napf und Bodensee*. Unpubl. PhD Thesis, Universität Bern, Bern, 402 p pp.

Kempf, O., Bolliger, T., Kälin, D., Engesser, B. and Matter, A. (1997): New magnetostratigraphic calibration of Early to Middle Miocene mammal biozones of the North Alpine foreland basin. In: *Actes du Congrès BiochroM'97* (Eds J.-P. Aguilar, S. Legendre and J. Michaux), *Mémoires et Travaux de l' E.P.H.E.*, **21**, pp. 547-561, Montpellier.

Kempf, O., Matter, A., Burbank, D.W. and Mange, M. (1999): Depositional and structural evolution of a foreland basin margin in a magnetostratigraphic framework: the eastern Swiss Molasse basin. *International Journal of Earth Sciences*, **88**: 253-275.

Kiderlen, H. (1931): Beiträge zur Stratigraphie und Paläogeographie des süddeutschen Tertiärs. *Neues Jahrbuch für Mineralogie, Geologie und Paläontologie*, **66**: 215-384.

Krenmayr, H.G. (1991): Sedimentologische Untersuchungen der Vöklaschichten (Innviertler Gruppe, Ottnangian) in der oberösterreichischen Molassezone im Gebiet der Vökla und der Ager. *Jahrbuch der Geologischen Bundesanstalt Wien*, **137**: 83-100.

Krenmayr, H.G. and Roetzel, R. (Eds) (1996): *Oligozäne und miozäne Becken- und Gezeitensedimente in der Molassezone Oberösterreichs, Exkursionsführer Sediment '96, Exkursion B2*, **33**. Geologische Bundesanstalt, Wien, 17 Abb., 43 pp.

Kuhlemann, J. (2000): Post-collisional sediment budget of circum-Alpine basins (Central Europe). *Memoire di Scienze Geologiche Padova*, **52**: 1-91.

Kuhlemann, J. and Kempf, O. (2002): Post-Eocene evolution of the North Alpine Foreland Basin and its response Alpine tectonics. *Sedimentary Geology*, **152**: 45-78.

Laubscher, H. (1965): Ein kinematisches Modell der Jurafaltung. *Eclogae geologicae Helvetiae*, **58**: 231-318.

Laubscher, H. (1992): Jura Kinematics and the Molasse Basin. *Eclogae geologicae Helvetiae*, **85**: 653-675.

Lemcke, K. (1973): Zur nachpermischen Geschichte des nördlichen Alpenvorlandes. *Geologica Bavarica*, **69**: 5-48.

Lemcke, K. (1988): *Geologie von Bayern. - I. Teil: Das bayerische Alpenvorland vor der Eiszeit*, **I**. E. Schweizerbart'sche Verlagsbuchhandlung, Stuttgart, 175 p pp.

Lickorish, W.H. and Ford, M. (1998): Sequential restoration of the external Alpine Digne thrust system, SE France, constrained by kinematic data and synorogenic sediments. In: *Cenozoic Foreland Basins of Western Europe* (Eds A. Mascle, C. Puigdefàbregas, H.P. Luterbacher and M. Fernàndez), *Geological Society Special Publication*, **134**, pp. 299-323, London.

Loutit, T.S., Hardenbol, J., Vail, P.R. and Baum, G.R. (1988): Condensed sections: the key to age datings and correlation of continental margin sequences. In: *Sea-level Changes: An Integrated Approach* (Eds C.K. Wilgus et al.), **42**, pp. 183.213. Soc. Econ. Paleontol. Mineral., Spec. Publ.

Luterbacher, H. (1997): Stratigraphy and facies evolution of a typical foreland basin; the Tertiary Molasse Basin (Lake Constance area and Allgäu). In: *18th IAS regional European meeting of sedimentology, Heidelberg, September 2-4, 1997; field trip guidebook* (Eds T. Bechstädt, P. Bengtson, R. Gaupp, R. Greiling and V. Schweizer), *Gaea Heidelbergensis*, **4**, pp. 123-140, Heidelberg.

Luterbacher, H., Köhler, J. and Winder, H. (1992): The northern margin of the Molasse Basin in SW Germany. *Eclogae geologicae Helvetiae*, **85**: 787-788.

Lynch, D.R. (1982): Unified Approach to Simulation on Deforming Elements, with Application to Phase Change. *Journal of Computational Physics*, **47**: 387-411.

Lynch, D.R., Holbroke, M.J. and Naimie, C.E. (1997): The Marine Coastal Current: Spring Climatological Circulation. *Continental Shelf Research*, **17**: 605-634.

Lynch, D.R., Ip, J.T.C., Naimie, C.E. and Werner, F.E. (1996): Comprehensive Coastal Circulation Model with Application to the Gulf of Maine. *Continental Shelf Research*, **12**: 37-64.

Lynch, D.R. and Werner, F.E. (1991): Three-Dimensional Hydrodynamics on Finite Elements. Part II: Non-linear Time-stepping Model. *International Journal for Numerical Methods in Fluids*, **12**: 507-533.

Malzer, O., Rögl, F., Seifert, P., Wagner, L., Wessely, G. and Brix, F. (1993): Die Molassezone und deren Untergrund. In: *Erdöl und Erdgas in Österreich* (Eds F. Brix and O. Schultz) 2nd edn, pp. 281-322. Naturhistorisches Museum Wien, Wien.

Martel, A.T., Allen, P.A. and Slingerland, R. (1994): Use of tidal-circulation modeling in paleogeographical studies: An example from the Tertiary of the Alpine perimeter. *Geology*, **22**: 925-928.

Matter, A., Homewood, P., Caron, C., Rigassi, D., Stuijvenberg, J.v., Weidmann, M. and Winkler, W. (1980): Flysch and Molasse of western and central Switzerland (Excursion No. 5). In: *Geology of Switzerland, a guide-book* (Eds R. Trümpy), *Schweizerische Geologische Kommission*, **Part B**, pp. 261-293. Wepf, Basel.

Mellor, G.L. and Yamada, T. (1982): Development of a turbulence closure model for geophysical fluid problems. *Reviews of Geophysics Space Physics*, **20**: 851-875.

Mugnier, J.L. and Menard, G. (1986): Le developpement du bassin molassique suisse et l'evolution des Alpes externes; un modele cinematique. Development of a Swiss molasse basin in the external Alps; a kinematic model. In: *La subsidence des bassins sedimentaires; Seminaire organise en hommage et a la memoire d'Etienne Winnock. Subsidence of sedimentary basins; a seminar organized in homage to and in memory of Etienne Winnock* (Eds Anonymous), **10 (1)**, pp. 167-180. Bulletin des Centres de Recherches Exploration-Production Elf-Aquitaine.

Naef, H., Diebold, P. and Schlanke, S. (1985): *Sedimentation und Tektonik im Tertiär der Nordschweiz.* NAGRA Technischer Bericht, **85-14**, 145 p pp.

Ritz, F. (1991): *Evolution du champ de contraintes dans les Alpes du Sud depuis la fin de l'Oligocène. Imlications sismotectoniques.* PhD thesis, Montpellier.

Roetzel, R. and Rupp, C. (1991): E/8 - Die westliche Molassezone in Salzburg und Oberösterreich. In: *Exkursionen im Tertiär Österreichs - Molassezone-Waschbergzone-Korneuburger Becken-Wiener Becken-Eisenstädter Becken* (Eds R.N. Roetzel, D.), pp. 114-57. Österreichische Paläontologische Gesellschaft, Wien.

Rögl, F. (1996): Stratigraphic correlation of the Paratethys Oligocene and Miocene. *Mitt. Ges. Geol. Bergbaustud. Österr.*, **41**: 65-73.

Rögl, F. (1999): Mediterranean and Paratethys. Facts and Hypotheses of an Oligocene to Miocene Paleogeography (short overview). *Geologica Carpathica*, **50**: 339-349.

Rögl, F. and Steininger, F.F. (1983): Vom Zerfall der Tethys zu Mediterran und Paratethys. Die neogene Paläogeographie und Palinspastik des zirkummediterranen Raumes. *Ann. Naturhist. Mus. Wien*, **85/A**: 135-163.

Rögl, F. and Steininger, F.F. (1984): *Neogene Patatethys, Mediterranean and Indo-pacific Seaways.* Fossils and Climate. John Wiley & Sons.

Rutte, E. (1952): Grobsand und Muschelsandstein in der miozänen Meeresmolasse des nordwestlichen Bodenseegebietes. *N. Jb. Geol. Paläont. Abh.*, **Mh**: 295-304.

Salvenmoser, S. (1999): Zur Sedimentologie gezeitenbeeinflusster Sande in der Oberen Meeresmolasse und Süssbrackwassermolasse (Ottnangium) von Niederbayern und Oberösterreich. *Münchner Geologische Hefte (A)*, **26**: 1-179.

Salvermoser, S. (1999): Zur Sedimentologie gezeitenbeeinflusster Sande in der Oberen Meeresmolasse und Süssbrackwassermolasse (Ottnangium) von Niederbayern und Oberösterreich. *Münchner Geologische Hefte (A)*, **26**: 1-179.

Schaad, W., Keller, B. and Matter, A. (1992): Die Obere Meeresmolasse (OMM) am Pfänder: Beispiel eines Gilbert-Deltakomplexes. *Eclogae geologicae Helvetiae*, **85**: 145-168.

Schlunegger, F., Burbank, D.W., Matter, A., Engesser, B. and Mödden, C. (1996): Magnetostratigraphic calibration of the Oligocene to Middle Miocene (30-15 Ma) mammal biozones and depositional sequences of the Swiss Molasse Basin. *Eclogae geologicae Helvetiae*, **89**: 753-788.

Schlunegger, F. and Hinderer, M. (2001): Crustal uplift in the Alps: Why the drainage pattern matters. *Terra Nova*, **13**.

Schlunegger, F., Leu, W. and Matter, A. (1997): Sedimentary sequences, Seismic Facies, Subsidence Analysis, and Evolution of the Burdigalian Upper

Marine Molasse Group (OMM), Central Switzerland. *American Association of Petroleum Geologists, Bulletin*, **81**: 1185-1207.

Schlunegger, F., Matter, A., Burbank, D.W. and Klaper, E.M. (1997): Magnetostratigraphic constraints on relationships between evolution of the central Swiss Molasse basin and Alpine orogenic events. *Geological Society of America, Bulletin*, **109**: 225-241.

Schlunegger, F., Matter, A. and Mange, M.A. (1993): Alluvial fan sedimentation and structure of the southern Molasse Basin margin, Lake Thun area, Switzerland. *Eclogae geologicae Helvetiae*, **86**: 717-750.

Schreiner, A. (1976): *Hegau und westlicher Bodensee*. Sammlung Geologischer Führer, **62**. Gebr. Bornträger, Berlin - Stuittgart, 337 pp.

Schreiner, A. and Luterbacher, H. (1999): Die Molasse zwischen Blumberg und Überlingen (Exkursion J am 9. April 1999. *Jahresberichte der Mitteilungen der oberrheinischen geologischen Vereinigung, Neue Folge*, **81**: 171-181.

Sinclair, H.D., Coakley, B.J., Allen, P.A. and Watts, A.B. (1991): Simulation of foreland basin stratigraphy using a diffusion model of mountain belt uplift and erosion: an example from the central Alps, Switzerland. *Tectonics*, **10**: 599-620.

Smagorinsky, J. (1963): General circulation experiments with the primitive equations I. The basic experiment. *Monthly Weather Review*, **91**.

Steininger, F. and Rögl, F. (1979): The Paratethys history - A contributiontowards the Neogene geodynamics of the Alpine Orogene (an abstract). *Annales géologique des pays Hellèniques, (hors serie)*, **3**: 1153-1165.

Steininger, F.F., Berggren, W.A., Kent, D.V., Bernor, R.L., Sen, S. and Agusti, J. (1996): Circum-Mediterranean Neogene (Miocene and Pliocene) marine-continental chronologic correlations of European mammal units. In: *The Evolution of Western Eurasian Neogene Mammal Faunas* (Eds R.L. Bernor, V. Fahlbusch and H.-W. Mittmann), pp. 7-46. Columbia University Press, New York.

Sündermann, J. and Lenz, W. (1983): *North Sea Dynamics*. Springer-Verlag.

Sztanó, O. & de Boer, P.L. (1995): Basin dimensions and morphology as controls on amplification of tidal motions (the early Miocene North Hungarian Bay). *Sedimentology*, **42**: 665-682.

Tessier, B. and Gigot, P. (1989): A vertical record of different tidal cyclicities: an example from the Miocene Molasse of Digne (Haute Provence, France). *Sedimentology*, **36**: 767-776.

Wagner, L. (1996): Stratigraphy and hydrocarbons in the Upper Austrian Molasse Foredeep (active margin). In: *Oil and Gas in the Alpidic Thrustbelts and Basins of the Central and Eastern Europe* (Eds G. Wessely and W. Liebl), **5**, pp. 217-235. EAGE Special Publication, London.

Wagner, L. (1998): Tectono-stratigraphy and hydrocarbons in the Molasse Foredeep of Salzburg, Upper and Lower Austria. In: *Cenozoic Foreland Basins* (Eds A. Mascle, C. Puigdefàbregas, H. Luterbacher and M. Fernàndez), **134**. Geological Society, Special Publications, London.

Wagner, L., Kuckelkorn, K. and Hiltmann (1986): Neue Ergebnisse zur alpinen Gebirgsbildung Oberösterreichs aus der Bohrung Oberhofen 1 - Stratigraphie, Fazies, Maturität und Tektonik. *Erdöl-Erdgas-Zeitschrift*, **102(1)**.

Werner, S.R., Beardsley, R.C. and Williams, A.J. (2003): Bottom friction and bed forms on the southern flank of Georges Bank. *Journal of Geophysical Research*, **108**: (C11), 8004, doi:10.1029/2000JC000692.

Zweigel, J. (1998): Reservoir analogue modelling of sandy tidal sediments, Upper Marine Molasse, SW Germany, Alpine foreland basin. In: *Cenozoic Foreland Basins of Western Europe* (Eds A. Mascle, C. Puigdefàbregas, H.-P. Luterbacher and M. Fernàndez), *Geological Society Special Publication*, **134**, pp. 325-337.

Zweigel, J., Aigner, T. and Luterbacher, H. (1998): Eustatic versus tectonic controls on Alpine foreland basin fill: sequence stratigraphy and subsidence analysis in the SE German Molasse. In: *Cenozoic Foreland Basins of Western Europe* (Eds A. Mascle, C. Puigdefàbregas, H.P. Luterbacher and M. Fernàndez), *Geological Society Special Publication*, **134**, pp. 299-323, London.

Chapter 4

Cross-stratified calcarenites: Nearshore deposits of the OMM and their transition towards the OSM (North Alpine Foreland Basin, Early Miocene)

4.1 Abstract

During early Ottnangian (c. 17.8 Ma) the central Molasse Basin was flooded by the shallow Upper Marine Molasse sea. In turn of the maximum flooding the Randengrobkalk, a bioclastic grainstone, was deposited at the northern coastline. The Randengrobkalk is separated into different sedimentary facies types according to sedimentary structures and the admixture of siliciclastics and carbonates. The bathymetric gradient from the coastline to the deeper water was dictated by the underlying morpohology of the Jurassic limestone, that was flexed down by the orogenic loading of the alpine orogene. This forms a bathymetric gradient, comparable to a shallow ramp.

Vertical and lateral transitions from carbonate to mixed siliciclastic-carbonate deposits are interpreted to represent a transition from a distal to proximal environment and thus progradation of the OMM coastline due to uplift or sea-level fall. Conglomeratic channel fill deposits of Alpine origin, are interpreted to form a 2nd order sequence boundary.

4.2 General Introduction

In this study, we concentrate on the northernmost coastal facies belt of the OMM, which is represented by the Randengrobkalk, a shelly calcarenite with varying siliciclastic content (shelly calcarenite to sandy limestone). It is distributed at the northern margin of the Upper Marine Molasse sea, which is in part represented by a wave-cut cliff in the Swabian and Frankonian Alb. The Randengrobkalk was deposited above the Jurassic limestone, but is also in part underlain by the "Ältere Juranagelfluh" (Fig. 4.1, J1). The Juranagelfluh is interpreted as incised valley fills and fluvial deposits of a SSE draining hinterland during the USM (Schaad 1908; Leuze 1921; Fischer 1933; Schreiner 1963, 1965).

Near Tengen the stratigraphy (see Fig. 4.2) of the marginal OMM deposits, were defined by Schreiner (1966a,b; Schreiner 1976 and Schreiner & Luterbacher 1999). A new quarry has allowed to map facies assemblages, and shed new light onto the "classic" stratigraphical succession.

As most of the old quarries and outcrops are decayed we had to concentrate on three localities (see Fig. 4.1; section Tengen, Zollhaus and Wiechs a. R.), where new stratigraphic sections were taken. The dense occurrence of outcrops in the Tengen section, along the same stratigraphical horizon allows lateral tracing of beds and the mapping of lateral facies development. Over 200m of outcrops along a transect of 1km were sketched with the assistance of

enlarged photomosaics. Surfaces both traverse and parallel to the bedform migration direction were documented. Grain fabric and modal composition were examined in petrographic thin sections (5x5 cm).

The purpose of a detailed facies analysis within the Randengrobkalk is threefold: 1) to document the composition and the sedimentology of these rocks; 2) to present a facies model for the sediments, and 3) to determine if there was response of the depositional system to relative sea-level changes.

The study puts special emphasis on

- the identification of the maximum flooding surface,
- the microfacies of the calcareous dominated sediments in order to deduce palaeoecological parameters,
- cross-bedded structures to reconstruct tidal, current and/or wave activity. This is especially relevant as it is reported for the Swiss (e.g. Diem 1985, Allen 1981, Allen 1984, Homewood & Allen 1981, Homewood et al. 1986 and Allen et al. 1985) and German area (e.g. Salvermoser 1999, Hülsemann 1955), that sediments of the OMM have been deposited within an at least meso-tidal regime,
- the reconstruction of the stratigraphical position of the "Alpine conglomerate".

Carbonates which have been deposited during the Upper Marine Molasse sea are rare and of limited spatial extent. Carbonate deposits are known as nearshore deposits from the Bohemian massif (Nebelsick 1989, 1992) and the Allgäu region (e.g. Scholz 1989). With the ongoing transgression of the OMM sea, nearshore deposits retrograded towards the north. This is marked by several several coquina beds or bryozoan sands (Schalch 1901; Gutmann 1910; Knupfer 1912; Lutzeier 1929, Haus 1951; Lemcke et al. 1953; Volz 1953; Hagn 1961, Werner 1966). The Randengrobkalk (Kiderlen 1931, Haus 1951, Schreiner 1966a,b, Schreiner 1976, Luterbacher & Schreiner 1997) represents the northernmost carbonate deposits of the OMM in this region and hence is expected to be linked to the maximum flooding .

4.2.1 OMM stratigraphy and depositional setting of the Molasse basin in SW Germany

In the Swiss Molasse basin the Upper Marine Molasse (OMM) has been traditionally subdivided into two lithostratigraphic units; the "Burdigalian" and "Helvetian" of Heim et al. (1928) and Büchi (1957, 1958); or the Luzern Formation and the St. Gallen Formation of Keller (1989) and Schaad et al. (1992). These two subdivisions are separated by a basin-wide transgressive surface at around 18 Ma (e.g. Keller 1989).

For the German Molasse basin, Lemcke (1970, 1972, 1973) also used the terms "Burdigalian" and "Helvetian" in accordance to the Swiss subdivisions. OMM sediments, discussed within this paper are deposited within the second unit ("Helvetian") and are referred to the Ottnangian Paratethyian stage.

Deposits of the OMM in SW-Germany have been generally divided into SW - NE striking stratigraphical units (Haus 1951; Kiderlen 1931). Facies belts are parallel towards the general striking of the Molasse basin.

The first marine sediments of the OMM ("Heidenlöcher beds") can be found in the area surrounding Lake Constance. They are discussed by Haus (1951), Schreiner (1976) and described in more detail by Winder (1983) and Zweigel (1998). According to their preserved structures and textures, sands and silts of this lithological unit are interpreted as sub- to intertidal.

The marine transgression towards the north starts with a basal conglomerate of reworked material from the underlying Lower Freshwater Molasse and nearhsore deposits of the retrograding sea (Basisschichten). The succeeding part of the Upper Marine Molasse ("Sandschiefer/Sandmergel") consists of in part laminated glauconitic sands and silty shales deposited within a deeper marine, low energetic environment. The "Sandschiefer" are overlain by sandstones of the "Baltringer beds" with a sharp and in part erosive base. The thin veneer of alpine pebbles ("Alpines Konglomerat") at the base of the "Bodman sands" passes into the "second cycle" of Lemcke et al. (1953). The "Baltringen beds" consist of glauconitic sands "Bodman sands" which show in most places tabular to sigmoidal foresets, generally dipping towards the NE (Luterbacher 1997). They are interpreted as representing subtidal sandwaves.

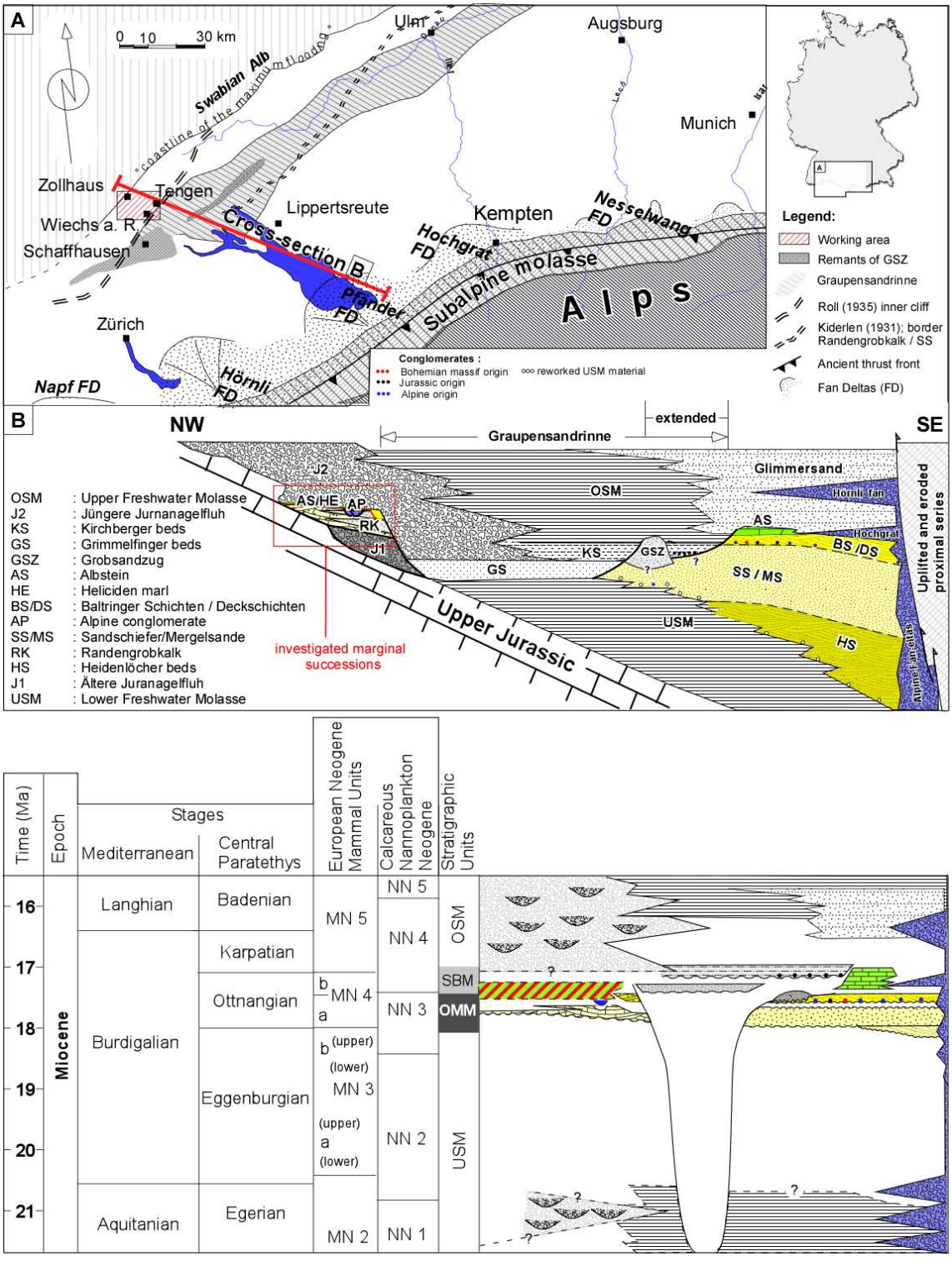

Figure 4.1: *(A) Overall setting of the study area and the morphological elements seen today - modified after Büchi & Hofmann (1960), Doppler (1989) (B) Lithostratigraphy and (C) Chronostratigraphic chart of the OMM in the western South-German Molasse basin - modified after Luterbacher et al. (1992) originally based on Schreiner (1965), Kempf (1997). Time scale according to Berggren et al. 1995, Rögl (1996) and Steininger et al. (1996) modified by Kuhlemann & Kempf (2002).*

Due to the regression of the OMM sea, a white limestone and a reddish palaeosoil ("Helicidenmergel") was deposited in exposed areas (named "Albsteinschwelle" or "Albsteinplatte"). Due to submarine erosion or in the course of the regression, a deep trench, running NE-SW, was formed. The origin and depositional processes (fluvial, estuarine or submarine) of this trench, named "Graupensandrinne", are still under discussion (see e.g. Luterbacher et al. 1992; Buchner et al. 1998; Reichenbacher 1989; Reichenbacher et al. 1998a,b; Buchner & Seyfried 1999; Asprion and Aigner 2000; Tipper et al. 2003). Deposits of the "Graupensandrinne" comprise the "Grimmelfingen" beds and "Kirchberg" beds. Both belong to the Freshwater-Brackish Molasse stage (SBM, see Fig. 4.1) which forms a transition towards the Upper Freshwater Molasse (OSM), where terrestrial conditions prevailed until the determination of deposition by c. 10 Ma.

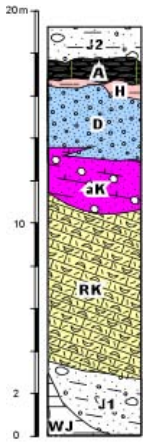

Figure 4.2: *Schematic stratigraphic profile of the marginal OMM successions after Schreiner (1966a,b); see Fig. 4.1 for legend.*

4.3 The Randengrobkalk

The Randengrobkalk is restricted to a small area parallel to the max. OMM coastline (Fig. 4.1). The Randengrobkalk shows a rapid change in thickness. Its maximum thickness of 10m in the vicinity of Tengen decreases towards the ancient coastline to around 2-2.5m (see Zollhaus section, Fig. 4.5). The "Randengrobkalk" is underlayed by the Jurassic limestone, but also in part by the "Ältere Juranagelfluh" (Fig. 4.1, J1).

Since the time of the Romans, the bioclastic limestone (Randengrobkalk) was used as a millstone or for building purposes. In general, the Randengrobkalk is a grey to yellowish skeletal grainstone with varying content of medium sand. A higher content of glaucony sometimes causes a greenish appearance. Due to its high moldic porosity, it looks similar to the Eocene coarse limestone of Paris, and termed 'Grobkalk' by Laffon (1847).

Although the heterogeneous appearance of the Randengrobkalk has been known for a long time, it has not been subdivided into different facies types, resulting in a number of different names e.g. "Sandkalk" (sandy limestone - Schalch 1908), "Citharellenkalk" of Leuze (1921) named after the most prominent gastropod *Melanopsis citharella Mer.* Other names used are "Muschelsand" (mollusc-sand), "Pectensand" (pectinid sand), "Turitellenkalk" (following the common occurence of the gastropod) and the quarryman's term "Muschelkalk". Rollier (1911, 1903) introduced the name Randengrobkalk. Heim (1919) extended the unit from the carbonate dominated exposures near the cliff (Zollhaus section) to the more siliciclastic limestones basinwards (Tengen section). Kiderlen (1931) with his review of the German Molasse Basin, designated the Randengrobalk according to its fossil components as Citharellen-, Turritella-limestone or pectinid sand. In the Swiss part of the Molasse basin, equivalents include the "Tennikerfluh" (Hofmann 1955) and the "Citharellen- and Sandkalke" (sandy limestone) in the vicinity of Schaffhausen (Braun 1953).

4.3.1 Fossil assemblages and petrographic analysis

The Randengrobkalk is largely composed of an mixture of skeletal fragments. Allochems include the remains of bryozoans, gastropods, epifaunal bivalves (pectinids and oysters), barnacles, gastropods and sparsely distributed echinids and foraminifera. Fossiliferous debris is not heavily fragmented and edges are angular to poorly-rounded. Fecal pellets are prevalent within all facies types. Bioerosion on shell material can also be observed.

Thin sections have been taken within all facies types. Based on the content of siliciclastics, we observe a transition from biosparite/calcarenite

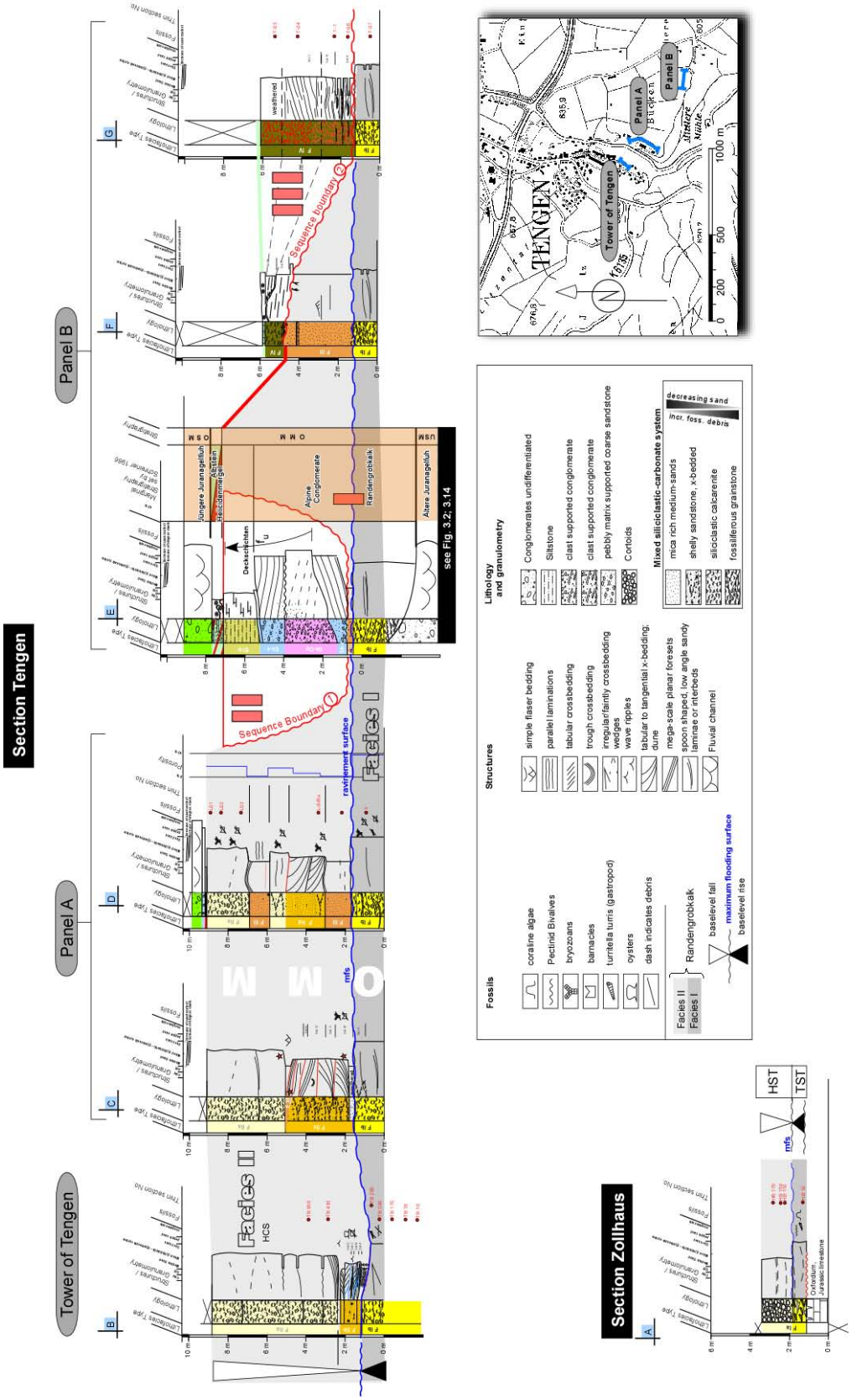

Figure 4.3: *Sedimentologic and stratigraphic columns for the Tengen and Zollhaus section, showing the evolution of the Upper Marine Molasse at the northern proximal basin border. Reddish upper case roman numerals denote the order of deposition. See also Fig. 4.1 for location and Fig. 4.21 for interpretation.*

or fossiliferous grainstone (Facies I) to fossiliferous sandstone (Facies II). Siliciclastics are non- to subangular rounded, fines have not been deposited.

Thin sections show a high porosity (visual porosity of up to 40%) when the amount of siliciclastic debris is low. With increasing sand debris, porosity decreases (10-20%). Two types of porosity can be observed. Interparticale (primary) porosity was generated during deposition and intraparticle (secondary or oo-moldic) porosity due to leaching of aragonitic shell material after deposition. Permeability seems to be moderate where aligned dissolved molluscs connect some few shells (separate vug-porsity).

Typically 70-90% of the calcite occurs as chemically precipitated inter- and intra-particle cement, the reminder 10-30% as skeletal fragments; dominantly the remains of bryozoans, bivalves, barnacles and to a less extend red-algae. Non-carbonate particles are mainly quartz and to a minor amount feldspar and mica. Cement fabrics are petrographically simple and of equant or blocky calcite spar, showing that there was no early marine phreatic cementation phase as none of the components is fringed by fibrous or acicular cement.

The abundant bio- and oo-moldic porosity indicates, that the earliest cements may have formed due to the selective solution of aragonitic shell material. This is generally considered to be caused either by subaerial exposure and/or fresh water influence under shallow water conditions or by undersaturated marine (pore-) waters with respect to aragonite (see Tucker & Wright 1990). After the leaching process, the resulting pore has been occluded by two distinct generations of sparite. Small crystals fringing the interior shell can be observed adjacent to the micritic envelope of shells. Small crystals show sometimes a diffuse fibrous fabric; individual crystallites are extremely difficult to differentiate, as they are so small and appear to be in a spatial continuity with their neighbours. Within a later stage (the second generation), coarse blocky sparite filled cavities as well inter- as intra-particle space. Almost all aragonitc shells appear as fabric inverted (neomorphism). Very common for dissolved aragnitic shell material and peloids is a micritic envelope which may have been formed by early microbial micritization (endolithic algae).

4.3.2 Facies types of the Randengrobkalk

Facies types are defined according to the ratio of sand to fossiliferous debris, sedimentary structures and microfacies. Both endmembers of a siliciclastic-carbonate system (Facies I and III), but also mixed-members (Facies II, IV) have been identified.

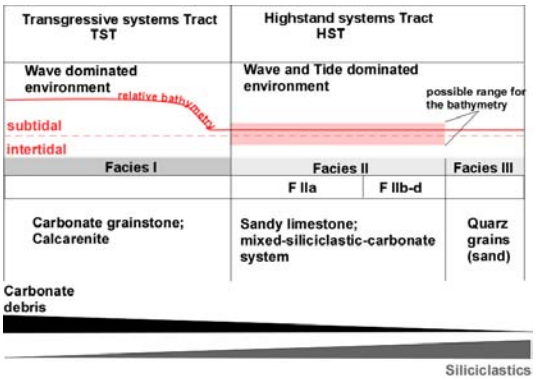

Figure 4.4: *Sand - Carbonate system - Sedimentary structures - diagram*

This results into 4 higher-ranking facies, starting with a discontinuous-curved, wavy, non-parallel cross-bedded grainstone at the base (Facies I). Facies I is characterized by a dominance of shell-hash material (shelly calcarenite) with an accessory amount of coarse quartz. Facies II is characterized by a mixed siliciclastic-cabonate system (sandy limestone). If the siliciclastic fraction is above a treshold of $\sim$ 70% it can be subdivided into Facies IIa-IIc according to the cross-bedding types. Facies III is characterized by pure siliciclastic wedge-shaped bodies. Facies IV is similar to Facies II according to its microfacies and the ratio of sand to fossiliferous debris, but persistent reddish stained.

Facies I: Gastropod-Bryozoan-Mollusc grainstone; sand content up to 5% - (Tengen and Zollhaus section)

Facies I consits of a skeletal grainstone. These rocks present the "classic" Randengrobkalk, which was favoured for quarrying. Within all outcrops, it is represented at the base. Except for the Zollhaus section (Facies Ia), no transition from the underlying Jurassic limestone or

"Ältere Juranagelfluh" is exposed.

Facies Ia:
Poorly sorted Algal-Bryozoan-Mollusc pack- to grainstone - (Zollhaus section)

Figure 4.5: *Facies Ia: Transition from the Jurassic limestone to the Randengrobkalk near Zollhaus at the western slope of Heilinbuck; see Fig. 4.3 for the detailed sedimentologic profile.*

Description:
Deposits of this facies type can be found about 8km NNE of Tengen near Zollhaus (see Fig. 4.1). The outcrop exhibits the transgression of the OMM onto the Jurassic limestone (Late Oxfordium). The transgressive surface shows borings of different organisms. At the base of the Randengrobkalk rounded Jurassic lithoclasts ranging from 1 to 3 cm in diameter can be found. This is in contrast to the Lindenbühl (approx. 1 km north of Heilinbuck), where the limestone lithoclasts are angular. The shelly limestone contains mostly gastropods, pectinids, oysters, bryozoans, barnacles but also red algae. The bedding is irregular to wavy planar, sometimes shallow troughs of 2-4m in plan shape can be recognized. Facies Ia has a maximum thickeness of 2-2.5m. From the base to the top of the succession a transition from from a coarse gastropod limestone to a fine limestone composed of cortoids can be observed. Cortoids consist of spherical and ovoid micritic grains, commonly without an internal structure, arranged in undulatory, faintly cross-bedded beds.

Interpretation:
The top of the Jurassic limestone marks the transgressive surface. This surface of nondeposition developed an in part organically bored surface (hardground), with fossils in growth position. The occurence of red algae indicates, a depostition in a more sheltered environment. Cortoids may have developed due to sea-level fall, when the underlying gastropod grainstone was reworked and the winnowed fractured particles have been constantly held in suspensionn, such the micritic envelope was formed by early microbial micritization (endolithic algae).

Facies Ib:
Gastropod grainstone - (Tengen section)

Description:
Facies Ib appears massive, distinct bundles of single events could not be observed. Sedimentary structures include subhorizontal cross-bedding of grainstone packages. quartz grains are rare, of medium to coarse grain size and poorly rounded. The top of facies Ib is sharp, slightly undulating or erosively cut by facies II.

Interpretation:
Facies Ib is influenced by permanent current action indicated by its massive appearance. It is interpreted as an amalgamated unit of instantaneous higher energy events, frequently reworked and incorporated into the "foreshore" package. Due to continuous wave or current action the fine material was bypassed, most probably in suspension. Deposition of the fossiliferous debris took place near to the carbonate factory, as the allochems are only slightly fragmented and edges only poorly rounded. This is an evidence for a more or less in-situ carbonate production, with reworking and transport over short distances.

Facies II: "intertidal" to subtidal bedforms within a mixed siliciclastic-carbonate system - (Tengen section)

This facies overlies facies I, with a sharp, erosive, mainly planar, but in case of facies IIb incised contact. Within this facies all transitions from pure siliciclastics (quartz grains) to carbonate rich sand (shelly sandstone) exist. Facies II is subdivided, depending on the ratio of sand to shelly debris and cross-bedding types.

Where sand content is above a treshold of 80%, cross-bedding is most obvious. This yields to a division into 3 more subfacies types (facies IIb-d). Bedforms and bedding structures which

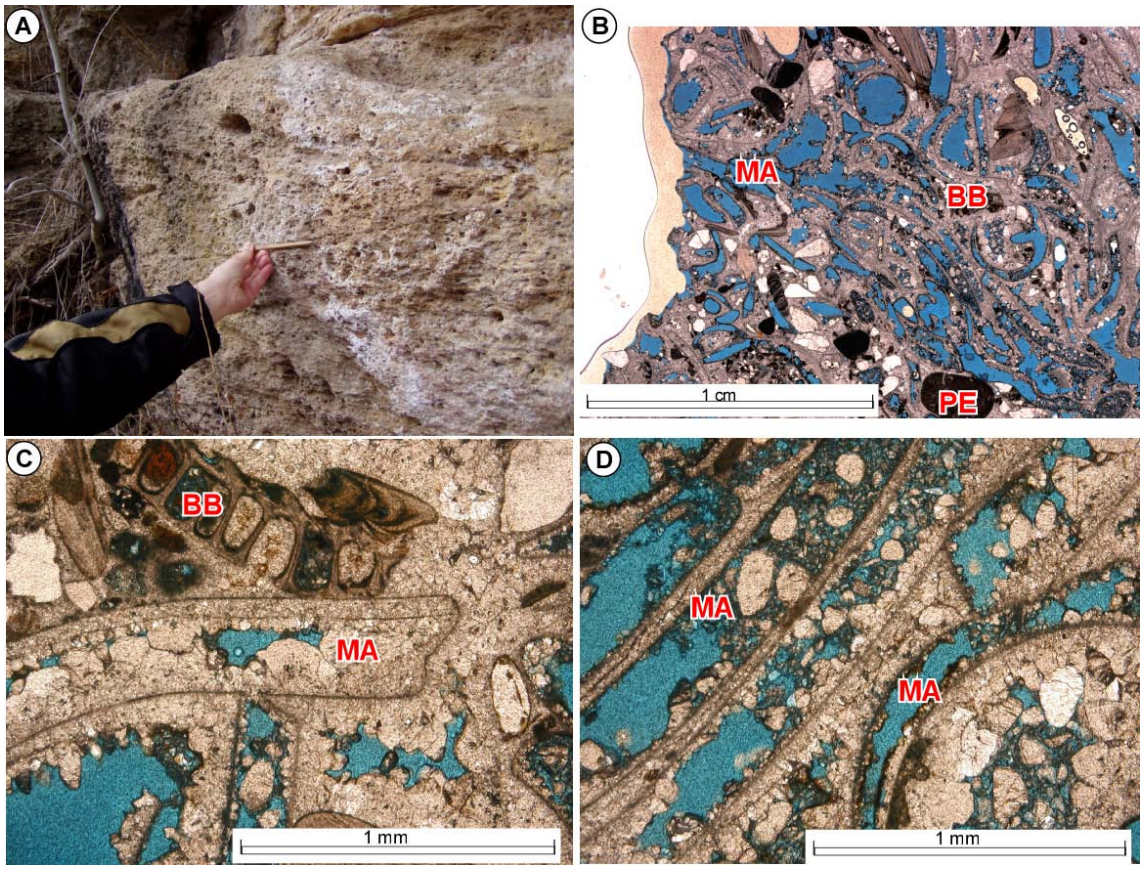

Figure 4.6: *Facies IB: [A] Pronounced wedge shaped stratification of the calcarenite below the tower of Tengen. [B] Photomicrograph of facies IB, showing a coarse bioclastic limestone with larger fragments of balanid barnacles (BB), moulds of aragonitic shelled bivalves (MA) and peloids (PE). Detailed photomicrographs [C] shows disarticulated balanid barnacles. Balanid plates show typical growth lines and pores. [D] High porosity (in blue) do to high percentage of moulds of aragonitic mollusc shells which are only partly filled with sparitic cements. Bivalves show micritic envelopes, which may have been formed by early microbial micritization and coarse blocky sparite as the next generation of infill.*

are different in scale and foreset shape, have been interpreted by using the terminology of Dalrymple & Rhodes (1995) adopted from Ashley (1990). Allen (1980) employs the term dunes to describe major bedforms, generated under unidirectional flow and the term sand-waves for bedforms associated with reversing tidal currents. Dunes may be 2D (having fairly straight, even crests, lacking local sours in the troughs) or 3D (sinous, often discontinous uneven crests and local sour pits in the troughs) see descriptions in e.g. Allen (1968), Costello & Southard (1981), Harms et al. (1982) and Rubin & McCullough (1980). 2D forms occur at lower speeds and three-dimensional forms at higher speeds, for a given grain size (Middleton and Southard 1986). Sandstones are classified according to McBride (1963) and bedding terms according to McKee & Weir (1963). Describing cross-bedding, attention must be paid to several attributes as illustrated by Allen (1963).

Facies IIa:
Faintly cross-bedded, mixed siliciclastic-carbonate facies

Description:
Facies IIa is composed of a moderate-sorted barnacle-bryozoan calcarenite with a high content (up to 50%) of medium to coarse sand. The sedimentary structures include 1 to 2cm thick and 1 to 2m wide, trough-shaped low angle interbeds of sand (Fig. 4.8). Due to interbeds of sand facies IIa appears as undulatory cross-bedded. These sandy layers are intercalated within mixed, unstructured siliciclastic-carbonate bodies. Sedimentary structures also include indistinct

HCS (Hummocky cross-stratification) structures incorporating at least 3m of the grainstone (Fig. 4.7A).

Interpretation:
Deposition of facies IIa was isochronous to facies IIb-d, but not incised by tidal channels.

Facies IIb:
Bundles of small-scale low angle trough cross-bedding structures - subaqueous tidal channel

Description:
This facies type is found at the footing of the castle in Tengen. The base of the facies is composed of sandy banks each few cm thick. They show a concave upward profile in plan view (some 6m wide) cutting down in the underlying facies I. The sandy banks wedge out towards the upper edge of the undercut structure. Each bank shows a coarsening upward trend, from medium grained sand to highly fragmented shells.

This is overlain with a sharp, slightly undulating contact by bundles of faintly to low-angle trough cross-bedded sandy units with a lateral extent of 6 to 12m. Facies IIb is characterized by medium to coarse-grained sand containing at times highly fragmented oyster bivalve shell debris.

The cross-stratification includes:

- semi tabular sets
- trough sets
- fill structures

The outcrop (see Fig. 4.8) shows bimodal inclination of foresets. The foresets in plan shape are planar to tangential in the toesets. Steep angle tabular crossbeds tend to form tangential, slightly inclined foresets with ongoing lateral accretion, resulting in a cross-bed set.

Other cross-stratified units appear as flat spoon-shaped, where bedding types seem to be concordant with the trough profile. Different co-sets can be found, separating two or more sets of strata or cross-bedding by surfaces of erosion, non-deposition or abrupt change in character. Individual sets are in dm-scale and commonly stack to several dm-thick co-sets. All sets show erosive bases and are also eroded at the top by the succeeding set. Single sets wedge out laterally within few meters.

Interpretation:
The base of this facies type is interpreted as a cut and fill structure with periods of waning stages, where transport energy was reduced to allow the deposition of shelly debris. This is transfered towards cross-beds with bidirectional foresetting, what is very common in tidal areas and taken as an evidence for two reversing currents (ebb and flood). Depositional elements such as fill structures, lateral accretion elements are interpreted as a shallow tidal channel (approx. 1.5m deep and several 10 meters wide) which migrates over time. The undercut structure is genetically related to the overlying amalgamated trough cross-bedded units.

According to Visser (1980), the slack water period is sometimes marked by a thin silty to muddy layer spreading over the foresets. This was not observed and might be explained by the lack of fines within the depositional system. It might also be hampered by tidal flow, which is able to remove the fines deposited on the foreset during the slack water period. Thinning and thickening of individual foresets, which is an evidence for neap- and spring-tides, is not observable.

Facies IIc:
Bedform complex with mega-scale planar sets and superimposed current ripples, single trough cross-bedding but also sets of dunes - A (tidal) bar

Description:
Palaeocurrent azimuths measured from the mega-scale foresets are strongly unimodal, indicating a migration direction of cross-beds towards the SSW. The foresets are inclined between 6° and 10°, thin-bedded and consist of few laminae, each 0.5 to 2cm in thickness. In detail, superimposed ripples can be observed indicating that paleocurrents flowed down the foreset slope. Wavelength range is in the order of 6-10cm, the amplitude in the order of 1.5-3cm. Each set reaches only few cm or dm in thickness but can be traced in the direction of foreset dip for at least 6m.

Single troughs and medium-scale dunes can also be observed within this bedform complex. The troughs are about 1 m wide and 20-40 cm in height. Single trough foresets are superimposed

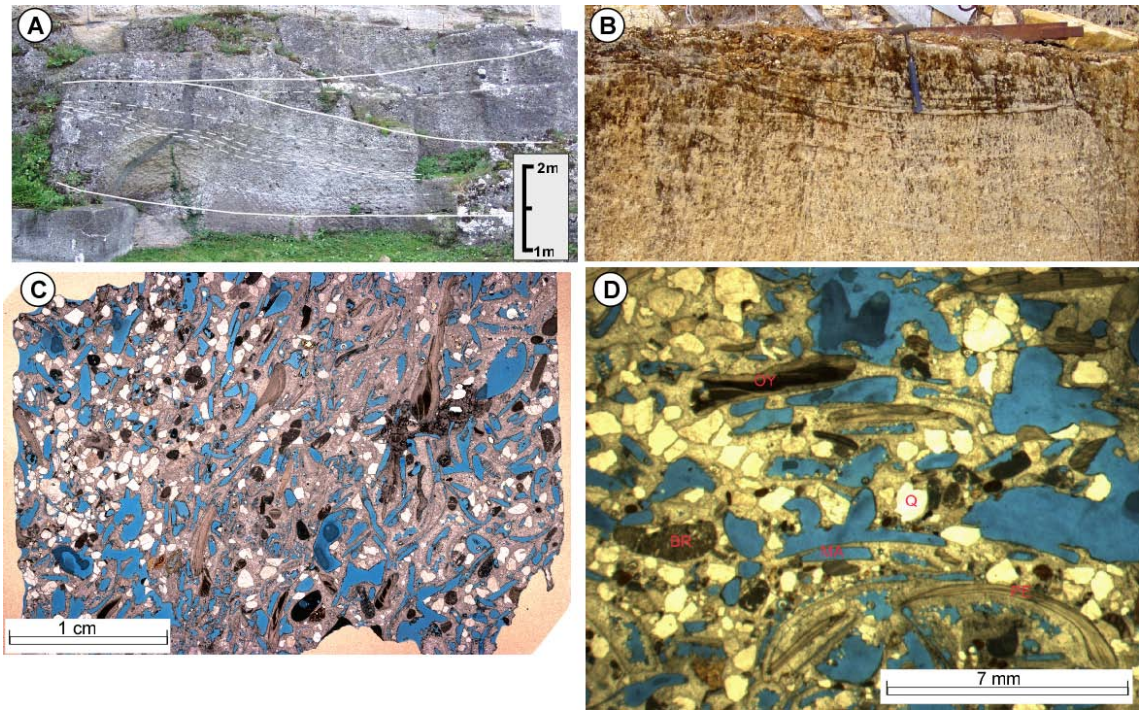

Figure 4.7: *Facies IIa: [A] Undulating cross-bedding of 2 to 3m grainstone packages, similar to larger-scale HCS structures. [B] Trough shaped cross-bedding due to sandy interbeds. [C,D] Photomicrographs of a coarse bioclastic limestone with high vugy porosity (in blue). The picture shows larger fragments of pectinid Bivalves (PE), Oysters (OY), bryozoans (BR). Some moulds of former aragonitic bivalve fragments (MA) can be recognized. Very angular quartz grains (Q) are common. Components are generally orientated parallel to bedding.*

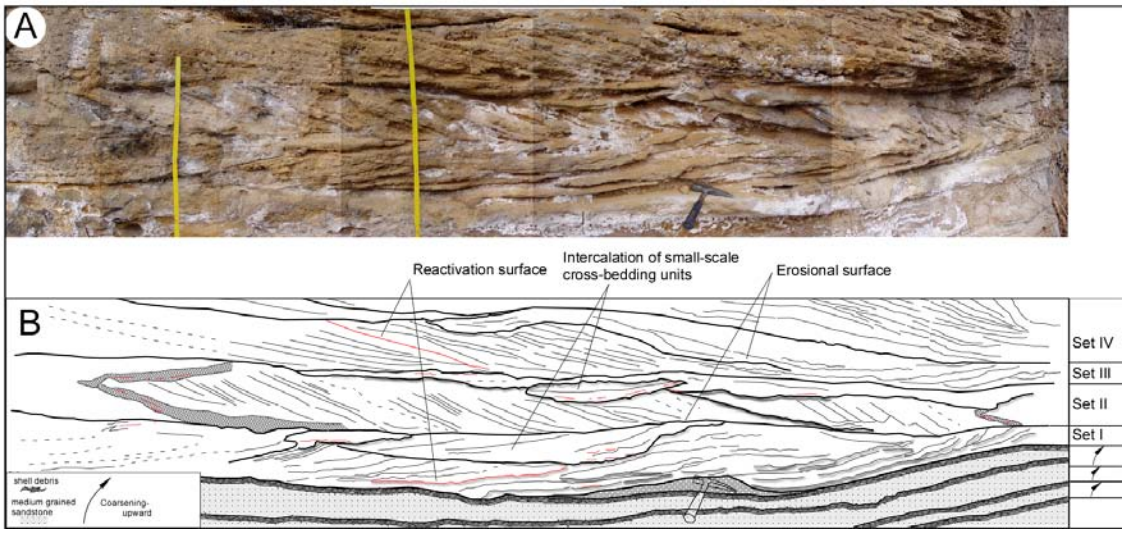

Figure 4.8: *Facies IIb: Decimeter-scale trough- to tabular-crosbedding with spoon-shaped, faintly inclined foresets and lateral accretion surfaces of a subtidal channel. Cross-bedding indicates a southern directed transport.*

by asymmetric ripples. Medium-scaled dunes are intercalated between the individual planar sets as horizontal packages of medium scale dunes with concave foresets aligned tangential towards the lower bounding surface. The set thickness is in the order of 1 to 1.5m. Cross-bedded foresets

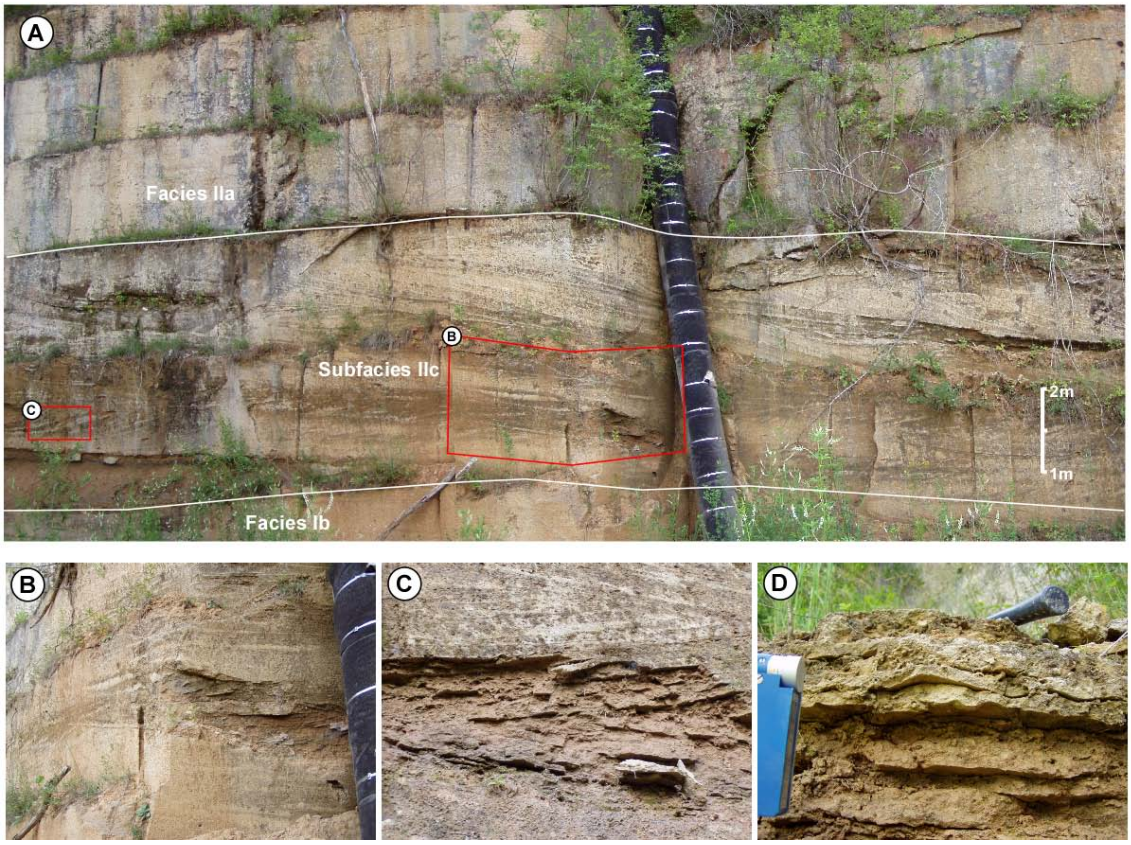

Figure 4.9: *FaciesIIc: The bedform complex shows (A) mega scale planar sets in the mid of the photograph, single troughs (B) with asymmetric current ripples (D)and 2D dunes with tangential foresets (C). The subhorizontal stripes are bulldozer markings generated by quarry operations. For location see Fig. 4.10*

of this type incline with a high angle of 18°. Bipolar crossbed orientation is common. The boundary towards the large-scale planar foresets is, if visible, strongly erosional.

Interpretation:
Single troughs with assymetric flow ripples on the foresets might be a indication for intertidal conditions. Such features may occur in a complex coastal morphology with bars and swales or perhaps barrier islands promoting systems like tidal inlets, which might have similar bedforms.

Facies IId:
Medium-scale subaqueous 2D dunes with no superimposed ripples

Description:
Foreset units are planar and in case of reactivation concave. The unidirectional foresets of the lateral sequence have dip angles ranging from 12° to 25°. On the face of the outcrop structure shows the 2D character of a dune, with a progradation direction towards the SE. The dune is characterized as 'simple' according to Ashley (1990). The superimposed dune migrates over the crest and down the main lee face overtaking the underlying one.

The top surface of the 2D dune is overlain by about 2m of trough cross-bedding. This subfacies is surrounded by facies IIa whereas no sharp bounding surface can be recognized.

Interpretation:
The geometry of the set suggests the filling of a broad depression, with an axis approximately rectilinear to the palaeo-shoreline. The depression is shallow ranging from 2m in the thalweg and 0.5m at the rim edge. The transition from the 2D dunes towards the trough-cross bedded unit marks the final stage of the infill of a "laterally migrating" channel by weakening

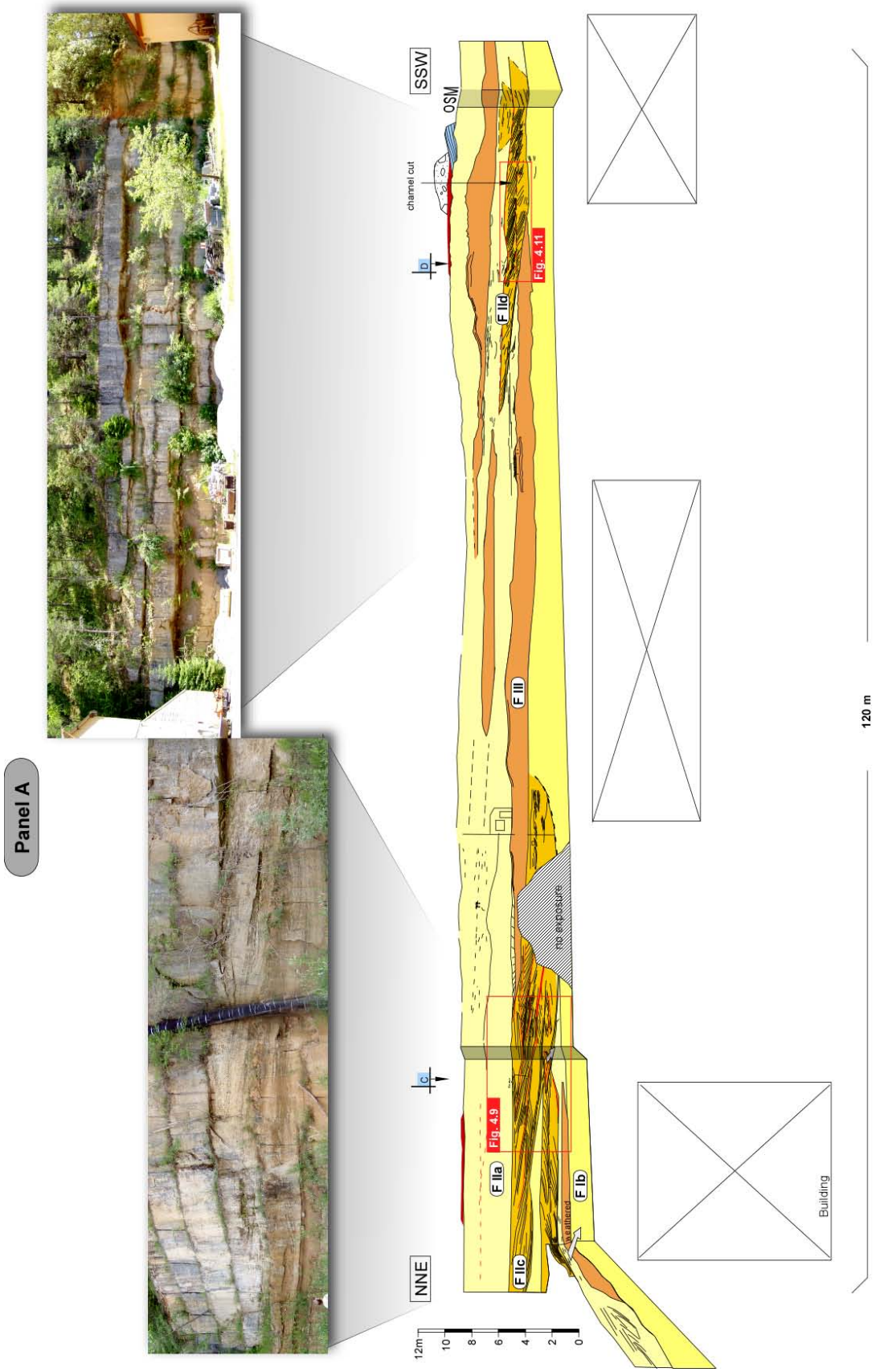

Figure 4.10: *Panel A of the Tengen section: The panel shows the progradation direction of facies II clinoforms towards the SSW. Incised channel facies IIc,d indicate for a SSW and respectively NE-SW progradation direction. For location see Fig. 4.3.*

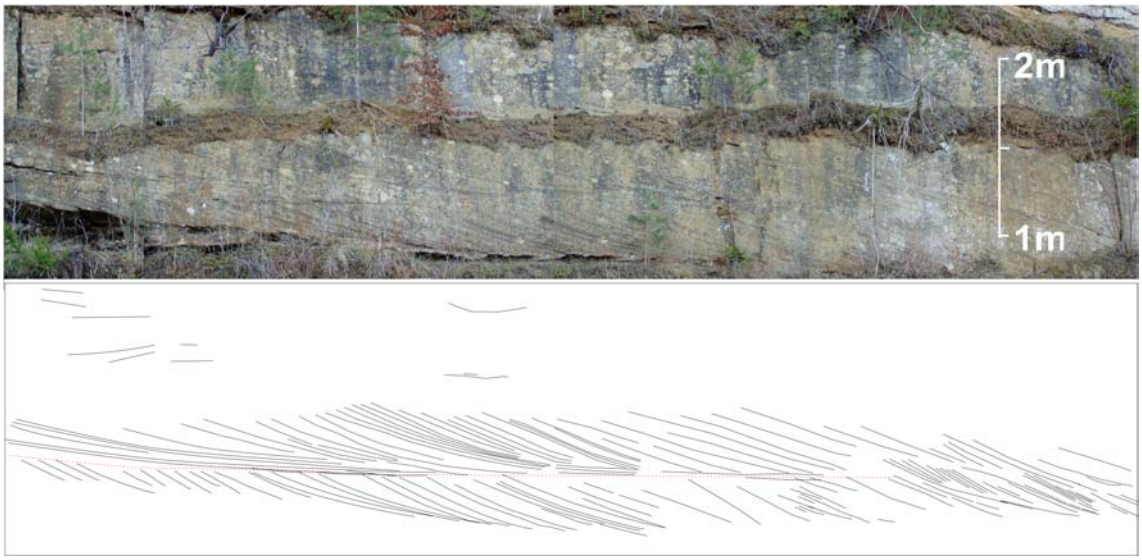

Figure 4.11: *Facies IId: The superimposed meso-scale 2D dune migrates down the main lee face and overtakes the underlying one. For location see Fig. 4.10.*

tidal currents. The depositional environment changes from an unidirectional, mostly sand bearing, dune forming environment to a gradual accumulating, wave dominated environment (trough shaped sets at the top).

Effects of semi-diurnal or diurnal, tidal-current reversals and changes in speed can only be observed rudimentary in some extremely weathered profiles (Fig. 4.11). Instead, longer-term flow unsteadiness related to neap-spring cycles, or storm events will be more likely in the unsteadiness of foreset thickness. Hydraulic behaviour of shelly debris might also be of crucial difference to its hydraulic equivalent sand particle.

Facies III - 1 to 2m thick and at least 80m wide lenticular bodies - sand wedges - - (Tengen section, Wiechs a. R. section)

Description:
The lower contact of facies III is marked by a sharp, (sub-)horizontal, erosive base. The upper boundary is sharp but undulatory (see Fig. 4.10). Sandy to marly, easily erodible, layers of almost 2m thickness pervade facies II. The packages form lens-shaped bodies with a observed lateral extension of 80m. Sedimentary structures are rare and restricted to horizontal sand lamination where individual sand laminae can be followed over distances of up to few meters. Towards the south, the height of the sandy wedges increases to observable 4m, but to the north they wedge out and are not recognized within the Zollhaus section.

Thin sections are dominated by medium grained quartz with subordinate peloids, feldspars and mica slate. quartz grains are mostly fractured, elongated to irregular shaped, with non to slightly rounded edges and dissolution features. quartz grains are often coated by a reddish crust.

Interpretation:
Facies III is interpreted as a "event unit", deposited during hydrodynamic highenergy conditions. Horizontal sand lamination may originate from selective settling of sand from suspension in turbulent water. This interpretation is supported by the fact that individual sand laminae may be followed over distances up to few meters. Selective settling is only possible if the turbulence of the water is so intensive that fine sand, silt, and clay if deposited, are easily and quickly resuspended (Terwindt 1971), before they become entrapped by overspreading coarser sand. The lower boundary of the sand lamination is usually very sharp, sometimes erosive. It represents a break in the existing sedimentation conditions. This facies forms a bed-form for the succeeding, overlying facies IIa.

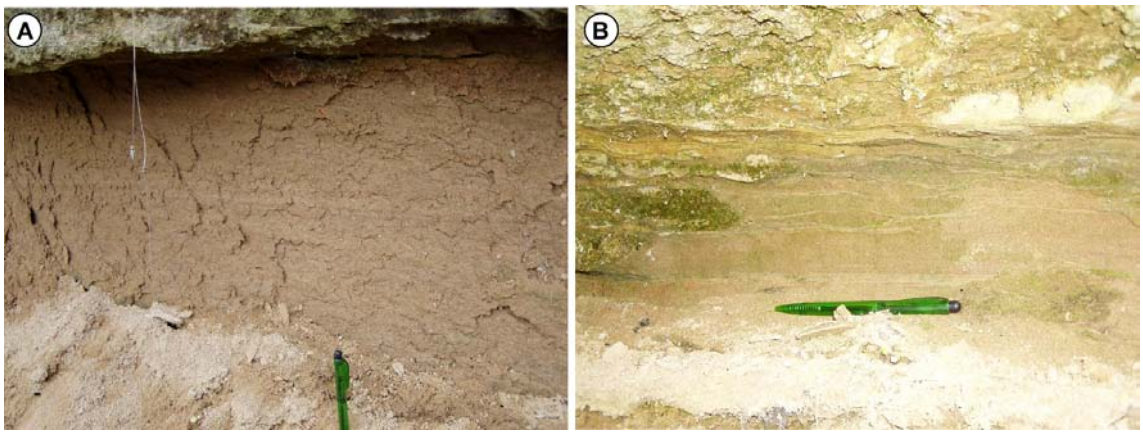

Figure 4.12: *Facies III: (A) The photograph shows horizontal lamination, persistent for some meters; (B) shows simple flaser bedding where facies III wedges out.*

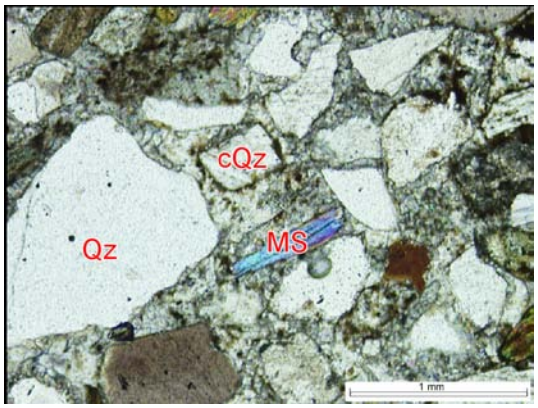

Figure 4.13: *Facies III: Photomicrograph showing skeletal quartz grains (QZ) and mica slate (MS). quartz grains are often coated witz a secondary matrix (cQz).*

Siliciclastic grains in thin sections commonly show weathering features including grain splitting and cavernous corrosion embayments (Fig. 4.13). Although this is also observable in facies I and II, it is most prominent in facies III. Such features are the result of the most intensive stages of chemical alteration (e.g Krinsley & Doornkamp 1973, Borger 2000). In natural environments intensive chemical quartz weathering of this type only occurs after exposure to prolonged periods of hot and humid conditions. This might have happened during the Eggenburgian, when the sandy deposits of the Lower Freshwater Molasse (USM) have been subaerialexposed and available for intensive, persistent tropical weathering. The weathering stage to which these etching features have progressed are stage two and three of six key stages, explained in Borger (2000). quartz grains show the earliest expression of alteration. As alteration advances, minor corrosion begins to affect fracture faces. Fractures may become coated with a secondary matrix (Fig. 4.13), often a kaolinite-goethite mixture (Borger 2000). Continued solution causes the pits to expand into one another, thus imparting an irregular form to the once smooth fracture faces. Whilst corrosion features of stage 2 are visible only in SEM (Scanning Electron Microscopy), at stage 3 they become increasingly deepened, and hence observable in thin sections.

FACIES IV - Beachface deposits - (Tengen section)

Description:
The deposition of this facies starts with an angular and erosional unconformity of 11 degree. Root-like structures penetrate the underlaying facies III. The lowermost part of facies IV contains few pebbles, mainly quartzite but also black cherts, averaging 1-2cm in diameter. The calcarenite is stained by reddish clay. In the lower part undulating and in part connected shallow troughs are present. They contain reddish silt to clay but also nodules of carbonate, which are similar to the "Albstein" (see section 4.5). In the upper part, the calcarenite forms subhorizontal bodies, with crudely to well stratified, subhorizontal to gently (1-4°) seaward dipping bedding planes. Facies IV directly overlies Facies I and III with a maximum thickness of 6m, wedging out towards the north.

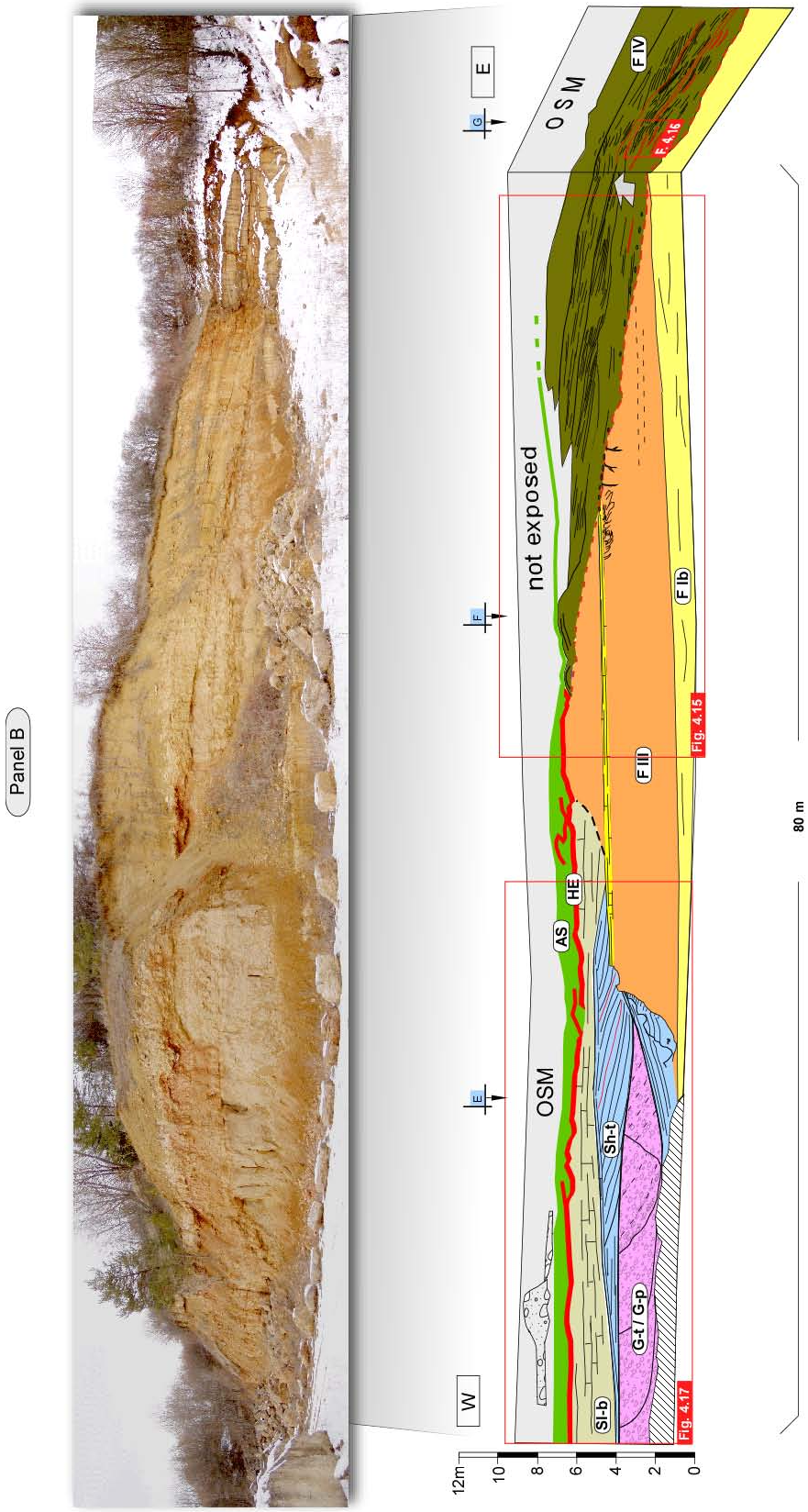

Figure 4.14: *Panel B: The quarry shows the whole maginal successions (for detailed stratigraphic profiles see Fig. 4.3), with the Randengrobakalk at the base, a sequence boundary marked by the Alpine conglomerate and another on by a steep erosional surface in the eastern part of the quarry. OMM sediments are overlain by terrestrial deposits of the Helicdenmarl and Albstein and discordantly overlain by the fluvial deposits of the OSM (Upper Freshwater Molasse). For location see 4.3.*

Interpretation:
This facies marks a transgressive phase, during which facies II was reworked and incorporatred into the beachface deposits of facies IV. The basis is marked by a ravinement surface with rare erosional lag deposits. A berm like structure limits the extent of facies IV. Reddish clay is distributed diffusive within facies IV and may be floated from the surrounding terrestrial area. The trough shaped, shallow forms, filled with the reddish clay and silt of the Helicidenmarl, indicate, that the basal layer fell dry so reddish silty to white calcrete nodules were formed.

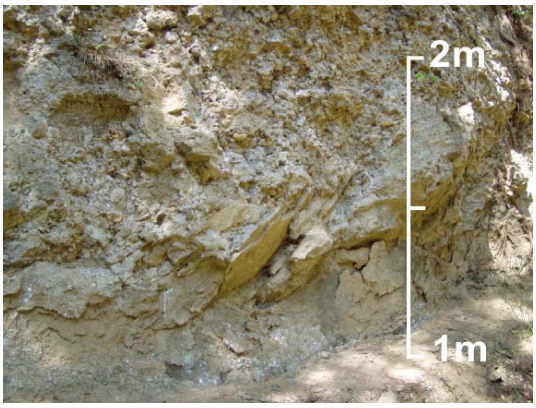

Figure 4.18: *Protruding base of a mass flow rudite, Prograded fill, lateral accretion element, more lenticular elements, record local shifting of bars and subchannels in the Wiechs a. R. section. For location see Wiechs a. R. in Fig. 4.1.*

4.4 The Alpine Conglomerate and Deckschichten

The stratigraphic term "Alpine Conglomerate" has so far been used for two different facies types. On one hand it describes a clast supported channel conglomerate, which was deposited as the distal remains of alpine fans and on the other hand it describes an concordant, veneer of alpine pepples at the base of the Bodeman sands (see Fig. 4.19 and e.g. Lemcke et al. (1953) for description).

The alpine conglomerate in the study area belongs to the first facies type. Within all sections it is cut into facies III (see Fig. 4.13, 4.16, 4.17, Tengen and Wiechs a.R.). According to Schreiner it is overlain by the "Deckschichten" that are interpreted to represent time equivalents of the fine sands above the cross-bedded "Bodman sands" also termed "Deckschichten". Analysing the components of the "Alpine conglomerate", the source is attributed to the Alpine fan deltas and mostly to the Napf fan delta (Schreiner 1965, 1974).

Within this section the so far used stratigraphic term "Deckschichten" (e.g. Schreiner 1966a,b, 1976; Schreiner & Luterbacher 1999) is discussed in the context of the depositional process of the "Alpine Conglomerate" and not used in a lithostratigraphic sense.

Alpine conglomerate - Distal fan delta, channel fill conglomerate - (Tengen section, Wiech a. R. section)

Description:
The Alpine Conglomerate (see Fig. 4.14, 4.17, 4.18 is characterized by a distinct erosive base with a sharp concave-up shape. The top is marked by a pronounced erosional surface cutting all the amalgamated structures. It reaches a thickness of 3 to 4m with lateral dimensions of few up to tens of few meters, whereas the lateral extents have not been exposed. Lithofacies types follow Miall (1996). The internal structure is composed of clast supported trough (Gt) to planar (Gp) cross-bedded sets or simply consist of poorly sorted massive clast-supported gravel (Gcm). The clast-supported, conglomerate lithofacies types are unconformably overlain by a sandy unit with loosely distributed pebbles, organized in crude flat bedded to low angle tabular cross-bedded sets (Sh-t). The upper bounding surface of the Sh-t unit is wavy to angular and wedges out to both sides lateraly. It is overlain by a unit of monotonous, banked silts (SIb).

Lithofacies Gt-Gp: This primarily consists of pebble to cobble-size clasts. Clasts are well rounded, moderate to poorely sorted. The matrix is silt or moderate to poorly sorted medium to coarse-grained sand and granules. Although imbrication is rare, some elongate clasts are oriented with their long axes in the direction of cross-bedding. Slightly fragmented oyster shells, marine gastropods and bored limestone clasts are also found.

Lithofacies Gcm: This lithofacies is known from the Wiechs a. R. section. Sedimentary structures are absent and distinct bedding planes are difficult to recognize; grading is

Figure 4.15: *Beach deposits showing well-developed foreshore lamination prograding of facies IV towards the south. See Fig. 4.3, 4.14 for location.*

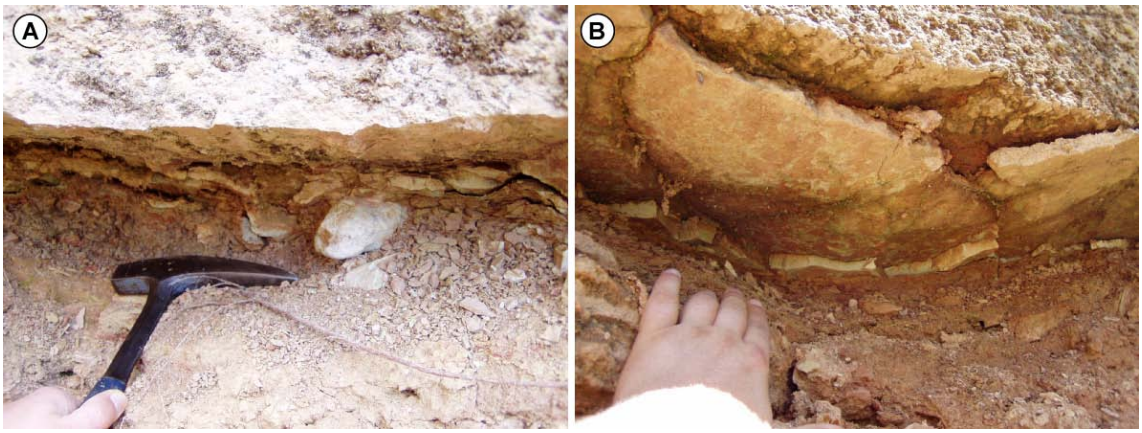

Figure 4.16: *Facies IV with tough-shaped bedforms, filled with redstained silty beds (B) and nodular limestones (A). See Fig. 4.3, 4.14 for location.*

uncommon. Conglomerate fabric is disorganized within lithofacies type Gcm. The conglomerate is polymict with well-rounded clasts of limestone, quartzite, reddish to black chert and subordinate of metamorphics.

Lithofacies Sh-t: This lithofacies cuts the underlaying Gt-Gp unit. The sandstone is predominantly coarse to very coarse-grained and includes well-rounded pebble size limestone clasts up to 1-3 cm in diameter. The clasts are either randomly scattered beds, or are present as pebble layers along the bedding planes and matrix-supported. Sedimentary structures change from horizontal bedding to slight angular sets.

Lithofacies SIb (former "Deckschichten"): Monotonous, banked silts are summarized within this lithofacies type. They overlay lithofacies Sh-t.

Interpretation:
The "Alpine Conglomerate" of the Tengen and Wiechs a. R. section can be divided into 3 architectural elements. Units of massive, clast-supported conglomerate (MCC) with indistinct bedding planes dominate, with smaller proportions of lateral accretion conglomerate (LAC) and channel-fill conglomerate (CH). Massive, matrix supported units coarse-grained sandstone (SS) pass into crudely horizontal bedded silty parts (SI). Boulder clasts have been transported by northward draining Alpine fan deltas during a period, when the OMM sea retreated and terres-

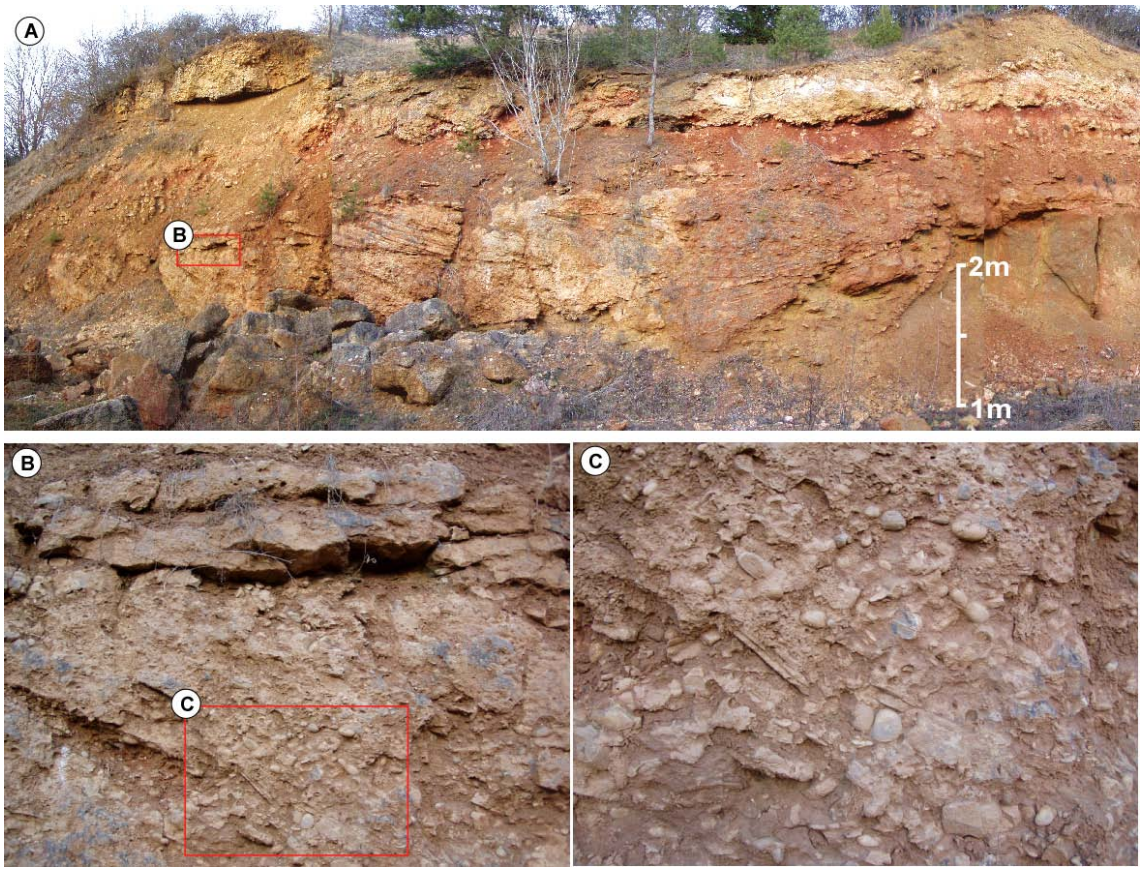

Figure 4.17: *"Cut and Fill" structure of the Alpine conglomerate (A), showing clast supported framework of well rounded pebbles and cobbles with a matrix of medium to coarse grained sand (C). Lithofacies G-t/G-p is erosively cut at the top and overlain by lithofacies Sh-t; see text for explanation and location Fig. 4.14.*

trial conditions prevailed. We propose that both facies types are derived from the alpine dispersal systems. Thus the interpretation of the "Alpine conglomerate" as a lag deposit (at the basal Bodman beds) is replaced by a limited short-time spread out of Alpine fan material (Fig. 4.19) due to progradation of the southern coastline during sea-level fall. After a rapid regression, conglomeratic fan deltas continued to grow at the mouths of northward-discharging intra-Alpine streams. Basin shape must have bee changed from wedge to at least tabular shaped. The basin changed to an overfilled stage, with a continuous northward dipping gradient from the Alpine orogen, with the deepest parts in the distal remains of the NFAB.

Processes, responsible for the transport of gravel material transverse towards the distal part of the Molasse Basin might be gravity induced debris-flow events or a northward dewatering channel system (stream flows). The fining upward succession from a gravel dominated lithofacies towards silts, is an indication of reducing hydroenergetic conditions.

The deposits known as Deckschichten, are genetically related to the underlying Alpine Conglomerate. Sheet like deposits are similar to the stratified sandstone during waning flow stages. Thus we propose that the bewildering lithostratigraphic Deckschichten unit should no more be used for the maringal successions. The observations in the Tengen quarry also indicate, that after the "Deckschichten" there was another marine ingression, thus the marginal Deckschichten could not be the same, as the more basinal "Deckschichten" indicating the transition to the terrestrial OSM.

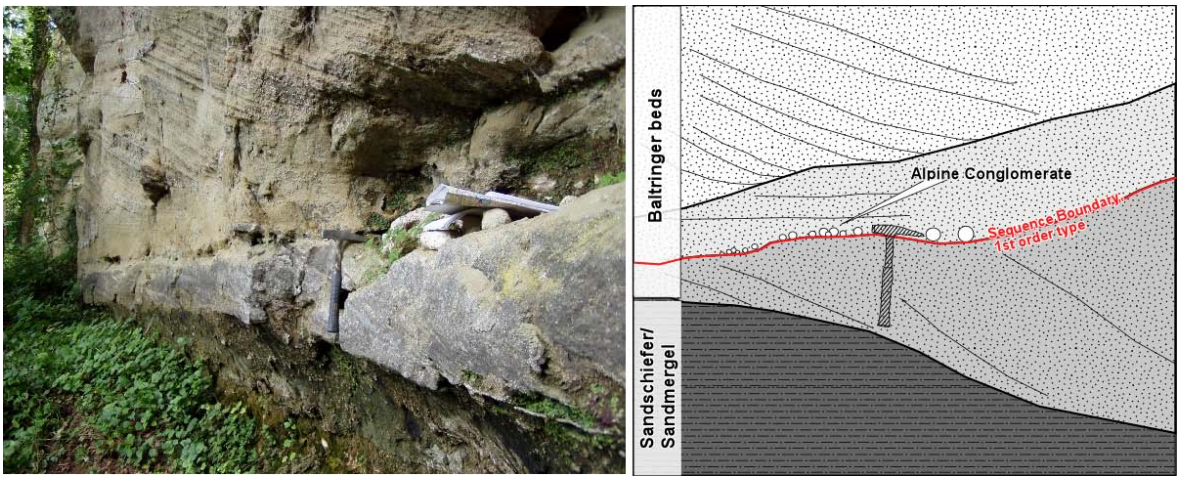

Figure 4.19: *Outcrop near Lippertreute showing the thin veneer of dispersed Alpine conglomerates at the base of the Baltringen beds. For location see 4.1.*

4.5 Heliciden beds and Albstein

Outcrops in Tengen show the reddish clay of the "Heliciden marl" (named according to its prominent gastropod) partly interbedded with the Albstein (see also Schreiner & Luterbacher 1999). The "Heliciden marl" consits of predominantly redish to sometimes yellowish clay with a maximum thickness of 0.5m. The "Albstein" limestone is present as aggraded pisolites of caliche nodules, cemented by a micritic matrix. The Albstein is discordant overlain by the OSM.

The genesis of the Albstein carbonate is still under discussion. Geyer & Gwinner (1991) interpret the Albstein as a calcrete. Zöbelein (1985) suggested that calcareous algae formed these carbonates in a shallow freshwater lake. Both ("Heliciden marl" and "Albstein") may have formed in subaerial environments, where weathering profiles have developed, including the development of caliche and calcrete but also the red palaeosoil of the "Heliciden marl".

4.6 Discussion

4.6.1 Palaeogeographic Reconstruction - Depositional Model

The deposits of the Randengrobkalk mark the maximum flooding of the western part of the German Molasse Basin. These deposits represent a shallow-water coastal environment and can be subdivided into a transgressive and regressive serie. Higher order, nested cycles are not observed. Fig. 4.20 illustrates the different palaeogeographic stages, which are explained below.

Facies I and II — Unit I

Transgressive series:
The lowermost unit of the Randengrobkalk is interpreted to represent transgressional deposits consisting of facies I. This Transgressive systems Tract (TST) is separated from the regressive series (Highstand systems Tract - HST) by a ravinement surface (see Fig. 4.3) marking the maximum flooding. Deposits of facies I are wave dominated. There is no indication for tidal influences. Due to flexural bending of the jurassic limestone in the course of the alpine orogenese, the Jurassic limestone, forms a natural southward dipping gentle gradient on which the transgression encroached. The depositional setting of facies I might have been similar to a shallow ramp. Remnants of the Older Juranagefluh (J1 - see Fig. 4.1) have not been removed by the transgression. This indicates, that the peneplenation of the OMM sea took place in a relatively short time, not being able to remove the loose shingle of the J1.
Regressive series:
Facies I is overlain by southward dipping clinoforms of facies II. Clinoforms (see Fig. 4.10) correspond to slope processes. Cross-bedding structures of facies II show a high variability in scale and foreset shape. Bidirectional foresetting of crossbeds, which is common in tidal areas, is constricted to facies IIb. The depositional environ-

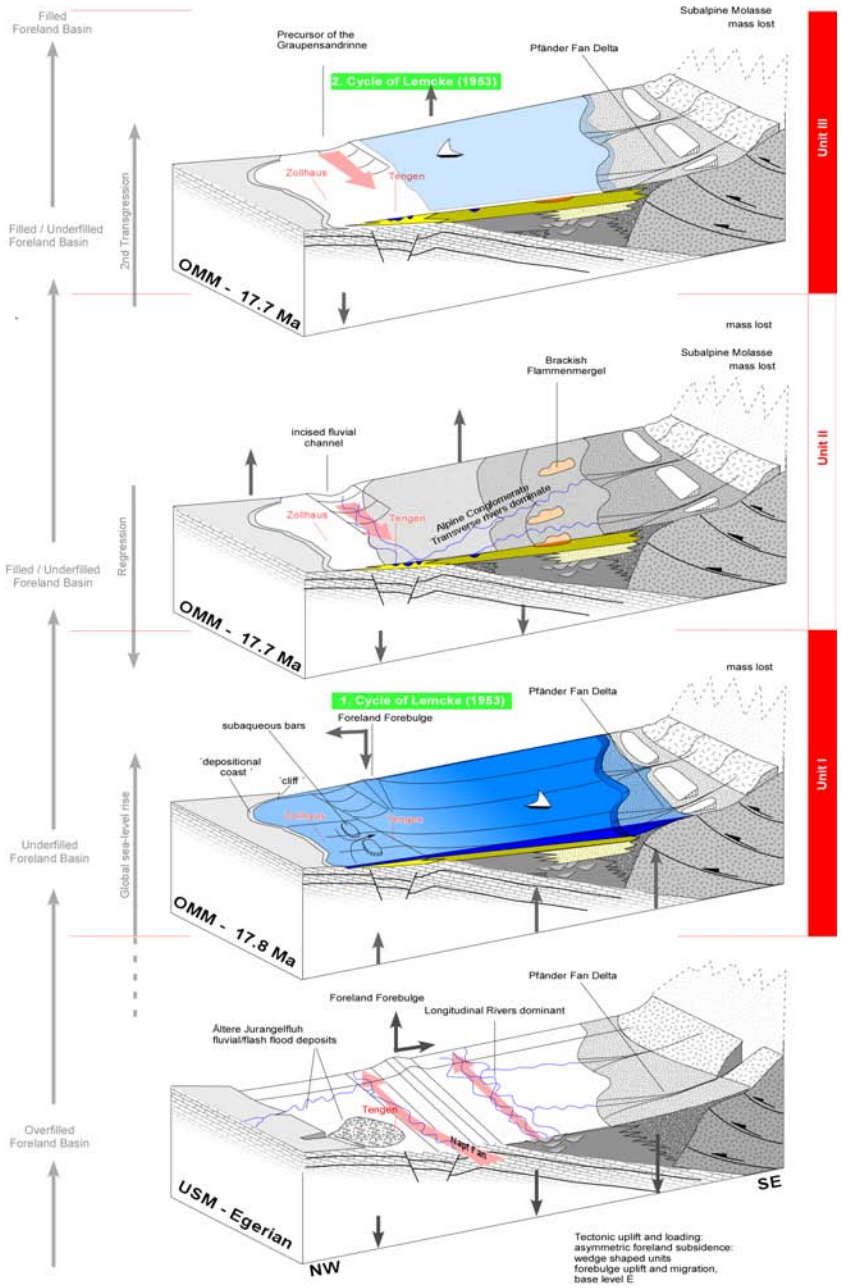

Figure 4.20: *3D palaeogeographic reconstructions of the depositional environmentfor the time of the Upper Marine Molasse within the southwestern German Molasse basin.*

ment of facies IIb-d is interpreted to represent sub- to inter-tidal channels with "cut and fill" structures. Characterisitcs and diagnostic criteria for a tidal regime as described by Clifton (1983), Terwindt (1988), Terwindt & Brouwer (1986) could not be found. In general it has to be noted, that the hydraulic behaviour of shelly debris is almost unknown. Thus thickening and thinnning of foresets according to neap- and spring-tide cycles might not be developed as known from siliciclastic tidal environments.

Alpine Conglomerate — Unit II

With the onset of facies II the marine basin shallowed and prograded towards the south. Parts of the NAFB fell dry and allowed conglomeratic fan deltas to grow at the mouths of northward-discharging intra-Alpine streams (2nd order type

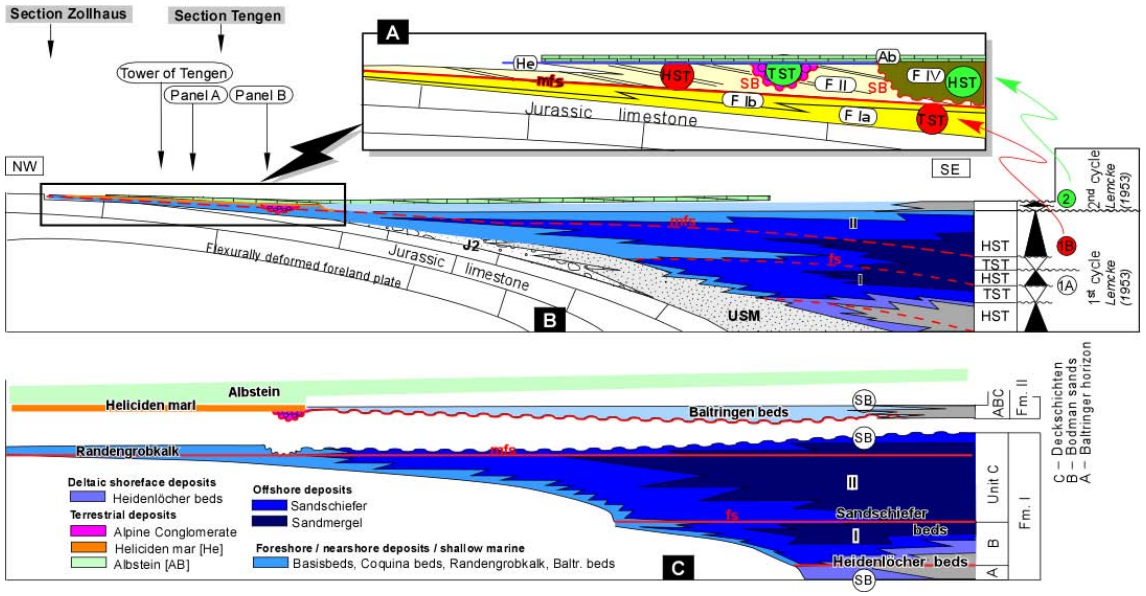

Figure 4.21: *(A) Revised stratigraphy of the marginal OMM deposits;(B) Sequence-stratigraphic correlation attempt (not to scale) towards the basinal OMM deposits; (C) Wheeler chart; based on conceptual ideas of Schreiner (1965, 1966a,b), Schreiner (1976), Naef et al. (1985), Luterbacher et al. (1992), Schreiner & Luterbacher (1999)*

sequence boundary). Basin shape must have changed toward the end of Unit I, from wedge to at least tabular shape, promoting a northward discharge of the alpine dispersal systems. Thus the deepest parts at this time must have been the distal remains of the NFAB, with a transverse draining system (see Fig. 4.20) bypassing the material towards the West. For the time of the OMM, Schlunegger (1999) reconstructed huge drainiage areas, with a maximum length of 50 - 70km, for the central Alps. The transport of gravel material transverse towards the northern margin of the Molasse Basin might have been driven by both gravity induced debrisflow events (lithofacies Gcm, see Fig. 4.18) and stream flows (lithofacies Gt-Gp, Sh-t, SIb; see Fig. 4.14, 4.17). Stream flows are characterized by lateral accretion elements and mass-flow deposits by a chaotic mixture of a clast supported pebbles with a sandy matrix. Local occurence of marine faunal elements (oysters) indicate that the Alpine Conglomerate has been reworked during the following transgression (TST).

The term Deckschichten (lithofacies SIb) shoud no more be used, as it is genetically related to the underlying Alpine Conglomerate, representing waning flow stages and thus deposits of a reduced hydroenergy of a stream-flow channel.

Facies IV — Unit III

The base of facies IV is marked by a sequence boundary of 2nd order type. Facies IV has been deposited at the time of the Baltringen beds, when a renewed transgression reached the northern part of the German Molasse Basin. Both deposits represent the HST of the next cylce in SW-Germany.

At this time the transgression established a shallow subtidal environment, reworking the upper part of the Randengrobkalk (facies II). Facies IV marks the northermost extent of the OMM coastline for that time in the Tengen region. The transgression did not extend up to the maximum flooding, as marked by facies I. The terrestrial Helicidenmarl were isochrouns deposited at the northern hinterland, floating into the marine realm, generating the reddish stained color of facies IV.

4.6.2 Origin of siliciclastics in the Randengrobkalk

The origin of siliciclastic quartz grains within the Randengrobkalk (facies I,II,III and IV) is of crucial interest. Because of the lack of sand bearing deposits in the northern hinterland (Jurassic limestone), sediment-yielding rivers were not able to transport siliciclastic material in the de-

positional environment of the OMM sea directly from the north.

There are three possible source regions, which might have provided sandy material. They are discussed in the following.

Alpine dispersal systems: They are charaterized by decreasing sediment input during the OMM (Kuhlemann 2000) and probably attribut only a minor content of siliciclastics to the basin. The elongate, skeletal shape of quartz grains, an effect of intensive chemical weathering could not be explained by using the Alpine hinterland as a source region (see explanation below).

Bohemian massif: Deriving sandy material from the Bohemian Massif can also be neglected. On one hand the quartz grains should have been more rounded on their long alongshore transport of some 100km. On the other hand tidal simulations (see chapter 3 and 5) suggested, that there must have been a NE directed sediment transport towards the Bohemian massif and not vice versa.

Reworked USM material: As shown above, siliciclastics (quartz grains) appear as single sheets (facies III) or in the mixed siliciclastic-carbonate system of facies I, II and IV. Within these facies types quartz grains are angular and mostly of skeletal and elongate shape. This is interpreted to represent weathering stages (e.g. **Borger** 2000). The shape of quartz grains but also accessory lithic components show the result of intensive weathering. It must be concluded that the deposits of the USM in south Germany have been exposed to intensive chemical weathering during the Eggenburgian. Thus sand, that was carried onshore (facies III) by wave action during marine regression, may originate from reworked USM deposits.

The importance of shoreward drift of sediment to beaches was deduced in the Isles of Scilly by Barrow (1906). Because of the lack of eroding cliffs and sediment-yielding rivers, sand and gravel (including shelly debris) was transported onshore from the surrounding sea-floor by wave action. Shoreward drift has occurred where the nearshore waters are shallow, or are becoming shallower because of land uplift or a falling sea-level. During repeated minor oscillations of sea-level fall a widespread shoreward transport took place.

This model is supported by our study, as facies I,II,III and IV belong to the regressive series of the Randengrobkalk indicating a sea-level fall. Further evidence for a short transport of sand is its lack of roundness. The sedimentary structures of facies III indicate that sand was not transported in a continuous way, but may represent storm generated event sheets, fringing the landward area (transition) zone.

4.6.3 Fossil assemblages

Allochems of all facies types (see section 4.3.2) can be interpreted as BryoMol or BiMol facies. Modern equivalents of these byrozoan-rich sediments are common on part of high-energy, open shelves around New Zealand and southern Australia (e.g. Wass et al. 1970; Nelson et al. 1988a,b; Boreen et al. 1993). Byrozoans as suspension feeders, are sensitive to the amount of sediment in suspension, and so a relatively low terrigenous sediment supply is a general prerequisite for bryozoan dominance (Ryland 1970). They will colonise particulate and flexible substrates, but diversity is highest on hard substrates, such as gravel, shell or rock. Bryozoans live at all shelf depth, the massive and encrusting forms favour the shallower, more turbulent waters, and the erect delicate forms generally deeper and calmer conditions (Ryland 1970).

4.7 Conclusion

- The Randengrobkalk is interpreted to represent a transgressive (facies I) and regressive (facies II) series, separated by the maximum flooding ravinement surface. Towards the end of unit I, the OMM sea retreated and intra-Alpine streams discharged towards the northern margin of the NAFB and bypassing the material towards the West. Local occurence of marine faunal elements (oysters) indicate that the Alpine Conglomerate has been reworked during the following transgression (TST). During the HST a shallow (10-20m) subtidal environment was established, during which the Baltringer beds (Fig. **??**), but also facies IV was deposited.
- Unit I: The transgressive series (facies I) is wave dominated; tidal signatures are found

in the regressive series (facies II).

⋆ Sequence-stratigraphic reconstructions showed, that during the maximum extent of the OMM sea, unit I was deposited. The succeeding transgression (unit III) did not encroach further towards the north.

⋆ The sequence-stratigraphic model (Fig. **??**) suggests, that the maximum flooding was coeval with the deposition of the Sandschiefer unit of the deeper basin. Thus the maximum transgression cannot be correlated with the Baltringen beds as proposed by e.g. Kiderlen (1931), Volz (1953), Erb et al. (1961), Gall (1974).

⋆ Two sequences (unit I / unit II,III) have been identified, which might be correlated with the two cycles of Lemcke et al. (1953).

⋆ Origin of siliciclastics (skeletal quartz grains of facies I,II, III, IV) might be reworked USM deposits.

4.8 References

Allen, J.R.L. (1963): The classification of cross-stratified units, with note on their origin. *Sedimentology*, **2**: 93-114.

Allen, J.R.L. (1968): The nature and origin of bed-form hierarchies. *Sedimentology*, **10**: 161-182.

Allen, J.R.L. (1980): Sand waves: A model of origin and internal structure. *Sedimentary Geology*, **26**: 281-328.

Allen, J.R.L. (1981): Palaeotidal speeds and ranges estimated from cross-bedding sets with mud drapes. *Nature*, **293**: 394-396.

Allen, P.A. (1984): Reconstruction of ancient sea conditions with an example from the Swiss Molasse. *Marine Geology*, **60**: 455-473.

Allen, P.A., Mange-Rajetzky, M., Matter, A. & Homewood, P. (1985): Dynamic palaeogeography of the open Burdigalian seaway, Swiss Molasse basin. *Eclogae geologicae Helvetiae*, **78**: 351-381.

Ashley, G.M. (1990): Classification of large-scale subaqueous bedforms: A new look at an old problem. *Journal of Sedimentary Petrology*, **60**: 160-172.

Asprion, U. & Aigner, T. (2000): Fazies- und Georadar (GPR) - Analyse in der süddeutschen Graupensandrinne. *Neues Jahrbuch für Geologie und Paläontologie, Abhandlungen*, **218**: 321-342.

Barrow, G. (1906): The Geology of the Isles of Scilly. *Memoirs of the Geological Survey, London.*

Berggren, W.A., Kent, D.V., Swisher, C.C. & Aubry, M.-P. (1995): A revised Cenozoic geochronology and chronostratigraphy. In: *Geochronology, time scales and global stratigraphic correlations* (Eds W.A. Berggren, D.V. Kent, M.-P. Aubry and J. Hardenbol), *SEPM, Special Publications*, **54**, pp. 17-28, Tulsa.

Boreen, T., James, N., Wilson, C. & Haggie, D. (1993): Surficial cool-water carbonate sediments on the Otway continental margin, southeastern Australia. *Marine Geology*, **112**: 35-56.

Braun, E.v. (1953): Geologische und sedimentpetrographische Untersuchungen im Hochrheingebiet zwischen Zurzach und Eglisau. *Eclogae geol. Helv.*, **46**: 143-170.

Büchi, U.P. (1957): Zur Gliederung des Burdigalien im Kanton Aargau. *Bulletin der Vereinigung Schweizerischer Petroleum-Geologen und -Ingenieure*, **23**: 33-41.

Büchi, U.P. (1958): Zur Geologie der Molasse zwischen Reuss und Seetal (Baldegger-/Hallwilersee/Aabach). *Eclogae geologicae Helvetiae*, **51**: 279-298.

Büchi, U.P. & Hofmann, F. (1960): Die Sedimentationsverhältnisse zur Zeit der Muschelsandsteine und Grobkalke im Gebiet des Beckennordrandes der Oberen Meeresmolasse zwischen Aarau und Schaffhausen. *Bulletin der Vereinigung Schweizerischer Petroleum-Geologen und -Ingenieure*, **27**: 11-22.

Buchner, E., Schweigert, G. & Seyfried, H. (1998): Revision der Stratigraphie der süddeutschen Brackwassermolasse. *Zeitschrift der deutschen geologischen Gesellschaft*, **149**: 305-320.

Buchner, E. & Seyfried, H. (1999): Die Grimmelfinger Schichten (Graupensande): fluviatile und/oder ästuarine Ablagerungen? *Jahreshefte Ges. Natur. Württemberg*, **155**: 5-25.

Clifton, H.E. (1983): Discrimination between subtidal and intertidal facies in Pleistocene deposits, Willapapa Bay, Washington. *Journal of Sedimentary Petrology*, **53**: 353-369.

Costello, W.R. & Southard, J.B. (1981): Flume experiments on lower flow regime bed forms in coarse sand. *J. sedim. Pterol.*, **51**: 849-864.

Dalrymple, R.W. & Rhodes, R.N. (1995): Estuarine dunes and bars. In: *Geomorphology and Sedimentology of Estuaries - Developments in Sedimentology* (Eds G.M.E. Perillo), **53**, pp. 359-422. Elsevier Science.

Diem, B. (1985): Analytical method for estimating palaeowave climate and water depth from wave ripple marks. *Sedimentology*, **32**: 705-720.

Erb, L., Haus, H.A. & Rutte, E. (1961): Erläuterungen zu Blatt 8120 Stockach. In: *Geologische Karte von Baden-Württemberg 1:25000.*

Fischer, G. (1933): Die Juranagelfluh Badens. *Mitt. bad. geol. L.-Anst.*, **11**: 91-212.

Gall, H. (1974): Neue Daten zum Verlauf der Klifflinie der oberen Meeresmolasse (Helvet) im südlichen Vorries. *Mitt. Bayer. Stattssamml. Paläont. hist. Geol.*, **14**: 81-101.

Geyer, O.F. & Gwinner, M.G. (1991): *Geologie von Baden-Württemberg.* Schweizerbart, 482 pp.

Gutmann, S. (1910): Gliederung der Molasse und Tektonik des östlichen Hegaus. *Mitt. bad. geol. Landesanst.*, **6**: 469-514.

Hagn, H. (1961): Die Gliederung der Oberen Meeresmolasse nördlich vom Überlinger See (Bodensee) in mikropaläontologischer Sicht. *Jh. geol. Landesamt Baden-Württemberg*, **5**: 293-321.

Harms, J.C., Southard, J.B. & Walker, R.G. (1982): Strutures and sequences in in clasatic rocks. *Society of Economic Paleontologists and Mineralogists Short Course*, **2**: 161.

Haus, H.A. (1951): Zur paläogeographischen Entwicklung des Molassetroges im Bodenseegebiet während des mittleren Miozäns. *Mitteilungsblatt der badischen geologischen Landesanstalt*, **1950**: 48-66.

Heim, A. (1919): *Geologie der Schweiz. 1. Molasseland und Juragebirge*. Tauchnitz, Leipzig.

Heim, A., Baumberger, E. & Stehlin, H.G. (1928): Die Subalpine Molasse des westichen Vorarlbergs. *Vierteljahresschrift der Naturforschenden Gesellschaft Zürich*, **73**: 1-65.

Hofmann, F. (1955): Neue geologische Untersuchungen in der Molasse der Nordostschweiz. *Eclogae geol. Helv.*, **48**: 100-124.

Homewood, P. & Allen, P. (1981): Wave-, tide-, and current-controlled sandbodies of Miocene molasse, Western Switzerland. *American Association of Petroleum Geologists, Bulletin*, **65**: 2534-2545.

Hülsemann, J. (1955): Großrippeln und Schrägschichtungs-Gefüge im Nordsee Watt und in der Molasse. *Senck. leth.*, **36**: 359-388.

Keller, B. (1989): *Fazies und Stratigraphie der Oberen Meeresmolasse (Unteres Miozän) zwischen Napf und Bodensee*. Unpubl. PhD Thesis, Universität Bern, Bern, 402 p pp.

Kempf, O., Bolliger, T., Kälin, D., Engesser, B. & Matter, A. (1997): New magnetostratigraphic calibration of Early to Middle Miocene mammal biozones of the North Alpine foreland basin. In: *Actes du Congrès BiochroM'97* (Eds J.-P. Aguilar, S. Legendre and J. Michaux), *Mémoires et Travaux de l' E.P.H.E.*, **21**, pp. 547-561, Montpellier.

Kiderlen, H. (1931): Beiträge zur Stratigraphie und Paläogeographie des süddeutschen Tertiärs. *Neues Jahrbuch für Mineralogie, Geologie und Paläontologie*, **66**: 215-384.

Knupfer, S. (1912): Molasse und Tektonik des südöstlichen Teils des Blattes Stockach der topographischen Karte von Baden. *Ber. Naturfr. Ges. Freiburg*, **19**.

Krinsley, D.H. & Doornkamp, J.C. (1973): *Atlas of quartz sand surfaces*. Cambridge University Press, 91 pp.

Kuhlemann, J. (2000): Post-collisional sediment budget of circum-Alpine basins (Central Europe). *Memoire di Scienze Geologiche Padova*, **52**: 1-91.

Kuhlemann, J. & Kempf, O. (2002): Post-Eocene evolution of the North Alpine Foreland Basin and its response Alpine tectonics. *Sedimentary Geology*, **152**: 45-78.

Laffon, J.C. (1847): Naturwissenschaftliche Skizzen des des Kantons Schaffhausen. *Verhandl. schweiz. naturf. Ges.*

Lemcke, K. (1970): Epirogenetische Tendenzen im Untergrund und in der Füllung des Molassebeckens nördlich der Alpen. *Bulletin der Vereinigung Schweizerischer Petroleum-Geologen und -Ingenieure*, **37**: 25-34.

Lemcke, K. (1972): Die Lagerung der jüngsten Molasse im nördlichen Alpenvorland. *Bulletin der Vereinigung Schweizerischer Petroleum-Geologen und -Ingenieure*, **39**: 29-41.

Lemcke, K. (1973): Zur nachpermischen Geschichte des nördlichen Alpenvorlandes. *Geologica Bavarica*, **69**: 5-48.

Lemcke, K., Engelhardt, W.v. & Füchtbauer, H. (1953): Geologische und sedimentpetrographische Untersuchungen im Westteil der ungefalteten Molasse des süddeutschen Alpenvorlandes. *Beih. Geol. Jb.*, **11**: 182.

Leuze, J. (1921): Die Citharellenkalke in Schwaben. *Neues Jh. Mineral. etc., Beil. Bd.*, **46**: 268-381.

Luterbacher, H. (1997): Stratigraphy and facies evolution of a typical foreland basin; the Tertiary Molasse Basin (Lake Constance area and Allgäu). In: *18th IAS regional European meeting of sedimentology, Heidelberg, September 2-4, 1997; field trip guidebook* (Eds T. Bechstädt, P. Bengtson, R. Gaupp, R. Greiling and V. Schweizer), *Gaea Heidelbergensis*, **4**, pp. 123-140, Heidelberg.

Luterbacher, H., Köhler, J. & Winder, H. (1992): The northern margin of the Molasse Basin in SW Germany. *Eclogae geologicae Helvetiae*, **85**: 787-788.

Lutzeier, H. (1929): Beiträge und Kenntnis der Meeresmolasse in der Ulmer Gegend. *N. Jb. Min Geol. Paläont., Beil Bd.*, **46**: 117-180.

McBride, E.F. (1963): A classification of common sandstones. *Journal of Sedimentary Petrology*, **33**: 664-669.

McKee, E.D. & Weir, G.W. (1963): Terminology for stratification and cross-stratification in sedimentary rocks. *Geological Society of America Bulletin*, **64**: 381-390.

Miall, A.D. (1996): *The Geology of fluvial deposits - Sedimentary Facies, Basin Analysis, and Petroleum Geology*. Springer Verlag, 582 pp.

Middleton, G.V. & Southard, J.B. (1986): *Mechanics of sediment movement*. 2nd ed.: SEPM Short Course No. 3, 246 pp.

Naef, H., Diebold, P. & Schlanke, S. (1985): *Sedimentation und Tektonik im Tertiär der Nordschweiz*. NAGRA Technischer Bericht, **85-14**, 145 p pp.

Nebelsick, J. (1989): Temperate Water Carbonate Facies of the Early Miocene Paratethys (Zogelsdorf Formation, Lower Austria). *Facies*, **21**: 11-40.

Nebelsick, J. (1992): Components analysis of sediment composition in Early Miocene temperate carbonates from the Austrian Paratethys. *Palaegeog. Palaeoclimatol. Palaeoecol.*, **91**: 59-69.

Nelson, C.H., Hyden, F.M., Keane, S.L., Leask, W.L. & Gordon, D.P. (1988a): Application of bryozoan zoarial growth-form studies in facies analysis of non-tropical carbonate deposits in New Zealand. *Sedimentary Geology*, **60**: 301-322.

Nelson, C.H., Keane, S.L. & Head, P.S. (1988b): Non-tropical carbonate deposits on the modern New Zealand shelf. *Sediment. Geol.*, **60**: 71-94.

Reichenbacher, B. (1989): Feinstratigraphische Gliederung der Kirchberger Schichten (Unter-Miozän) an der Typuslokalität Illerkirchberg bei Ulm. *Geologica Bavarica*, **94**: 135-177.

Reichenbacher, B., Böttcher, R., Bracher, H., Doppler, G., Engelhardt, W.v., Gregor, H.-J., Heissig, K., Heizmann, E.P.J., Hofmann, F., Kälin, D., Lemcke, K., Luterbacher, H., Martini, E., Pfeil, F.H., Reiff, W., Schreiner, A. & Steininger, F.F. (1998a): Graupensandrinne - Ries - Impakt: zur Stratigraphie der Grimmelfinger Schichten,Kirchberger Schichten und Oberen Süßwassermolasse: Kommentar zur 'Revision der Stratigraphie der süddeutschen Brackwassermolasse'. *Z. dt. geol. Ges.*, **149**: 127-161.

Reichenbacher, B., Doppler, G., Schreiner, A., Böttcher, R., Heissig, K. & Heizmann, E.P.J.

(1998b): Lagerungsverhältnisse von Grimmelfinger Schichten und Kirchberger Schichten: Kommentar zur 'Revision der Stratigraphie der süddeutschen Brackwassermolasse'. *Zeitschrift der deutschen geologischen Gesellschaft*, **149**: 321-326.

Rögl, F. (1996): Stratigraphic correlation of the Paratethys Oligocene and Miocene. *Mitt. Ges. Geol. Bergbaustud. Österr.*, **41**: 65-73.

Rollier, L. (1903): Über das Verhältnis von Helvétien zum Randengrobkalk in der Nordostschweiz. *Zentralbl. f. Min.*

Rollier, L. (1911): Revision de la Stratigraphie et la Tektonique de la Molasse. *Denkschrift schweiz. naturf. Ges.*

Rubin, D.M. & McCullough, D.S. (1980): Single and superimposed bedforms of San Francisco Bay and flume observations. *Sedim. Geol.*, **26**: 207-231.

Ryland, J.S. (1970): *Bryozoans.* Hutchinson, London, 175 pp.

Salvermoser, S. (1999): Zur Sedimentologie gezeitenbeeinflusster Sande in der Oberen Meeresmolasse und Süssbrackwassermolasse (Ottnangium) von Niederbayern und Oberösterreich. *Münchner Geologische Hefte (A)*, **26**: 1-179.

Schaad, E. (1908): Die Juranagefluh. *Beitr. geol. Karte Schweiz, N.F.*, **22**: 1-51.

Schaad, W., Keller, B. & Matter, A. (1992): Die Obere Meeresmolasse (OMM) am Pfänder: Beispiel eines Gilbert-Deltakomplexes. *Eclogae geologicae Helvetiae*, **85**: 145-168.

Schalch, F. (1901): Bemerkungen über die Molasse der badischen Halbinsel und des Überlinger Seegebiets. *Mittlg. Bad. Geolog. Landesanst.*, **4**.

Schalch, F. (1908): Erläuterungen zu Blatt Blumberg - Geologische Spezialkarte des Großherzogtum Baden, Heidelberg.

Schlunegger, F. (1999): Controls of surface erosion on the evolution of the Alps: constraints from the stratigraphies of the adjacent foreland basins. *International Journal of Earth Sciences*, **88**: 285-304.

Scholz, H. (1989): Die Obere Meeresmolasse (OMM) am Südrand des Molassebeckens im Allgäu. *Geologica Bavarica*, **94**: 49-81.

Schreiner, A. (1963): Geologische Untersuchungen am Höwenegg/Hegau. *Jh. geol. Landesamt Baden-Württemberg*, **6**: 395-420.

Schreiner, A. (1965): Die Juranagelfluh im Hegau. *Jh. geol. Landesamt Baden-Württemberg*, **7**: 303-354.

Schreiner, A. (1966a): Erläuterungen zu Blatt 8118 Engen; Geologische Karte von Baden-Württemberg 1:25000. Geologisches Landesamt Baden-Württemberg, Stuttgart.

Schreiner, A. (1966b): Zur Stratigraphie der Oberen Meeresmolasse zwischen der Oberen Donau und dem Überlinger See (Baden-Württemberg). *Jber. u. Mitt. oberrh. geol. Ver.*, **48**: 91-104.

Schreiner, A. (1974): Erläuterungen zur geologischen Karte des Landkreises Konstanz mit Umgebung 2. edn. Geol. Landesamt Baden-Württemberg, Freiburg i. Br.

Schreiner, A. (1976): *Hegau und westlicher Bodensee.* Sammlung Geologischer Führer, **62**. Gebr. Bornträger, Berlin - Stuittgart, 337 pp.

Schreiner, A. & Luterbacher, H. (1999): Die Molasse zwischen Blumberg und Überlingen (Exkursion J am 9. April 1999). *Jber. Mitt. oberrh. geol. Ver.*, **N.F. 81**: 171-181.

Steininger, F.F., Berggren, W.A., Kent, D.V., Bernor, R.L., Sen, S. & Agusti, J. (1996): Circum-Mediterranean Neogene (Miocene and Pliocene) marine-continental chronologic correlations of European mammal units. In: *The Evolution of Western Eurasian Neogene Mammal Faunas* (Eds R.L. Bernor, V. Fahlbusch and H.-W. Mittmann), pp. 7-46. Columbia University Press, New York.

Terwindt, J.H.J. (1971): Litho-Facies of inshore estuarine and tidal-inlet deposits. *Geologie en Mijnbouw*, **50**: 515-526.

Terwindt, J.H.J. (1988): Palaeo-tidal reconstructions of inshore tidal depositional environments. In: *Tide-influenced sedimentary environments and facies* (Eds P.L. de Boer, A. van Gelder and S.D. Nio), pp. 233-263. D. Reidel Publ. Co., Dordrecht, Netherlands (NLD).

Terwindt, J.H.J. & Brouwer, M.J.N. (1986): The behaviour of intertidal sandwaves during neap-spring tide cycles and the relevance for palaeoflow reconstructions. *Sedimentology*, **33**.

Tipper, J., Sach, V.J. & Heizmann, E.P.J. (2003): Loading fractures and Liesegang laminae: new sedimentary structures found in the north-western North Alpine Foreland Basin (Oligocene-Miocene, southwest Germany). *Sedimentology*, **Online publication date: 18-Jul-2003**.

Tucker, M.E. & Wright, V.P. (1990): *Carbonate Sedimentology.* Blackwell Scientific Publications, 482 pp.

Visser, M.J. (1980): Neap-spring cycles reflected in Holocene subtidal large-scale bedform deposits: A preliminary note. *Geology*, **8**: 543-456.

Volz, E. (1953): Geologische Untersuchungen in der tertiären Molasse des Saulgauer Gebiets. *Neues Jb. Geol. u. Paläontol.*, **97**: 189-219.

Wass, R.E., Conolly, J.R. & MacIntyre, R.J. (1970): Bryozoan carbonate sand continuous along southern Australia. *Marine Geology*, **60**: 63-74.

Werner, J. (1966): Ergebnisse der Auswertung von Flachbohrungen im Bereich des Gobsandzuges der Oberen Meeresmolasse (Gebiet Stockach - Pfullendorf). *Jber. Mitt. oberrh. geol. Ver.*, **N. F. 48**: 105-120.

Winder, H. (1983): *Untersuchung der Fazies der Oberen Meeresmolasse nördlich des Überlinger Sees (Bodensee).* Diplomarbeit, Tübingen.

Zöbelein, H.K. (1985): Helicidenschichten und Albstein in der miozänen Vorlandmolasse Südwestdeutschlands. *Jahreshefte des Geologischen Landesamtes Baden-Württemberg*, **27**: 41-92.

Zweigel, J. (1998): Reservoir analogue modelling of sandy tidal sediments, Upper Marine Molasse, SW Germany, Alpine foreland basin. In: *Cenozoic Foreland Basins of Western Europe* (Eds A. Mascle, C. Puigdefàbregas, H.-P. Luterbacher and M. Fernàndez), *Geological Society Special Publication*, **134**, pp. 325-337.

Chapter 5

Palaeogeographic evolution of the Upper Marine Molasse basin and its impact on circulation pattern and sediment transport pathways

5.1 Abstract

In previous chapters modeling of global and regional tidal waves has been introduced. This chapter presents further studies. Alternative reconstructions for the circum-mediterranean realm are presented, to evaluate possible ranges in tidal amplitude distribution, which might have co-oscillated with the shallow water model of the Burdigalian Seaway. Moreover the regional model of the Burdigalian Seaway was reconstructed for different palaeogeographic key stages. This allowed us to retrace changes of tidal amplitudes due to changes in the palaeogeography and palaeobathymetry of the seaway. To evaluate changes in net-sediment transport directions, the regional model was also driven by river influx and atmospheric forcing.

5.2 Global M_2 simulation

As shown in Chapter 2, simulations of the global M_2 oscillation system were used, to derive boundary conditions (tidal amplitudes and phases) for both open boundaries of the Burdigalian Seaway. The numerical constraints, which have been calculated in chapter 2 are understood to represent a minimum estimate.

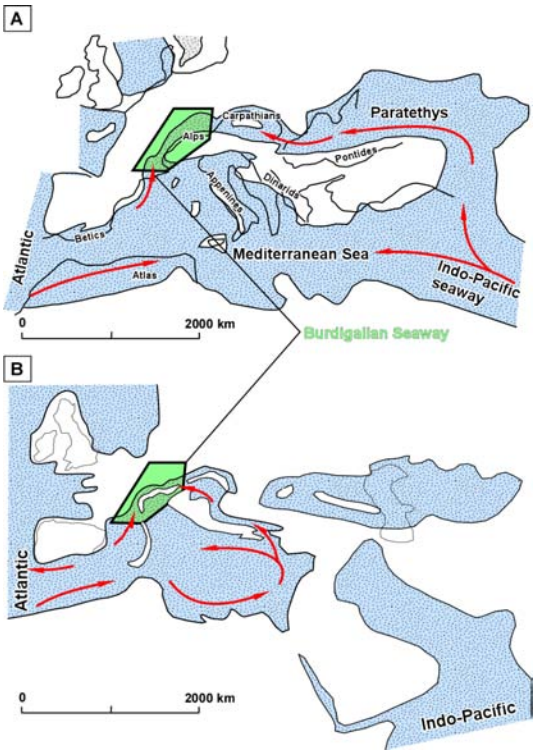

Figure 5.1: *Palaeogeographic sketch maps of early Miocene basin shape of the circum-Mediterranean realm accounting ideas of [A] Dercourt et al. (1993) and [B] Rögl (1998). Red arows indicate possible propagation routes for tidal waves.*

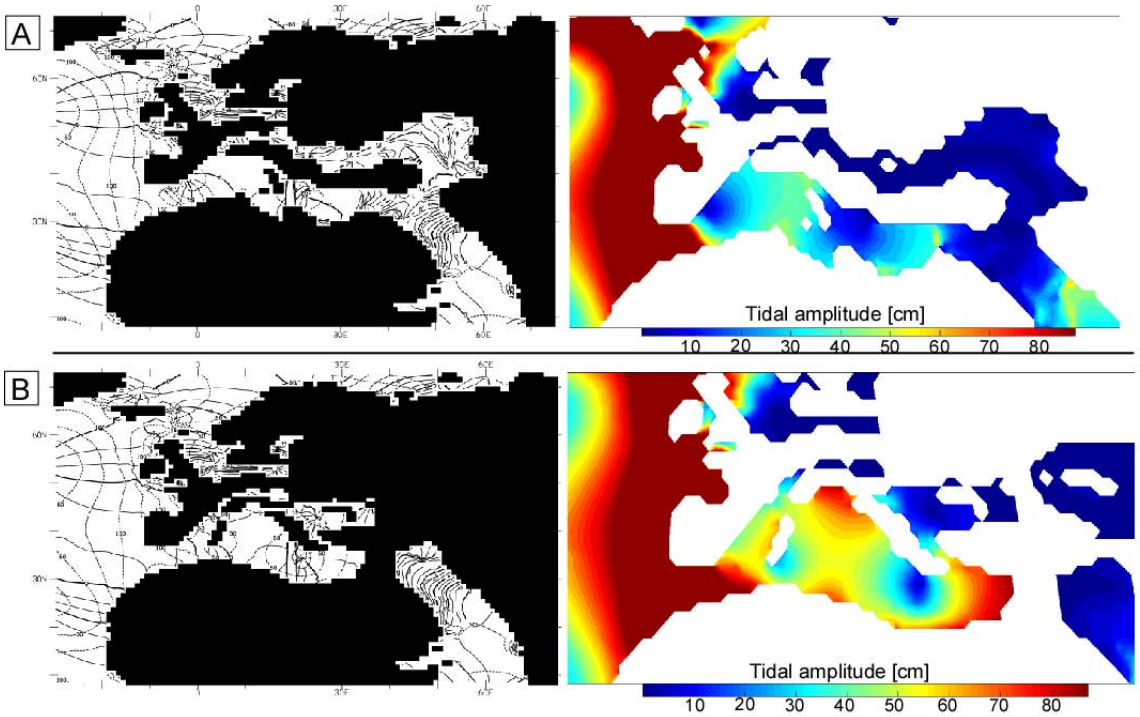

Figure 5.2: *Two alternative palaeogeographic reconstructions of the circum-Mediterranean realm accounting ideas of [A] Dercourt et al. (1993) and [B] Rögl (1998). The monochrome figure shows the simulation results with co-range lines and co-tidal lines. For a better understanding tidal amplitudes are color coded on the right part of the figure.*

Further models runs have been carried out using

- ⋆ the palaeogeographical reconstruction of chap. 2, with widened and deepened seaways towards the Atlantic and the Indian Ocean and removal of emergent areas within the Mediterranean, to allow tidal propagation more easily (see Fig. 5.2 [A]),
- ⋆ an alternative palaeogeographical reconstruction as proposed by Rögl (1998); (see Fig. 5.2 [B]).

Model runs using a modified palaeogeograpy (widened gateways towards the Atlantic and Indic Ocean; removal of small-scale emergent areas) of chapter 2 (Fig. 5.2 [A]) yield minimum estimates of tidal amplitudes both the region in SE France and Austria. A maximum of tidal amplitudes were calculated for the western Mediterranean by using an alternative reconstruction as proposed by Rögl (1998) (see Fig. 5.2 [B]). Tidal amplitudes in this case are in the order of 1.40m and belong to a meso-tidal system which has been established in the Mediterranean sea. At the southern gateway of the Burdigalian Seaway, maximum values are simulated to have reached around 60cm. It might be well possible to increase them further by changing the basin shape (most likely by realigning slightly the tectonic block of Corsica and Sardegna).

Tidal amplitudes for the Austrian region reach values of some 20cm within all the simulations. The simulations show, that tidal waves are damped (tidal friction) either on their way from the Indo Pacific (see Fig. 5.2 [A]) but also on their way through the constricted corridors towards the Austrian realm (see Fig. 5.2 [B]).

5.3 Palaeogeographic evolution of the North Alpine Foreland basin during the Upper Marine Molasse

During the deposition of the Upper Marine Molasse, the North Alpine Foreland Basin was flooded by a shallow marine sea. The aim of the chapter is to present 6 sketch maps describing the spatial extent and relative bathymetry of the OMM sea. The stratigraphic data were compiled from literature and research carried out in

the field (chapter 4). A detailed stratigraphic framework is absolutely necessary to constrain the shallow water model. This allows to accomodate the shift of tidal loci and thus changes in the tidal regime and meso-scale current system.

For an overall discussion of the evolution of the NAFB, see e.g. Kuhlemann & Kempf (2002), Sissingh (1997), Berger et al. (2005 a,b) and for the Rhône-Bresse Gaben system see e.g. Sissingh (1998, 2001), Dermarq & Perriaux (1984).

The facies distribution in the NAFB is generally controlled by eustatic sea-level changes and structural developments that can be assigned to major tectonic processes.

- Tectonic subsidence caused by orogenic loading. Alpine tectonics at the thrust front and also indirectly the uplift of the crystalline domes in Austria and Switzerland redirected the Alpine dispersal systems.

- "Interference Zone" Lake Constance region: Between two isostatic unequal domains the Alps and the Upper Rhine Graben system (Black Forest, Vosges) respectively. Recently Berger (2005a,b) showed that uplift of the Vosges startet already during USM times. Uplift of the Black Forest possibly started during the OMM (Liniger 1925). A palaeohigh west of Lake Constance (Lägern area) is proposed by Naef et al. (1985), Berger et al. (2005). It is possible that sub-basins, may have formed in the the "interference zone" also enhanced by reactivate structure of the Permo-Carbon trough. The extenional regime of the Northern Upper Rhein Graben rotated counterclockwise from ESE to NE during the OMM, possibly related to a major change in the direction of convergence in the Alpine domain south of the Rhine Graben (Meier & Eisbacher 1991). This might have turned the foreland bulge to a SW directed striking structure, enabling a SW directed draining fluvial system (see discussion of the "Grobsandzug" below).

- In the later stage of the OMM (Upper Ottnagian, $\sim$ 17.5 Ma) the eastern Alps collided with the Bohemian spur and closed the marine connection towards the Paratethys.

5.3.1 USM - Aquitanian, late Egerian, 22 Ma - Fig. 5.4

During the Aquitanian the continental sedimentation persisted in the western and central part of the Molasse basin. Supplied sediment was equal or in excess of the accommodation space. The western and central part of the Molasse basin was dominated by the accumulation of thick mainly conglomeratic alluvial fan deposits. Northward-flowing, marginal intra-Alpine streams formed a series of individual and partly lateral interfingering deltaic fans along the alpine thrust front (cf. Berger 1996; Schlunegger & Pfiffner 2001; Kuhlemann & Kempf 2002). The thrust wedge fringing fans were characterized by steep proximal areas and dominated by braided rivers. Downstream these gave way to relatively low-gradient floodplains typified by meandering rivers. Farther away from the rising mountain belt, lakes and swamps occurred within a fluvial system *draining to the east* (Füchtbauer 1964; Büchi et al. 1965; Füchtbauer 1967; Büchi & Schlanke 1977), that was additionally fed by a southward draining palaeo-Main (Lemcke 1985). At the northern margin ephermal flash floods cut into the Swabian platform draining southwards, delivering conglomeratic deposits of the "Ältere Juranagelfluh" towards the south (Schreiner 1965).

Within the Austrian part of the Molasse Basin, deep marine conditions prevailed from UMM times. Within the Puchkirchen Basin, an axial channel belt runs approximately parallel to the Alpine thrust front (deRuig 2003). It is 3-5 km wide and of low sinuosity. The channel fill consists of predominantly coarse-grained conglomeratic debris flow and turbidite deposits. Overbank areas are characterized by fine-grained turbidite sands. Main sediment transport direction was from west to east. The water depth of the Puchkirchen Basin is considered to have been in the order of 1000 to 1500m based on foraminiferal assemblages (Rögl et al. 1979; Robinson & Zimmer 1989). It is generally accepted, that a series of lobate submarine fans, which were fed by a series of intramontane streams cutting through the narrow, tectonically unstable southern shelf (Moiolo 1976; Kollmann & Malzer 1980). In front of the thrust front various fans overlapped to form a belt of amalgamated turbidite fans, locally disturbed by submarine slides and slumps. Sediment supply was predominantly from south to north, although sediment reworking was postulated

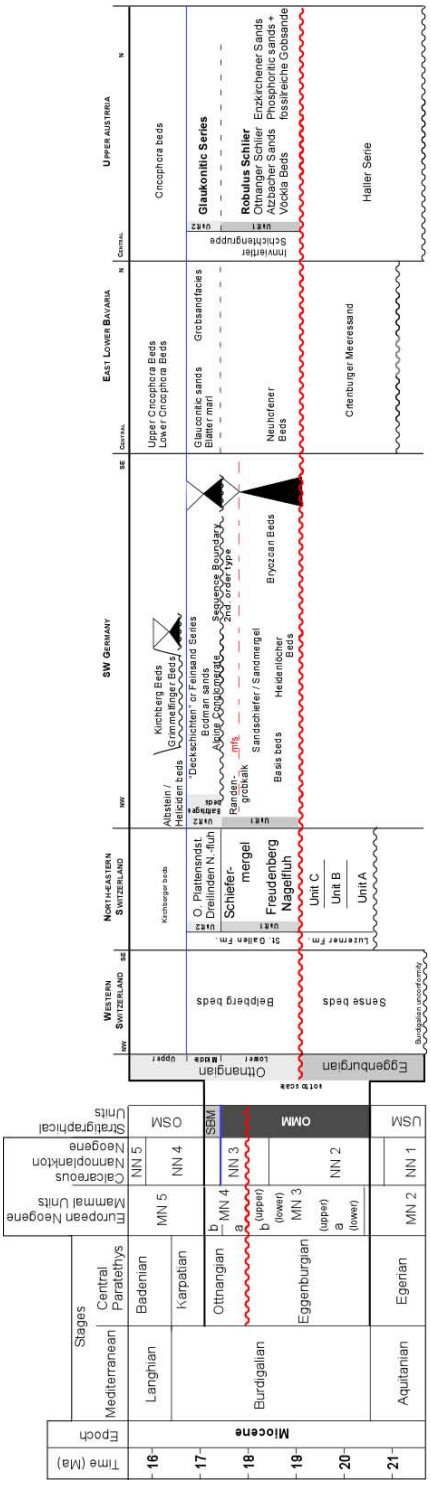

Figure 5.3: *Stratigraphic chart of Upper Marine Deposits from the North Alpine Foreland Basin, note that the detailed lithostratigraphy is not to scale accrding to time. Modified according to Rögl & Steininger (1984), Scholz (1989), Luterbacher et al. (1992), Reichenbacher (1993), Egger et al. (1996) Schlunegger (1997), Burkhard & Sommaruga (1998), Salvermoser (1999), Strunck (2001), Kuhlemann & Kempf (2002).*

by Wagner (1996, 1998). Robinson & Zimmer (1989) recognized in a seismic stratigrapic study (based on 2D seismic), that part of the submarine fan complex was channelized. This part is interpreted as proximal feeder channels of the fan complex. Using a 3D seismic survey, it became clear that the turbidite fan lobe model of the Puchkirchen system is inaccurate. Linzer (2001) described the Puchkirchen system as a broad, roughly west-east trending axial channel complex. There is no evidence for the lobe geometries of the classical turbidite fan model of Walker (1978). Recently deRuig (2003) published an 3D seismic investigation, where different depositional elements like e.g. levee deposits, crevasse splays and terraces have been identified within the deep water channel complex of the Puchkichen system.

5.3.2 Upper Marine Molasse (OMM) - Eggenburgian and Ottnangian times

At the beginning of the Burdigalian $\sim$ 21Ma, a widespread and rapid transgression occurred (see also chap. 3). While this can be correlated with the global eustatic sea level curve of Haq et al. (1987, 1988), several short-lived facies and basin geometry modifications between 18Ma and 17Ma, which can be observed in the South German molasse basin (see e.g. Doppler 1989) are partly related to eustatic sea-level fluctuations (Lemcke 1983; Lemcke 1988; Zweigel et al. 1998; Jin et al. 1995) but also to alpine processes (Gall 1975; Kempf et al. 1997; Schlunegger et al. 1997; Spiegel et al. 2001; Kuhlemann & Kempf 2002).

Whether the transgression occurred from the west or the east has been discussed intensively several times in the past with varying answers see e.g. Rigassi (1957), Berger (1985), Allen & Bass (1993), Luterbacher (1997), Schlunegger et al. (1997), Strunck (2001) and Kempf (unpublished seismic data). In general we have to assume that sediment series have been deposited diachronously from west to east, but also from the central towards the external basin.

Siliciclastic sediments of the Upper Marine Molasse are subdivided into two transgressive-regressive fining upward cycles, separated by a hiatus between 18.3-17.8 Ma in the Molasse basin of eastern Switzerland (Kempf et al. 1999) and between 18.1-17.7 Ma in central Switzerland (Schlunegger et al. 1997). With the beginning

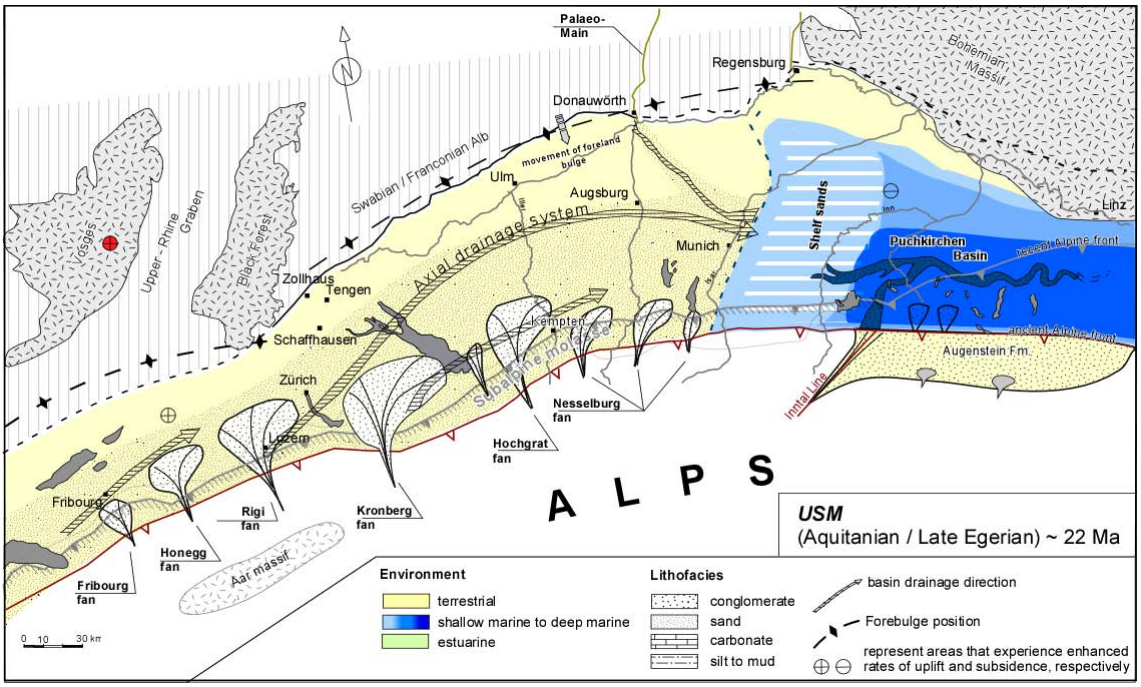

Figure 5.4: *Palaeogeography of the NAFB during late USM times. Dispersal systems at the Swiss thrust front fed the Basin with sediment. The east directed fluvial system, transported sand towards the residual sea in eastern Bavaria (the Puchkirchen Basin). In Austria an axial, deepwater channel complex runs subparallel to the Alpine thrust front - for explanation see text.*

of the OMM transgression, accomodation space formation occured at higher rates than sediment accumulation. Hence the transgression of the OMM marks a change in the central and western NAFB from overfilled to underfilled conditions.

Middle Eggenburgian ca. 19Ma - Fig. 5.5

During the Eggenburgian, the marine transgression reached eastern Switzerland, establishing a shallow wave- and tide-controlled seaway (Allen et al. 1985, Keller 1989, Schaad et al. 1992 - Luzern Fm. in eastern Switzerland).

Potentially, a narrow trench was flooded due to enhanced subsidence in front of the alpine thrust wedge, linking the residual sea in Bavaria with the western part (Zweigel et al. 1998) along the central part of the Molasse Basin (Bachmann Müller 1991: Fig. 20:13). In the course of the marine transgression, the top of the underlying Freshwater Molasse was eroded.

In terms of an intermittend regression of the OMM sea towards west-Switzerland, continental conditions arised for a short time.

Early Lower Ottnangian ca. 17.9 Ma. - Fig. 5.6

A subsequent transgression is marked by a regional erosional unconformity (Lemcke 1988) with reworking and erosion of Molasse sediments in Bavaria up to 250m (Zweigel et al. 1998) and in western Switzerland of around 50m (Morend 2000). The transgression reached the Lake Constance reagion. Within eastern Switzerland the St. Gallen unit starts to be deposited. This transgression generated the maximum flooding of the NAFB. Stacking pattern of sediments can be subdivided into a retrogradational (TST - Transgressive systems tract) and a progradational (Highstand systems tract - HST) parasequence set. The stacking pattern describe one cycle but not 2 cycles, as proposed by Lemcke et al. (1953).

Late Lower Ottnangian; "transgressive series - TST" - 1^{st} cycle of Lemcke et al. (1953) - Fig. 5.7

For the German Molasse basin, we propose the onset of the maximum flooding at this stage. This is in contradiction to the accepted opinion that the most widespread transgression occurred during the 2^{nd} cylcle of Lemcke et al. (1953), see

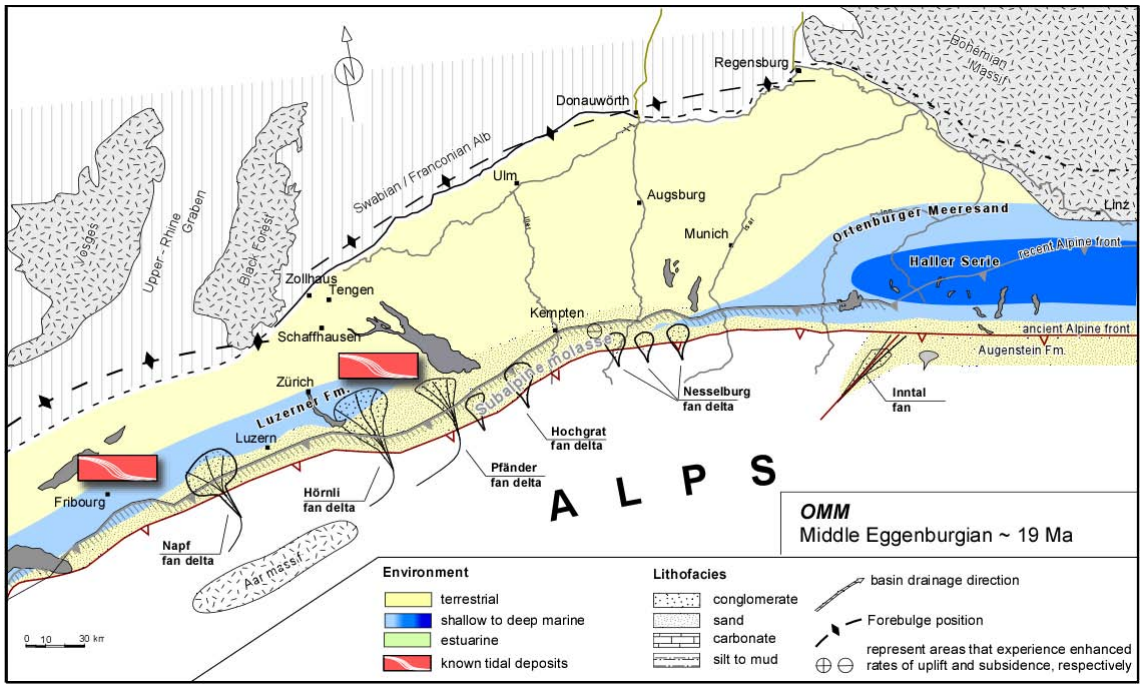

Figure 5.5: *Palaeogeographic reconstruction of the NAFB for the Middle Eggenburgian (ca. 19 Ma). The possible position of the forebulge was adopted from Laubscher (1992) and Zweigel & Zweigel (1998). The direction of the transgression is discussed in the text.*

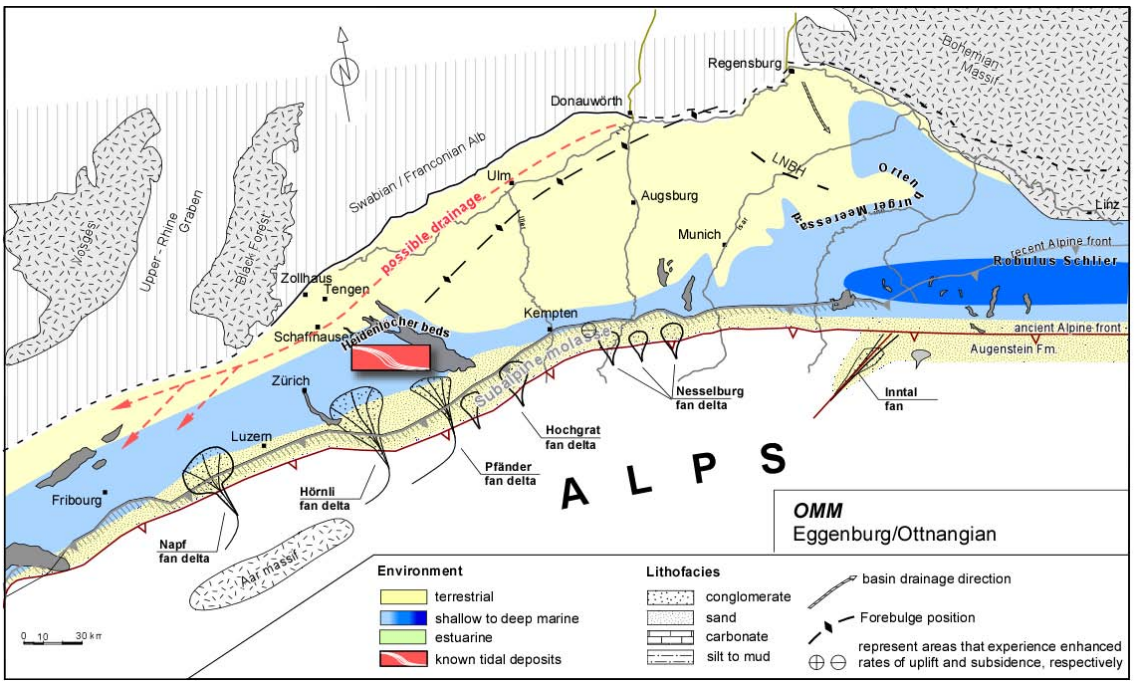

Figure 5.6: *Palaeogeographic reconstruction of the NAFB in thr turn of the Eggenburgian, Ottnangian. The figure was modified after Wenger (1987), Kuhlemann & Kempf (2002).*

e.g. Volz (1953), Kiderlen (1931), Gall (1975), Hüttner (1961), Erb et al. (1961), Doppler et al. (in press). So far it is not clear if there was a forced transgression or if the onset of the flooding took place in a more gradual way forming a complex coastline of various extents with

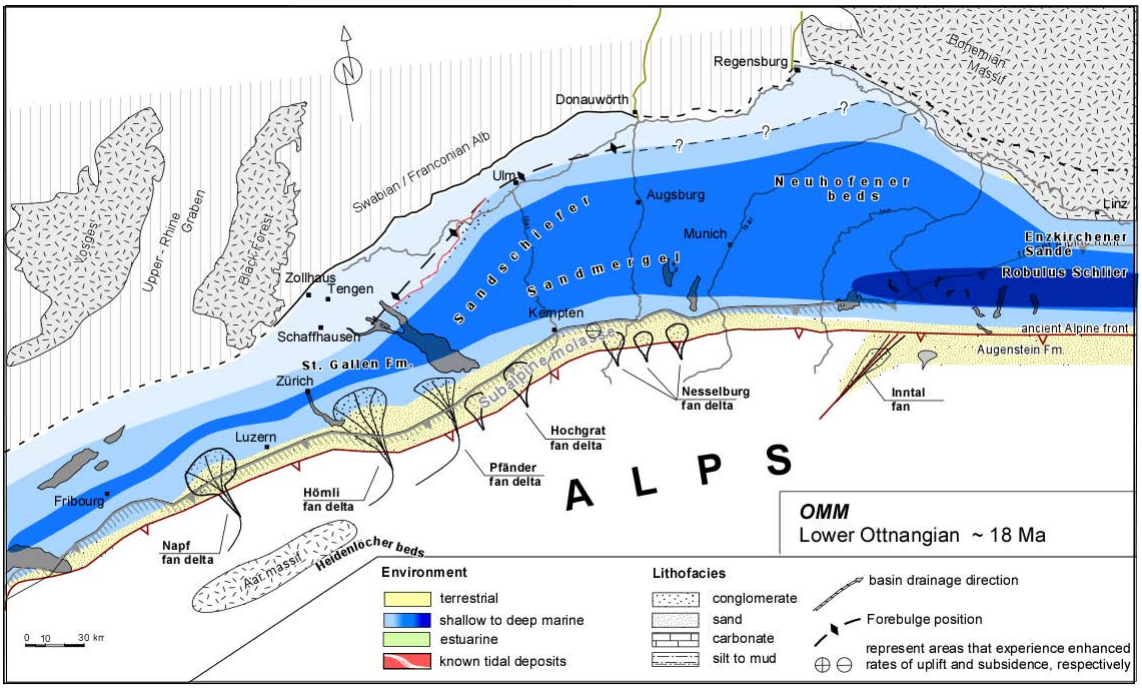

Figure 5.7: *Palaeogeograpic reconstruction of the NAFB during the Lower Ottnangian (~ 17.8 Ma), during the maximum flooding; depth distribubution was asymmetric with the deepest bathymetry next to the alpine thrust front.*

stairways of coastal terraces (cf. "inner cliff" of Roll (1935)). The retrogradation of the shoreline is marked by several coquina beds, described in Gutmann (1910), Haus (1951), Knupfer (1912), Schalch (1901), Lemcke et al. (1953).

The transgressive unit is formed by the basinal "Basisschichten", the "Sandschiefer/Sandmergel" series and the near-shore equvalent the "Randengrobkalk". Basin shape is asymmetric, with the greatest bathymetry near the alpine thrust front tapering of towards the Swabian and Franconian platform. Accomodation space which was created due to the eustatic sea-level rise and subsidence was filled slowly.

In the eastern Molasse basin the "Neuhofen beds" in Bavaria (e.g. Heermann 1954; Paulus 1964 - Bavaria) and the equivalent "Robulus Schlier" in Austria were deposited in the Lower Ottnangian.

Middle Ottnangian - 2^{nd} cycle of Lemcke et al. (1953) - Fig. 5.8

The maximum flooding surface, which separates the transgressive systems tract from the high-stand systems tract, represents the maximum landwart extent of marine conditions. This has been identified in the Randengrobkalk (see chapt. 4). A drop in sea-level is attended by the retreat of the northern as well the southern shoreline and a northward progradation of the alpine dispersal system. At this time the German Molasse Basin was overfilled, changing from a wedge to a tabular shaped basin (see also Schlunegger et al. 1997).

The Alpine Conglomerate was deposited above a sequence boundary when accomodation space was sufficient to allow deposition. Local occurence of marine faunal elements (oysters) indicate that the Alpine Conglomerate has been reworked during the transgression (TST).

The Baltringen beds are descibed by eg. Kiderlen (1931), Haus (1951), Hülsemann (1955), Erb et al. (1961), Luterbacher (1997). They represent the HST of the next sequence in SW-Germany. The Glaukonitsand facies in Bavaria (Neumaier & Wieseneder 1939, Zöbelein 1940, Wenger 1987, Salvermoser 1999) and the e.g the "Phosphoritsande" in lower-Austria (for further local stratigraphic units see e.g. Faupl & Roetzel 1990, Krenmayr & Roetzel 1996, Wagner 1996) represent time equivalent deposits of the Baltringen beds.

A differing facies in the northeastern vicinity

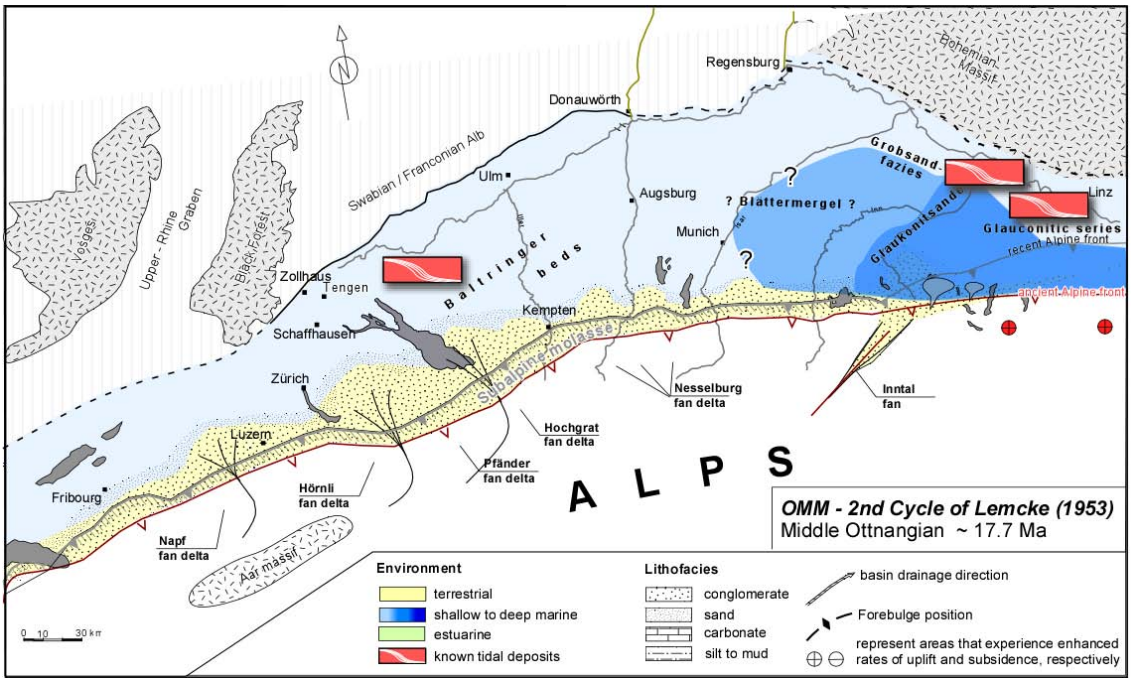

Figure 5.8: *Palaeogeograpic reconstruction of the NAFB during the Middle Ottnangian (∼ 17.7 Ma)*

of Lake Constance was firstly described by Gutmann (1910) and named by Haus (1951) "Grobsandzug Friedingen-Rengetsweiler". The "Grobsandzug" forms an elongate body, running 20-25 km parallel to the northern margin of the later "Graupensandrinne". The "Grobsandzug" is discussed by many authors, see e.g. Teike (1921), Teike (1923), Kiderlen (1931), Rutte (1952), Volz (1953), Erb et al. (1961), Haus (1960), Werner (1966). The chronostratigraphic setting of this unit is unknown and discussed controverse (see e.g. Kiderlen 1931, Haus 1951, Rutte 1952). We propose that the "Grobsandzug" belongs to the uppermost regessive unit, where a estuarine system was established in the backbulge area. Nevertheless there is evidence, that during Eggenburgian times, when continental conditions prevailed for the northern part of the German molasse basin, a SW draining fluvial system existed (Kiderlen 1931, Kuhlemann & Kempf 2002). The change of the drainage direction, shortly after the USM, cannot be correlated with an orogenic phase of the alps, but may originate from the interplay of the Alpine and the Upper Rhine Graben stress system and results in a complex system of bars and swales (subbasins). For a possible position of the peripheral bulge see e.g. Volz (1953).

The morphological rim of the backbulge with a tentative graben system (Werner 1966) formed the natural course of the "Grobsandzug" river (Haus 1951; Rutte 1952; Werner 1966) and thus was the precursor of the Graupensandrinne. The tentative graben system might also be originated in a reacitvation of Permo-Carboniferous trough structures (Naef et al. 1985).

It's discussed by e.g Büchi and Hofmann (1960), Büchi & Schlanke (1977), Büchi et al. (1965), Hofmann (1955), Hofmann (1976), Schreiner (1966), Allen et al. (1985) that based on heavy mineral analysis and key clasts (accessory andalusit, dark cherts) medium- to coarse grained sand was transported from the Bohemian Massif towards the Swiss realm. This was confirmed early by Kiderlen (1931) who recognized dark cherts from the Frankenwald in the vicinity of Donauwörth and Ulm in the Eggenburgian. The fluvial system of Kiderlen (1931) was fed by the palaeo-Main (see also Büchi & Hofmann 1960).

SBM - Late Ottnangian - Collision of Austrian thrust front with the Bohemian spur - renewed transgression from the west - Fig. 5.9

The Upper Marine Molasse is unconformably overlain by the estuarine, fluvial and brackish to limnic deposits of the Freshwater-Brackish Mo-

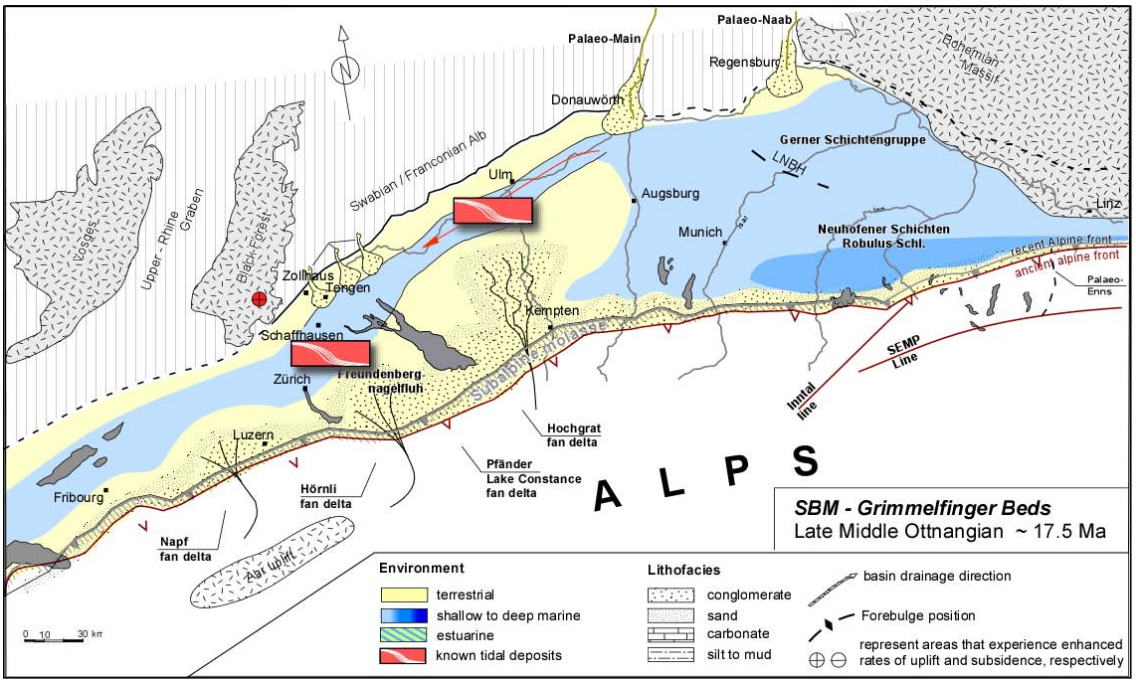

Figure 5.9: *Palaeogeography of the NAFB during the Lower Upper Ottnangian (∼ 17.5 Ma), during the SBM (Freshwater-Brackish Molasse) - modified according to Lemcke (1988), Doppler (1989), Reichenbacher (1993); SEPM Line = Salzach-Enns-Mariazell-Puchberg Line after Ratschbacher et al. (1991).*

lasse (SBM). At this time, the sea retreated towards the southwest (Swiss central plain and Rhône Valley).

Along the northern border of the German molasse basin, the "Graupensandrinne" was cut and filled with predominantly quarzitic gravel and coarse sand. The transgressive brackish to limnic upper part of the Freshwater-Brackish Molasse grades towards the top into the continental deposits of the Upper Freshwater Molasse (OSM).

The depositional environment of the Grimmelfinger Schichten was interpreted by most authors to be fluvial (Buchner & Seyfried 1999, Graf 1991, Kiderlen 1931, Lemcke 1985, Moos 1925, Bader et al. 2000). Recently, however, it has been reinterpreted as being largely estuarine (Asprion & Aigner 2000, Luterbacher et al. 1992, Reichenbacher et al. 1998a,b) or fully marine (Tipper et al. 2003) as suggested by marine vertebrate fossils that they contain (Sach & Heizmann 2001).

Both the fluvial or estuarine interpretations of the Grimmelfinger Schichten foresee the Graupensandrinne as a fluvially incised valley cut in response to a sharp fall in sea-level. The belief, that the Graupensandrinne was a fluvially incised valley is deeply entranched. Tipper et al. (2003) reinterpretated the origin of the "Graupensandrinne" as a valley of a 'drowned river' or eventually cut by marine erosion (e.g. Werner 1966). A boulder-bed at the base of the Grimmelfinger Schichten has been dated by Sach and Heizmann (2001) as belonging to mammal zone MN4 (c. 17.5 Ma).

The collision of the eastern Alpine thrust front with the Bohemian massif, leads to an uplift in the eastern part of the Molasse basin and changed the basin drainage gradient towards the west. This is the transport direction of the Glimmersande.

5.4 Numerical results of a sensitivity analysis using different palaeogeographic key stages

Fluctuations in eustatic, tectonic, and climatic conditions of the seaway caused key oceanographic parameters (palaeogeography, palaeobathymetry, stratification, wind stresses and boundary tides) to vary widely throughout the seaway's history. These fluctutions, in turn must have caused variations in its circulation and sediment-transport regimes.

Based on the presented palaeogeographic reconstructions two additional key stages have been chosen according to the widespread occurence of tidal deposits during each time interval.

- ⋆ Mid-Eggenburgian: Forced by one M_2 tidal wave form the southwest.
- ⋆ Mid-Ottnangian: For detailed M_2 simulation results see chapter 3; this section evaluates the response of residual currents according to different driving methods (atmospheric forcing, river influx).
- ⋆ Upper-Ottnangian:Forced by a combination of one M_2 tide and river influx form the Palaeo-Naab and Palaeo-Main.

While chapter 3 analyses tidal forcing of the Burdigalian seaway using different initial conditions. This section determines the influence of different forcing mechanisms on the residual velocities generated by the M_2 waves in the "Mid-Ottnangian model" of chapter 3. Forcing of the Burdigalian Seaway was enhanced by strong wind but also freshwater influx.

5.4.1 Mid-Eggenburgian model

Based on the palaeogeographical reconstruction (semi-enclosed basin), the model was driven with one incident M_2 wave of 2m amplitude (Fig. 5.11). As basin length is a multiple of the quarter M_2 wavelength, tidal waves are reflected (and amplified) at the head of the semi-enclosed basin. Thus the basin reacts with resonance according to the forcing M_2 wave and a standing wave was generated with an amphidromic point in western Switzerland. The computed residual velocities show distinct circulation cells between the Napf and Hörnli Fan system, similar to what is described by Allen et al. (1985). Net sediment transport in the Basse-Dauphiné and Rhône area is directed towards the southwest, with a main current in the mid of the sea, flanked by clockwise and anti-clockwise rotating circulations cells towards the western and eastern coastlines. Circulation cells themself can be separated in terms of branches into subordinate circulation cells promoting the general current system.

5.4.2 Mid-Ottnangian model

Chapter 3 shows in detail the response of the Mid-Ottnangian model towards changed tidal boundary conditions. The numerical results presented in this section evaluate how "unidirectional" forcing mechanisms (wind, point sources) influence the residual velocites generated by two incident tidal waves of 2m amplitude.

Including atmospheric forcing to the Mid-Ottnangian model

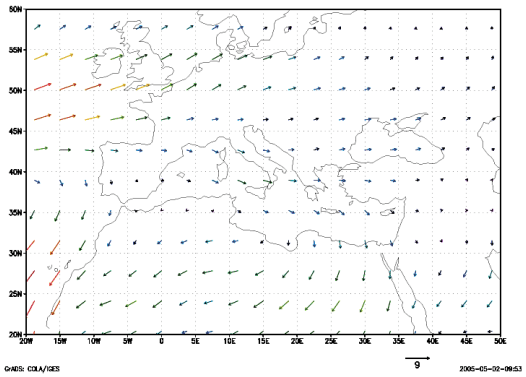

Figure 5.13: *Simulated annual wind field for the Tortonian, taken from the ECHAM4/ML simulations of Micheels (2003).*

In a separate set of experiments we applied a uniform wind field. The wind forced the model instantaneous after it has achieved its dynamic equilibrium with the M_2 tide.

In a first test a wind field directed towards the SSE was applied. This is based on a reconstruction of the wave climate for the Swiss part of the Burdigalian Seaway presented by Allen et al. (1985). Similar wind directions are derived from Tortonian ECHAM4/ML simulations by Micheels (2003). Wind stress is directed towards 292° clockwise from true north. The strength of the wind is estimated to be 20m/s (equal to 8 BFT). During the Quoddy simulation, the wind field was linearly ramped up over 2 tidal periods. For the remaining tidal cycle, the wind field was held constant.

The residual velocities (Fig. 5.12) display a general increase with a magnitude in the order of 3 (see reference vector. Apparent in these unstratified (barotropic) results is the deep penetration of the wind. Within the south German part of the model, eastward directed residual velocities are amplified by the wind field, generating a strong clockwise rotating velocity field. Alongshore currents along the western coastline of the Bohemian massif are also intensified. Since

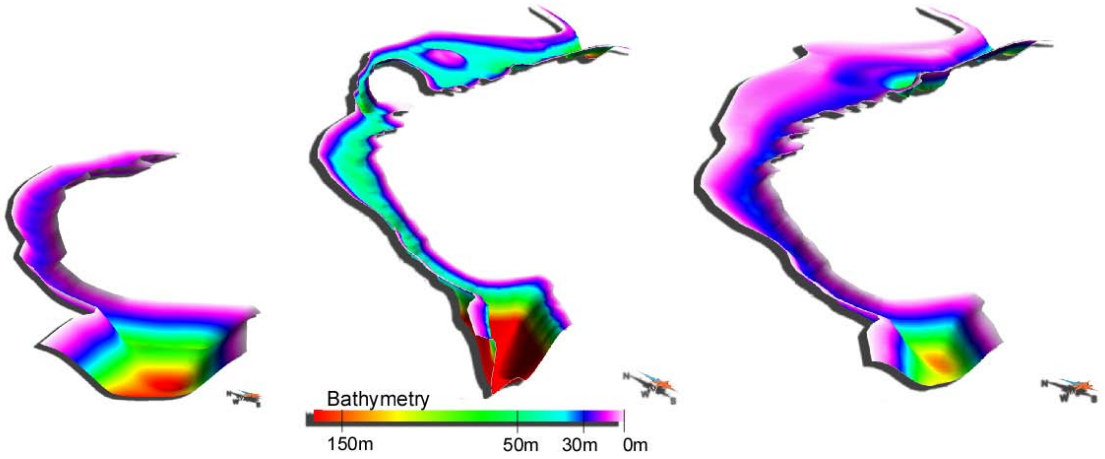

Figure 5.10: *Reconstructed 3D palaeobathymetry: from left to the right; Mid-Eggenburgian, Mid-Ottnangian, Upper-Ottnangian*

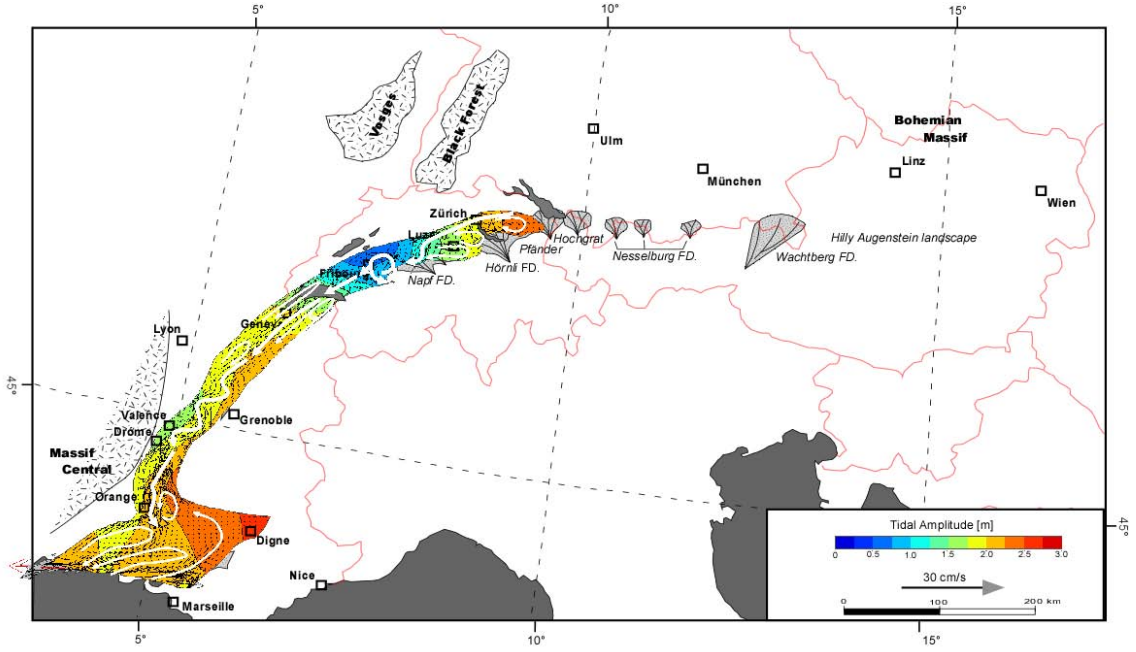

Figure 5.11: *Residual velocities and tidal amplitudes of the Mid-Eggenburg model. The model is initiated with one tide entering the seaway at it southwestern open boundary.*

the wind field was applied over the whole model domain with the same strength and direction, residual velocities in Switzerland and the Rhône area are as expected directed strongly towards the southwest.

Evaluating river influx from the surrounding domains for the Mid-Ottnangian model

The prognostic calculations of river influx into the model require an additional spin up of some days for the nonlinearities and additional dynamics of the baroclinic model to be established. Therefore the simulation is run for 7 extra M_2 tidal periods (total of 12 days). Runoff rates from the surrounding domains have been estimated (Kuhlemann pers. com.) and used within the study.

Simulation results show, that river runoff in general corresponds to a intensification of residual currents (Fig. 5.15). Three circuits are generated, parting the sediment transport east

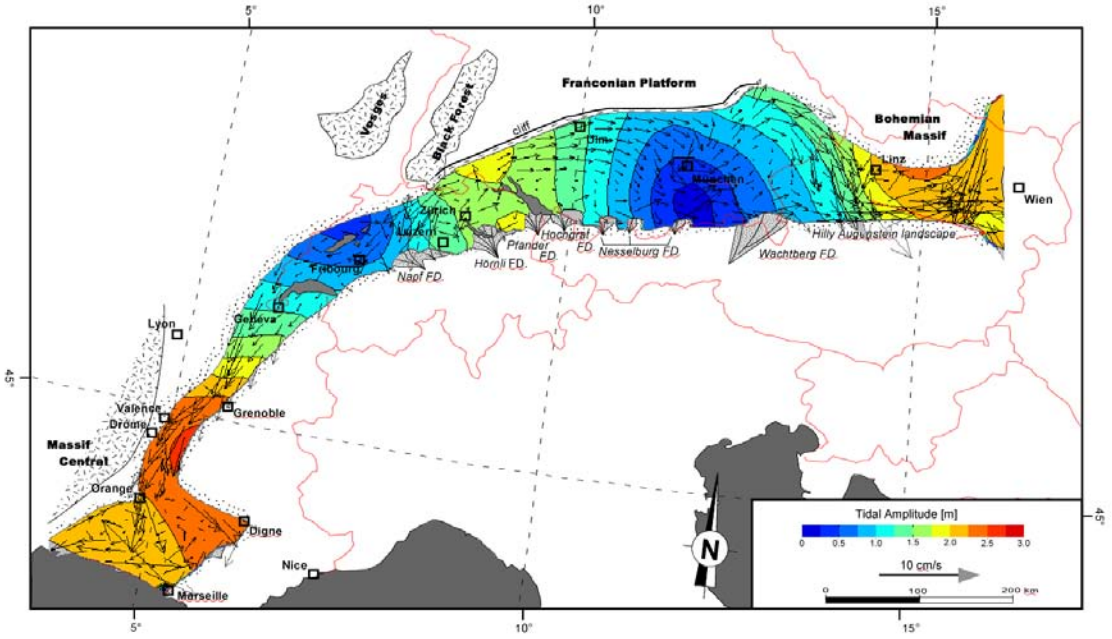

Figure 5.12: *Middle Ottnangian model: Residual velocietes and tidal amplitudes after the model was driven by two incident M_2 waves and a windstress (storm with 20 m/s from the NNE).*

Source	Drainage Area [m^2]	Flow rate [m^3/s]
Napf Fan Delta	4000	90
Hörnli Fan Delta	3000	72
Palaeo-Rhine	5000	115
Hochgrat Fan Delta	2500	60
Nesselburg Fan Deltas	-	total 20
Palaeo-Inn	12000	285
Palaeo-Main	22000	280
Palaeo-Naab	5000	63

Table 5.1: *Flow rates were kindly provided by PD Dr. J. Kuhlemann (University of Tübingen). For S-Germany a precipitation rate of 1000mm/a with a runoff of 40% and respectively 1500mm/a and 50% runoff for the Alps have been accounted.*

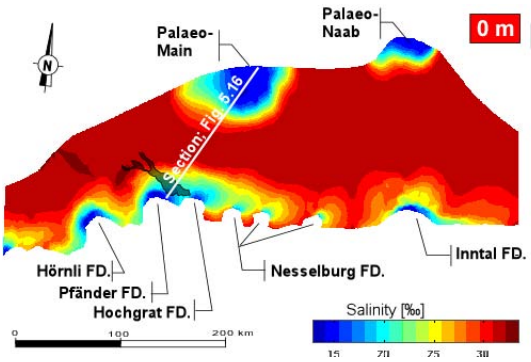

Figure 5.14: *Middle-Ottnangian model: Salinity distribution at the sea surface of the central Molasse Basin, if the model is forced by two incident M_2 waves and freshwater influx from the surrounded domains (fan deltas and rivers).*

of Lake constance towards the east and west of Luzern towards the southwest. Between the two systems a depositional system that is closed for sediment transport is simulated. The generated flow circuit forms a meandering, eastward directed arm. The computational results also show uniform SW directed residual currents west of Fribourg.

A horizontal slice at the sea surface (0m) is shown in Fig. 5.14, highlighting the salnity at the river plume areas of the central Molasse Basin. Isohalines along the Swiss transect (Fig. 5.16) show mixing of saline with freshwater, resulting in downwelling. This forced the isohalines to be more vertical.

Lagrangian Passive Particle Tracking

To study bedload transport, a Lagrangian particle tracking approach has been applied, in which a finite number of sediment paricles are released and tracked. The method yields pathways and sediment accumulations.

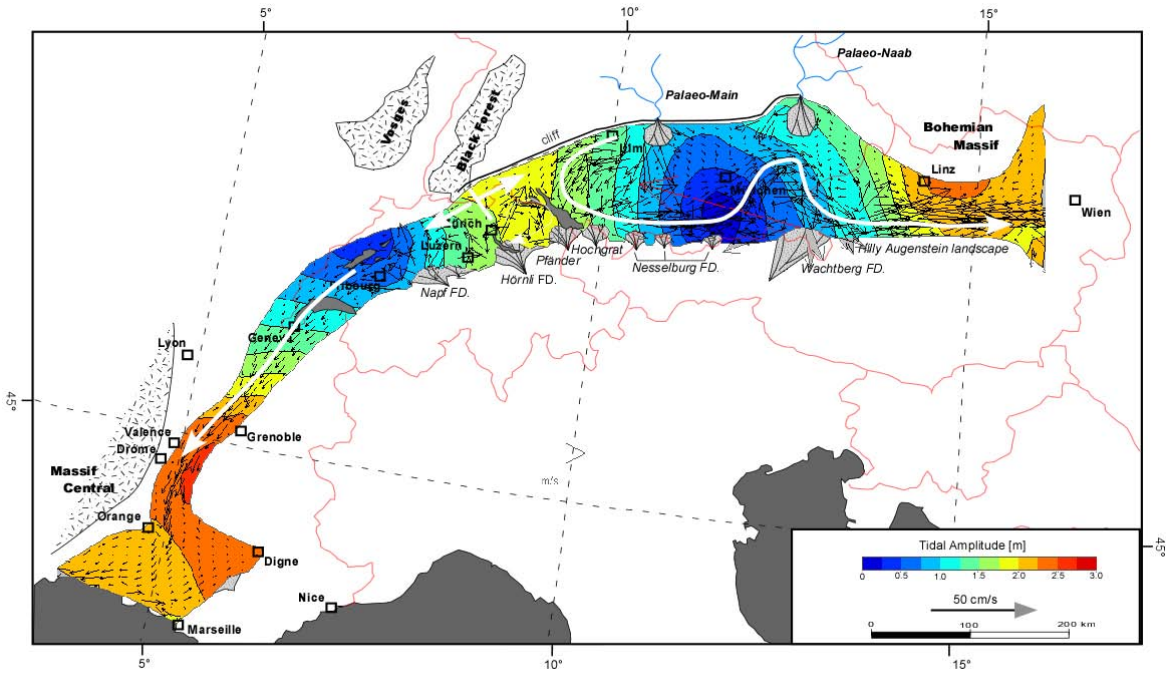

Figure 5.15: *Middle-Ottnangian model: Residual velocities and tidal amplitudes if the model is driven by two incident M_2 waves and forced by freshwater influx from the surrounded domains (fan deltas and rivers)*

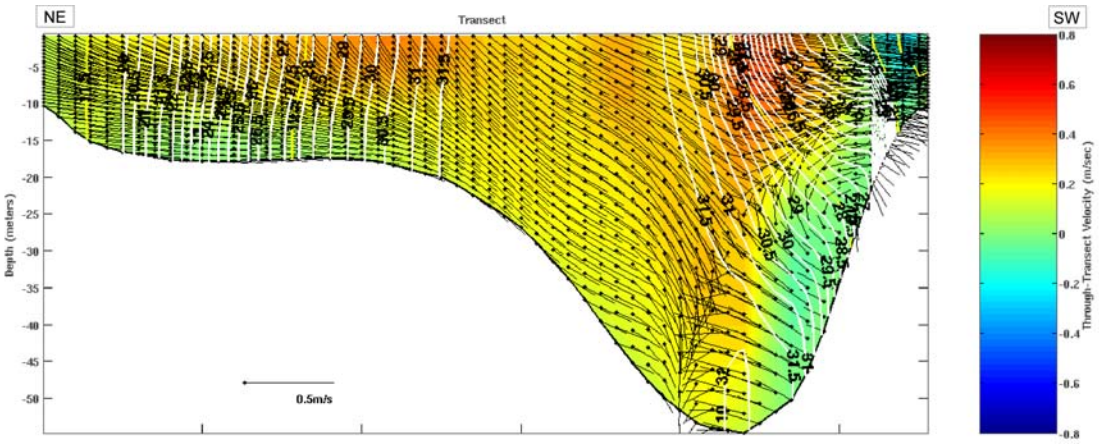

Figure 5.16: *Velocity and salinity (isolines) transect of the central Molasse Basin, if the model is forced by two incident M_2 waves and freshwater influx. Location of the section see fig. 5.14.*

Lagrangian particle trajectories are calculated using a time-stepping particle tracking algorithm (Blanton 1995a,b), which uses a fourth order Runge-Kutta integration scheme to compute particle movements in a given velocity field over a time interval.

The particles were placed along the 10m, 30m, 50m isobaths. The purpose of these placements is to test a conceptual model, where particles within all isobaths are drifted in nearly the same direction and suggest possible transport pathways. The particles are allowed to advect for 30 days. The magnified area, highlighted in figure 5.17 displays the circular, elliposoidal shaped pathways of the particles due to to- and fro-movements in the course of ebb and flood.

Bed-load sediment transport within the shallow marine Burdigalian Seaway is an important

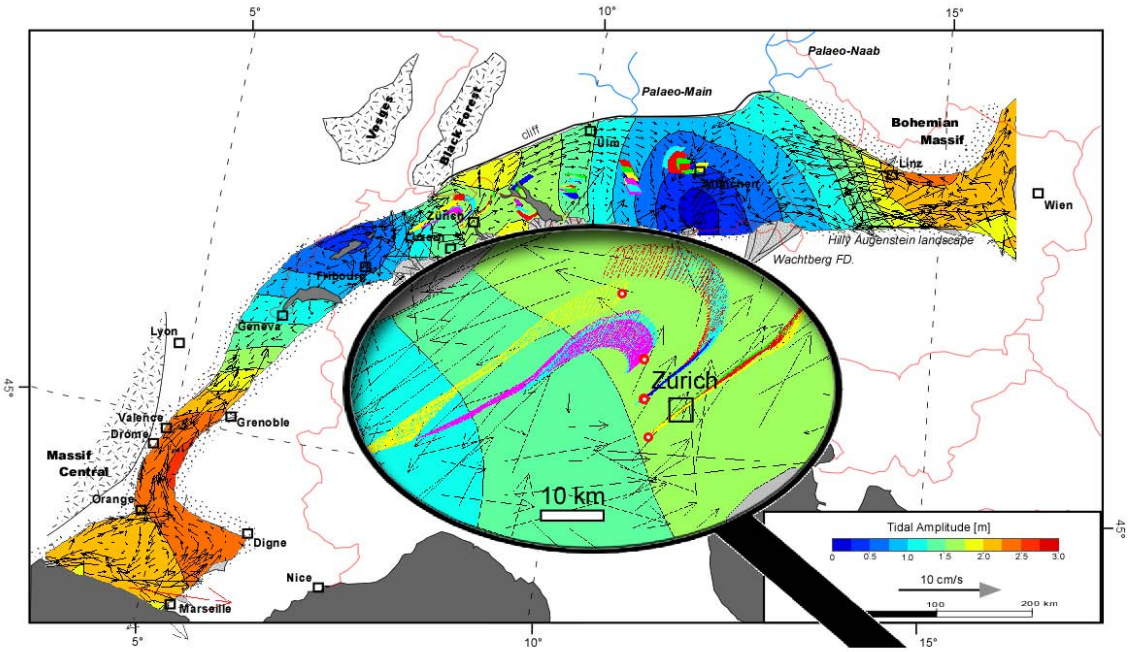

Figure 5.17: *Middle Ottnangian simulation: The model was driven by two incident M_2 waves. Particles have been placed in different isobaths and tracked for 30 days. The magnifier shows in more detail the pathways of the particles. Red points define the starting point for each drogue.*

process which might have the potential of causing long-term environmental effects (e.g. barrier islands). Net transport is dominated by asymmetries in tidal currents, which can be created by the strongly non-linear hydrodynamics and their complex interaction with basin geometry. These asymmetries can export (ebb dominant) or import (tide dominant) sediment from/to the domain, but may also cause deposition and erosion in the form of converging and, respectively, diverging bed-load flux vectors.

5.4.3 Upper-Ottnangian model

In this computational model we calculated the distribution of tidal amplitudes and residual velocites for the time of the Graupensandrinne. The model (Fig. 5.18) was initiated with a tidal amplitude of 2m entering the seaway from France. The eastern boundary was kept close. River runoff from the Swabian and Franconian Alp was accounted by the Palaeo-Main and Palaeo-Naab. As shown above, river influx is able to steer and increase the residual velocities. The simulation indicates that the Palaeo-Main generates a strong southwestward directed currents system. Nevertheless funneling of tides at the SW mouth of the Graupensandrinne allows tidal amplitudes to be amplified towards a meso-tidal system in the Graupensandrinne.

5.5 Discussion

The global M_2 simulations: When reconstructing the circum-Mediterranean realm for the late Eggenburgian/early Ottnangian, we faced the problem, that palaeogeograpic reconstructions concerning the circum-Mediterranean account time intervals of some million years (e.g. Dercourt 1993) and proposed reconstructions differ greatly (see Fig. 5.1). However in the case of the Burdigalian Seaway, we reconstructed palaeogeographic maps accounting for a stratigraphic resolution of some ky. This is of special interest, as circum-Mediterranean reconstructions propose changing gateways towards Austria and opening of the seaways cannot be dated exactly towards the higher resolution Budigalian Seaway sketch maps.

Shallow water simulations of the Burdigalian Seaway showed, that meso-tidal conditions can

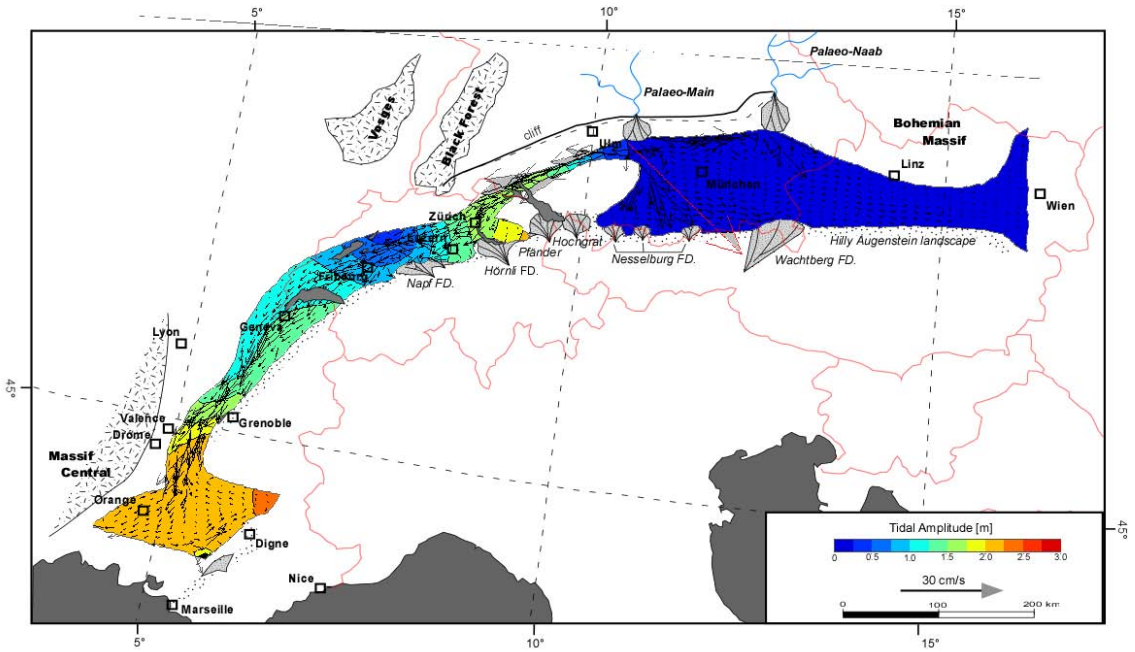

Figure 5.18: *Upper Ottnangian simulation: The model is driven by one incident M_2 wave from SW; the northeastern boundary of the model was kept close and not initiated with a tidal wave. Fresh water influx from the Palaeo-Main and -Naab was also included. Residual velocities are high and directed towards the southwest in the Graupensandrinne. Tidal amplitudes within the rim reach meso-tidal values.*

only be simulated in the NAFB when 2 tidal waves from the open bounderies propagate towards each other. The global M_2 simulations presented, suggest that the general configuration of the circum-Mediterranean illustrated in Fig. 5.1, depicts a best approximation to explain marine faunal relations and potential continental migration bridges, but does not account for the resonance behavior of tidal waves which is dependend on basin shape. Thus the used circum-Mediterranean reconstructions might be still fragmentary and incorrect in many details (already suggested by Rögl 1998).

For further global simulations it is recommended to evaluate the natural modes of oscillation for each circum-Mediterranean basin reconstruction. This should provide a maximum estimate of tidal amplitudes, which can be expected for each basin shape reconstruction. To do this, the frequency for which the resonance is found, is decomposed (harmonic analysis) into all of its diurnal constituents (K_1, O_1, P_1) and all of its semidiurnal constituents (M_2, S_2, N_2, K_2). Each constituent represents a periodic change or variation in the relative positions of the Earth, Moon and Sun and has to be considered for a proper analysis of the forcing tides.

The Burdigalian Seaway simulations: Fluctuations in eustatic, tectonic and climatic conditions in the Burdigalian Seaway caused key oceanographic parameters (palaeogeography, palaeobathymetry, stratification, wind stress and boundary tides) to vary widely throughout the seaway's history. These fluctutions in turn must have caused variations in circulation and sediment-transport regimes. For this reason palaeogeographic key stages of the OMM have been derived and used for further tidal simulations.

Although global M_2 simulations could not yet evidence a meso-tidal system for the Western Paratethys, necessary for the generation of a meso-tidal system within the NAFB (see chapter 3); it seems best to explain tidal signatures by using a tidal wave entering the Burdigalian Seaway from the NE with a tidal amplitude of 2m (see also Krenmayr & Roetzel 1996).

Driving the shallow waters of the Burdigalian Seaway additionally by atmospheric forcing and freshwater influx provides a best estimate for possible meso-scale current systems, without explicitly accounting the observation of meso-tidal conditions.

5.6 Conclusion

Global and regional modeling of tidal amplitudes provide a tool, which allows to retrace the distribution of tidal amplitudes and residual velocities. Using different boundary conditions allowed us to evaluate the response of both model scales to different boundary conditions.

The global M_2 simulations revealed:

- ⋆ No resonance of tidal waves in the semi-enclosed Paratethys realm.
- ⋆ So far it was not possible to evaluate proper tidal amplitudes for the open boundaries of the Burdigalian Seaway. Tidal waves towards the Paratethys are damped on their runtime from the eastern Mediteranean realm and due to constricted gateways. Only a micro-tidal system was computed to the western Paratethys for both model cases.

Shallow water simulations revealed:

Tidal driven:

- ⋆ A meso-tidal system in the Burdigalian Seaway can only be simulated by two tidal waves, entering the seaway at its open boundaries.
- ⋆ It is not possible to generate a meso-tidal system in the Burdigalian Seaway by using one tidal wave co-oscillating with the open boundary in SE France as proposed by Sztanó & deBoer (1994) and Sztanó (1994, 1995). They suggested that the seaway was blocked in Austria during the maximum flooding and acted like a semi-enclosed basin. A tidal wave comming from SE France should be reflected at the closed head of the basin (vicinity of Amstetten). Due to resonance between the incident and the reflected wave, a standing wave should be generated. Numerical studies showed that this is not possible as the tidal wave is damped (tidal friction) on its long way from France to Austria. However the authors identified the standing wave as the main reason why high tidal amplitudes can be observed in the mid of the Burdigalian Seaway.
- ⋆ If the model is only driven by M_2 waves, especially within the Swiss realm, meso-scale circulation pattern display circulation cells, which might be closed for sediment transport (see also Allen et al. 1985).
- ⋆ If we additionally use fresh water as a driving force, residual vectors chamge to a SW direction from western Switzerland to the Rhône area. This indicates for an export of sediment from the Swiss realm towards the western Mediterranean. Moreover in the Central Molasse basin residual velocities form a semi-circular, counter-clockwise rotating cell which continues in a meandering branch towards the eastern open boundary. Such the Burdigalian Seaway is split in the center of the basin into two directly opposed net-sediment transport systems, supporting as well the ideas of Kulemann (2000) as Lemcke (1973) and Freudenberger & Schwerd (1996).

Atmospheric forcing:

- ⋆ Residual currents generated by tidal waves are overprinted by uniform directed currents, generated by the tangential forces of a uniform wind field. If we use atmospheric forcing directed from the NNW, residual currents in the central basin are reinforced and strong SE directed alongshore currents are suggested at the western coastline of the Bohemian Massif.

River influx:

- ⋆ Large river runoff rate of the Palae-Main has a great impact on the residual current system in the central seaway.
- ⋆ Coastal flow near the Swiss fan deltas is modulated by the river influx and directed towards the southwest.
- ⋆ A strong SW directed net-sediment transport can be simulated for the Upper-Ottnangian model in the Graupensandrinne. The numerical simulation is driven by one incident M_2 wave from the southwest and river influx from the palaeo-Main. This might explain the transport of quarz granules of the Grimmelfinger beds.

5.6.1 References

Allen, P.A. & Bass, J.P. (1993): Sedimentology of the Upper Marine Molasse of the Rhône-Alp region, Eastern France: Implications for basin evolution. *Eclogae geologicae Helvetiae*, **86**: 121-171.

Allen, P.A., Mange-Rajetzky, M., Matter, A. & Homewood, P. (1985): Dynamic palaeogeography of the open Burdigalian seaway, Swiss Molasse basin. *Eclogae geologicae Helvetiae*, **78**: 351-381.

Asprion, U. & Aigner, T. (2000): Fazies- und Georadar (GPR) - Analyse in der süddeutschen Graupensandrinne. *Neues Jahrbuch für Geologie und Paläontologie, Abhandlungen*, **218**: 321-342.

Bader, K., Meyer, R.K.F. & Brunold, H. (2000): Graupensandrinne-Urnaabrinne, ihre Verbindung und tektonische Verstellung zwischen Donauwörth und Regensburg. *Geologica Bavarica*, **105**: 243-250.

Berger, J.-P. (1985): *La transgression de la molasse marine supérieure (OMM) en Suisse occidentale.* Münchner Geowissenschaftliche Abhandlungen (A), **5**. Verlag Friedrich Pfeil, München, 1-208 pp.

Berger, J.-P. (1996): Cartes paléogéographiques-palinspastiques du bassin molassique suisse (Oligocène inférieur - Miocène moyen). *Neues Jahrbuch für Geologie und Paläontologie, Abhandlungen*, **202**: 1-44.

Berger, J.-P., Reichenbacher, B., Becker, D., Grimm, M., Grimm, K., Picot, L., Storni, A., Pirkenseer, C., Derer, C. & Schäfer, A. (in press, a): Palaeogeography of the Upper Rhine Graben (URG) and the Swiss Molasse Basin (SMB) from Eocene to Pliocene. *Int. J. Earth Sciences (Geol. Rundsch.).*

Berger, J.-P., Reichenbacher, B., Becker, D., Grimm, M., Grimm, K., Picot, L., Storni, A., Pirkenseer, C. & Schäfer, A. (in press, b): Eocene-Pliocene time scale and stratigraphy of the Upper Rhine Graben (URG) and the Swiss Molasse Basin (SMB). *Int. J. Earth Sciences (Geol. Rundsch.).*

Blanton, B.O. (1995a): Drog3d: User's manual for 3-dimensional drogue tracking on a finite element grid with linear finite elements, University of North Carolina at Chapel Hill.

Blanton, B.O. (1995b): Modifications to Quoddy2 time-stepping code to include Drog3ddt - Memorandum to GLOBEC team, University of North Carolina at Chapel Hill.

Büchi, U.P. & Hofmann, F. (1960): Die Sedimentationsverhältnisse zur Zeit der Muschelsandsteine und Grobkalke im Gebiet des Beckennordrandes der Oberen Meeresmolasse zwischen Aarau und Schaffhausen. *Bulletin der Vereinigung Schweizerischer Petroleum-Geologen und -Ingenieure*, **27**: 11-22.

Büchi, U.P. & Schlanke, S. (1977): Zur Paläogeographie der schweizerischen Molasse. *Erdöl-Erdgas-Zeitung*, **93**: 57-69.

Büchi, U.P., Wiener, G. & Hofmann, F. (1965): Neue Erkenntnisse im Molassebecken auf Grund von Erdöltiefbohrungen in der Zentral- und Ostschweiz. *Eclogae geologicae Helvetiae*, **58**: 87-108.

Buchner, E. & Seyfried, H. (1999): Die Grimmelfinger Schichten (Graupensande): fluviatile und/oder ästuarine Ablagerungen? *Jahreshefte Ges. Natur. Württemberg*, **155**: 5-25.

Burkhard, M. & Sommaruga, A. (1998): Evolution of the western Swiss Molasse basin: structural relations with the Alps and the Jura belt. In: *Cenozoic Foreland Basins of Western Europe* (Eds A. Mascle, C. Puigdefàbregas, H.P. Luterbacher and M. Fernàndez), *Geological Society Special Publication*, **134**, pp. 279-298.

de Ruig, M.J. (2003): Deep Marine Sedimentation and Gas Reservoir Distribution in Upper Austria. *OIL GAS European Magazine*, **2**: OG1-OG7.

Demarcq, G. & Perriaux, J. (1984): Neogene. In: *Synthèse géologique du Sud-Est de la France: Stratigraphie et paléogeographie* (Eds D.-P.e. al.), **Bureau de Récherches Géologiques et Minières, Mémoire 125**, pp. 469-519.

Dercourt, J., Ricou, L.E. & Vrielynck, B. (1993): *Atlas Tethys Palaeoenvironmental Maps.* Gauthier-Villars, Paris, 307 pp.

Doppler, G. (1989): Zur Stratigraphie der nördlichen Vorlandmolasse in Bayrisch-Schwaben. *Geologica Bavarica*, **94**: 83-133.

Doppler, G., Heissig, K. & Reichenbacher, B. (in press): Die Gliederung des Tertiärs im süddeutschen Molassebecken. *Newsl. Stratigr.*

Egger, H., Hofmann, T. & Rupp, C. (1996): Exkursionsunterlagen für die Wandertagung 1996 - Ein Querschnitt durch die Geologie Oberösterreichs - 7. Oktober bis 11. Oktober 1996 in Wels. *Österreichische Geologischen Gesellschaft*, **16**.

Erb, L., Haus, H.A. & Rutte, E. (1961): Erläuterungen zu Blatt 8120 Stockach. In: *Geologische Karte von Baden-Württemberg 1:25000.*

Faupl, P. & Roetzel, R. (1990): Die Phosphoritsande und Fossilreichen Grobsande; Gezeitenbeeinflusste Ablagerungen der Innviertler Gruppe (Ottnangien) in der oberoesterreichischen Molassezone. *Jahrbuch der Geologischen Bundesanstalt Wien*, **132**: 157-180.

Freudenberger, W. & Schwerd, K. (1996): *Erläuterungen zur Geologischen Karte von Bayern 1:500000.* Bayerisches Geologisches Landesamt, München.

Füchtbauer, H. (1964): Sedimentpetrographische Untersuchungen in der älteren Molasse nördlich der Alpen. *Eclogae geol. Helv.*, **57**: 157-298.

Füchtbauer, H. (1967): Die Sandsteine in der Molasse nördlich der Alpen. *Geol. Rundsch.*, **56**: 266-300.

Gall, H. (1974): Neue Daten zum Verlauf der Klifflinie der oberen Meeresmolasse (Helvet) im südlichen Vorries. *Mitt. Bayer. Stattssamml. Paläont. hist. Geol.*, **14**: 81-101.

Gall, H. (1975): Der III. Zyklus der oberen Meeresmolasse (Helvet) am Südrand der Schwäbisch-Fränkischen Alb. *Mitt. Bayer. Stattssamml. Paläont. hist. Geol.*, **15**: 179-205.

Graf, H. (1991): Die OMM und USM im Gebiet des Kleinen Randen (südlicher badischer Klettgau). *Mitt. Naturforsch. Ges. Schaffhausen*, **36**: 1-44.

Gutmann, S. (1910): Gliederung der Molasse und Tektonik des östlichen Hegaus. *Mitt. bad. geol. Landesanst.*, **6**: 469-514.

Haq, B.U., Hardenbol, J. & Vail, P.R. (1987): Chronology of fluctuating sea levels since the Triassic. *Science*, **235**: 1156-1167.

Haq, B.U., Hardenbol, J. & Vail, P.R. (1988): Mesozoic and Cenozoic chronostratigraphy and cycles of sea-level change. In: *Sea-level changes: An integrated approach* (Eds C.K. Wilgus et al.), *SEPM, Special Publications*, **42**, pp. 71-108. SEPM (Society of Economic Paleontologists and Mineralogists), Tulsa.

Haus, H.A. (1951): Zur paläogeographischen Entwicklung des Molassetroges im Bodenseegebiet während des mittleren Miozäns. *Mitteilungsblatt der badischen geologischen Landesanstalt*, **1950**: 48-66.

Haus, H.A. (1960): Mönchsrot als Ölfeld im Westabschnitt der süddeutschen Vorlandsmolase. *Bull. Ver.*

Schweizer Petrol.-Geol. u. -Ing., **26**: 49-71.

Heermann, O. (1954): Erdölgeologische Grundlagen der Aufschlußarbeiten im ostbayerischen Molassebecken. *Bull. Ver. Schweizer Petrol.-Geol. u. -Ing.*, **21**: 5-22.

Hofmann, F. (1955): Neue geologische Untersuchungen in der Molasse der Nordostschweiz. *Eclogae geol. Helv.*, **48**: 100-124.

Hofmann, F. (1976): Überblick über die geologische Entwicklungsgeschichte der Region Schaffhausen seit dem Ende der Jurazeit. *Bull. Ver. Schweizer Petrol.-Geol. u. -Ing.*, **42**: 1-16.

Hülsemann, J. (1955): Großrippeln und Schrägschichtungs-Gefüge im Nordsee Watt und in der Molasse. *Senck. leth.*, **36**: 359-388.

Hüttner, R. (1961): Geologischer Bau und Landschaftsgeschichte des östlichen Härtsfelds. *Jh. geol. Landesamt Baden-Württemberg*, **4**: 49-126.

Jin, J., Aigner, T., Luterbacher, H.P., Bachmann, G.H. & Müller, M. (1995): Sequence stratigraphy and depositional history in the south-eastern German Molasse Basin. *Marine and Petroleum Geology*, **12**: 929 - 940.

Keller, B. (1989): *Fazies und Stratigraphie der Oberen Meeresmolasse (Unteres Miozän) zwischen Napf und Bodensee*. Unpubl. PhD Thesis, Universität Bern, Bern, 402 p pp.

Kempf, O., Bolliger, T., Kälin, D., Engesser, B. & Matter, A. (1997): New magnetostratigraphic calibration of Early to Middle Miocene mammal biozones of the North Alpine foreland basin. In: *Actes du Congrès BiochroM'97* (Eds J.-P. Aguilar, S. Legendre and J. Michaux), *Mémoires et Travaux de l' E.P.H.E.*, **21**, pp. 547-561, Montpellier.

Kempf, O., Matter, A., Burbank, D.W. & Mange, M. (1999): Depositional and structural evolution of a foreland basin margin in a magnetostratigraphic framework: the eastern Swiss Molasse basin. *International Journal of Earth Sciences*, **88**: 253-275.

Kiderlen, H. (1931): Beiträge zur Stratigraphie und Paläogeographie des süddeutschen Tertiärs. *Neues Jahrbuch für Mineralogie, Geologie und Paläontologie*, **66**: 215-384.

Knupfer, S. (1912): Molasse und Tektonik des südöstlichen Teils des Blattes Stockach der topographischen Karte von Baden. *Ber. Naturfr. Ges. Freiburg*, **19**.

Kollmann, K. & Malzer, O. (1980): Die Österreichischen Erdöl- und Erdgasprovinzen: Die Molassezone Oberösterreichs und Salzburgs. In: *Erdöl und Erdgas in Österreich* (Eds F. Brix), pp. 179-201. Naturhistorisches Museum Wien, Wien.

Krenmayr, H.G. & Roetzel, R. (Eds) (1996): *Oligozäne und miozäne Becken- und Gezeitensedimente in der Molassezone Oberösterreichs, Exkursionsführer Sediment '96, Exkursion B2*, **33**. Geologische Bundesanstalt, Wien, 17 Abb., 43 pp.

Kuhlemann, J. (2000): Post-collisional sediment budget of circum-Alpine basins (Central Europe). *Memoire di Scienze Geologiche Padova*, **52**: 1-91.

Kuhlemann, J. & Kempf, O. (2002): Post-Eocene evolution of the North Alpine Foreland Basin and its response Alpine tectonics. *Sedimentary Geology*, **152**: 45-78.

Laubscher, H. (1992): Jura Kinematics and the Molasse Basin. *Eclogae geologicae Helvetiae*, **85**: 653-675.

Lemcke, K. (1973): Zur nachpermischen Geschichte des nördlichen Alpenvorlandes. *Geologica Bavarica*, **69**: 5-48.

Lemcke, K. (1985): Flußfracht von Ur-Main und Ur-Naab in der Schweiz und im deutschen Molassebecken. *Bull. Ver. Schweizer Petrol.-Geol. u. -Ing.*, **51**: 13-21.

Lemcke, K. (1988): *Geologie von Bayern. - I. Teil: Das bayerische Alpenvorland vor der Eiszeit*, **I**. E. Schweizerbart'sche Verlagsbuchhandlung, Stuttgart, 175 p pp.

Lemcke, K., Engelhardt, W.v. & Füchtbauer, H. (1953): Geologische und sedimentpetrographische Untersuchungen im Westteil der ungefalteten Molasse des süddeutschen Alpenvorlandes. *Beih. Geol. Jb.*, **11**: 182.

Liniger, H. (1925): Geologie des Delsberger Beckens und der Umgebung von Movelier. *Beitr. geol. Karte Schweiz, N.F.*, **55**.

Linzer, H.G. (2001): Cyclic Channel systems in the Molasse Foreland Basin of the Eastern Alps - the Effect of Late Oligocene Foreland Thrusting and Early Miocene Lateral Escape. *AAPG Bulletin, Supplement A*, **85**: 118.

Luterbacher, H. (1997): Stratigraphy and facies evolution of a typical foreland basin; the Tertiary Molasse Basin (Lake Constance area and Allgäu). In: *18th IAS regional European meeting of sedimentology, Heidelberg, September 2-4, 1997; field trip guidebook* (Eds T. Bechstädt, P. Bengtson, R. Gaupp, R. Greiling and V. Schweizer), *Gaea Heidelbergensis*, **4**, pp. 123-140, Heidelberg.

Luterbacher, H., Köhler, J. & Winder, H. (1992): The northern margin of the Molasse Basin in SW Germany. *Eclogae geologicae Helvetiae*, **85**: 787-788.

Micheels, A. (2003): *Late Miocene climate modelling with ECHAM4/ML - The effects of the palaeovegetation on the Tortonian climate.*, PhD Thesis, University of Tübingen, 135 pp.

Moiola, R.J. (1976): Environmental analysis of Teritary reservoir sandstones and conglomerates, Molasse Basin, Austria. *International report, Mobil Research and Development Corporation, Technical Service Job 256-69055*.

Moos, A. (1925): Beiträge zur Geologie des Tertiärs zwischen Ulm und Donauwörth. *Geognost. Jh.*, **37**: 167-252.

Morend, D. (2000): High-resolution seismic facies of alluvial depositional systems in the Lower Freshwater Molasse (Oligocene-early Miocene, western Swiss Molasse Basin). *Terre Environ*, **23**: 1-97.

Naef, H., Diebold, P. & Schlanke, S. (1985): *Sedimentation und Tektonik im Tertiär der Nordschweiz.* NAGRA Technischer Bericht, **85-14**, 145 p pp.

Neumaier, F. & Wieseneder, H. (1939): Geologische und sedimentpetrographische Untersuchungen im nierderbayerischen Tertiär. *Sber. Bayer. Akad. Wiss., math.-naturw. Abt.*177-252.

Paulus, B. (1964): Der tiefere Untergrund unter besonderer Berücksichtigung des von den Bohrungen Landsham 1 und Pliening 101-105 erschlossenen Tertiärs. *Erläuterungen z. Geol. Kte. v. Bayern 1:25000*, **Bl. Nr. 7736 Ismaning**: 9-53.

Reichenbacher, B. (1993): Mikrofaunen, Paläogeographie und Biostratigraphie der miozänen Brack- und Süßwassermolasse in der westlichen Paratethys unter

besonderer Berücksichtigung der Fisch-Otolithen. *Senckenbergiana lethaea*, **73**: 277-374.

Reichenbacher, B., Böttcher, R., Bracher, H., Doppler, G., Engelhardt, W.v., Gregor, H.-J., Heissig, K., Heizmann, E.P.J., Hofmann, F., Kälin, D., Lemcke, K., Luterbacher, H., Martini, E., Pfeil, F.H., Reiff, W., Schreiner, A. & Steininger, F.F. (1998a): Graupensandrinne - Ries - Impakt: zur Stratigraphie der Grimmelfinger Schichten,Kirchberger Schichten und Oberen Süßwassermolasse: Kommentar zur 'Revision der Stratigraphie der süddeutschen Brackwassermolasse'. *Z. dt. geol. Ges.*, **149**: 127-161.

Reichenbacher, B., Doppler, G., Schreiner, A., Böttcher, R., Heissig, K. & Heizmann, E.P.J. (1998b): Lagerungsverhältnisse von Grimmelfinger Schichten und Kirchberger Schichten: Kommentar zur 'Revision der Stratigraphie der süddeutschen Brackwassermolasse'. *Zeitschrift der deutschen geologischen Gesellschaft*, **149**: 321-326.

Rigassi, D. (1957): Le tertiaire de la region genevoise et savoisienne. *Bulletin der Vereinigung Schweizerisches Petroleum -Geologen und -Ingenieur.*, **24**: 19-34.

Robinson, D. & Zimmer, W. (1989): Seismic stratigraphy of Late Oligocene Puchkirchen Formation of Upper Austria. *Geologische Rundschau*, **78**: 49-79.

Rögl, F. (1998): Palaeogeographic Considerations for Mediterranean and Paratethys Seaways (Oligocene to Miocene). *Ann. Naturhist. Mus. Wien*, **99A**: 279-310.

Rögl, F., Hochuli, P.A. & Müller, C. (1979): Oligocene-Early Miocene stratigraphic correlations in the Molasse Basin of Austria. *Annales géologique des pays Hellèniques, Tome 5*1045-1050.

Rögl, F. & Steininger, F.F. (1984): *Neogene Patatethys, Mediterranean and Indo-pacific Seaways.* Fossils and Climate. John Wiley & Sons.

Roll, A. (1935): Beobachtungen längs der Küste des burdigalen Meeres auf der Schwäbischen Alb. *Z. dt. geol. Ges.*, **5**: 281-307.

Rutte, E. (1952): Grobsand und Muschelsandstein in der miozänen Meeresmolasse des nordwestlichen Bodenseegebietes. *N. Jb. Geol. Paläont. Abh.*, **Mh**: 295-304.

Sach, V.J. & Heizmann, E.P.J. (2001): Stratigraphie und Säugetierfaunen der Brackwassermolasse in der Umgebung von Ulm (Südwestdeutschland). *Stuttgarter Beitr. Naturk., Ser. B*, **310**: 95.

Salvermoser, S. (1999): Zur Sedimentologie gezeitenbeeinflusster Sande in der Oberen Meeresmolasse und Süssbrackwassermolasse (Ottnangium) von Niederbayern und Oberösterreich. *Münchner Geologische Hefte (A)*, **26**: 1-179.

Schaad, W., Keller, B. & Matter, A. (1992): Die Obere Meeresmolasse (OMM) am Pfänder: Beispiel eines Gilbert-Deltakomplexes. *Eclogae geologicae Helvetiae*, **85**: 145-168.

Schalch, F. (1901): Bemerkungen über die Molasse der badischen Halbinsel und des Überlinger Seegebiets. *Mittlg. Bad. Geolog. Landesanst.*, **4**.

Schlunegger, F., Leu, W. & Matter, A. (1997): Sedimentary sequences, Seismic Facies, Subsidence Analysis, and Evolution of the Burdigalian Upper Marine Molasse Group (OMM), Central Switzerland. *American Association of Petroleum Geologists, Bulletin*, **81**: 1185-1207.

Schlunegger, F. & Pfiffner, O.A. (2001): The sedimentary response of the North Alpine Foreland Basin to changes in erosional processes in the Alps (Excursion P9). In: *IAS 2001, 21st Meeting* (Eds H. Funk and U.G. Wortmann), *Excursion Guides*, pp. 85-99. IAS (International Association of Sedimentologists), Davos.

Scholz, H. (1989): Die Obere Meeresmolasse (OMM) am Südrand des Molassebeckens im Allgäu. *Geologica Bavarica*, **94**: 49-81.

Schreiner, A. (1965): Die Juranagelfluh im Hegau. *Jh. geol. Landesamt Baden-Württemberg*, **7**: 303-354.

Schreiner, A. (1966): Zur Stratigraphie der Oberen Meeresmolasse zwischen der Oberen Donau und dem Überlinger See (Baden-Württemberg). *Jber. u. Mitt. oberrh. geol. Ver.*, **48**: 91-104.

Sissingh, W. (1997): Tectonostratigraphy of the North Alpine Foreland Basin: correlation of Tertiary depositional cycles and orogenic phases. *Tectonophysics*, **282**: 223-256.

Sissingh, W. (1998): Comparative Tertiary stratigraphy of the Rhine Graben, Bresse Graben and Molasse Basin: correlation of Alpine foreland events. *Tectonophysics*, **300**: 249-284.

Sissingh, W. (2001): Tectonostratigraphy of the West Alpine Foreland: correlation of Tertiary sedimentary sequences, changes in eustatic sea-level and stress regimes. *Tectonophysics*, **333**: 361-400.

Spiegel, C., Kuhlemann, J., Dunkl, I. & Frisch, W. (2001): Paleogeography and catchment evolution in a mobile orogenic belt: the Central Alps in Oligo-Miocene times. *Tectonophysics*, **341**: 33-47.

Strunck, P. (2001): *The Molasse of western Switzerland.* PhD Thesis, University of Bern, 246 pp.

Sztanó, O. (1994): *The tide-influences Pétervására sandstone, early Miocene, Northern Hungary: Sedimentology, Palaeogeography and basin development.* Phd., Universiteit Utrecht, Utrecht, 155 pp.

Sztanó, O. (1995): Palaeogeographic significance of tidal deposits; an example from an early Miocene Paratethys embayment, northern Hungary. *Palaeogeography, Palaeoclimatology, Palaeoecology*, **113**: 173-187.

Sztanó, O. & de Boer, P.L. (1995): Basin dimensions and morphology as controls on amplification of tidal motions (the early Miocene North Hungarian Bay). *Sedimentology*, **42**: 665-682.

Teike, M. (1921): *Die Molasse im Linzgau und ihre Tektonik.* Phd - unpubl.

Teike, M. (1923): Die Molasse im bad.-württ. Grenzgebiet südlich von Sigmaringen. *Mitt. bad. geol. Landesanst.*, **9**: 408-426.

Tipper, J., Sach, V.J. & Heizmann, E.P.J. (2003): Loading fractures and Liesegang laminae: new sedimentary structures found in the north-western North Alpine Foreland Basin (Oligocene-Miocene, southwest Germany). *Sedimentology*, **Online publication date: 18-Jul-2003**.

Volz, E. (1953): Geologische Untersuchungen in der tertiären Molasse des Saulgauer Gebiets. *Neues Jb. Geol. u. Paläontol.*, **97**: 189-219.

Wagner, L. (1996): Stratigraphy and hydrocarbons in the Upper Austrian Molasse Foredeep (active margin). In: *Oil and Gas in the Alpidic Thrustbelts and Basins of the Central and Eastern Europe* (Eds G. Wessely and W. Liebl), **5**, pp. 217-235. EAGE Special Publication, London.

Wagner, L. (1998): Tectono-stratigraphy and hydrocarbons in the Molasse Foredeep of Salzburg, Upper and Lower Austria. In: *Cenozoic Foreland Basins* (Eds A. Mascle, C. Puigdefàbregas, H. Luterbacher and M. Fernàndez), **134**. Geological Society, Special Publications, London.

Walker, R.G. (1978): Deep-water sandstone facies and ancient submarine fans: Models for exploration for stratigraphic traps. *AAPG Bulletin*, **62**: 932-966.

Wenger, W.F. (1987): Die Foraminiferen des Miozäns der bayerischen Molasse und ihre stratigraphische sowie paläontologische Auswertung. *Zitteliana*, **16**: 173-340.

Werner, J. (1966): Ergebnisse der Auswertung von Flachbohrungen im Bereich des Gobsandzuges der Oberen Meeresmolasse (Gebiet Stockach - Pfullendorf). *Jber. Mitt. oberrh. geol. Ver.*, **N. F. 48**: 105-120.

Zöbelein, H.K. (1940): Geologische und sedimentpetrographische Untersuchungen im nierderbayerischen Tertiär (Blatt Pfarrkirchen). *N. Jb. Min Geol. Paläont., Beil Bd.*, **84**: 233-302.

Zweigel, J., Aigner, T. & Luterbacher, H. (1998): Eustatic versus tectonic controls on Alpine foreland basin fill: sequence stratigraphy and subsidence analysis in the SE German Molasse. In: *Cenozoic Foreland Basins of Western Europe* (Eds A. Mascle, C. Puigdefàbregas, H.P. Luterbacher and M. Fernàndez), *Geological Society Special Publication*, **134**, pp. 299-323, London.

Chapter 6

APPENDIX

6.1 Conversion Tool: gOcad Surface File → Quoddy Geomety and Property Files

```
1
2  #include <stdio.h>
3  #include <math.h>
4  #include <string.h>
5  #include <malloc.h>
6
7  #define Boolean int
8  #define False 0
9  #define True 1
10 #define NDV -99999
11
12
13
14 /* Definition der Funktionen */
15
16 static Boolean fend ( FILE* ) ;
17 static void line_skip (FILE*);
18 static char* addstr (char*, char*);
19 static float* addfloat (float* , float*);
20 static int isort(int*, int);
21 static float vangle(float *, float *, float *);
22 static float vproduct(float *, float *, float *);
23 static int isright(float *, float *, float *);
24
25 // ******** Hauptprogramm *****************************************//
26 main (int argc,char **argv)
27
28 {
29 float **xyz, fread[6], *fa2, **fan, A[3],B[3],C[3];
30 int trn[3], **segments, Snumber,*seg[3], **san, **triangles, Tnumber=0;
31 int **borders,bnumber=0, **bstones,bsnumber=0;
32 int anumber=0,**aris,bt[5];
33 FILE *fp, *fp1, *fp2;
34 int drinn,i,j,Number,lbuffer1,sort,a,b,c;
35 char lbuffer[256];
36 char fname[24];
37
38
39
40    xyz=(float **) calloc(1,sizeof(float *));
41    xyz[0]=(float *) calloc(6,sizeof(float));  /* 6 ,da x,y,z,Phase,Amplitude,.. !! Definiert wird xyz[][6] !! */
42
43    segments=(int **) calloc (1, sizeof(int *));
44    segments[0]=(int *) calloc(2,sizeof(int));
45
46    borders=(int **) calloc (1, sizeof(int *));
47    borders[0]=(int *) calloc(3,sizeof(int));
48
49    triangles=(int **) calloc (1, sizeof(int *));
50    triangles[0]=(int *) calloc(3,sizeof(int));
51
52    bstones=(int **) calloc (1, sizeof(int *));
53    bstones[0]=(int *) calloc(2,sizeof(int));
54
55    aris=(int **) calloc (1, sizeof(int *));
56    aris[0]=(int *) calloc(1,sizeof(int));
57
58
59    sprintf(fname,"%s",strtok(argv[1],"."));
60    printf("\n###### %s Mesh wird bearbeitet: #######\n\n", &fname);
61
62    fp = fopen (strcat(fname,".ts"), "r" ) ;
63
64
65 /****************** Read the TSurf ***************************/
66 /*************************************************************/
```

```
67    printf("TSurf wird eingelesen");
68
69  while(!fend(fp))
70
71  {
72
73     sprintf(lbuffer,"\n");
74     lbufferl=fscanf(fp,"%[^\n]s",lbuffer);
75
76     if (strstr(strtok(lbuffer," "),"VRTX"))
77     {
78         sscanf (&lbuffer[6],"%d %f %f %f %f %f %f",&Number, &fread[0],&fread[1],&fread[2],&fread[3],&fread[4],&fread[5]);
79         fan=xyz;
80         xyz= (float **) realloc (fan,Number*sizeof(float *));
81         xyz[Number-1]=(float *) calloc(6,sizeof(float));
82         xyz[Number-1][0]=fread[0];
83         xyz[Number-1][1]=fread[1];
84         xyz[Number-1][2]=fread[2];
85         xyz[Number-1][3]=fread[3];
86         xyz[Number-1][4]=fread[4];
87         xyz[Number-1][5]=fread[5];
88     }
89
90     if (strstr(strtok(lbuffer," "),"TRGL"))
91     {
92        Tnumber++;
93
94        /* Generate List of Triangles */
95        san=triangles;
96        triangles = ( int **) realloc (triangles,Tnumber*sizeof(int *));
97        triangles[Tnumber-1]=(int *) calloc(3,sizeof(int));
98
99        /*Generate List of Segmenents */
100       san=segments;
101       segments = ( int **) realloc (san,(3*Tnumber)*sizeof(int *));
102       seg[2]= segments[3*Tnumber-1]=(int *) calloc(2,sizeof(int));
103       seg[1]= segments[3*Tnumber-2]=(int *) calloc(2,sizeof(int));
104       seg[0]= segments[3*Tnumber-3]=(int *) calloc(2,sizeof(int));
105
106       sscanf (&lbuffer[5],"%d %d %d",&trn[0],&trn[1],&trn[2]);
107       triangles[Tnumber-1][0]=trn[0];
108       triangles[Tnumber-1][1]=trn[1];
109       triangles[Tnumber-1][2]=trn[2];
110
111       isort(trn,3);
112
113        //printf("\n Triangle: %d Nodes: %d %d %d",Tnumber, trn[0], trn[1], trn[2]);
114
115       seg[2][0]=seg[0][0]=trn[0];
116       seg[0][1]=seg[1][0]=trn[1];
117       seg[1][1]=seg[2][1]=trn[2];
118
119        //printf("\nSeg1: %d %d, Seg2: %d %d, Seg3: %d %d",seg[0][0],seg[0][1],seg[1][0],seg[1][1],seg[2][0],seg[2][1]);
120
121    }
122
123    if (strstr(strtok(lbuffer, " "),"BORDER"))
124    {  bsnumber++;
125       san=bstones;
126       bstones = ( int **) realloc (san,(bsnumber)*sizeof(int *));
127       bstones[bsnumber-1]=(int *) calloc(2,sizeof(int));
128       sscanf (&lbuffer[7]," %*d %d %d", &bstones[bsnumber-1][0], &bstones[bsnumber-1][1]);
129
130    }
131
132    if (strstr(strtok(lbuffer, " "),"ARI"))
133    {
134       anumber++;
135       san=aris;
136       aris=(int **)realloc(san,anumber*sizeof(int*));             /* REALLOC */
137       aris[anumber-1]=(int *) calloc(1,sizeof(int));
138       // Original:   sscanf(&lbuffer[4],"%*d %d %d %d %d %d",&bt[0],&bt[1],&bt[2],&bt[3],&bt[4]); jetzt wird doppelt bestimmt
139       sscanf(&lbuffer[4],"%d %d %d %d %d %d",&anumber,&bt[0],&bt[1],&bt[2],&bt[3],&bt[4]);
140       aris[anumber-1][0]=0;
141       for(i=0;i<5;i++)
142          if(bt[i]==1) aris[anumber-1][0]=i+1;
143          /* printf("\n %d %d",anumber,aris[anumber-1][0]);*/
144    }
145
146  line_skip(fp);
147  }
148   // printf("\n Number of Points: %d, Number of Triangles: %d, Number of Segments: %d",Number,Tnumber,Tnumber*3);
149
150
151
152
153 // ******************** Generate List of Segments and Borders ***** //
154 // ************************************************************** //
155    printf("\nGenerate List of Segments ...\n");
156    drinn=0;
157    j=0;
158
159    for(i=0;i<3*Tnumber-1;i++)
160       {
161           drinn=0;
162          /*printf ("\nsegment nr%d: %d %d",i,segments[i][0],segments[i][1]);*/
163
164           while(!drinn && (j<3*Tnumber))
165           {
166             if(segments[i][0]==segments[j][0] && segments[i][1]==segments[j][1] && (i!=j))
167             {
168                drinn=1;
169                /*printf("\n Drinn!!: %d %d %d %d",i,j,segments[i][0],segments[i][1]); */
170             }
171             j++;
172           }
```

```
         j=0;

         if(drinn==0)
         {
            san=borders;
            /*    printf("\n Randsegment!! Segment: %d Nodes:%d %d",i,segments[i][0],segments[i][1]);*/
            bnumber++;
            borders = ( int **) realloc (san,(3*Tnumber)*sizeof(int *));
            borders[bnumber-1]=(int *) calloc(3,sizeof(int));
            borders[bnumber-1][0]=segments[i][0];
            borders[bnumber-1][1]=segments[i][1];
            borders[bnumber-1][2]=i/3; // i/3=int Wert des Triangles
         }
      }
      printf("BorderKnoten = %d\n",bnumber);

/************* Now output all files one by one *********************/
/*******************************************************************/
   printf("Output all Files one by one ..\n");
   sprintf(fname,"%s%s",strtok(fname,"."),".nod");
   fpl = fopen ( fname, "w" ) ;
      for(i=0;i<Number;i++)
      fprintf(fpl,"%d %f %f\n",i+1,xyz[i][0],xyz[i][1]);
   fclose(fpl);

   sprintf(fname,"%s%s",strtok(fname,"."),".ele");
   fpl = fopen ( fname, "w" ) ;
      for(i=0;i<Tnumber;i++)
      fprintf(fpl,"%d %d %d %d\n",i+1,triangles[i][2],triangles[i][1],triangles[i][0]); // 0...1...2 ehem=Neg. Area
   fclose(fpl);

   sprintf(fname,"%s%s",strtok(fname,"."),".bat");
   fpl = fopen ( fname, "w" ) ;
      for(i=0;i<Number;i++)
      fprintf(fpl,"%d %f\n",i+1,-1.*xyz[i][2]);
   fclose(fpl);



   sprintf(fname,"%s%s",strtok(fname,"."),".bcs.s2c");
   fpl = fopen ( fname, "w" ) ;
   fprintf(fpl,"%s\nM2 BCs for %s - elevations\n0.1405E-03\n",strtok(fname,"."),&fname);
      for(i=0;i<Number;i++)
      {
         if(xyz[i][3]!=NDV)
            fprintf(fpl,"%d %f %f\n",i+1,xyz[i][3], xyz[i][4]);
      }
      fclose(fpl);

   sprintf(fname,"%s%s",strtok(fname,"."),".bcs.s2r");
      fpl = fopen ( fname, "w" ) ;
      fprintf(fpl,"%s\nM2 BCs for %s - residuals\n",strtok(fname,"."),&fname);
      for(i=0;i<Number;i++)
      {
         if(xyz[i][3]!=NDV)
               fprintf(fpl,"%d %f \n",i+1,xyz[i][5]);
      }
      fclose(fpl);


/*************** Find the correct direction of the borders *******/
/*******************************************************************/

sprintf(fname,"%s%s",&fname,".bel");
fpl = fopen ( fname, "w" ) ;
fprintf(fpl,"%s Mesh from Gocad\nnodes with neighbourhood\n",strtok(fname,"."));

for (i=0;i<bnumber;i++)
{
   a=borders[i][0];
   b=borders[i][1];

   for(j=0;j<3;j++) // Border Triangles werden nach dem 3.,innnen liegenden Punkt durchsucht
   {
      if(triangles[borders[i][2]][j]!=a && triangles[borders[i][2]][j]!=b)
      c=triangles[borders[i][2]][j];
   }

   //    printf("Nodes %d %d %d, Angle: %f, VProduct %d\n",a,b,c,vangle(xyz[a-1],xyz[b-1],xyz[c-1]),isright(xyz[a-1],xyz[b-1],xyz[c-1]));
   //    printf("\nXYZ[B]: %f %f %f",xyz[b-1][0],xyz[b-1][1],xyz[b-1][2]);


   if(!isright(xyz[a-1],xyz[b-1],xyz[c-1]))
   {
      b=borders[i][0];
      a=borders[i][1];
   }

   c=aris[a-1][0]; // Border IdentifikationsWert von Punkt A

   //    for(j=0;j<bsnumber;j++)
   //    if(a==bstones[j][0]) c=aris[b-1][0];

   fprintf(fpl,"%d %d %d %d 0 \n",i+1,b,a,c);

}
fclose(fpl);


   //    for(i=0;i<bnumber;i++)
   //    printf("\n bnumber %d, Nodes(ARI): %d:%d %d:%d Triangle: %d",i,borders[i][0],borders[i][1],aris[borders[i][0]-1][0],aris[borders[i
         ][1]-1][0],borders[i][2]);

fclose(fp);
return (0);
}
```

```
278
279 /*************************************/
280 /****** SUBROUTINEN *****************/
281
282 static Boolean fend ( FILE *fp )
283 {
284     int ch = fgetc (fp) ;
285       if (ch==EOF)
286          return True ;
287     else
288          {
289             ungetc (ch, fp) ;
290             return False ;
291               }
292 }
293
294 /*************************************/
295 static void line_skip ( FILE *fp )
296 {
297     char c;
298
299       do c=(int)getc(fp);
300     while ( c!='\n' && c!=EOF );
301 }
302
303 /*********************************************/
304 static int isort (int *zahl, int anzahl)
305 {
306    int i, sortiert=0, hilf;
307    while(!sortiert)
308    {
309    sortiert=1;
310    for(i=1;i<anzahl; i++)
311       if(zahl[i-1]>zahl[i])
312       {
313       sortiert=0;
314       hilf=zahl[i];
315       zahl[i]=zahl[i-1];
316       zahl[i-1]=hilf;
317       }
318    }
319 return(1);
320 }
321
322 /************************************************/
323 static float vangle (float *A, float *B, float *C)
324 {
325    float phi,uv,u,v;
326
327    u=sqrt(((B[0]-A[0])*(B[0]-A[0]))+((B[1]-A[1])*(B[1]-A[1])));
328    v=sqrt(((C[0]-A[0])*(C[0]-A[0]))+((C[1]-A[1])*(C[1]-A[1])));
329    uv=(B[0]-A[0])*(C[0]-A[0])+(B[1]-A[1])*(C[1]-A[1]);
330    phi=acos(uv/(u*v));
331    return(phi);
332 }
333
334 /************************************************/
335 static float vproduct (float *A, float *B, float *C)
336 {
337    float u[2],v[2],vp;
338
339    u[0]=B[0]-A[0];
340    u[1]=B[1]-A[1];
341    v[0]=C[0]-A[0];
342    v[1]=C[1]-A[1];
343
344    vp=u[0]*v[1]-u[1]*v[0];
345
346    return (vp);
347 }
348
349 /************************************************/
350 static int isright (float *A, float *B, float *C)
351 {
352      float u[2],v[2];
353      int ind;
354
355      u[0]=B[0]-A[0];
356      u[1]=B[1]-A[1];
357      v[0]=C[0]-A[0];
358      v[1]=C[1]-A[1];
359      ind=0;
360      if((u[0]*v[1]-u[1]*v[0])>0) ind=1;
361
362      return (ind);
363 }
```

Listing 6.1: *Conversion program to read gOcad surface files with the corresponding values for the boundary conditions and writing the input files for Quoddy (geometry and boundary conditions)*

6.2 Conversion Tool: Quoddy Results → gOcad Property Surface File

```
1
2  ////////////////////////////////////////////////////////////////////////////
3  //                                  QUODDY->GOCAD
4  //--------------------------------------------------------------------------
5  //
6  //
7  ////////////////////////////////////////////////////////////////////////////
8
9  #include <stdio.h>
10 #include <string.h>
11 #include <malloc.h>
12 #include <stdlib.h>
13 #include <math.h>
14 const float pi=3.141592654;
15 /* Definition der Struktur */
16 typedef struct node{
17            struct node *next;      // Zeiger auf die Struktur des selben Typs
18            struct node *search;    // Zeiger auf die Suchkette
19
20            int ARI[3];             // ARI = Atom Region Indicator
21            int EleNr;
22            float vector[3];
23            float RealVelocityField[2];
24            float SurfElev;
25            float TidalAmplitude;
26            float phaselag;
27            float ZMID[21];
28            float ZOLD[21];
29            float UZMID[21];
30            float VZMID[21];
31            float WZMID[21];
32            float Q2MID[21];
33            float Q2LMID[21];
34            float TMID[21];
35            float SMID[21];
36            float Svelocity[202][3];
37            float Bvelocity[202][3];
38            float Sheight[202];
39            float Resid_zeta[202];
40            float Resid_vbar[202][2];
41      }element;                     // Name der Struktur
42
43 typedef element *ptr;               // Typdendefinition ZEIGER AUF STRUKTUR
44
45 //*************************************************************
46 //*** Definition der Funktionsköpfe          ***
47
48 int LeseDFTULI( ptr *anker );
49 int DatenEinhaengen( ptr *anker, ptr neues );
50 int SchreibeDFTULI( ptr anker );
51 int SucheElemente( ptr *anker, ptr neues, int z1,int z2);
52 static int Getline( FILE *, char *);
53 static float vangle (float x,float y);
54 static float meanv(float x, float y, float z);
55
56
57 /*************************************************************/
58 /*************************************************************/
59 static float vangle (float x, float y)
60 {
61
62    float angle,hypo;
63
64    hypo=(float)sqrt(pow(x,2)+pow(y,2));
65    angle=fabs(asin(y/hypo)/(pi/180));
66    return(angle);
67 }
68
69 static float meanv(float x, float y, float z)
70 {
71    float m;
72    m=sqrt(pow(x,2)+pow(y,2)+pow(z,2));
73
74    return(m);
75 }
76
77 //*************************************************************
78 //*************************************************************
79 static int Getline(FILE *input, char *p)
80 {
81    int c;
82    while(c=fgetc(input),(c!=EOF && c!='\n'))
83    *p++ =c;
84    if(c!=EOF) *p++=c;
85    *p++='\0';
86    return c;
87 }
88
89
90 //*************************************************************
91 /*** Setzt die Search-Zeiger der Listenelemente so, dass
92     die Daten, die auf das suchEleNr zutreffen direkt
93     miteinander verkettet werden
94     Gibt einen Zeiger auf das erste passende Element zurück ***/
95
96 /*********************************************************************/
97 int SucheElemente( ptr *anker, ptr neues, int z1,int z2 )
98 {
99    ptr   start=NULL;       // Zeiger auf das erste passende Element
```

```
   ptr   zeiger=NULL;      // Interner durchlaufzeiger
   ptr   altes=NULL;       // Zeiger auf das zuletzt gefundene Element
   int   status = 0;       // <> 0 --> noch kein element gefunden
   int test,test1,i,erg;



      for( zeiger = *anker,i=0; zeiger != NULL && status==0; zeiger = zeiger->next,i++ )
      {
         test=zeiger->EleNr;
         //printf("z1= %d ..i=%d\n",z1,i);
         //if(z1==z2) z1=z1+1;
         if( test == z2 )
         {
            /*** Passendes Element gefunden ***/
            zeiger->Sheight[z1-1]=neues->Sheight[z1-1];
            zeiger->Svelocity[z1-1][0]=neues->Svelocity[z1-1][0];
            zeiger->Svelocity[z1-1][1]=neues->Svelocity[z1-1][1];
            zeiger->Svelocity[z1-1][2]=neues->Svelocity[z1-1][2];
            zeiger->Bvelocity[z1-1][0]=neues->Bvelocity[z1-1][0];
            zeiger->Bvelocity[z1-1][1]=neues->Bvelocity[z1-1][1];
            zeiger->Bvelocity[z1-1][2]=neues->Bvelocity[z1-1][2];
            zeiger->Resid_vbar[z1-1][0]=neues->Resid_vbar[z1-1][0];
            zeiger->Resid_vbar[z1-1][1]=neues->Resid_vbar[z1-1][1];
            //zeiger->Resid_zeta[z1-1]=neues->Resid_zeta[z1-1];

            //printf("Level %d KnotenNr %d ZMID %f\n",z1,(*anker)->EleNr,(*anker)->ZMID[z2]);
            status=1;
         }
      }
      erg=1;


   return erg;

}

//*****************************************************
//*****************************************************

int LeseDFTULI( ptr *anker)
{
   FILE  *fp,*fp1,*fp2,*fp3,*fp4,*fp5,*fp6,*fp7,*fp8;
   ptr   zeiger,cpzeiger,gefZeiger;
   int   i, erg =-1,j,knoten,test,n,NPRD,STEP;
   char  zeile[180]="",fname1[40],fname2[40],fname3[30],fname4[30],fname5[25],cSTEP[5],cNPRD[5];
   double modulus;


   //
   // Öffnen der EingabeFiles
   //

   fp=fopen("perialpine.nod","rt");
   fp1=fopen("perialpine.bat","rt");
   fp5=fopen("perialpine.ele","rt");

         // TEST mit 17 = 1 Tidal M2 Zyklus sonst 192
         for (n=1;n<192;n++) // 16 Files pro Tidal Period (16 insg.) = 192 Files die eingelesen werden müssen
            {


            NPRD=(int)(((182*n)/2910)+1); // ehem. 256 nun 2992
               if (((182*n)%2910) == 0) NPRD=NPRD-1; // ehem. 16 anstatt 187; und 256 anstatt 2992
               sprintf(strtok(cNPRD," "),"%d",NPRD);
               STEP=(182*n)-1; sprintf(strtok(cSTEP," "),"%d",STEP);


               printf("-- Durchgang Nr.%d\n\n",n);
               sprintf(fname1,"Svelocity_%s_iter_%s.s2r",cNPRD,cSTEP);
               sprintf(&fname2[0],"Bvelocity_%s_iter_%s.s2r",cNPRD,cSTEP);
               sprintf(fname3,"Sheight_%s_iter_%s.s2r",cNPRD,cSTEP);
               sprintf(&fname4[0],"resid_vbar_%s_iter_%s.v2r",cNPRD,cSTEP);
               sprintf(&fname5[0],"resid_zeta_%s_iter%s.s2r",cNPRD,cSTEP);//

               printf("%s\n%s\n%s\n\n",fname1,fname2,fname3);

               fp2=fopen(fname1,"r"); if (fp2==NULL) printf("!! %s nicht vorhanden !!\n",fname1);
               fp3=fopen(fname2,"r"); if (fp3==NULL) printf("!! %s nicht vorhanden !!\n",fname2);
               fp4=fopen(fname3,"r"); if (fp4==NULL) printf("!! %s nicht vorhanden !!\n",fname3);
               fp7=fopen(fname4,"r"); if (fp7==NULL) printf("!! %s nicht vorhanden !!\n",fname4);
               fp8=fopen(fname5,"r"); if (fp8==NULL) printf("!! %s nicht vorhanden !!\n",fname5);//

               for (j=0;j<2;j++) {fgets (zeile,180,fp2);printf(" %s",zeile);}
               for (j=0;j<2;j++) {fgets (zeile,180,fp3);printf(" %s",zeile);}
               for (j=0;j<2;j++) {fgets (zeile,180,fp4);printf(" %s",zeile);}
               for (j=0;j<2;j++) {fgets (zeile,180,fp7);printf(" %s",zeile);}
               for (j=0;j<2;j++) {fgets (zeile,180,fp8);printf(" %s",zeile);} //


               printf("\n\n");

                     if (n<2)
                     {
                        while ( !feof(fp))
                        {
                           zeiger = (ptr)malloc( sizeof(element) ); // Speicher reservieren
                           zeiger->next = NULL;              // Zeiger vorbelegen
                           zeiger->search = NULL;
                           fscanf(fp," %d %f %f ",&zeiger->EleNr,&zeiger->vector[0],&zeiger->vector[1]);
                           fscanf(fp1," %d %f ",&test,&zeiger->vector[2]);
                           fscanf(fp5," %*d %d %d %d",&zeiger->ARI[0],&zeiger->ARI[1],&zeiger->ARI[2]);

                           fscanf(fp2,"%*d %f %f %f",&zeiger->Svelocity[n-1][0],&zeiger->Svelocity[n-1][1],&zeiger->Svelocity[n-1][2]);
                           fscanf(fp3,"%*d %f %f %f",&zeiger->Bvelocity[n-1][0],&zeiger->Bvelocity[n-1][1],&zeiger->Bvelocity[n-1][2]);
```

```
                           fscanf(fp4,"%*d %f ",&zeiger->Sheight[n-1]);
                           fscanf(fp7,"%*d %f %f",&zeiger->Resid_vbar[n-1][0],&zeiger->Resid_vbar[n-1][1]);
                           fscanf(fp8,"%*d %f",&zeiger->Resid_zeta[n-1]);//
                           DatenEinhaengen( anker, zeiger );
                        }
                           fclose( fp );fclose( fp1 );fclose( fp2 );fclose( fp3);fclose( fp4 );fclose( fp5 );
                     }
                     else
                     {

                        cpzeiger = (ptr)malloc( sizeof(element) ); // Speicher reservieren
                        cpzeiger->next = NULL;           // Zeiger vorbelegen
                        cpzeiger->search = NULL;
                        i=1;
                        while ( !feof(fp2))
                        {
                           fscanf(fp2,"%*d %f %f %f",&cpzeiger->Svelocity[n-1][0],&cpzeiger->Svelocity[n-1][1],&cpzeiger->Svelocity[n-1][2]);
                           fscanf(fp3,"%*d %f %f %f",&cpzeiger->Bvelocity[n-1][0],&cpzeiger->Bvelocity[n-1][1],&cpzeiger->Bvelocity[n-1][2]);
                           fscanf(fp4,"%*d %f",&cpzeiger->Sheight[n]);
                           fscanf(fp7,"%*d %f %f",&cpzeiger->Resid_vbar[n-1][0],&cpzeiger->Resid_vbar[n-1][1]);
                           fscanf(fp8,"%*d %f",&zeiger->Resid_zeta[n]);//
                           SucheElemente (anker,cpzeiger,n,i);
                           i++;
                        }
                        fclose( fp2 );fclose( fp3);fclose( fp4 );fclose( fp7 );
                        fclose( fp8 );//
                     }

         /*          if (n>16)
                     {

                        cpzeiger = (ptr)malloc( sizeof(element) ); // Speicher reservieren
                        cpzeiger->next = NULL;           // Zeiger vorbelegen
                        cpzeiger->search = NULL;
                        i=0;
                        while ( !feof(fp2))
                        {
                           fscanf(fp2,"%*d %f %f %f",&cpzeiger->Svelocity[n-1][0],&cpzeiger->Svelocity[n-1][1],&cpzeiger->Svelocity[n-1][2]);
                           fscanf(fp3,"%*d %f %f %f",&cpzeiger->Bvelocity[n-1][0],&cpzeiger->Bvelocity[n-1][1],&cpzeiger->Bvelocity[n-1][2]);
                           fscanf(fp4,"%*d %f",&cpzeiger->Sheight[n-1]);
                           fscanf(fp7,"%*d %f %f",&cpzeiger->Resid_vbar[n-1][0],&cpzeiger->Resid_vbar[n-1][1]);
                           //fscanf(fp8,"%*d %f",&zeiger->Resid_zeta[n]);
                           SucheElemente (anker,cpzeiger,n,i);
                           i++;
                        }
                        fclose( fp2 );fclose( fp3);fclose( fp4 );fclose( fp7 );
                        //fclose( fp8 );
                     }
         */
            }


         erg = i;







   return erg;
}

// ************************************************************
// ************************************************************
// *** Schreibt die Surface/Bottom Velocity Files ... ***
// ***                                              ***
// *** Schreibe TS Files für jede TidalPeriod lM2 ***
// *** = 16 SBW-Files, die 2*(Ebbe und Flut) beinhalten ***

int SchreibeDFTULI( ptr anker )
{
   FILE  *fp,*fp1,*fp2;    // *** Zeiger auf die Datei
   ptr   zeiger;
   int   i, erg = -1,j,z,NPRD,STEP,aux=0,test4,test5,test6,status;
   float knoten=1,test1,test2,test3,angle;
   char  EXT[4]=".ts", step[11]="_TimeStep_";
   char  cNPRD[3],cSTEP[3],fname[24],fnamel[24],cj[3];

   printf("\n Svelocity, Bvelocity, Wave height Files are being processed ....\n");

      for (j=1;j<16;j++) // Number of Tidal Periods = 16 = äußere Schleife = 16 Files
      {
         sprintf(strtok(cj," "),"%d",j);
         sprintf(fname,"3D_IAS_TP_%s.ts",cj);
         fp= fopen(fname,"wt");
         sprintf(fnamel,"speed_direction_5m_TP_%s.txt",cj);
         printf("\n AusgabeFiles: %s AND %s\n",fname,fname);
         fp2 = fopen(fnamel,"wt");

         fprintf(fp,"GOCAD Tsurf 1\nHEADER {\nname:3D_ohh_%d\n}\n\
            PROPERTIES Svel_16 Svel_32 Svel_48 Svel_64 Svel_80 Svel_96 Svel_112 Svel_128 Svel_144 Svel_160 Svel_176 Svel_192 Svel_208 Svel_224
                  Svel_240 Svel_256\
                    Bvel_16 Bvel_32 Bvel_48 Bvel_64 Bvel_80 Bvel_96 Bvel_112 Bvel_128 Bvel_144 Bvel_160 Bvel_176 Bvel_192 Bvel_208 Bvel_224
                          Bvel_240 Bvel_256\
                    vbar_16 vbar_32 vbar_48 vbar_64 vbar_80 vbar_96 vbar_112 vbar_128 vbar_144 vbar_160 vbar_176 vbar_192 vbar_208 vbar_224
                          vbar_240 vbar_256 \
                    Sheight_16 Sheight_32 Sheight_48 Sheight_64 Sheight_80 Sheight_96 Sheight_112 Sheight_128 Sheight_144 Sheight_160 Sheight_176
                          Sheight_192 Sheight_208 Sheight_224 Sheight_240 Sheight_256 \
                    bvelo_mean_16 bvelo_mean_32 bvelo_mean_48 bvelo_mean_64 bvelo_mean_80 bvelo_mean_96 bvelo_mean_112 bvelo_mean_128
                          bvelo_mean_144 bvelo_mean_160 bvelo_mean_176 bvelo_mean_192 bvelo_mean_208 bvelo_mean_224 bvelo_mean_240 bvelo_mean_256
                          \
                  \nESIZES \
                      3 3 3 3 3 3 3 3 3 3 3 3 3 3 3 3 \
                      3 3 3 3 3 3 3 3 3 3 3 3 3 3 3 3 \
                      3 3 3 3 3 3 3 3 3 3 3 3 3 3 3 3 \
                      1 1 1 1 1 1 1 1 1 1 1 1 1 1 1 1 \
                      1 1 1 1 1 1 1 1 1 1 1 1 1 1 1 1 \
```

```
306                  \n\nTFACE\n",j);
307
308          // Schleife über alle Knoten
309          for( zeiger=anker; zeiger != NULL; zeiger=zeiger->next)
310          {
311
312
313                fprintf(fp,"PVRTX %d %-2.3f %f %f",                    \
314                   zeiger->EleNr,                                      \
315                   zeiger->vector[0],                                  \
316                   zeiger->vector[1],                                  \
317                   zeiger->vector[2]);
318
319
320                // 16 Bvelocities[3] pro TidalPeriod... innere Schleife
321                // !!!! KORREKTUR DER WERTE, damit GOCAD die 3D Vektoren richtig mittelt !!!!!
322                for (i=0;i<16;i++)
323                {
324                   test1=zeiger->Svelocity[i+aux][0];test2=zeiger->Svelocity[i+aux][1];test3=zeiger->Svelocity[i+aux][2];
325                   //if (zeiger->Svelocity[i+aux][0]>5 || zeiger->Svelocity[i+aux][0]<-5) zeiger->Svelocity[i+aux][0]=0.00;
326                   //if (zeiger->Svelocity[i+aux][1]>5 || zeiger->Svelocity[i+aux][1]<-5) zeiger->Svelocity[i+aux][1]=0.00;
327                   //if (zeiger->Svelocity[i+aux][2]>0 || zeiger->Svelocity[i+aux][2]<0) zeiger->Svelocity[i+aux][2]=0.00;
328                   fprintf(fp," %f %f %f",zeiger->Svelocity[i+aux][0],zeiger->Svelocity[i+aux][1],zeiger->Svelocity[i+aux][2]);
329                }
330
331                for (i=0;i<16;i++)
332                {
333                   test1=zeiger->Bvelocity[i+aux][0];test2=zeiger->Bvelocity[i+aux][1];test3=zeiger->Bvelocity[i+aux][2];
334                   //if (zeiger->Bvelocity[i+aux][0]>5 || zeiger->Bvelocity[i+aux][0]<-5) zeiger->Bvelocity[i+aux][0]=0.00;
335                   //if (zeiger->Bvelocity[i+aux][1]>5 || zeiger->Bvelocity[i+aux][1]<-5) zeiger->Bvelocity[i+aux][1]=0.00;
336                   //if (zeiger->Bvelocity[i+aux][2]>5 || zeiger->Bvelocity[i+aux][2]<-5) zeiger->Bvelocity[i+aux][2]=0.00;
337                   fprintf(fp," %f %f %f",zeiger->Bvelocity[i+aux][0],zeiger->Bvelocity[i+aux][1],zeiger->Bvelocity[i+aux][2]);
338                }
339
340
341                for (i=0;i<16;i++)
342                {
343                   test1=zeiger->Resid_vbar[i+aux][0];test2=zeiger->Resid_vbar[i+aux][1];
344                   //if (zeiger->Bvelocity[i+aux][0]>5 || zeiger->Bvelocity[i+aux][0]<-5) zeiger->Bvelocity[i+aux][0]=0.00;
345                   //if (zeiger->Bvelocity[i+aux][1]>5 || zeiger->Bvelocity[i+aux][1]<-5) zeiger->Bvelocity[i+aux][1]=0.00;
346                   //if (zeiger->Bvelocity[i+aux][2]>5 || zeiger->Bvelocity[i+aux][2]<-5) zeiger->Bvelocity[i+aux][2]=0.00;
347                   fprintf(fp," %f %f 0.00",zeiger->Resid_vbar[i+aux][0]*500,zeiger->Resid_vbar[i+aux][1]*500);
348                }
349
350                for (i=0;i<16;i++) fprintf(fp," %f",zeiger->Sheight[i+aux]);
351
352                for (i=0;i<16;i++)
353                {
354                   test1=zeiger->Bvelocity[i+aux][0];test2=zeiger->Bvelocity[i+aux][1],test3=zeiger->Bvelocity[i+aux][2];
355                   fprintf(fp," %f",meanv(test1,test2,test3));
356                }
357
358                // HERAUSSCHREIBEN IN EINE SEPARATE DATEI für MATLAB //////
359                // ------------------------------------------------------
360
361                   for (i=0;i<16;i++)
362                   {
363                      test1=zeiger->Bvelocity[i+aux][0];test2=zeiger->Bvelocity[i+aux][1];test3=zeiger->Bvelocity[i+aux][2];
364                      // ------------------------------------------------------
365                      // Preparation for MEAN VEOLCITY - FLOW DIRECTION Diagramm für alle Knoten -- BVelocity(x,y)
366                      if (zeiger->Bvelocity[i+aux][0]>0 && zeiger->Bvelocity[i+aux][1]>0) angle=90-vangle(test1,test2); // SECTOR UR
367                      if (zeiger->Bvelocity[i+aux][0]>0 && zeiger->Bvelocity[i+aux][1]<0) angle=90+vangle(test1,test2); // SECTOR LR
368                      if (zeiger->Bvelocity[i+aux][0]<0 && zeiger->Bvelocity[i+aux][1]<0) angle=270-vangle(test1,test2); // SECTOR LL
369                      if (zeiger->Bvelocity[i+aux][0]<0 && zeiger->Bvelocity[i+aux][1]<0) angle=270+vangle(test1,test2); // SECTOR UL
370
371                      fprintf(fp2,"%d %f",zeiger->EleNr,angle);
372                      // ------------------------------------------------------
373                   }
374
375                   for (i=0;i<16;i++)
376                   {
377                      test1=zeiger->Bvelocity[i+aux][0];test2=zeiger->Bvelocity[i+aux][1];test3=zeiger->Bvelocity[i+aux][2];
378                      fprintf(fp2," %f",meanv(test1,test2,test3));
379                   }
380                // ------------------------------------------------------
381
382                fprintf(fp2,"\n");
383                fprintf(fp,"\n");
384
385          } // For Schleife für alle Knoten
386
387          //+++ TRIANGLES bzw. ELE File auslesen
388
389          fpl = fopen("perialpine.ele","r");
390          while ( !feof(fpl))
391          {
392             fscanf(fpl,"%*d %d %d %d",&test4,&test5,&test6);
393             fprintf(fp,"TRGL %d %d %d\n",test4,test5,test6);
394          }
395
396          //+++ Abschluß der VSet Datei +++
397          fprintf(fp,"\nEND");
398
399          fclose( fp );fclose(fpl);fclose(fp2);
400
401          erg = i;
402          aux=aux+16;
403       } // Number of TidalPeriods
404
405    return erg;
406
407 }
408
409 //*************************************************************
410 //*************************************************************
411 /*** Hängt ein neues Element in die Liste einn ***/
```

```
412 int DatenEinhaengen( ptr *anker, ptr neues )
413 {
414       ptr   suchzeiger;  // Zeiger für die Suche
415       ptr   nachlauf;   // Zeiger auf den Suchzeiger
416       int   status = 0;  // Status für IN DIE LISTE EINGEHÄNGT
417       int   erg=0;
418
419       // Adresse des neuen Elementes gültig ?
420       if( neues != NULL )
421       {
422
423          // Ist noch kein Element in der Liste ?
424          if( *anker == NULL )
425          {
426             // Ja, dann so
427             *anker = neues;
428             erg = 1;
429          }
430          else // sonst suchen, wo es hingehört
431          {
432
433             if( (neues->EleNr)<((*anker)->EleNr) )
434             {
435                // An den Listenanfang hängen, wenn EleNr des neuen Eingabewertes < als EleNr
436                // im Aktuellen Listenplatz ANKER ist
437                neues->next = *anker;
438                neues->search = *anker;
439                *anker = neues;
440                erg=1;
441             }
442             else // Nein, dann
443             {
444                // In die Listenmitte hängen ?
445                // Vorbelegung für suchzeiger und nachlauf
446                suchzeiger = (*anker)->next;
447                nachlauf = *anker;
448
449                // Solange unser suchzeiger nicht ins leere zeigt
450                // und das zeichen noch nicht in die liste gehängt wurde
451                while( suchzeiger != NULL && status == 0 )
452                {
453                   // vergleiche das neue zeichen mit der aktuellen position
454                   if( (neues->EleNr) < (suchzeiger->EleNr) )
455                   {
456                      neues->next = suchzeiger;
457                      neues->search = suchzeiger;
458                      nachlauf->next = neues;
459                      nachlauf->search = neues;
460                      status = 1;  // In die Liste aufgenommen!
461                   }
462
463
464                      // setze den suchzeiger auf das nächste listenelement
465                      suchzeiger = suchzeiger->next;
466                      // ziehe den nachlaufzeiger ebenfalls um eins nach vorne
467                      nachlauf = nachlauf->next;
468                      erg++;
469
470                }
471
472
473                if( status == 0 )
474                {
475                   // Listenende erreicht aber noch nicht
476                   // neues element eingehängt, dann
477                   // Ans Listenende
478                   nachlauf->next = neues;
479                   nachlauf->search = neues;
480                   erg++;
481                }
482             } // Ende LISTENMITTE/ENDE
483          } // Ende der Suche
484       } // ENDE MALLOC-Abfrage
485       else
486       {
487          erg = -1;
488       }
489       return erg;
490 }
491
492 /*********************************************************************************************
493 ++++++++++++++++++++++++++  H A U P T P R O G R A M M  ++++++++++++++++++++++++++++++++++
494 *********************************************************************************************/
495
496
497
498 int main(void)
499 {
500    ptr   anker=NULL;    // Der Anker für die Struktur
501    ptr   ausgabe=NULL;  // Für die Ausgabe der Liste
502    ptr   neues=NULL;    // Platz für ein neues Element
503
504
505
506    LeseDFTULI(&anker);
507    SchreibeDFTULI( anker );
508
509    return 0;
510 }
```

Listing 6.2: *Conversion program to read Quoddy results and generate gOcad surface files to display e.g. tidal amplitudes and flow velocities.*

6.3 Enhancements of QUODDY

6.3.1 Atmospheric Forcing

```
1
2  C*************************************************************
3  C*************************************************************
4       SUBROUTINE ATMOSQ5(KD,SECKD,ITER,NN,NNV,XNOD,YNOD,TMID,SMID,
5      &ATMX,ATMY,ATEMP,BTEMP,PME)
6  C Include file for parameter statements
7       INCLUDE 'DCMS.DIM'
8  C Fixed global variables
9       REAL XNOD(NNDIM),YNOD(NNDIM),TMID(NNDIM,NNVDIM),SMID(NNDIM,NNVDIM)
10      REAL ATMX(1:NNDIM),ATMY(1:NNDIM),ATEMP(NNDIM),BTEMP(NNDIM),
11     %PME(NNDIM)
12 C declare u,v to be same size as ATMX,ATMY
13      REAL U(1:NNDIM),V(1:NNDIM),RAMPUP
14      save RAMPUP_EXTENT,GEOFAC,PI
15
16 CBOB for rampup calculation
17      COMMON/TIDEINFO/NPRD,FREQ
18 C----------------------------------------
19
20
21 C
22 C on iter.eq.0, set some static stuff
23      IF(ITER.eq.0)THEN
24
25           PI=ACOS(-1.0)
26           GEOFAC=PI/180.
27
28 C define wind magnitude,direction
29           ANGLE=292*GEOREF ! counterclockwise from true east
30           WINDMAG=20.     ! m/s
31
32           ! this sets a rampup length of 3 m2 cycles
33           RAMPUP_EXTENT=3.
34         END IF ! iter>0
35
36 C
37 C Wind wird nach dem 7. Durchlauf 2910*7 eingeschaltet sobald sich ein
38 C dyn. Gleichgewicht durch die M2 Gezeit eingestellt hat
39 C
40       IF (ITER.gt.20370) THEN
41
42 C In fortran 90, there is no need to explicitly loop
43 C over the size of the arrays
44
45           DO I=1,NN
46             U(I)=WINDMAG*cos(ANGLE)
47             V(I)=WINDMAG*sin(ANGLE)
48           enddo
49
50 C more generally, what we do here is read in a wind field from a
51 c meteorological model, which is usually specified as U,V
52 c something like:
53 c         open(22,file='wind at time "now"')
54 c         READ(22,*) (K,U(I),V(I),I=1,NN)
55 c         close(22)
56
57           CALL WIND_STRESS(NN,U,V,ATMX,ATMY)
58
59 C        end
60
61 C compute rampup for this iteration, and scale ATMX,ATMY
62         RAMPUP=AMIN1(FLOAT(ITER)/NPRD/RAMPUP_EXTENT,1.)
63
64         DO I=1,NN
65           ATMX(I)=ATMX(I)*RAMPUP
66           ATMY(I)=ATMY(I)*RAMPUP
67         enddo
68
69         END IF
70
71 C End of routine
72 C
73      RETURN
74      END
```

Listing 6.3: *Soubroutine ATMOSQ5 added in the TIDE_Q5_1.1.USER.f file*

```
1
2  C***********************************************
3  C***********************************************
4       SUBROUTINE WIND_STRESS(NN,U,V,ATMX,ATMY)
5         INCLUDE 'DCMS.DIM'
6         REAL U(1:NNDIM),V(1:NNDIM),ATMX(1:NNDIM),ATMY(1:NNDIM)
7         REAL WINDMAG(1:NNDIM),CD(1:NNDIM),Q(1:NNDIM)
8         RHOAIR=1.225
9         RHOH2O=1024
10
11 C     Hsu wind stress
12
13        DO I=1,NN
14          WINDMAG(I)=SQRT(U(I)*U(I)+V(I)*V(I))
15          Q(I)=max(.1,WINDMAG(I))
16          CD(I)=max(6.0e-04,(0.4/(14.56-2*log(Q(I))))**2)
17          ATMX(I)=RHOAIR*CD(I)*U(I)*WINDMAG(I)/RHOH2O
18          ATMY(I)=RHOAIR*CD(I)*V(I)*WINDMAG(I)/RHOH2O
19        enddo
20
21       END
22
23 C End of routine
24 C
```

Listing 6.4: *Soubroutine WIND_STRESS which is used by the ATMOSQ5 routine*

6.3.2 Point Source

```
1
2       SUBROUTINE POINTSOURCEQ5(KD,SECKD,ITER,NN,NNV,Z,
3      &SRCRATE,USRC,VSRC,TSRC,SSRC)
4  C Include file for parameter statements
5       INCLUDE 'DCMS.DIM'
6  C Fixed global variables
7       REAL Z(NNDIM,NNVDIM),USRC(NNDIM,NNVDIM),VSRC(NNDIM,NNVDIM),
8      &TSRC(NNDIM,NNVDIM),SSRC(NNDIM,NNVDIM)
9       REAL SRCRATE(NNDIM,NNVDIM)
10
11 C...Set number of cycles for ramping up the river source
12 C    NPRD=Number of time step per cycle
13 C    NRAMP=Number of cycles for ramping up
14 C
15      NPRD=256
16      NRAMP=3
17      RAMPUP=REAL(ITER)/REAL(NPRD*NRAMP)
18 c     IF (RAMPUP.GT.1) RAMPUP=1.
19 C...no rampup for hot-start
20 C     RAMPUP=1.0
21 C
22 C...Surface element number
23      NEV=NNV-1
24 C
25 c - Napf FAN DELTA
26      STRENGTH=90
27      II=1801
28      SSRC(II,NNV)=1.0
29      TSRC(II,NNV)=1.0
30      DO KK=10,20
31        SRCRATE(II,kk)=STRENGTH*RAMPUP
32        SSRC(II,kk)=15.
33        TSRC(II,kk)=12.
34      END DO
35 RETURN
36 END
```

Listing 6.5: *Soubroutine POINTSOURCEQ5 to acknowledge resh water influx from the surrounding domains.*

6.4 Generate a PGM Bitmap

```
1
2  % Konvertiere Matrix in PGM
3  % Uli Bieg - März 2004
4
5  wk1read uli1_neu.wk1
6  %bathy_uli.wk1
7  %csvread uli.csv
8
9  % Bestimmt die Größe des Zeilen und Spaltenvektors und
10 % legt die Hilfsmatrix
11 % lalo an, in der die auf 256 Grauwerte reduzierten
12 % Werte stehen
13 % Zeilenvektor x = [ x1 x2 x3];
14 % Spaltenvektor x = [x1; x2];
15
16 %long=max(size(ans));
17 %lat=min(size(ans));
18
19 lalo=ones(362,362);
20
21 % Bestimmung des größten Bathymetriewertes in der Matrix
22 % Da ans eine Matrix ist, so ergibt sich ein Vektor,
```

```
% der die größten Elemente
% einer jeden Spalte enthält; danach wird der max Wert
% des Spaltenvektors
% ermittelt.

bb=max(ans)
bb1=max(bb);
multiplikator=256/bb1

% Bathymetrie mit max. Wert 256 wird erstellt

for y=1:362
   for x=1:180
      if ans(y,x)>0
         lalo(x,y)=round(ans(y,x)*multiplikator);
      end
   end
end

% Erzeugung eines pgm Files
% Portable Graymap File Format

% Header schreiben
fp=fopen('Batyhmetry.pgm','w');
fprintf(fp,'P2\n');
fprintf(fp,'# Bathymetry.pgm\n');
fprintf(fp,'361 180\n');
fprintf(fp,'256\n');

%
for y=1:180
   for x=361:-1:1
      fprintf(fp,' %d,',lalo(y,x));
      end
      fprintf(fp,'\n');
   end
end

fclose(fp);
```

Listing 6.6: *Matlab code snippet to generate a PGM bitmap file from a simple matrix. This can be used and converted to a arbitrary bitmap file.*